Gene Editing of Tumour Infiltrating Lymphocytes for the Generation of Adoptive Cellular Therapeutics against Cancer

UCL Cancer Institute

University College London

A thesis presented for the Degree of Doctorate in Philosophy

Mariana Werner Sunderland

November 2019

Declaration

I, Mariana Werner Sunderland, confirm that the work presented in this thesis is my own. Where information has been derived from other sources, I confirm that this has been indicated in the thesis.

Abstract

Cancer treatments that are based on the reactivation, expansion, or mobilisation of the immune system, such as adoptive cellular therapies and immune-checkpoint blockade, have achieved long-lasting anti-tumour responses in cancer patients. However, there is still a high proportion of patients that do not benefit from these treatments. This highlights the need for more effective therapies.

Based on the notion that adoptive cell therapies do work and are likely limited *in vivo* by the activation of immune modulatory pathways, this project focused on ablating negative regulation and increasing the intra-tumoural effector activity of tumour-reactive T cells. Specifically, my project aimed to genetically modify tumour infiltrating T cells by knocking-out the expression of immune-checkpoints on their surface so as to render them resistant to checkpoint inhibition, thus generating potent and long-lasting anti-tumour immunity. For this purpose, the CRISPR/Cas9 technology was used to genome edit tumour-reactive T cells using primary human tumour-infiltrating lymphocytes (TILs) obtained from melanoma and non-small-cell lung carcinoma (NSCLC) patients.

The project initially focused on the generation of PD1-deficient tumour-reactive T cells as a proof of concept, as targeting this pathway with antibodies has shown clear efficacy in the clinic (Suzanne L. Topalian et al., 2012). Following the generation of PD1-deficient gene edited T cells, we developed LAG3-deficient and TIGIT-deficient tumour-reactive T cells, as well as T cells that were deficient for both PD1 and LAG3 expression.

In sum, the overall purpose of this project was to utilise cutting edge gene editing tools to engineer tumour-reactive lymphocytes and render them resistant to checkpoint inhibition. The results from this work have established a clinically relevant pipeline for the generation of potent adoptive cell therapy products for the treatment of cancer.

Impact Statement

For many years, the cornerstones of cancer treatment have been surgery, chemotherapy, and radiation therapy. These treatments have been suboptimal, and this has called for new strategies in the fight against this disease. Moreover, in recent years we have seen the emergence of cancer immunotherapy, in which treatments harness the power of a patient's immune system to battle against their disease. This field has rapidly become a promising one in the fight against cancer, however there are still many improvements that could be done to existing clinical treatments to achieve better survival rates.

Long-lasting responses have been observed in a fraction of patients treated with adoptive cellular therapies (ACT) or immune checkpoint blockade (ICB) treatments (R. Andersen et al., 2016; Frank Stephen Hodi et al., 2018; McDermott, Haanen, Chen, Lorigan, & O'Day, 2013; Rosenberg et al., 2011). However, to date, only a small percentage of patients with advanced malignancies can benefit from either of these immune-based treatment modalities. Furthermore, immune-related adverse events (irAEs) are frequent in patients treated with ICB and in some cases these events can be fatal (F. Stephen Hodi et al., 2010; Robert et al., 2015). These irAEs occur in up to 90% of patients treated with an anti-CTLA4 antibody (F. Stephen Hodi et al., 2010) and in 70% of patients treated with an anti-PD1 antibody (Suzanne L. Topalian et al., 2012). Therefore, there is a need to develop therapies that can achieve complete responses in a higher proportion of patients and that can minimise or prevent the toxicities observed with the systemic blockade of immune checkpoints.

To address this need, this project was focused on generating a proof-of-concept for the combination of adoptive cellular therapy of tumour infiltrating lymphocytes (TILs) with immune checkpoint inhibition via gene engineering of the TILs. We hypothesised that by genetically knocking down the expression of immune checkpoints only on the tumour-reactive T cells (or, if possible, in the neoantigen-reactive T cells), we would be able to eliminate the negative regulation and increase the intra-tumoural effector activity of tumour-reactive T cells whilst preventing or at least reducing the toxicities associated with systemic blockade of immune checkpoints.

In this project we succeeded in optimising a methodology for the genomic engineering of primary human TILs using the CRISPR/Cas9 technology. We demonstrated that the use of this methodology can achieve high efficiencies of gene editing whilst maintaining a high viability of the cells post-editing. The methodology developed in this project can be used to generate powerful preclinical and translational adoptive cellular therapeutics.

Acknowledgments

I am truly thankful to my supervisors, Professor Sergio Quezada and Professor Karl Peggs for giving me the opportunity to come to their laboratory and work on this project, as well as for their support and advice during the course of my PhD. It was a pleasure working for the both of you. I also want to thank the Mexican National Council for Science and Technology for the scholarship they awarded me, without it I would not have been able to embark in this PhD.

I am hugely grateful to all of the past and present members of the Quezada/Peggs laboratory: Fred Arce, Pablo Becker, Assma Ben Aissa, Jo Clancy, Cristobal Costoya, Dafne Franz, Felipe Galvez, Andy Georgiou, Ehsan Ghorani, Emine Hatipoglu, Jake Henry, Kroopa Joshi, Chen Qing, James Reading, Marc Robert De Massy, Manar Shafat, Anna Sledzinska, Isabelle Solomon, Maria Vila de Mucha, Sophia Wong, and Dimitrios Zervas. I am thankful for their help and advice, as well as for the valuable life lessons they all gave me.

Special thanks go to Dafne Franz, Emine Hatipoglu, Anna Sledzinska, and Isabelle Solomon. Thank you for your unwavering friendship, I don't think I could have finished this PhD with a sane mind without you and our coffee breaks. Also, I would like to give a special thank you to Pablo Becker for his enthusiasm, example, and mentorship.

I would also like to thank all of the people from the UCL Cancer Institute. This institute is filled with students and staff members that are always willing to lend a hand, to explain things, or to discuss ideas. The good-naturedness of my colleagues and friends made working with them a real pleasure and an unforgettable work- and life-experience.

My family and friends outside of science are also owed my thanks. Especially my mother and sister, Clara Sunderland and Jimena Werner, who have always encouraged me in any undertaking I pursue. Their unwavering support was indispensable for me throughout this period.

Last, but definitely not least, I am the most grateful to my husband Alexandre Leskanich. Even while undertaking a PhD of his own, he was continually supportive of me and my work. Thank you for your perspective, motivation, and love. Your constant companionship made this academic journey pleasurable.

Table of contents

DECLARATION **2**

ABSTRACT **3**

IMPACT STATEMENT **4**

ACKNOWLEDGMENTS **6**

LIST OF FIGURES **12**

LIST OF TABLES **15**

ABBREVIATIONS **16**

CHAPTER 1. INTRODUCTION **19**

1.1. THE IMMUNE SYSTEM AND CANCER 19

1.1.1. Cell-Mediated Immune Responses *22*

1.1.2. Molecular Mechanisms of T cell Co-Stimulation and Co-Inhibition . *25*

1.1.3. Co-Inhibitory Receptors and their Signalling Pathways *27*

1.1.3.1. CTLA4 27

1.1.3.2. PD1 28

1.1.3.3. TIM3 30

1.1.3.4. LAG3 32

1.1.3.5. TIGIT 33

1.2. IMMUNOTHERAPY 34

1.2.1. Immune Checkpoint Blockade *34*

1.2.2. Adoptive Cell Therapy *36*

1.2.2.1. Tumour Infiltrating Lymphocytes 36

1.2.2.2. Neoantigens 37

1.2.2.3. Chimeric Antigen Receptor T Cell 38

1.3. NEXT GENERATION CELL THERAPIES 39

1.3.1. Gene Editing Technologies *41*

1.3.1.1. Meganucleases 42

1.3.1.2. Zinc Finger Nucleases 42

1.3.1.3. Transcription Activator-Like Effector Nucleases 43

1.3.1.4. The CRISPR/Cas9 System 44
1.4. HYPOTHESIS AND AIMS 46
1.5. EXPERIMENTAL PLAN 47

CHAPTER 2. MATERIALS AND METHODS 49

2.1 MATERIALS 49
2.1.1. Cell lines and primary cells 49
2.1.2. Plasmids and Cas9 protein 50
2.1.3. crRNAs oligos for cloning into Cas9 plasmid and commercially synthesised crRNAs:tracrRNAs complexes 51
2.1.4. Flow cytometry antibodies 53
2.1.5. Mice 54
2.2 METHODS 55
2.2.1. Molecular biology techniques 55
2.2.1.1. Cloning of crRNAs oligos into SpCas9 and chimeric guide RNA expression plasmid 55
2.2.1.2. Bacteria transformation 55
2.2.1.3. Plasmid purification from bacteria 55
2.2.1.4. Complete and diagnostic digestions 56
2.2.1.5. Sanger sequencing for confirmation of correct cloning 57
2.2.1.6. Gel extraction/purification 57
2.2.1.7. Generation of SFG.TIGIT and SFG.LAG3 plasmids 57
2.2.1.8. In vitro transcription of GFP, Cas9 and gRNAs 58
2.2.1.9. DNA isolation from cells 59
2.2.1.10. Genomic confirmation of gene editing 59
2.2.1.10.1 TIDE and ICE Analysis 59
2.2.1.10.2 MiSeq Analysis 59
2.2.2. Cell culture techniques 59
2.2.2.1. Transfection of adherent HEK293T cell line 59
2.2.2.2. Transduction of adherent HEK293T cell line 60
2.2.2.3. Human peripheral blood mononuclear cell isolation 60
2.2.2.4. Activation of human T cells 60
2.2.2.5. Expansion of human TILs using the pre-REP and Rapid Expansion Protocol (REP) 61

2.2.2.6. Electroporation of primary T cells 61
2.2.2.6.1. BTX electroporator machine 61
2.2.2.6.2. Amaxa 4D Nucleofector machine 62
2.2.3. CRISPR cRNAs design and Cas9 RNP complex production 62
2.2.4. Flow cytometry staining and analysis 63
2.2.4.1. Staining protocol 63
2.2.4.2. Compensation 63
2.2.4.3. Fluorescence cell sorting 64
2.2.5. Statistical analysis 64
2.2.6. In vitro functional assays 64
2.2.6.1. Recall assay 64
2.2.6.2. CFSE proliferation assay 64
2.2.6.3. Killing assay 65
2.2.6.4. Peptide screen 65
2.2.7. Single cell suspensions of tumours for flow cytometry analysis 66

CHAPTER 3. CRISPR/CAS9-MEDIATED GENE EDITING IN CELL LINES, PRIMARY T CELLS AND TUMOUR INFILTRATING LYMPHOCYTES 67

3.1. OVERVIEW 67
3.2. INTRODUCTION 67
3.2.1. CRISPR/Cas9 gRNAs design 67
3.2.2. Delivery of CRISPR/Cas9 components 69
3.2.2.1. Viral vectors 69
3.2.2.2. Non-viral vectors 71
3.2.2.3. Physical delivery 72
3.3. AIMS 74
3.4. DESIGN OF CRRNAS AND LIGATION INTO CAS9 VECTOR 75
3.5. GENERATION OF HEK293T CELL LINES CONSTITUTIVELY EXPRESSING CHECKPOINTS OF INTEREST 78
3.6. CRISPR/CAS9-MEDIATED KNOCKDOWN OF TARGETS VIA DNA TRANSFECTION INTO CELL LINES CONSTITUTIVELY EXPRESSING CHECKPOINTS OF INTEREST 82
3.7. ELECTROPORATION OF CELL LINE AND PRIMARY T CELLS (BTX ELECTROPORATOR) 90

3.8. CAS9 RNP COMPLEX ELECTROPORATION OF PRIMARY T CELLS AND OF TILS (AMAXA 4D NUCLEOFECTOR) 99
3.8.1. Healthy donors PBMCs 99
3.8.2. Melanoma and Non-Small-Cell Lung Carcinoma (NSCLC) Patient's TILs 110
3.9. DISCUSSION 122

CHAPTER 4. EXPANSION AND CHARACTERISATION OF MELANOMA-REACTIVE T CELLS 125

4.1. OVERVIEW 125
4.2. INTRODUCTION 125
4.2.1. Ex vivo expansion of tumour infiltrating lymphocytes for adoptive cellular therapies 125
4.2.2. Detection and expansion of neoantigen reactive T cells 128
4.3. AIMS 130
4.4 CHARACTERISATION OF EXPANDED MX063 TUMOUR INFILTRATING LYMPHOCYTES AND OF AUTOLOGOUS PRIMARY TUMOUR CELL LINE 130
4.5. EXPANSION AND SELECTION OF TUMOUR-REACTIVE T CELLS 135
4.6. PEPTIDE SCREENING OF MX063 TUMOUR INFILTRATING LYMPHOCYTES IN SEARCH OF NEOANTIGEN REACTIVE T CELLS 140
4.7. DISCUSSION 147

CHAPTER 5. DEVELOPMENT OF *IN VITRO* AND *IN VIVO* FUNCTIONAL ASSAYS FOR THE CHARACTERISATION OF TUMOUR INFILTRATING LYMPHOCYTES 151

5.1. OVERVIEW 151
5.2. INTRODUCTION 151
5.2.1. Patient derived xenografts as a model for adoptive cellular therapies 151
5.3. AIMS 154
5.4. FUNCTIONAL *IN VITRO* ASSAYS OF MX063 TUMOUR INFILTRATING LYMPHOCYTES (EDITED AND NON-EDITED) VS. AUTOLOGOUS PRIMARY CELL LINE 154
5.5. OPTIMISATION OF AN *IN VIVO* MODEL TO TEST ADOPTIVE CELLULAR THERAPIES 163

5.6. DISCUSSION 172

CHAPTER 6. CONCLUSION AND FUTURE WORK 176

6.1. CONCLUDING REMARKS 176

6.2. OUTLOOK FOR FUTURE WORK 178

6.2.1. Selective expansion of tumour-reactive or neoantigen-reactive T cells 178

6.2.2. Generation of in vitro and in vivo models to test adoptive cellular therapies 179

6.2.3. Targets for future work 181

7. REFERENCES 182

8. APPENDIX 218

List of Figures

Figure 1.1. The three phases of the cancer immunoediting process 21
Figure 1.2. Class I MHC-restricted cross-presentation by dendritic cells 23
Figure 1.3. The MHC class I and MHC class II antigen-presentation pathways25
Figure 1.4. Comparison of intracellular signalling by CTLA4 and PD1 30
Figure 1.5. The TIM3 pathway 31
Figure 1.6. The LAG3 pathway 33
Figure 1.7. The CD226/TIGIT pathway 34
Figure 1.8. Experimental plan devised to achieve the aims of this project 48
Figure 3.1. E-CRISP workflow 69
Figure 3.2. Cloning of crRNAs into a human codon-optimised SpCas9 and chimeric guide RNA expression plasmid 77
Figure 3.3. Generation of HEK293T cell line constitutively expressing TIGIT for validation of gRNAs 80
Figure 3.4. Generation of HEK293T cell line constitutively expressing LAG3 for validation of gRNAs 81
Figure 3.5. CRISPR/Cas9-mediated Knockdown of PD1 83
Figure 3.6. CRISPR/Cas9-mediated Knockdown of TIM3 85
Figure 3.7. CRISPR/Cas9-mediated Knockdown of CTLA4 87
Figure 3.8. CRISPR/Cas9-mediated Knockdown of TIGIT 89
Figure 3.9. CRISPR/Cas9-mediated Knockdown of LAG3 90
Figure 3.10. Electroporation of HEK293T PD1/TIM3 cells with Cas9:gRNA mRNA and with Cas9 RNP complex 93
Figure 3.11. Electroporation of healthy donor PBMCs and of TILs with *in vitro* transcribed GFP 95
Figure 3.12. Electroporation of healthy donor PBMCs with *in vitro* transcribed Cas9 and gRNA or with *in vitro* transcribed GFP 97
Figure 3.13. Electroporation of healthy donor PBMCs with Cas9 RNP complex 98
Figure 3.14. Electroporation of unstimulated healthy donor PBMCs with pmaxGFP vector 100
Figure 3.15. Amaxa electroporation of healthy donor PBMCs with Cas9 RNP complexes 102

Figure 3.16. Dual gRNA electroporation targeting PD1 exon 1 104
Figure 3.17. PD1 editing of healthy donor PBMCs with Cas9 RNP complexes with different molar ratios and with combination of PD1 gRNAs 106
Figure 3.18. Gene editing of four different healthy donors PBMCs with either PD1, TIGIT, or LAG3 gRNA 109
Figure 3.19. Gene editing of MX063 TILs with gRNAs targeting TIM3 or TIGIT 112
Figure 3.20. Gene editing of MX063 TILs with gRNAs targeting LAG3 114
Figure 3.21. Gene editing of TILs during REP 117
Figure 3.22. Genomic confirmation of gene editing on LTX997 edited TILs ... 119
Figure 3.23. Efficient and persistent co-editing of PD1 and LAG3 on MX063 TILs 121
Figure 4.1. Checkpoint expression in expanded MX063 TILs after stimulation 132
Figure 4.2. Characterisation of MX063 primary tumour cell line 134
Figure 4.3. Upregulation of PD-L1 by IFNγ in MX063 primary tumour cell line 135
Figure 4.4. Recall assay for expanded TILs against autologous tumour cell line 137
Figure 4.5. Sorting of tumour-reactive MX063 TILs 138
Figure 4.6. Sorting of tumour-reactive TILs from MX063 TILs expanded using the 'REP' 140
Figure 4.7. Indels peptide screening of MX063 'REP*' TILs 143
Figure 4.8. Indels peptide screening of MX063 'pre-REP+REP' TILs 144
Figure 4.9. SNV peptide screening of MX063 'pre-REP+REP' TILs 146
Figure 5.1. Killing assay of MX063 edited TILs against autologous tumour cell line 155
Figure 5.2. Killing assay of MX063 edited TILs (single and double edited) against autologous tumour cell line 157
Figure 5.3. Recall assay of MX063 edited TILs (single and double edited) against autologous tumour cell line 159
Figure 5.4. Recall assay of MX063 'REP' edited TILs (single and double edited) against autologous tumour cell line 162

Figure 5.5. Co-injection of MX063 tumour primary cell line and non-edited autologous tumour infiltrating lymphocytes into NSG mice 165
Figure 5.6. Flow cytometry analysis of tumours 41 days post-injection of cells 167
Figure 5.7. Treatment of MX063 tumour-bearing NSG mice with autologous tumour infiltrating lymphocytes 169
Figure 5.8. Flow cytometry analysis of tumours 43 days post-injection of cells 170
Figure 5.9. T cell infiltration of tumours 28 days post-injection of TILs 171
Supplementary Figure 8.1. Validation of correct ligation via Sanger sequencing 218
Supplementary Figure 8.2. GFP expression of HEK293T cells transfected with SFG.LAG3 plasmid 219
Supplementary Figure 8.3. Percentage of HEK293T cells expressing targets of interest after gene editing 220
Supplementary Figure 8.4. Percentage of PD1 expression on edited PBMCs221
Supplementary Figure 8.5. TIM3 and CTLA4 gRNA validation in healthy donor PBMCs 223
Supplementary Figure 8.6. Gene editing of four different healthy donors PBMCs with either PD1, TIGIT, or LAG3 gRNA 223
Supplementary Figure 8.7. Gene editing of MX063 TILs with gRNAs targeting TIM3 224
Supplementary Figure 8.8. Viability of TILs edited during REP 224
Supplementary Figure 8.9. Gene editing of TILs during REP 225
Supplementary Figure 8.10. Efficient and persistent co-editing of PD1 and LAG3 on LTX1000 TILs 226
Supplementary Figure 8.11. Fluorescence minus one (FMO) controls for the staining of MX063 primary tumour cell line 227
Supplementary Figure 8.12. Percentage of $CD4^+$ and $CD8^+$ cells in expanded MX063 TILs that were edited to knockdown either LAG3, PD1, or a combination of both 228
Supplementary Figure 8.13. Successful gene editing of TIGIT, LAG3, PD1, and combination of LAG3 and PD1 229

List of Tables

Table 1.1. Comparison of different gene editing technologies..... 41
Table 2.1. Oligos ordered for crRNAs..... 51
Table 2.2. Commercially synthesised crRNAs..... 52
Table 2.3. Antibodies used for flow cytometry staining..... 54
Table 2.4. Reaction performed for enzymatic digestion of plasmid and purified PCR products..... 56
Table 2.5. Reaction performed for diagnostic digestion of SFG.TIGIT and SFG.LAG3 plasmids 57
Table 2.6. Reaction performed for ligation of SFG vector with TIGIT or LAG3 ORF 58
Table 2.7. Reactions made for transfections of HEK293T cells 60
Table 2.8. Electrical variables for electroporation of primary T cells 62
Table 3.1. Designed crRNAs 76

Abbreviations

AAV:	Adeno-associated virus
ACT:	Adoptive cellular therapy
ANOVA:	Analysis of variance
APC:	Antigen presenting cell
ATP:	Adenosine triphosphate
bp:	Basepair
CAR:	Chimeric antigen receptor
Cas9:	CRISPR-associated protein 9
CD:	Cluster of differentiation
cDNA:	Complementary DNA
CDX:	Cell line derived xenograft
CEACAM1:	Carcinoembryonic antigen cell adhesion molecule 1
CFSE:	Carboxyfluorescein succinimidyl ester
CMV:	Cytomegalovirus
Cpf1:	CRISPR from *Prevotella* and *Francisella* 1
CRISPR:	Clustered regularly interspaced short palindromic repeats
CRISPRa:	CRISPR activation
CRISPRi:	CRISPR interference
crRNAs:	CRISPR RNAs
CRS:	Cytokine release syndrome
CTLA4:	Cytotoxic T lymphocyte associated protein 4
CTLs:	Cytotoxic T lymphocytes
DAMPs:	Damage-associated molecular patterns
DC:	Dendritic cell
DMEM:	Dulbecco's modified eagle's medium
DMSO:	Dimethyl sulfoxide
DNA:	Deoxyribonucleic acid
DTT:	Dithiothreitol
E:T ratio:	Effector to target ratio
eGFP:	Enhanced green fluorescence protein
ER:	Endoplasmic reticulum
FACS:	Fluorescence-activated cell sorting
FBS:	Foetal bovine serum
FMO:	Fluorescence minus one
FoxP3:	Forkhead box P3
Gal-9:	Galectin-9

GFP: Green fluorescence protein
gRNA: Guide RNA
HDR: Homology directed repair
HEK: Human embryonic kidney
HLA: Human leukocyte antigen
HMGB1: High mobility group box 1
ICB: Immune checkpoint blockade
ICE: Inference of CRISPR Edits
IFNγ: Interferon gamma
IFNs: Interferons
IgSF: Immunoglobulin (Ig) superfamily
IL-10: Interleukin-10
IL-15: Interleukin-15
IL-2: Interleukin-2
IL-21: Interleukin-21
IL-7: Interleukin-7
IMDM: Iscove's modified eagle's medium
Indels: Insertions or deletions
iPSCs: Induced pluripotent stem cells
irAEs: Immune-related adverse events
IRES: Internal ribosome entry site
ITIM: Immunoreceptor tyrosine-based inhibitory motif
ITSM: Immunoreceptor tyrosine-based switch motif
IVT: *In vitro* transcription
kb: Kilobase
LAG3: Lymphocyte activation gene 3
LSECtin: Liver and lymph node sinusoidal endothelial cell C-type lectin
LTR: Long terminal repeat
MDSCs: Myeloid-derived suppressor cells
MHC: Major histocompatibility complex
MMLV: Moloney murine leukaemia virus
mRNA: Messenger RNA
NFAT: Nuclear factor of activated T-cells
NGS: Next generation sequencing
NHEJ: Non-homologous end joining
NK cells: Natural killer cells
NKT cells: Natural killer T cells
NLS: Nuclear localization sequence
NSCLC: Non-small cell lung cancer

NSG: NOD *scid* gamma
ORF: Open reading frame
PAM: Protospacer adjacent motif
PAMPs: Pathogen-associated molecular patterns
PBMCs: Peripheral blood mononuclear cells
PD-L1: Programmed death-ligand 1
PD-L2: Programmed death-ligand 2
PD1: Programmed cell death protein 1
PDX: Patient derived xenograft
PtdSer: Phosphatidyl serine
REP: Rapid expansion protocol
RNA: Ribonucleic acid
RNases: Ribonucleases
RNP: Ribonucleoprotein
RPMI: Roswell Park Memorial Institute medium 1640
SaCas9: *Staphylococcus aureus* Cas9
SEB: Staphylococcus aureus Enterotoxin Type B
SHIP-1: SH-2 containing inositol 5' polyphosphatase 1
SHP: Src homology region 2 domain-containing phosphatase
SNV: Single nucleotide variant
SpCas9: *Streptococcus pyogenes* Cas9
T4 PNK: T4 polynucleotide kinase
TAA: Tumour-associated antigen
TALEN: Transcription activator-like effector (TALE) nucleases
TCR: T cell receptor
Tfh: T follicular helper cells
TGF-β: Transforming growth factor-β
TIDE: Tracking of indels by decomposition
TIGIT: T cell Immunoglobulin and ITIM domain
TILs: Tumour infiltrating lymphocytes
TIM3: T cell immunoglobulin and mucin-domain containing 3
TNFα: Tumour necrosis factor alpha
TNFRSF: Tumour necrosis factor (TNF) receptor superfamily
TRACERx: Tracking cancer evolution through therapy (Rx)
tracrRNA: Trans-activating crRNA
Treg: Regulatory T cells
TSS: Transcription start site
ZFN: Zinc finger (ZF) nucleases

Chapter 1. Introduction

1.1. The Immune System and Cancer

The immune system is the assortment of cells, tissues and molecules that defend our bodies against pathogens. This system can be classified into two main categories: innate immune system and adaptive immune system. The innate immune system is, as its name indicates, the first line of defence that we are born with; it is comprised of epithelial barriers, the complement system, natural killer (NK) cells, mast cells, eosinophils, basophils, macrophages, neutrophils and dendritic cells (DC). This immune response provides immediate protection against infection by recognizing structures that are common to many pathogens but are absent in normal host cells. These structures are called pathogen-associated molecular patterns (PAMPs). The innate immune system is also able to recognise damage-associated molecular patterns (DAMPs), which are molecules that are released from injured or necrotic host cells. The cells of the innate immune system are immediately available to fight a broad variety of pathogens without needing prior exposure. This immediacy is one of the key advantages of the innate immune response, however, it has the limitation of not recalling prior encounters with pathogens and returning to baseline after each encounter. In contrast, adaptive immune responses have evolved to provide a more specialised defence against infection that also yields increased protection against successive reinfection with the same pathogen, a phenomenon known as immunological memory. The adaptive immune system is comprised of lymphocytes (T cells and B cells) and their products (such as antibodies). These lymphocytes express T and B cell receptors that identify in a specific way a much broader range of molecules produced by microbes as well as non-infectious substances. The adaptive immune response is further categorized into two groups: humoural immune responses and cell-mediated immune responses. In humoural immune responses, B cells produce proteins called antibodies to fight pathogens. In contrast, in cell-mediated immune responses, as the name states, the cells themselves are the ones that fight the pathogens or malignant cells (Abbas, Abul K, Lichtman, Andrew H. and Pillai, 2015).

The immune system has the capacity to recognise and eradicate

cancerous and/or precancerous cells on the basis of their expression of tumour-specific antigens or molecules induced by cellular stress (a process known as immune surveillance). However, despite the immune surveillance, tumours manage to develop in the presence of a functioning immune system. This observation combined with recent findings led to the generation of the updated concept of tumour immunoediting. Tumour immunoediting is a dynamic process composed of 3 phases: elimination, equilibrium, and escape (Figure 1.1). The first phase (i.e. elimination) is the same process of immune surveillance described before, in which the immune system identifies and eradicates the developing tumour and protects the host from tumour formation. This phase can be complete (when all of the tumour cells are cleared) or incomplete (when a portion of the tumour cells remain). If the elimination phase is incomplete, the remaining tumour cells may enter the equilibrium phase, where they are either maintained in a dormant state or they continue to evolve to “escape” the tumour control enforced by the immune system. During this phase the immune system exerts a selective pressure by eliminating the susceptible tumour clones. Hence, if the immune system is not able to completely eliminate the tumour cells during this phase, the tumour clones that are the fittest to resist, avoid, or supress the anti-tumour immune response will be the ones to survive and escape. During the escape phase the tumour clones that were able to surpass the immunological restraints of the equilibrium phase finally grow unimpeded and this results in a progressively growing tumour (Dunn, Old, & Schreiber, 2004; Swann & Smyth, 2007).

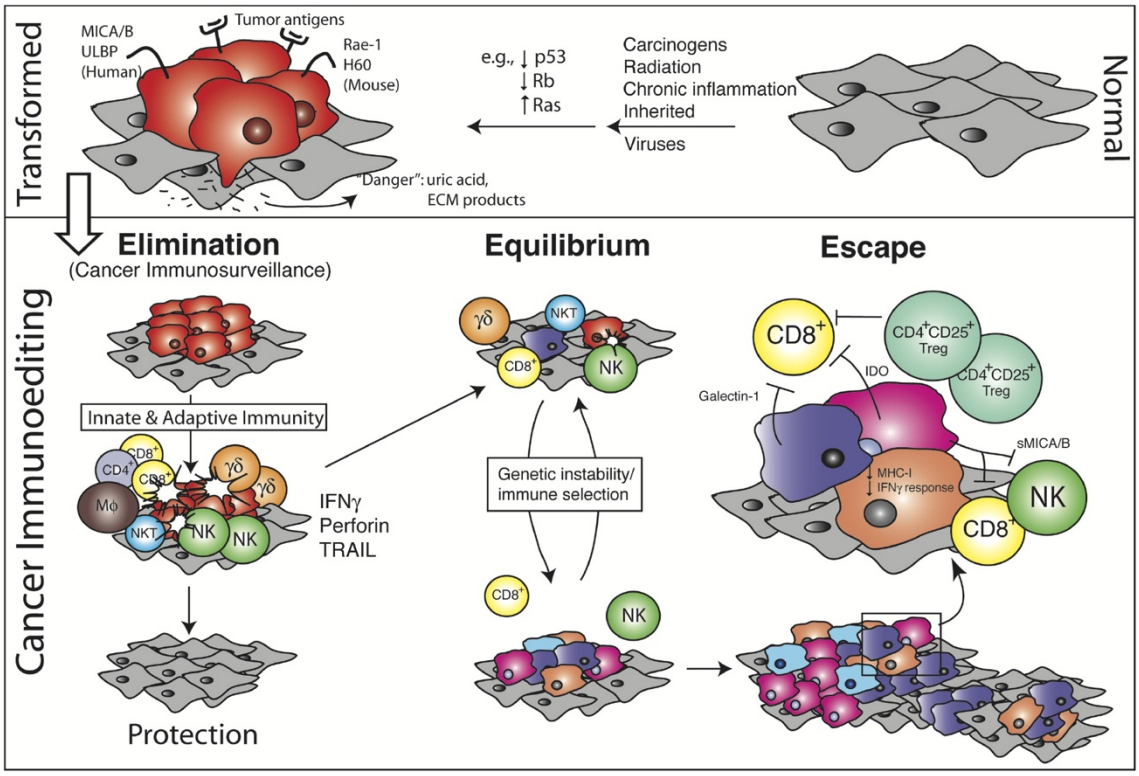

Figure 1.1. The three phases of the cancer immunoediting process. Normal cells (grey) can become tumour cells (red) (top). At the early stages of tumourigenesis, these cells may express tumour-specific antigens or molecules induced by cellular stress that initiate the cancer immunoediting process (bottom) (Dunn et al., 2004).

As part of the equilibrium and escape phases of the immunoediting process, tumour cells can evade being eliminated by the immune system by numerous mechanisms, such as:

- Low immunogenicity: Spontaneous tumours may not have mutations that generate tumour-specific antigens, instead expressing self-antigens to which T cells have been centrally tolerised. Furthermore, tumour cells can downregulate or lose MHC class I expression as a further means to escape the immune response (Algarra, García-Lora, Cabrera, Ruiz-Cabello, & Garrido, 2004).
- Tumour treated as self-antigen: When tumour-specific antigens are presented by antigen-presenting cells (APCs) without co-stimulation (signal 2) it induces tolerance in the T cells instead of activation.
- Antigenic modulation: Tumour cells can initially display antigens that the immune system can respond to and hence these tumour cells may be eliminated during the elimination or equilibrium phase of the tumour

immunoediting process. The remaining tumour cells that lack immunogenic antigens will then expand during the equilibrium phase. This modulation is driven by the selective pressure exerted by the immune system and by the genomic instability of the tumour (Dunn et al., 2004).

- Tumour-induced immune suppression: Tumour cells are also able to evade an immune response by producing an immunosuppressive microenvironment. In this regard, tumours can produce immunosuppressive cytokines such as transforming growth factor-β (TGF-β) and interleukin 10 (IL-10). Furthermore, the tumour cells can also recruit regulatory T cells (Treg), which can inhibit the function of cytotoxic $CD8^+$ T cells and $CD4^+$ effector T cells. Moreover, the microenvironment of some tumours can contain populations of myeloid-derived suppressor cells (MDSCs), which can inhibit T cell activation inside the tumour. Finally, some tumours express cell-surface ligands for different immune checkpoints (such as PD-L1), which directly inhibit immune responses (Murphy, Weaver, Mowat, Berg, & Chaplin, 2017).
- Tumour-induced privileged site: Tumour cells can produce and secrete molecules such as collagen that create a physical barrier around the tumour that prevents the infiltration of immune cells.

1.1.1. Cell-Mediated Immune Responses

The principal immune mechanism of tumour elimination is the killing of tumour cells by cell-mediated immune responses. This type of immune response is performed by T cells and requires an antigen-presenting cell (APC) that will capture antigens and display them for the T lymphocyte to recognise. APCs are able to display endogenous and exogenous peptides in the context of major histocompatibility complex (MHC) molecules. The MHC molecules are membrane proteins on APCs that are in charge of binding and displaying peptides derived from protein antigens. Internal peptides are usually loaded and presented on MHC class I whilst extracellular antigens phagocytosed by specialized APCs are processed in specialized intracellular compartments,

bound and presented via MHC class II.

APCs can be divided into two categories: professional and amateur. Professional APCs such as dendritic cells, macrophages, B cells, and monocytes, are cells that are dedicated to antigen presentation as an essential part of their role in the generation of the immune response. Amateur APCs such as endothelial cells, tumour cells, fibroblasts, glial cells, keratinocytes, and even T cells, are cells that have the ability to present antigens under select conditions. In this regard, it has been shown that T cell-T cell interactions can induce T cell activation, proliferation, and differentiation of both $CD4^+$ and $CD8^+$ T cells (Gérard et al., 2013; Ramming, Thümmler, Schulze-Koops, & Skapenko, 2009; Taams, Eden, & Wauben, 1999).

A subset of classical dendritic cells can ingest infected host cells, microbes, dead tumour cells, and microbial and tumour antigens. Then they transport these ingested antigens into the cytosol, where they enter the MHC class I pathway. This process is called cross-presentation (or cross-priming), to indicate that one type of cell (i.e. dendritic cells) can present the antigens of other (infected or dying) cells and prime naïve T cells specific for these antigens (Figure 1.2) (Abbas, Abul K, Lichtman, Andrew H. and Pillai, 2015).

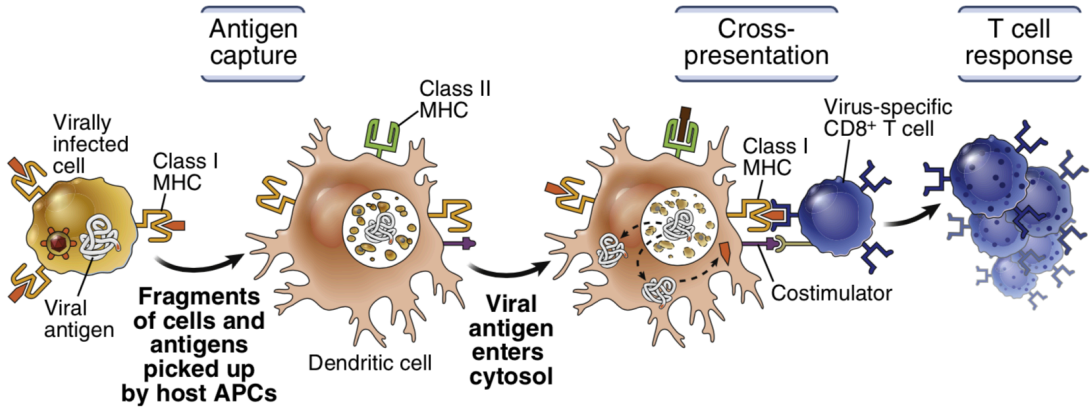

Figure 1.2. Class I MHC-restricted cross-presentation by dendritic cells. Fragments of cells infected with intracellular microbes or antigens produced in these cells are ingested by dendritic cells, and the antigens of the infectious microbes are broken down and presented in association with class I MHC molecules of the antigen-presenting cells (APCs). T cells recognize the microbial antigens expressed on the APCs, and the T cells are activated (Abbas, Abul K, Lichtman, Andrew H. and Pillai, 2015).

The class I MHC pathway begins with the processing of proteins that are in the cytosol of any nucleated cell (Figure 1.3A). Within the cell, protein

complexes called proteasomes carry out the digestion of proteins into peptides. Afterwards the peptides are transported from the cytosol into the endoplasmic reticulum (ER) in order to form peptide/MHC class I complexes. When a peptide/MHC class I complex is formed, it is transported to the cell surface and presented to $CD8^+$ T cells. After recognising the peptide/MHC complex via their T cell receptor (TCR), $CD8^+$ T cells then differentiate into cytotoxic T lymphocytes (CTLs) able to kill the cells producing the antigens (Abbas, Abul K, Lichtman, Andrew H. and Pillai, 2015).

The class II MHC pathway starts with the internalisation of extracellular antigens by specialized APCs (Figure 1.3B). After internalisation, the antigenic proteins are digested into peptides in intracellular vesicles called endosomes or phagosomes, which may fuse with lysosomes. MHC class II molecules are targeted from the ER (where they are synthesized) to the late endosomal/lysosomal vesicles that contain the digested peptides. Once the peptide/MHC class II complexes are formed in these vesicles, they are exported to the cell surface and presented to $CD4^+$ T cells. These T lymphocytes then differentiate into effector T cells that produce cytokines that help CD8+ T cell responses as well as helping B lymphocytes generate antibodies and help phagocytes eradicate ingested microbes. In addition to $CD4^+$ helper T cells, there is a subset of $CD4^+$ T cells, named regulatory T cells, that develop on recognition of self-antigens and that limit immune responses (Abbas, Abul K, Lichtman, Andrew H. and Pillai, 2015; Murphy et al., 2017).

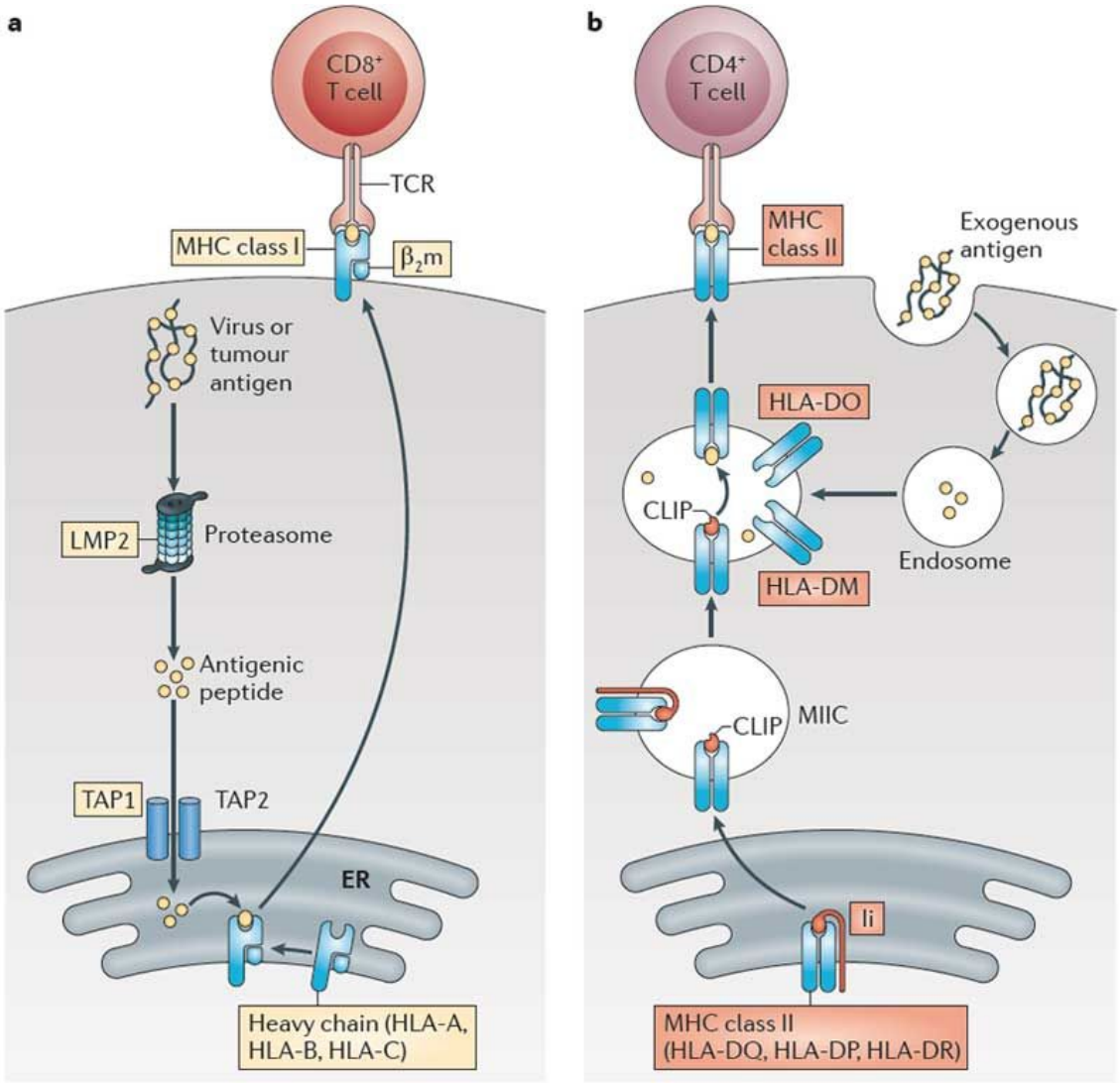

Figure 1.3. The MHC class I and MHC class II antigen-presentation pathways. (A) MHC class I antigen presentation pathway. **(B)** MHC class II antigen presentation pathway. MIIC, MHC class II compartment; TAP, transporter associated with antigen processing; TCR, T cell receptor; ER, endoplasmic reticulum; CLIP, class II-associated invariant chain peptide; Ii, MHC class II-associated invariant chain (Kobayashi & Van Den Elsen, 2012).

1.1.2. Molecular Mechanisms of T cell Co-Stimulation and Co-Inhibition

For a naïve T cell to be activated, in addition to the specificity signal provided by peptide/MHC-TCR interactions (signal 1), a second signal, also known as co-stimulatory signal, needs to be provided by the APC. These two signals then drive the expansion and differentiation of antigen-specific T cells. This classical two-signal model (P. A. Bretscher, 1999; P. Bretscher & Cohn, 1970) was depicted with the identification of the co-stimulatory receptor CD28 and its ligand, B7-1 (June, Ledbetter, Gillespie, Lindsten, & Thompson, 1987;

Linsley, Clark, & Ledbetter, 1990). However, with the identification of cytotoxic T lymphocyte antigen 4 (CTLA4) (a co-inhibitory receptor that also binds to B7-1) and of a second ligand (B7-2), which binds to both CD28 and CTLA4, the two-signal model evolved into a more complex regulatory system (Azuma et al., 1993; Linsley et al., 1991). Hence, it was discovered that in addition to the co-stimulatory receptors, T cells also express co-inhibitory receptors on their surface which negatively regulate T cell function upon interaction with co-inhibitory ligands on APCs, normal and transformed tissue.

The collection of co-stimulatory and co-inhibitory receptors expressed on T cells is highly adaptable and responsive to changes in the tissue microenvironment. Hence, the ligands that are expressed on the surface of the cells that interact with the T cells will determine the signals that are received from the co-stimulatory and co-inhibitory receptors. These co-stimulatory and co-inhibitory ligands have been identified on many different cell types, but their expression has been described in the most detail on professional APCs (Liechtenstein, Dufait, Lanna, Breckpot, & Escors, 2012).

Hence, T cell-mediated immune responses are firmly regulated by an array of mechanisms that vary from central tolerance by negative selection in the thymus to the modulation of T cell activation in the periphery via the interplay of signal 1 and co-activatory and co–inhibitory receptors. This interplay between positive and negative signals into T cells in addition to the inflammatory microenvironment surrounding T cell priming help determine the activation, function, and longevity of effector, memory, and regulatory T cell responses (Schildberg, Klein, Freeman, & Sharpe, 2016). Furthermore, it is now known that co-inhibitory or immune checkpoint receptors play a crucial part in the preservation of immune homeostasis. Given that APCs and normal tissue upregulate the co-inhibitory ligands upon inflammatory stimuli to help dampen and negatively control the immune response, the expression of co-inhibitory receptors on effector T cells guarantees the proper ceasing of effector T cell responses and their expression on regulatory T cells ensures the proper function of them to control effector T cells.

The co-stimulatory and co-inhibitory molecules are divided into two major superfamilies: the immunoglobulin (Ig) superfamily (IgSF) and tumour necrosis factor (TNF) receptor superfamily (TNFRSF). On the basis of their primary amino

acid sequence, protein structure and function, these molecules can be further subcategorized into specific families like the B7-CD28, TIM, CD226-TIGIT-CD96 families, among others (Chen & Flies, 2013).

1.1.3. Co-Inhibitory Receptors and their Signalling Pathways

1.1.3.1. CTLA4

Cytotoxic T lymphocyte-associated antigen 4 (CTLA4, CD152) is an inhibitory receptor member of the IgSF and of the B7-CD28 family. It consists of an extracellular IgV-like domain comprising the B7 binding motif (MYPPPY), a stalk comprising a cysteine that mediates homodimerization, a transmembrane domain, and a cytoplasmic tail (Brunet et al., 1987). CTLA4 is a CD28 homologue and because of this it binds to the same ligands as this co-stimulatory receptor. However, CTLA4 has 10 times higher affinity to B7-1 (CD80) and B7-2 (CD86) than CD28. Hence, CTLA4 competes with CD28 for the binding of ligands and in that way prevents CD28-mediated T cell activation (Greene et al., 1996) (Figure 1.4). In addition, it has been shown that CTLA4 can capture its ligands (i.e. CD80 and CD86) from opposing cells by a process of trans-endocytosis. After removal, these costimulatory ligands are degraded inside CTLA4–expressing cells, resulting in impaired co-stimulation via CD28 (Qureshi et al., 2011).

Mouse models have provided evidence of the checkpoint function of CTLA4 in controlling T cell activation. It was shown that $Ctla4^{-/-}$ mice rapidly developed lymphoproliferative disease with multiorgan lymphocytic infiltration and tissue destruction, dying at around 3-4 weeks of age (Tivol et al., 1995; Waterhouse et al., 1995).

CTLA4 is mainly expressed by T cells, however its expression has also been reported in B cells, dendritic cells, fibroblasts, and embryonic cells, among others. Regulatory T cells (Treg) constitutively express high levels of CTLA4, while naïve T cells upregulate CTLA4 only after activation, reaching the maximum level 2-3 days post activation *in vitro* with anti-CD3 (Walunas et al., 1994). After T cell activation, CTLA4 is translocated to the membrane and it is there where it competes with CD28 for the binding of their ligands expressed on APCs.

Foxp3 and NFAT regulate CTLA4 expression transcriptionally, and the 3' UTR of CTLA4 and microRNAs (miR-145 and miR-155) regulate CTLA4

expression post-transcriptionally. Furthermore, the tyrosine phosphorylation status of CTLA4 cytoplasmic domain controls the localization of CTLA4 protein within T cells. The majority of CTLA4 molecules are located in intracellular vesicles, hence there is a regular cycle of CTLA4 trafficking to the cell surface, followed by swift internalisation of CTLA4 with unphosphorylated cytoplasmic domains and either the recycling of it to the plasma membrane or the degradation of it in lysosomes (Schneider et al., 1999).

Despite many efforts, little is known about the intracellular signalling pathways initiated upon CTLA4 binding by its ligands and there are still many unresolved mechanistic questions about how CTLA4 exerts its inhibitory effects. However, it has been shown that the cytoplasmic domain of CTLA4 can associate with members of the PP2A family of serine/threonine phosphatases, which might inhibit signalling downstream (Figure 1.4) (Chuang et al., 2000).

1.1.3.2. PD1

Programmed cell death 1 (PD1, CD279) is a cell surface molecule member of the IgSF. PD1 consists of an N-terminal IgV-like domain, a stalk, a transmembrane domain, and a cytoplasmic domain that contains an immunoreceptor tyrosine-based inhibitory motif (ITIM) and an immunoreceptor tyrosine-based switch motif (ITSM) (Ishida, Agata, Shibahara, & Honjo, 1992; Shinohara, Taniwaki, Ishida, Kawaichi, & Honjo, 1994; Zak et al., 2015). There are four splice variants of PD1 expressed in human PBMCs and the expression of all of them can be induced by *in vitro* stimulation of T cells with anti-CD3 and anti-CD28 (C. Nielsen, Ohm-Laursen, Barington, Husby, & Lillevang, 2005).

Transgenic mouse models have provided evidence that suggested that PD1 is involved in the maintenance of peripheral self-tolerance by serving as a negative regulator of immune responses. In this regard, it has been shown that aged C57BL/6 $PD1^{-/-}$ congenic mice spontaneously develop lupus-like proliferative arthritis and glomerulonephritis, whilst 2C-TCR $PD1^{-/-}$ transgenic mice develop a chronic and systemic graft-versus-host-like disease (Nishimura, Nose, Hiai, Minato, & Honjo, 1999). It has also been shown that PD1 deficiency accelerates the onset and frequency of type I diabetes in NOD (non-obese diabetic) mice (Jian Wang et al., 2005). Furthermore, $CD4^+$ and $CD8^+$ T cell

responses were markedly enhanced in a PD-L1$^{-/-}$ mice model compared with wild-type mice both *in vitro* and *in vivo*, showing that PD-L1 on T cells, APCs, and host tissue inhibits naïve and effector T cell responses and plays a critical role in T cell tolerance (Latchman et al., 2004).

PD1 expression on T cells can be induced by TCR signalling (Agata et al., 1996) and by cytokines (common γ chain cytokines IL-2, IL-7, IL-15, IL-21 and type I IFNs) (Kinter et al., 2008; Terawaki et al., 2011). The expression of this molecule is high on activated T cells, B cells, NK cells, NKT cells, macrophages and some DC subsets. Furthermore, PD1 can be found on the surface of naïve T cells 24 hours after activation but this expression is transient, decreasing following loss of TCR stimulation. PD1 signalling is initiated by binding to one of its ligands (PD-L1 or PD-L2) and the subsequent phosphorylation of PD1 ITIM and ITSM tyrosine motifs. This phosphorylation leads to the recruitment of SH2-domain containing protein tyrosine phosphatases (SHP-1 and/or SHP-2) to the ITSM cytoplasmic region of PD1, which inhibits downstream signals of TCR (or BCR) through dephosphorylation of signalling intermediates (Figure 1.4) (Chemnitz, Parry, Nichols, June, & Riley, 2004; Okazaki, Maeda, Nishimura, Kurosaki, & Honjo, 2001; Sheppard et al., 2004).

The binding of PD-L1 or PD-L2 to PD1 inhibits two important pathways; it inhibits the PI3K-Akt signalling by inhibiting PI3K activation and it also inhibits the Ras-MEK-ERK signalling possibly by SHP-2 dephosphorylation of PLCγ1. In turn, the inhibition of these two pathways inhibits cell cycle progression (Figure 1.4) (Patsoukis et al., 2012; Patsoukis, Li, Sari, Petkova, & Boussiotis, 2013).

PD1 also modulates T cell effector function further downstream by diminishing the expression of cytokines and transcription factors connected with effector cell function (such as GATA-3, Tbet, and Eomes) (Nurieva et al., 2006). Hence, PD1 signalling can modify T cells in different ways that operate jointly to inhibit immune responses.

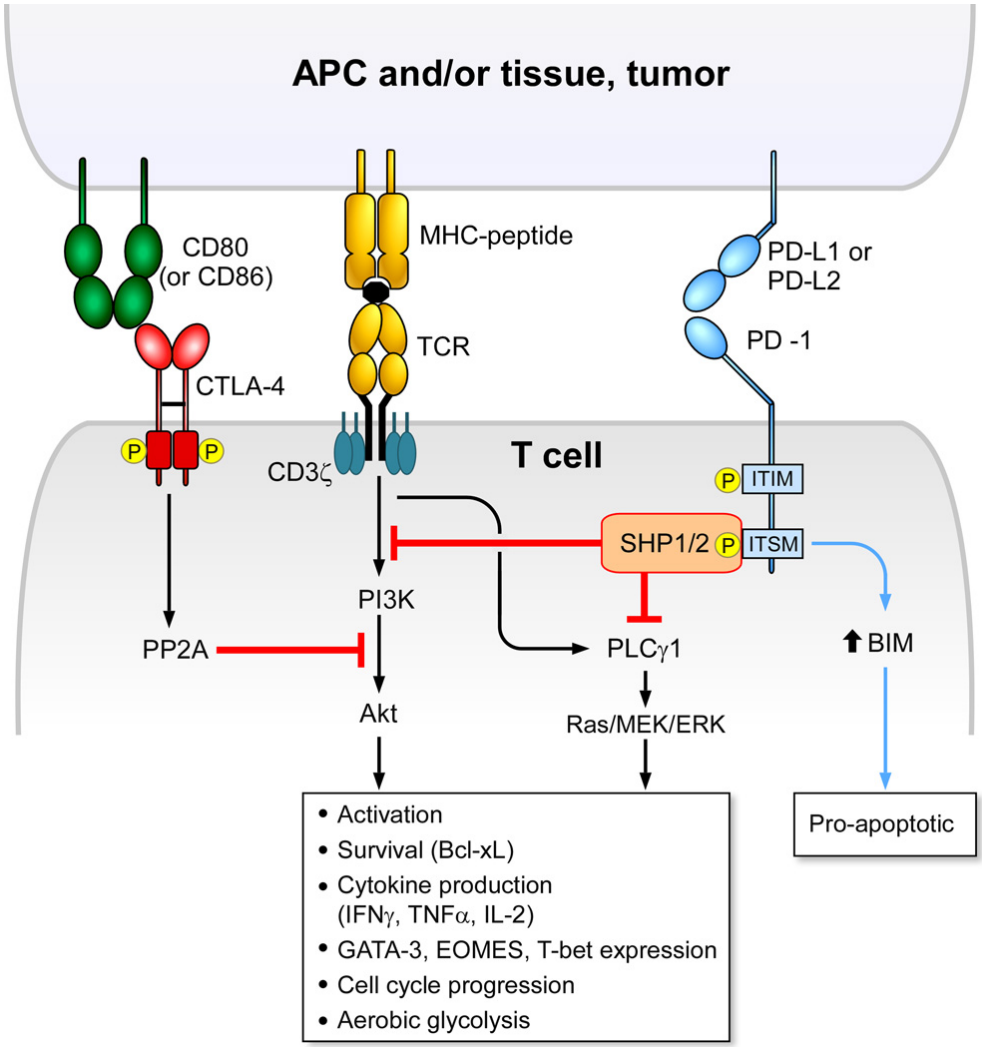

Figure 1.4. Comparison of intracellular signalling by CTLA4 and PD1. PD1 and CTLA4 both inhibit Akt activation, but they target different signalling molecules (Schildberg et al., 2016).

1.1.3.3. TIM3

T cell immunoglobulin 3 (TIM3, CD366) is a cell surface molecule member of the IgSF and of the TIM family. TIM3 consists of a single IgV domain, a mucin domain, a stalk, and a cytoplasmic tail comprising a tyrosine-based signalling motif (Cao et al., 2007; Santiago et al., 2007). TIM3 expression has been identified on activated $CD4^+$ and $CD8^+$ T cells, regulatory T cells, and on innate immune cells (DCs, NK cells, and monocytes). TIM3 expression can be upregulated in an inflammatory environment rich in cytokines (IL-2, IL-7, IL-15, IL-21) independently of TCR stimulation.

Several ligands for TIM3 have been identified, some of which primarily have a role in innate immune cells, like phosphatidyl serine (PtdSer) and high mobility group box 1 (HMGB1). At the moment, there are only two other ligands

for TIM3 that have been identified and that directly impact T cell responses; these are galectin-9 (Gal-9) and carcinoembryonic antigen cell adhesion molecule 1 (CEACAM1) (Figure 1.5). Galectin-9 is a C-type lectin and TIM3 can bind to it via its two carbohydrate recognition domains. This binding is crucial for inducing cell death of antigen specific $CD4^+$ and $CD8^+$ T cells (Sehrawat et al., 2010; Zhu et al., 2005). CEACAM1 has been shown to co-express with TIM3 on $CD4^+$ T cells upon tolerance induction and with $CD8^+$ TILs that show the exhausted phenotype. Importantly, the regulatory function of TIM3 is defective in the absence of CEACAM1, indicating a need for the interaction between CEACAM1 and TIM3 for the proper function of TIM3 (Y. H. Huang et al., 2015).

To date, the signalling pathway downstream of TIM3 has not been completely elucidated. However, it is known that HLA-B associated transcript 3 (Bat3) is bound to TIM3 when there is no ligand-mediated TIM3 signalling, and that it blocks SH2 domain-binding sites in the TIM3 tail. Binding of galectin-9 and/or CEACAM1 to TIM3 leads to the phosphorylation of two tyrosine residues of the cytoplasmic tail of TIM3 and to the release of Bat3 from the TIM3 tail. This allows the binding of SH2 domain-containing Src kinases and the successive regulation of TCR signalling. Moreover, it is known that both CEACAM1-L and TIM3 can engage SHP-1/SHP-2 phosphatases, respectively, at the immune synapse leading to the suppression of the TCR signalling (Y. H. Huang et al., 2015; Rangachari et al., 2012).

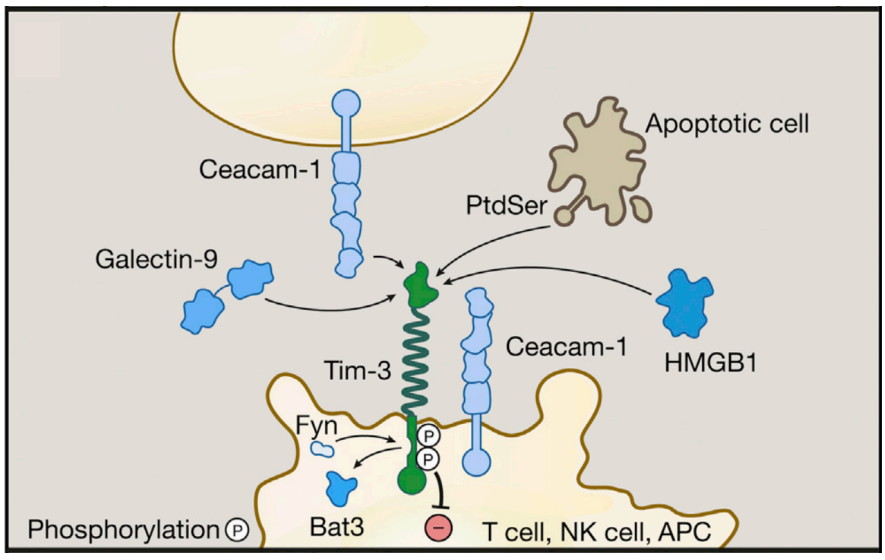

Figure 1.5. The TIM3 pathway. TIM3 ligands include soluble ligands (galectin-9 and HMGB1) and cell surface ligands (Ceacam-1 and Phosphatidyl serine [PtdSer]). Bat-3 and Fyn bind to the same region on the cytoplasmic tail of TIM3. Ligand binding triggers the dissociation of Bat-3 from

the cytoplasmic tail of TIM3, thus allowing Fyn to bind and promote the inhibitory function of TIM3 (Anderson, Joller, & Kuchroo, 2016).

1.1.3.4. LAG3

Lymphocyte activation gene 3 (LAG3, CD223) is a membrane protein belonging to the IgSF. LAG3 structure resembles the CD4 co-receptor, and even though both LAG3 and CD4 bind to MHC class II, LAG3 does it with a higher affinity (Huard, Prigent, Tournier, Bruniquel, & Triebel, 1995).

LAG3 expression is upregulated in activated T and NK cells. The level of LAG3 expression is particularly high in activated regulatory T cells and in $CD8^+$ T cells that present the exhausted phenotype (C. T. Huang et al., 2004; Wherry et al., 2007). In view of LAG3 having an effect on $CD8^+$ T cells and NK cells, neither of which interact with MHC class II, the existence of other ligands for LAG3 has been hypothesised. To this effect, it has been suggested that another ligand for LAG3 is LSECtin, a member of the DC-SIGN family of molecules (Xu et al., 2014).

LAG3 is associated with the stimulation of Treg cell-mediated suppression and with the inhibition of effector T cells; however, it is still not known how LAG3 signals in these different T cell subsets to accomplish its inhibitory effects. To date, most of what we know about LAG3 signalling is that it associates with TCR/CD3 complexes on effector T cells and that crosslinking of LAG3 together with CD3 prevents T cell proliferation, calcium flux and cytokine production (Hannier, Tournier, Bismuth, & Triebel, 1998). It has also been established that the inhibitory function of LAG3 on effector T cells requires the conserved KIEELE motif in the cytoplasmic tail of this co-receptor; however, the proteins that bind to this motif have not been identified (Figure 1.6). Furthermore, it is not known if this motif is necessary for the effects of LAG3 on Treg cells (Workman, Dugger, & Vignali, 2002).

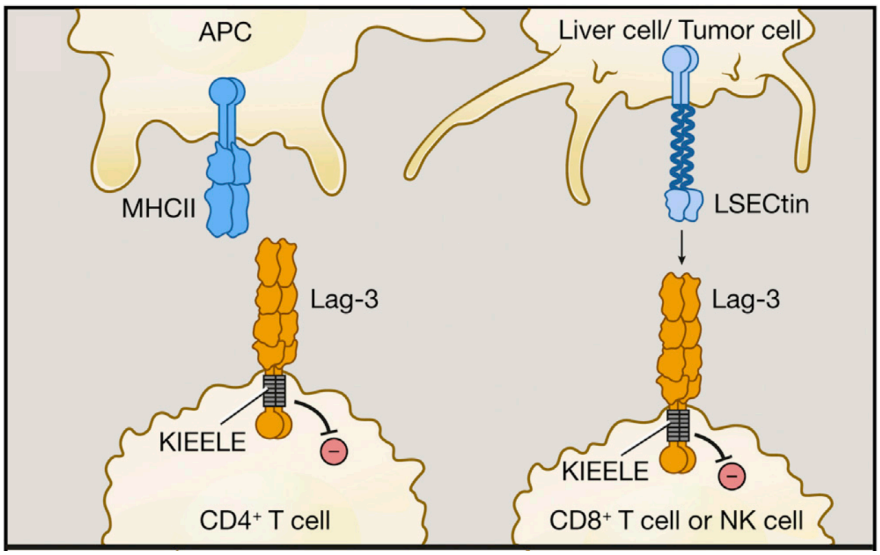

Figure 1.6. The LAG3 pathway. Left: LAG3 is expressed on $CD4^+$ T cells and binds to MHC class II on antigen-presenting cells. Right: LAG3 is expressed on $CD8^+$ T cells and NK cells and binds to L-SECtin on tumour cells or liver cells. The cytoplasmic tail of LAG3 contains a unique KIEELE motif that is essential for its inhibitory function (Anderson et al., 2016).

1.1.3.5. TIGIT

T cell immunoreceptor with Ig and ITIM domains (TIGIT) is a protein of the IgSF. It is formed of an extracellular IgV domain, a transmembrane region and a cytoplasmic tail containing an ITIM and an immunoglobulin tail tyrosine (ITT)-like motif. TIGIT is expressed on Tregs (resting and activated), $CD8^+$ and $CD4^+$ effectors, NK cells, follicular T helper (Tfh) cells, and memory cells (Boles et al., 2009; Levin et al., 2011; Stanietsky et al., 2009; Yu et al., 2009).

TIGIT binds to two ligands with high affinity, CD155 (poliovirus receptor (PVR), NECL5) and CD112 (PVRL2, NECTIN-2), and with lower affinity to CD113 (PVRL3, NECTIN-3). Because they bind to the same ligands, TIGIT forms a pathway with CD226 (DNAM-1) and CD96 (Tactile) where CD226 works as a co-stimulatory receptor and CD96 and TIGIT work as co-inhibitory ones. Binding of TIGIT to CD155 induces the phosphorylation of its cytoplasmic tail in either the ITIM motif or the ITT-like motif and the recruitment of SH2 domain-containing inositol-5-phosphatase 1 (SHIP-1). The recruitment of SHIP-1 blocks signal transduction through the phosphoinositide 3-kinase (PI3K) pathway and the mitogen-activated protein kinase (MAPK) pathway, and it also limits nuclear factor-κB (NF-κB) signalling. This in turn reduces NK cytotoxicity, granule polarization and cytokine secretion in NK cells (M. Li et al., 2014; S. Liu et al.,

2013; Stanietsky et al., 2009). Furthermore, elements of the TCR complex as well as key regulators of the TCR signalling cascade are downregulated when TIGIT is engaged. This causes the blocking of T cell activation, proliferation and acquisition of effector functions. However, although TIGIT engagement inhibits T cell activation, it also assists in their maintenance by inducing anti-apoptotic molecules as well as upregulating the receptors for IL-2, IL-7, and IL-15, which promote T cell survival (Joller et al., 2011; Levin et al., 2011).

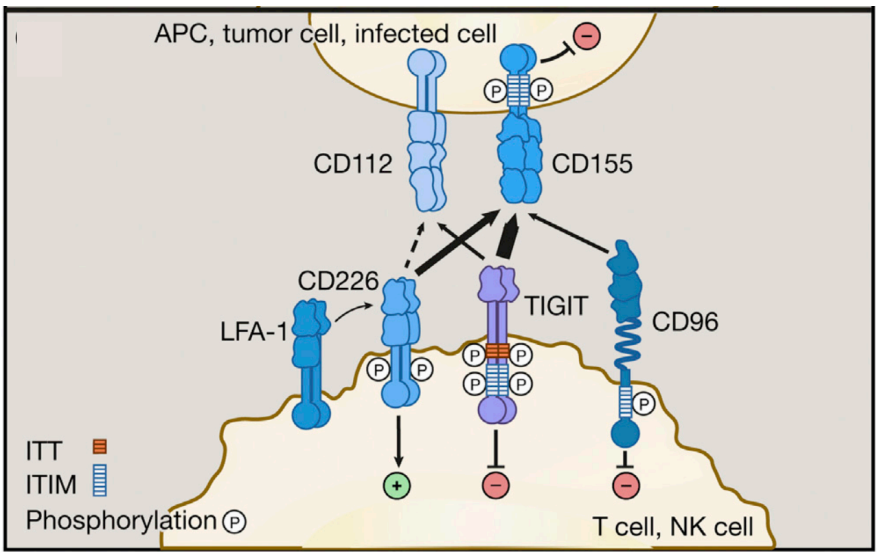

Figure 1.7. The CD226/TIGIT pathway. CD226, TIGIT, and CD96 are expressed on T cells and NK cells and share the ligands CD112 and CD155, which are expressed on APCs and other cells such as tumour cells. CD226 associates with the integrin LFA-1 and delivers a positive signal. TIGIT, CD96, and CD155 contain ITIM motifs in their cytoplasmic tails and can deliver inhibitory signals. TIGIT further contains an ITT-like motif (Anderson et al., 2016).

1.2. Immunotherapy

1.2.1. Immune Checkpoint Blockade

In the last two decades the field of immunotherapy has experienced a great expansion of knowledge that has led to new possibilities for development of immunotherapies for the treatment of cancer. In this regard, the blockade of immune checkpoints has been shown to be a very promising approach to activate therapeutic anti-tumour immunity. This is due to the fact that tumours co-opt immune-checkpoint pathways as a way of misleading the immune system into stopping the immune response against them.

Immune checkpoint inhibitors are antibodies that block either co-inhibitory receptors expressed on the surface of lymphocytes or their ligands in order to enhance anti-tumour activity. In 1996, preclinical data demonstrated that blocking one of these co-inhibitory receptors (CTLA4) with monoclonal antibodies promoted the rejection of established mouse tumours (Leach, Krummel, & Allison, 1996). Furthermore, in the early 2000's there were two publications that demonstrated that another one of these co-inhibitory receptors (PD1) was essential to anti-tumour immunity (H. Dong et al., 2002; Freeman et al., 2000). In 2011, US Food and Drug Administration (FDA) approval was given for Ipilimumab (a CTLA4 antibody), the first of this class of immunotherapeutics (Pardoll, 2012). Just a few years later, FDA approval was given for yet another one of these checkpoint inhibitors: Pembrolizumab, an antibody blocking the PD1/PD-L1 interaction. Both of these immune checkpoint inhibitors have shown remarkable success in the clinic, and combination therapy with the two of them was shown to have impressive clinical efficacy in advance-stage malignant melanoma (Wolchok et al., 2013). Since then, a plethora of agents targeting immune checkpoints are being tested in clinical trials (Smyth, Ngiow, Ribas, & Teng, 2016).

Even though these FDA-approved immune checkpoint inhibitors have shown clinically significant anti-tumour responses, they have also been associated with a unique set of toxicities called immune-related adverse events (irAEs). These toxicities are very different from toxicities observed with conventional chemotherapy. The most common reported irAEs are dermatologic toxicity, diarrhea/colitis, hepatotoxicity, and endocrinopathies. These irAEs can be reversed as long as they are recognised and treated (usually with immunosuppression) early, however, if left unattended they can lead to severe toxicity or even death (Villadolid & Amin, 2015).

Because of the toxicity that these immune checkpoint inhibitors present, as well as the fact that they are limited to tumours that exhibit endogenous population of tumour-reactive T cells at sufficient frequencies, other approaches targeting the immune system are continuously being explored, such as adoptive cell therapy with lymphocytes.

1.2.2. Adoptive Cell Therapy

1.2.2.1. Tumour Infiltrating Lymphocytes

Before the targeting of immune checkpoints with monoclonal antibodies, the first evidence that tumour regression could be promoted by manipulation of the host immune system was supplied by the successful trials of metastatic melanoma and renal cell cancer patients treated with interleukin-2 (IL-2) (Fisher, Rosenberg, & Fyfe, 2000; Smith et al., 2008). This stimulation of the complete lymphocyte repertoire generated durable results in a small fraction of patients. Additionally, studies in mice had shown that lymphokine-activated killer (LAK) cells could mediate tumour regression (Ettinghausen & Rosenberg, 1986), and this promoted the generation of a randomized human clinical trial comparing treatment with IL-2 alone or in conjunction with LAK cells. The results from this trial showed no difference in response rate between the two conditions (Rosenberg et al., 1993), demonstrating that the anti-tumour effects were due to IL-2 alone. Nevertheless, tumour infiltrating lymphocytes (TILs) were shown to be 50 to 100 times more effective in their therapeutic potency than LAK cells in murine models of metastatic melanoma (Rosenberg, Spiess, & Lafreniere, 1986), and hence were hypothesised to be a better starting population for adoptive cellular therapies.

Adoptive cell therapy (ACT) with tumour infiltrating lymphocytes (TILs) requires the selection and expansion of autologous T cells that have anti-tumour activity. The process for the *ex vivo* expansion of TILs for ACT will be reviewed in more detail in Chapter 4. Briefly, these TILs are produced by the processing of freshly resected tumour followed by culture in media supplemented with high-dose IL-2. The TILs then undergo a rapid expansion to achieve the quantity needed for infusion. The current method for adoptive cellular therapy with autologous TILs consists of nonmyeloablative preparative chemotherapy (cyclophosphamide and fludarabine), passive transfer of cells (generally 3–10 × 10^{10} in a one-time infusion), and post-transfer support with high-dose IL-2 (Goff et al., 2016). The use of this method in patients with metastatic melanoma has consistently reported objective response rates of 40%–50% (including complete tumour regression in 10%–20% of treated patients) (Besser et al., 2013; Goff et al., 2016; Pilon-Thomas et al., 2012; Rosenberg et al., 2011).

1.2.2.2. Neoantigens

Effective cancer immunotherapy is based on the recognition and attack of tumour-antigens by the host's adaptive immune system. Until recently, identification of these antigens had been limited to self-antigens that possess an aberrant expression in cancer, such as overexpressed or tumour differentiation antigens. Tumour-antigens that are expressed exclusively in the tumour cells (i.e. neoantigens) had been ignored as these mutations are patient specific and rare. However, the recent availability of whole exome sequencing of tumour DNA has allowed the identification of the somatic mutations in cancer cells that generate these neoantigens.

Neoantigens can be categorised into two groups: clonal and subclonal. Clonal neoantigens derive from somatic mutations that accumulated at the beginning of the transformation of a normal cell into a cancerous one and hence are carried by all the tumour cells (McGranahan et al., 2016). Subclonal neoantigens derive from secondary mutations that appeared later and hence will be present only in a portion of the tumour cells. The clonality of a neoantigen is important when designing immunotherapies, as the most efficient therapies will be the ones that target clonal neoantigens. Immunotherapies that target subclonal neoantigens may result in immunoediting, as the elimination phase would be incomplete given that only a portion of the tumour cells would be targeted.

Neoantigens are highly attractive antigens for immune interventions across the spectrum of solid and hematologic malignancies, as therapies that target neoantigens have possible advantages over those that target self-antigens that are aberrantly expressed in cancer. First, T cell responses against neoantigens should not lead to autoimmunity as the antigens are only present in the tumour cells. Second, T cells that recognise neoantigens are not exposed to central tolerance, and therefore should express higher-affinity T cell receptors (TCRs) compared to those that recognise self-antigens (Heemskerk, Kvistborg, & Schumacher, 2013). Furthermore, recent data suggests that neoantigens are critical targets for effective anti-tumour T cell responses, with many studies showing that the greatest clinical activity of checkpoint inhibitors targeting CTLA4

and PD1 happens against cancer types that have the greatest average number of somatic mutations (Rizvi et al., 2015; Snyder et al., 2014; Van Allen et al., 2015). Even within cancer type, patients whose tumours had a relatively high mutation load were more likely to benefit from checkpoint-blockade therapy than those with a lower mutation burden (McGranahan et al., 2016; Snyder et al., 2014). These correlations suggest that specific targeting of cancer neoantigens can result in tumour regression. To directly demonstrate that this is the case, adoptive cellular therapies that consist in their entirety of neoantigen-reactive T cells would be needed. The methods for the detection and selective expansion of neoantigen-reactive T cells will be reviewed in more detail in Chapter 4.

1.2.2.3. Chimeric Antigen Receptor T Cell

Chimeric antigen receptor (CAR) T cell therapy consists of the adoptive transfer of autologous T cells that have been genetically engineered to express a synthetic receptor that recognises a specific antigen expressed on malignant cells (i.e. tumour-associated antigen (TAA)). These engineered T cells combine the effector functions of T cells with the ability of antibodies to recognise surface antigens in a non-MHC restricted way.

CARs are usually formed by a binding domain (single chain antibody fragment, scFv), a transmembrane domain, and one or more intracellular signalling domains that mediate T cell activation. The first generation of CARs consisted of an scFv linked to the CD3ζ intracellular signalling domain of the TCR (Irving & Weiss, 1991), while the second generation of chimeric receptors also incorporated a co-stimulatory endodomain (i.e. 4-1BB/CD3ζ, CD28/CD3ζ, or OX40/CD3ζ). The addition of these co-stimulatory domains considerably improved T cell proliferation and persistence. To further optimise T cell efficacy, studies with third generation of CARs containing multiple co-stimulatory signalling modules are underway (Abate-Daga & Davila, 2016).

The key advantage of using CAR T cell therapies is that the scFv is derived from an antibody that has affinities several orders of magnitude higher than TCRs (Stone & Kranz, 2013). In addition, as scFvs has the ability to recognise intact cell-surface proteins, targeting of tumour cells with CARs is independent of antigen processing and presentation. Furthermore, CARs can target antigens

that cannot be easily recognised, if at all, by TCRs (e.g. glycolipids or aberrantly glycosylated proteins).

Results from clinical trials have shown that CAR T cells have the capacity to deliver powerful anti-tumour effects. However, to date, the success of CAR T cell therapies has largely been in haematological malignancies (Maude et al., 2014; Porter, Levine, Kalos, Bagg, & June, 2011; Schuster et al., 2017; Wei, Ding, Wang, Hu, & Huang, 2017). Despite extensive research, the success of this type of therapy in treating solid tumours has been limited. This could be explained by the fact that it is more difficult to find an ideal target antigen in solid tumours. Unlike haematological malignancies in which all the tumour cells express the B cell marker CD19, solid tumours very rarely express one universal tumour-specific antigen. In solid tumours it is common to find tumour-associated antigens (TAAs), but these would not be good targets as they are enriched on tumours but also expressed on normal tissues.

Finally, although most patients treated with CAR T cells show mild to moderate side effects, severe side effects are still possible with this therapy. The most notable severe side effects include cytokine release syndrome (CRS), insertional oncogenesis, and neurologic toxicity (Bonifant, Jackson, Brentjens, & Curran, 2016; Brudno & Kochenderfer, 2016).

1.3. Next Generation Cell Therapies

There is a strong rationale for combining adoptive cell therapies (ACT) with immune checkpoint blockade (ICB), as it has been demonstrated that tumour-reactive $CD8^+$ T cells that persist in patient PBMCs for up to 1 year after ACT are mostly polyfunctional; however they express high levels of PD1, rendering them sensitive to PD-L1 (Marco Donia et al., 2017). Hence, impaired T cell activity via the different immune checkpoint signalling pathways may be responsible for relapses observed in some patients treated with ACT. Moreover, it has been observed that the combination of ACT with ICB promotes tumour regression in different mouse models (Blake et al., 2015; John et al., 2013; L. Z. Shi, Gao, Allison, & Sharma, 2018). Furthermore, ACT of tumour antigen-specific cytotoxic T cells in combination with CTLA4 systemic blockade has shown promising clinical results (Chapuis, Lee, et al., 2016; Chapuis, Roberts, et al., 2016).

In this regard, there are two advantages to the genetic engineering of T cells in ACT to knockout immune checkpoints compared to immune checkpoint inhibitors. The first is that there is greater certainty in the proper targeting of immune checkpoints by genetic engineering than by antibody-mediated blockade of them. This is because it is difficult to predict for any given patient to what extent the antibodies will actually block the targeted immune checkpoints. On the contrary, by engineering the cells to create knockouts of the genes encoding immune checkpoints and subsequently multiplying the cells that have been successfully edited, there can be no doubt of the proper deletion of the immune checkpoint of interest. The second advantage is that immune checkpoint inhibitors target T cells in a non-specific way, which causes toxicity due to an excessive autoimmune response. ACT of genetic engineered T cells provides a platform where TILs that are neoantigen reactive (i.e. that recognise antigens only present on tumour cells) could be identified and selectively targeted for gene editing. In this way, one could hypothesise, the toxicity and side effects relating to autoimmune responses could be avoided.

However, genetic engineering of T cells also has a few disadvantages. Firstly, given that it is a type of personalized medicine, the procedure will not be as easily scalable and affordable as checkpoint inhibitors. Secondly, and most importantly, the genetic engineering of human cells is not without its concerns. These editing technologies are known to have “off-target” effects, which means that other parts of the genome may be mutated without our knowledge. However, as these technologies are advancing rapidly, more and more improvements are being performed on them to diminish or completely eliminate off-target events (Fu, Sander, Reyon, Cascio, & Joung, 2014; Kleinstiver et al., 2016; Slaymaker et al., 2016).

The field of ACT combined with genetic manipulation of cells is progressing rapidly, with a number of clinical trials using CRISPR-edited autologous lymphocytes already underway (NCT03399448, NCT03081715, NCT02793856). Furthermore, a clinical trial using a TALEN-edited universal CAR-T cell (NCT03190278) has also started.

1.3.1. Gene Editing Technologies

The rapid advancement of gene editing technologies has considerably improved our ability to make precise changes in the genomes of eukaryotic cells. These editing technologies can be divided into four main groups, which will be described in more detail below. A brief comparison of the main advantages and disadvantages of the different groups is shown in Table 1.1.

Technology	Mode of action	Advantages	Disadvantages
Meganucleases	-They generate a 3' overhang that anneals with the coding sequence of the meganuclease via the homology-directed repair pathway.	-Highly specific because of the integrated nature of DNA recognition and cleavage.	-Their integrated nature makes them complex to reprogram for the recognition of novel DNA targets.
Zinc Finger Nucleases (ZFN)	-They are the combination of zinc finger transcription factors with the FokI restriction enzyme. The DNA recognition comes from the zinc finger domain, which makes contact with 3bp in the major groove of the DNA, and the endonuclease activity comes from the FokI.	-Modular construction. -Can increase sequence specificity by rendering them obligate heterodimers.	-Nuclease design and assembly are complex. -Context-dependence in DNA recognition (i.e. some zinc fingers do not retain their expected triplet specificity once linked into a new zinc finger array).
Transcription Activator-Like Effector Nucleases (TALEN)	-Paired fusion proteins that bind DNA at adjoining sites and combine to produce a double-strand break.	-Modular construction. -Extensive targeting range.	-Nuclease design and assembly are very labour intensive. -Susceptible to rearrangements.
CRISPR/Cas9 System	-The gRNA leads the Cas9 to the genomic target sequence so that the wild-type endonuclease can cut both strands of DNA causing a double strand break.	-Simple design and assembly. -High targeting efficiencies with most gRNAs. -Multiplex capacity.	-Possible off-target effects.

Table 1.1. Comparison of different gene editing technologies. The main advantages and disadvantages of the different gene editing technologies are described.

1.3.1.1. Meganucleases

Meganucleases (also called homing endonucleases) are sequence-specific endonuclease proteins that can be found in a number of prokaryotes, archaea, and unicellular eukaryotes. The function of these proteins in nature is to support horizontal gene transfer of their coding sequences (Stoddard, 2005). They are named “mega” because their DNA recognition sites are in the range of 20-30bp in length (Stoddard, 2011), and hence these sites are significantly bigger than those of the type II restriction endonucleases commonly used in recombinant DNA technology. The double-strand break that is generated by these enzymes results in a 3’ overhang that then anneals with the coding sequence of the meganuclease via the homology-directed repair (HDR) pathway.

With the understanding of the function of the DNA-binding motif of this class of enzymes, meganucleases were established as useful tools for genome editing. Although many different DNA sequence specificities exist in wild-type meganucleases, it was still necessary to generate enzymes that included a larger repertoire of binding specificities. The relative difficulty of engineering these proteins with novel specificities, as well as the difficulty in separating the DNA-binding and cleavage domains of the meganucleases has limited the use of this platform. Hence, meganucleases have not attained widespread adoption as tools for genome engineering.

1.3.1.2. Zinc Finger Nucleases

Zinc fingers (ZF) are the most abundant class of DNA-binding transcription factors. In these proteins, one ZF domain makes contact with 3bp in the major groove of the DNA. Many attempts have been made to generate libraries of ZFs that could bind all possible DNA triplets (Jamieson, Kim, & Wells, 1994; Nardelli, Gibson, & Charnay, 1992). However, it was found that generation of ZFs with optimal DNA binding strength required a guanine nucleotide in the first position of the DNA triplet (Jamieson, Wang, & Kim, 1996).

As ZFs do not have endonuclease activity, the coupling of these DNA-binding transcription factors with a restriction enzyme was needed to generate a powerful genome editing tool. This was achieved by generating hybrid ZF/FokI enzymes that combined the DNA recognition of the ZF with the endonuclease

activity of the FokI restriction enzyme (Y. G. Kim, Cha, & Chandrasegaran, 1996). This technology was further optimised by generating paired ZFNs that heterodimerize upon binding DNA to form a catalytically active nuclease complex (Bibikova et al., 2001). Furthermore, to increase sequence specificity, mutant FokI monomers were introduced to render them obligate heterodimers (Miller et al., 2007).

A key advantage of the use of ZFNs is their modular construction. As each ZF domain binds three nucleotides, linking several together generates a recombinant protein that recognises a multiple of three genomic bases. However, a significant amount of the binding specificity of any ZF depends on the context of its neighbouring ZFs (Cornu et al., 2008). This context dependence causes uncertainty in the suitability of designed ZFNs, hence, for any targeted locus multiple ZFNs have to be constructed to guarantee a successful targeting of a specific genomic region. Additionally, another disadvantage of the system is that the requirement for dimerization introduces the possibility of restricting cleavage to very long and rare sequences.

1.3.1.3. Transcription Activator-Like Effector Nucleases

The discovery of a simple code by which TALE proteins from the plant pathogen *Xanthomonas* recognise a given DNA sequence introduced the possibility of a new customisable tool for genome engineering (Boch et al., 2009). Tools for TALEN experimentation developed rapidly, as many of the technical issues related to the generation of fusion proteins had already been solved through ZFN research. In this regard, TALENs design is similar to that of ZFNs, with paired fusion proteins that bind DNA at adjoining sites and combine to produce a double-strand break. Moreover, as with ZFNs, modular TALE repeats can be stringed together to generate long arrays with custom DNA-binding specificities (Christian et al., 2010; T. Li et al., 2011; Miller et al., 2011; F. Zhang et al., 2011).

A major difference between ZFNs and TALENs is that TALENs can be engineered to target virtually any sequence as their only restraint is the requirement of a 5' T for each array. Because of this extensive targeting range and the ease of engineering compared to meganucleases or ZFNs, TALENs

became an attractive platform for targeted genomic engineering. However, the considerable size and repetitive essence of TALE arrays is considered a limitation for *in vivo* delivery of these proteins. The delivery of both TALEN monomers in a single viral vector can be impeded by the fact that TALENs require 34 amino acids to bind a single base pair of DNA and that the viral vector has a limited packaging capacity. Furthermore, another disadvantage of this technology is that the unstable nature of tandem repeats present in TALENs make them susceptible to rearrangements (Holkers et al., 2013).

1.3.1.4. The CRISPR/Cas9 System

The CRISPR (clustered regularly interspaced short palindromic repeats)/Cas9 is a prokaryotic adaptive immune system that uses RNA-guided nucleases to cleave foreign genetic elements in a site-specific manner. There are three types of CRISPR systems (I-III) that have been found across the prokaryotic kingdoms. From these, the type II CRISPR system is one of the best characterised and it is the one on which the CRISPR/Cas9 technology is based. The type II CRISPR system consists of the nuclease Cas9, the crRNA cluster that encodes the guide RNAs, and a required auxiliary trans-activating crRNA (tracrRNA) that facilitates the processing of the crRNA array into distinct units. The crRNA array is formed by repetitive sequences (direct repeats) interspaced by short variable sequences known as protospacers. Within the DNA target, each protospacer is always related with a protospacer adjacent motif (PAM) sequence. After the processing of the crRNA cluster into distinct units, each of them contains a 20 nucleotide guide sequence and a partial direct repeat, where the former directs the Cas9 nuclease to a 20 base-pair DNA target via Watson-Crick base pairing (Cong et al., 2013).

In 2013, Mali *et al.* demonstrated for the first time that the CRISPR/Cas9 technology could be used to achieve genome editing of human cells. For this, they synthesised a human codon-optimised Cas9 protein with an SV40 nuclear localisation domain and cloned it into a plasmid to be expressed under the cytomegalovirus (CMV) promoter. Then, they designed a second plasmid expression system that combines the endogenous bacterial crRNA and tracrRNA into a single chimeric guide RNA (gRNA) transcript, which is expressed under the

human U6 polymerase III promoter (Mali et al., 2013). The gRNA combines the targeting specificity of the crRNA with the scaffolding properties of the tracrRNA.

For this technology only two components are needed: (1) a guide RNA and (2) an endonuclease (in this case Cas9 nuclease); when both of these elements are expressed in the cell, the genomic target sequence can be modified or permanently disrupted. The gRNA leads the Cas9 to the genomic target sequence so that the wild-type endonuclease can cut both strands of DNA causing a double strand break (DSB). A DSB is repaired through either the non-homologous end joining (NHEJ) or through the homology directed repair (HDR) DNA repair pathways. The NHEJ repair pathway is error-prone, resulting in random insertions/deletions (indels) at the site of the DSB; this can lead to frameshifts and/or premature stop codons disrupting gene function. The HDR pathway needs a repair template, which is used to fix the DSB. HDR faithfully copies the sequence of the repair template to the cut target sequence and by doing so it allows for specific nucleotide changes to be introduced into a targeted gene.

An alternative to the DSB executed by the Cas9 nuclease is to convert this nuclease into a nickase mutant (Cas9n) to nick rather than cleave DNA to yield single-stranded breaks. This in turn facilitates the preferentially homology-directed repair with minimal mutagenic activity. Additionally, pairs of gRNA can guide the Cas9n to simultaneously nick both strands of the target DNA to mediate a DSB with more specificity (Ran et al., 2013).

In addition to the knockout of a specific gene, the CRISPR/Cas9 technology can be used for other applications, such as post-transcriptional gene-silencing (by knocking down the expression of coding and noncoding RNAs with the CasRx) (Konermann et al., 2018), and directional gene transfer (using the Cpf1 (i.e. Cas12a) endonuclease, which creates double-stranded breaks with a short 3' overhang) (Zetsche et al., 2015). Additionally, the Cas9 endonuclease can be rendered inactive by point mutations, resulting in a nuclease dead Cas9 (dCas9) molecule that cannot cleave target DNA. The dCas9 can be fused with transcriptional repressors (CRISPRi) or activators (CRISPRa) for targeted gene regulation (Bikard et al., 2013; Gilbert et al., 2013; Qi et al., 2013). The dCas9 can also be fused to epigenetic modifiers to create programmable epigenome-engineering tools that can modify methylation states or induce acetylation (Hilton

et al., 2015; X. S. Liu et al., 2016). Furthermore, the CRISPR/Cas9 technology has been recently used to perform targeted insertions, deletions, and point mutations without requiring double-strand breaks or donor DNA template (this was done with a catalytically impaired Cas9 fused to an engineered reverse transcriptase, programmed with a prime editing guide RNA) (Anzalone et al., 2019).

In contrast to the three nuclease systems discussed above, the CRISPR/Cas9 technology does not entail the engineering of novel proteins for each DNA target site. Given its ease of implementation and multiplexing capacity, the CRISPR/Cas9 system has been used to generate a plethora of engineered eukaryotic cells carrying specific mutations via both NHEJ and HDR. Furthermore, direct injection of gRNA and mRNA encoding Cas9 into embryos has enabled the rapid generation of transgenic mice with numerous modified alleles (Ran et al., 2013).

In addition to producing powerful research tools, genome editing with CRISPR/Cas9 also holds great promise in the production of therapeutic agents such as universal CAR-T cells (Cooper et al., 2018; J. Ren, Zhang, et al., 2017) that are genetically edited to ablate PD1 expression (J. Ren, Liu, et al., 2017). Although any of the DNA editing technologies previously described could be used for the production of these therapeutic agents, the ease of implementation and inexpensive reprogramming of Cas9 gives CRISPR/Cas9 technology a clear advantage in a clinical context in which many different loci may need to be targeted at the same time.

1.4. Hypothesis and Aims

By genetically engineering tumour infiltrating T cells to knockout the expression of immune-checkpoints in their surface, we will render them resistant to checkpoint inhibition. We hypothesise that this will render the transferred T cells resistant to negative regulation exerted by cancerous cells and their surrounding microenvironment. Furthermore, by genetically engineering only the T cells that are tumour-reactive, we hypothesise that we will be able to prevent or at least reduce toxicities associated with systemic blockade of immune

checkpoints as the ones seen in the clinic with immune checkpoint inhibitors. To achieve this, the main aims of this project are divided in three parts:

- Aim 1: To develop a methodology that allows for the efficient gene editing of primary tumour infiltrating T cells (enriched for tumour reactivity) using the CRISPR/Cas9 technology.
- Aim 2: To generate a method to be able to selectively expand tumour-reactive (or, if possible, neoantigen-reactive) T cells from tumour infiltrating lymphocytes (TILs).
- Aim 3: To target relevant immune checkpoints in TILs using the developed methodology and to test both *in vitro* and *in vivo* if these edited TILs have enhanced anti-tumour activity.

1.5. Experimental Plan

To achieve the aims described above, the following experimental plan was devised (Figure 1.2):

1) To design the crRNAs for the human immune checkpoints we wish to target and to clone these into the Cas9 vector.
2) To create cell lines constitutively expressing the checkpoints of interest and to validate the gRNAs with DNA transfection into these cell lines followed by knockdown confirmation of the targets by flow cytometry.
3) To generate Cas9 ribonucleoprotein (RNP) complexes and electroporate them into human primary TILs.
4) To generate patient derived xenografts (PDX) of different tumours in immunodeficient mice.
5) To treat the immunodeficient mice by injecting autologous edited TILs that correspond to the PDX previously generated (to have matched PDX with TILs from the same patient).

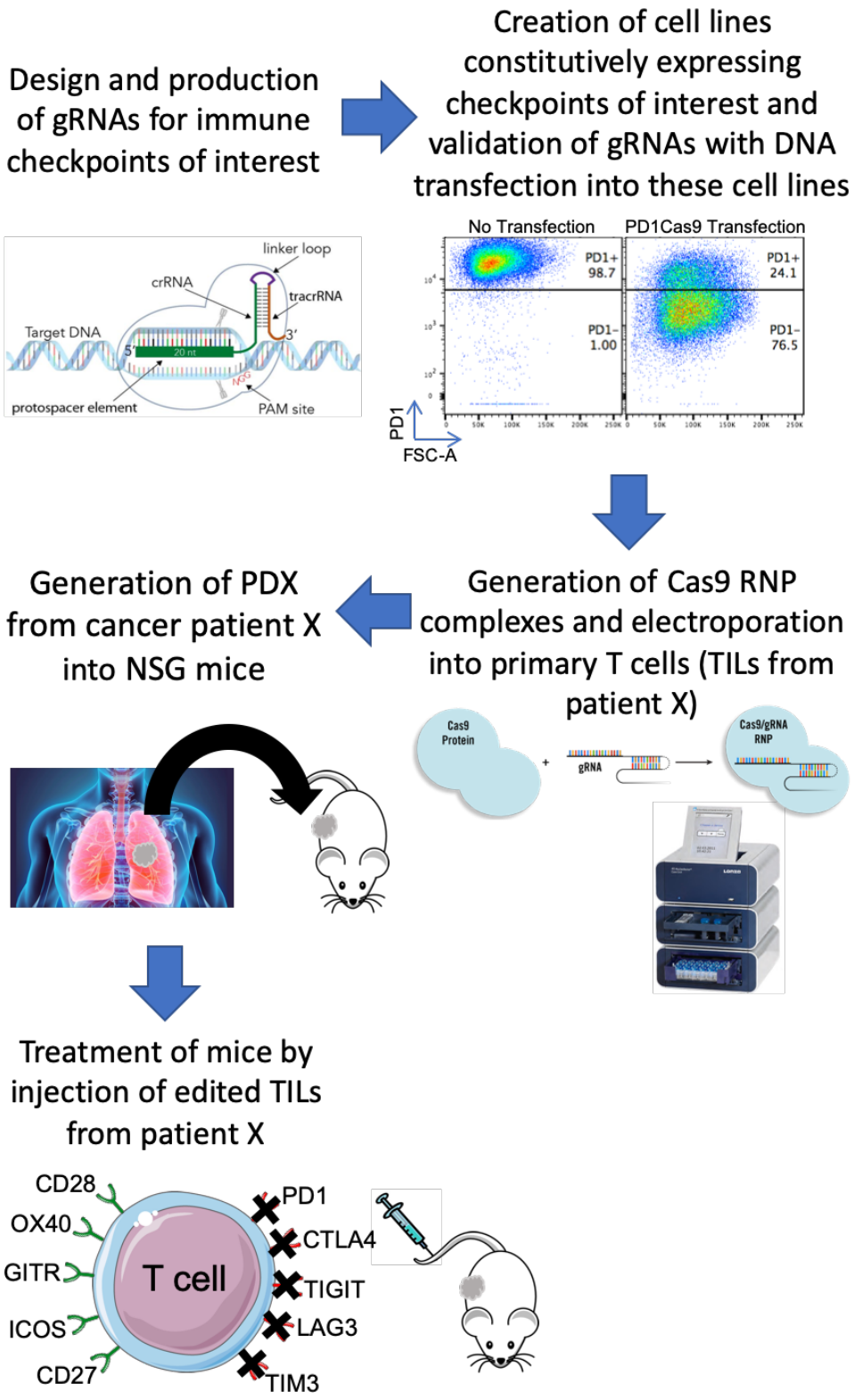

Figure 1.8. Experimental plan devised to achieve the aims of this project.

Chapter 2. Materials and Methods

2.1 Materials

2.1.1. Cell lines and primary cells

For this project the following cell lines were used:

- HEK293T cells: Highly transfectable cells derived of human embryonic kidney 293 cells. These were kindly provided by Dr Martin Pule's laboratory from UCL Cancer Institute.
- HEK293T PD1/TIM3 cells: HEK293T cells overexpressing PD1 and TIM3. These were kindly provided by Professor Andy Sewell's laboratory from Cardiff University.
- 293T.huCTLA4.I.d.CD34ngg: HEK293T cells overexpressing CTLA4 (sorted for high expression of CTLA4). These were kindly provided by Dr Martin Pule's laboratory from UCL Cancer Institute.

It is important to note that all of the cell lines were mycoplasma tested before starting any work on them and they all returned a negative result for mycoplasma contamination.

This project also made use of the following primary cells:

- Peripheral Blood Mononuclear Cells (PBMCs) from different healthy donors.
- Tumour Infiltrating Lymphocytes (TILs) from melanoma and lung patients (patients MX063, LTX11, LTX997, and LTX1000).
- MX063 tumour cell line: Primary tumour cell line generated in the lab by Sophia Wong from a fragment of tumour tissue resected from a melanoma patient (patient MX063).

The HEK293T cells and 293T.huCTLA4.I.d.CD34ngg cells were cultured in Iscove's Modified Eagle's Medium (IMDM, Sigma Aldrich) supplemented with 10% Foetal Bovine Serum (FBS, Gibco), 2mM L-Glutamine (Sigma Aldrich), and 100U/mL Penicillin with 100µg/mL Streptomycin (Sigma Aldrich). The HEK293T PD1/TIM3 cells were cultured in Dulbecco's Modified Eagle's Medium (DMEM, Sigma Aldrich) supplemented in the same way. The melanoma tumour cell line

and the PBMCs were grown in Roswell Park Memorial Institute medium 1640 (RPMI, Sigma Aldrich) supplemented in the same way. TILs were cultured in a 1:1 mixture of AIM V medium (GIBCO/Thermo Fisher Scientific) and Roswell Park Memorial Institute medium 1640 (RPMI, Sigma Aldrich) supplemented with 10% human serum (Sigma Aldrich), 2mM L-Glutamine (Sigma Aldrich), 100U/mL Penicillin with 100µg/mL Streptomycin (Sigma Aldrich), and 25 mmol/L HEPES pH 7.2. All the cells were grown at 37ºC with 5% CO_2.

The human TILs and tumour cell line derived from two translational studies, each approved by local institutional review board and Research Ethics Committee (Melanoma - REC no. 11/LO/0003, The Royal Marsden NHS Foundation Trust; NSCLC – REC no.13/LO/1546, University College London Hospital). The handling of these samples was conducted in accordance with the provisions of the Declaration of Helsinki and with Good Clinical Practice guidelines as defined by the International Conference on Harmonization.

2.1.2. Plasmids and Cas9 protein

The plasmids used for this project were mainly for the transfection of the CRISPR/Cas9 components into the cell lines, as well as for the transduction of the HEK293T cells to constitutively express the targets of interest. The plasmids used were the following:

- pX330-U6-Chimeric_BB-CBh-hSpCas9: Human codon-optimised SpCas9 and chimeric guide RNA expression plasmid that was produced by the laboratory of Dr Feng Zhang. This plasmid was purchased from Addgene (Cat #42230).
- pMONO.RD114env_wt.I.neo: An RD114 envelope in a splicing vector. This plasmid was kindly provided by Dr Martin Pule's laboratory from UCL Cancer Institute.
- SFG.CD25.mIgG1.I.GFP: Moloney Murine Leukemia Virus derived retroviral vector with an eGFP cassette. This plasmid was kindly provided by Dr Martin Pule's laboratory from UCL Cancer Institute.
- pEQ-Pam3-E: Moloney Murine Leukemia Virus gag-pol expression plasmid. This plasmid was kindly provided by Dr Martin Pule's laboratory from UCL Cancer Institute.

- pGEM-LAG3: Human LAG3 gene cDNA clone plasmid. This plasmid was purchased from Sino Biological Inc. (Cat #HG16498-G).
- pmaxGFP Control Vector: Fluorescent positive control vector provided by Lonza in their electroporation kits.

Two Cas9 proteins were used for this project: First the Alt-R SpCas9 Nuclease 3NLS from IDT (Cat #1074182) was employed. Then, as this version was discontinued, the new version was used: Alt-R SpCas9 Nuclease V3 (Cat #1081059).

2.1.3. crRNAs oligos for cloning into Cas9 plasmid and commercially synthesised crRNAs:tracrRNAs complexes

The crRNAs for the validation stage of this project (DNA transfection into easy-to-transfect cell lines) were designed and ordered as oligos from IDT. The target sequences (crRNAs) are described in more detail in Chapter 3. The oligos ordered from IDT were the following:

Name	Target Gene	Oligo 1 (Forward)	Oligo 2 (Reverse)
PD1e1 gRNA*	*PD1*	CACCGGGCGGTGCTACAACTGGGC	AAACGCCCAGTTGTAGCACCGCCC
TIM3e2 gRNA	*TIM3*	CACCGGGCACGAGGTTCCCTGGGG	AAACCCCCAGGGAACCTCGTGCCC
TIM3e3 gRNA*	*TIM3*	CACCGAGGTCACCCCTGCACCGACT	AAACAGTCGGTGCAGGGGTGACCTC
CTLA4e 1 gRNA	*CTLA4*	CACCGTGGCTTGCCTTGGATTTCAG	AAACCTGAAATCCAAGGCAAGCCAC
CTLA4e 2 gRNA	*CTLA4*	CACCGGGACTCTACATCTGCAAGG	AAACCCTTGCAGATGTAGAGTCCC
TIGITe1 gRNA	*TIGIT*	CACCGCCCCTGGGCCCAGATCAGG	AAACCCTGATCTGGGCCCAGGGGC
TIGITe2 gRNA	*TIGIT*	CACCGGCCATTTGTAATGCTGACT	AAACAGTCAGCATTACAAATGGCC
LAG3e1 gRNA	*LAG3*	CACCGACCATAGGAGAGATGTGGG	AAACCCCACATCTCTCCTATGGTC
LAG3e2 gRNA	*LAG3*	CACCGGGCTGAGGTCCCGGTGGTG	AAACCACCACCGGGACCTCAGCCC

Table 2.1. Oligos ordered for crRNAs. In blue are the overhangs that the oligos need to have to be cloned into the Cas9 plasmid, and in red are the bases that were not part of the target sequence but that were added because of the transcription initiation requirement of a 'G' base for

the U6 promoter. *The validated target sequences for these crRNAs were kindly provided to our laboratory by Professor Andy Sewell's laboratory from Cardiff University.

The sequences for the commercially synthesised crRNAs were the following:

Name	Target sequence	Synthesised crRNA sequence
PD1e1	GGGCGGTGCTACAACTGGGC	5'- /AltR1/ rGrGrG rCrGrG rUrGrC rUrArC rArArC rUrGrG rGrCrG rUrUrU rUrArG rArGrC rUrArU rGrCrU /AltR2/ -3'
PD1e1 (J. Ren, Liu, et al., 2017)	GGCCAGGATGGTTCTTAGGT	5'- /AltR1/ rGrGrC rCrArG rGrArU rGrGrU rUrCrU rUrArG rGrUrG rUrUrU rUrArG rArGrC rUrArU rGrCrU /AltR2/ -3'
TIM3e2	GGGCACGAGGTTCCCTGGGG	5'- /AltR1/ rGrGrG rCrArC rGrArG rGrUrU rCrCrC rUrGrG rGrGrG rUrUrU rUrArG rArGrC rUrArU rGrCrU /AltR2/ -3'
TIM3e3	AGGTCACCCCTGCACCGACT	5'- /AltR1/ rArGrG rUrCrA rCrCrC rCrUrG rCrArC rCrGrA rCrUrG rUrUrU rUrArG rArGrC rUrArU rGrCrU /AltR2/ -3'
CTLA4e1	TGGCTTGCCTTGGATTTCAG	5'- /AltR1/ rUrGrG rCrUrU rGrCrC rUrUrG rGrArU rUrUrC rArGrG rUrUrU rUrArG rArGrC rUrArU rGrCrU /AltR2/ -3'
CTLA4e2	GGGACTCTACATCTGCAAGG	5'- /AltR1/ rGrGrG rArCrU rCrUrA rCrArU rCrUrG rCrArA rGrGrG rUrUrU rUrArG rArGrC rUrArU rGrCrU /AltR2/ -3'
TIGITe1	GCCCCTGGGCCCAGATCAGG	5'- /AltR1/ rGrCrC rCrCrU rGrGrG rCrCrC rArGrA rUrCrA rGrGrG rUrUrU rUrArG rArGrC rUrArU rGrCrU /AltR2/ -3'
TIGITe2	GGCCATTTGTAATGCTGACT	5'- /AltR1/ rGrGrC rCrArU rUrUrG rUrArA rUrGrC rUrGrA rCrUrG rUrUrU rUrArG rArGrC rUrArU rGrCrU /AltR2/ -3'
LAG3e1	GACCATAGGAGAGATGTGGG	5'- /AltR1/ rGrArC rCrArU rArGrG rArGrA rGrArU rGrUrG rGrGrG rUrUrU rUrArG rArGrC rUrArU rGrCrU /AltR2/ -3'
LAG3e2	GGGCTGAGGTCCCGGTGGTG	5'- /AltR1/ rGrGrG rCrUrG rArGrG rUrCrC rCrGrG rUrGrG rUrGrG rUrUrU rUrArG rArGrC rUrArU rGrCrU /AltR2/ -3'

Table 2.2. Commercially synthesised crRNAs. The target sequence for the different checkpoints of interest as well as the optimised 36 base crRNA sequence from IDT's 'Alt-R CRISPR-Cas9 System' is shown. These chemical synthesised crRNAs have chemical modifications that confer resistance to nucleases and reduce immunogenicity.

The tracrRNA used was the same for all of the complexes. It was the 'Alt-R CRISPR-Cas9 tracrRNA' from IDT (Catalog #1072534). This 67 base chemical synthesised tracrRNA includes chemical modifications that reduce immunogenicity and provide resistance to nucleases. The sequence (without the proprietary IDT modifications) is:

rArGrCrArUrArGrCrArArGrUrUrArArArArUrArArGrGrCrUrArGrUrCrCrGrUrUrArUrCrArArCrUrUrGrArArArArArGrUrGrGrCrArCrCrGrArGrUrCrGrGrUrGrCrUrUrU.

2.1.4. Flow cytometry antibodies

The following antibodies were used to stain the cells for flow cytometry analysis:

Antigen	Clone	Conjugate	Supplier	Catalogue Number	Staining
B7-H3	MIH42	PE-Cy7	BioLegend	351008	Surface
CD3	OKT3	Brilliant Violet 785	BioLegend	317330	Surface
CD4	OKT4	Alexa Fluor 700	ThermoFisher Scientific	56-0048-82	Surface
CD8	SK1	BV510	BD Biosciences	563919	Surface
CD8	SK1	V500	BD Biosciences	561618	Surface
CD45	HI30	Brilliant Violet 605	BioLegend	304041	Surface
CD45	HI30	Brilliant Violet 650	BioLegend	304044	Surface
CD45 (mouse)	30-F11	PE-Cy7	BioLegend	103114	Surface
CD56	HCD56	Brilliant Violet 711	BioLegend	318336	Surface
CD112	TX31	APC	BioLegend	337411	Surface
CD155	SKII.4	PerCP-Cyanine5.5	BioLegend	337611	Surface
CTLA4	L3D10	APC	BioLegend	349907	Intracellular
CTLA4	BNI3	PE	BioLegend	369604	Intracellular
Galectin-9	9M1-3	PE	BD Biosciences	565890	Surface
HLA-ABC	W6/32	Brilliant Violet 605	BioLegend	311431	Surface
HLA-ABC	W6/32	FITC	ThermoFisher Scientific	11-9983-42	Surface
HLA-DR	G46-6	BV711	BD Biosciences	563696	Surface
IFNγ	4S.B3	PE	ThermoFisher Scientific	12-7319-42	Intracellular
LAG3	3DS223H	PE-Cyanine7	ThermoFisher Scientific	25-2239-42	Surface
PD1	EH12.2H7	Brilliant Violet 605	BioLegend	329924	Surface

PD-L1	29E.2A3	APC	BioLegend	329708	Surface
PD-L1	MIH2	FITC	BioLegend	393605	Surface
PD-L2	MIH18	BV421	BD Biosciences	563842	Surface
TIGIT	MBSA43	PE	ThermoFisher Scientific	12-9500-42	Surface
TIM3	F38-2E2	Brilliant Violet 650	BioLegend	345028	Surface
TIM3	F38-2E2	PE	BioLegend	345006	Surface
TNFα	MAb11	FITC	ThermoFisher Scientific	11-7349-82	Intracellular
Viability Dye	-	eFluor 780	ThermoFisher Scientific	65-0865-18	Surface

Table 2.3. Antibodies used for flow cytometry staining. The clones and catalogue numbers for the different antibodies used are shown. It is also indicated if the antibody was used in a surface or intracellular staining.

2.1.5. Mice

For the *in vivo* experiments 6-8 weeks old NOD.Cg-*Prkdc*^{scid} *Il2rg*^{tm1Wjl}/SzJ (commonly known as NOD *scid* gamma (NSG)) female mice were used. The mice were obtained from UCL P-Block. The NSG mice are characterised by the absence of mature T cells, B cells, and functional NK cells. They have defective dendritic cells and macrophages and have a complete knockout of the gamma chain of the interleukin 2 receptor gene leading to a deficiency in cytokine signalling.

All animals were maintained in individually ventilated cages and pathogen-free conditions at UCL Biological Service Unit (BSU) following arrival, in accordance with Home Office and institutional guidelines. All animal studies were performed under University College London and UK Home Office ethical approval and regulations and were in accordance with the Animal (Scientific Procedures) Act 1986 guidelines by the UK Home Office.

2.2 Methods

2.2.1. Molecular biology techniques

2.2.1.1. Cloning of crRNAs oligos into SpCas9 and chimeric guide RNA expression plasmid

The oligo annealing and cloning into the pX330 backbone vector was performed following Zhang's lab single-step digestion-ligation protocol (Ran et al., 2013). Briefly, the complimentary oligos ordered from IDT (Table 2.1) were resuspended to 100μM and mixed with 10X T4 Ligation Buffer (NEB) and T4 PNK (NEB). Then they were phosphorylated and annealed in a thermocycler by using the following parameters: 37°C for 30 min; 95°C for 5 min; ramp down to 25°C at 5°C/min. The phosphorylated and annealed oligos were diluted 250-fold and a digestion-ligation reaction was set up with 2μL of the oligo duplex and 100ng of the pX330 plasmid in the presence of 10X Tango Buffer (ThermoFisher Scientific), DTT (10mM), ATP (10mM), FastDigest BbsI (ThermoFisher Scientific), and T7 DNA Ligase (NEB). The ligation reaction was incubated in a thermocycler for 6 cycles of 37°C for 5 min; 23°C for 5 min.

2.2.1.2. Bacteria transformation

For the bacteria transformations, NEB 5-alpha Competent *E. coli* (High Efficiency) bacteria was used (NEB; Cat #C2987). For each transformation, a vial of this bacteria was thawed on ice for 10 minutes, and 1.5μL (for the pX330+crRNA clonings) or 5μL (for the SFG.TIGIT and SFG.LAG3 clonings) of the cloning product was added without vortexing or pipetting (the tube was gently flicked to mix the cells). After incubating the sample for 30 minutes on ice, bacteria were heat shocked for 2 minutes at 37ºC and immediately transferred to ice for 5 minutes to recover. Bacteria were plated on a LB agar plate with ampicillin (50μg/mL) and incubated overnight at 37ºC.

2.2.1.3. Plasmid purification from bacteria

Single colonies were selected from each LB agar plate and grown overnight at 37ºC in 4mL of LB broth medium with ampicillin (50μg/mL). Afterwards, plasmid DNA was purified using QIAprep Spin Miniprep Kit (Qiagen; Cat #27106), following the manufacturer's instructions. When a larger amount of

plasmid was needed, a midiprep was performed by growing a colony overnight at 37ºC in 200mL of LB broth medium with ampicillin (50µg/mL). Plasmid DNA was then purified using NucleoBond Xtra Midi Kit (Macherey-Nagel; Cat #740410.100), following the manufacturer's instructions.

2.2.1.4. Complete and diagnostic digestions

For the cloning of the TIGIT or LAG3 open reading frame (ORF) into the SFG plasmid, the purified TIGIT or LAG3 PCR products and the SFG.CD25.mIgG1.I.GFP plasmid were subjected to an enzymatic digestion with the BglII (NEB) and MluI (NEB) restriction enzymes in order to generate cloning DNA fragments with 'sticky' compatible ends to allow DNA ligation. The complete digestion of the plasmid and the PCR products was achieved by performing the reaction shown in Table 2.4.

Reagents	**Volumes per reaction**
Plasmid or purified PCR product	50µL
BglII (NEB)	1µL
MluI-HF (NEB)	1µL
Buffer 3.1 (NEB)	6µL
ddH_2O	2µL
Incubate at 37ºC for 4 hours	

Table 2.4. Reaction performed for enzymatic digestion of plasmid and purified PCR products. Volumes of reagents for one reaction are shown.

After the cloning of the TIGIT or LAG3 ORF into the SFG.GFP plasmid was performed, diagnostic digestions were carried out by following the reaction shown in Table 2.5.

Reagents	Volumes per reaction
Plasmid DNA	2µL
NcoI-HF (NEB) (for SFG.TIGIT) or MluI-HF (NEB) (for SFG.LAG3)	0.5µL
SacI (NEB)	0.5µL
Cutsmart Buffer (NEB)	2µL
ddH_2O	15µL
Incubate at 37ºC for 1 hour	

Table 2.5. Reaction performed for diagnostic digestion of SFG.TIGIT and SFG.LAG3 plasmids. Volumes of reagents for one reaction are shown.

2.2.1.5. Sanger sequencing for confirmation of correct cloning

The SFG.TIGIT, SFG.LAG3, and the Cas9+crRNAs plasmids were further validated by Sanger sequencing. Purified plasmid DNA samples (100ng/µL) were sent to GATC with the appropriate sequencing primer (5µM). The sequencing results were analysed and aligned to the reference map using SnapGene 3.0.

2.2.1.6. Gel extraction/purification

Following separation of DNA fragments by agarose gel electrophoresis, bands were visualised using a dark reader blue light transilluminator to prevent UV-mediated mutagenesis. DNA was then extracted using the QIAquick Gel Extraction Kit (Qiagen) according to manufacturer's instructions.

2.2.1.7. Generation of SFG.TIGIT and SFG.LAG3 plasmids

For the generation of the SFG.TIGIT plasmid, a GBlock was ordered from IDT that contained TIGIT's open reading frame (ORF) as well as the restriction sites for BglII and MluI flanking the ORF. For the generation of the SFG.LAG3 plasmid, a LAG3 cDNA plasmid was purchased from Sino Biological Inc. (pGEM-LAG3; Cat #HG16498-G). Afterwards, PCRs were performed for the GBlock and the LAG3 cDNA plasmid following the manufacturer's instructions (for the LAG3 PCR, primers that were specific for the LAG3 ORF and that had overhangs for the restriction sites BglII and MluI were used). The amplified fragments of the expected size were gel purified as previously described. Subsequently, both the

purified PCR products and the SFG.CD25.mIgG1.I.GFP plasmid were digested with BglII (NEB) and MluI (NEB) as previously described; this was to open the vector and cut out the CD25.mIgG1 part of the plasmid and to create the proper overhangs on the insert so that the ligation could be achieved. After the digestion, gel purification was performed for both the vector and the inserts. The digested vector was ligated with the digested TIGIT or digested LAG3 ORF using T4 DNA Ligase (NEB) by performing the reaction shown in Table 2.6.

Reagents	Volumes per reaction
Digested Insert (either TIGIT or LAG3)	4μL
Digested Vector (SFG.GFP vector)	4μL
T4 Ligase Buffer (10x) (NEB)	1μL
T4 DNA Ligase (NEB)	1μL
Incubate at room temperature for 20 minutes	

Table 2.6. Reaction performed for ligation of SFG vector with TIGIT or LAG3 ORF. Volumes of reagents for one reaction are shown.

The ligations were followed by transformation of competent bacteria (NEB 5-alpha Competent *E. coli*) as previously described. A test digestion was performed for 10 colonies of the SFG.TIGIT using NcoI (NEB) and SacI (NEB) and 3 of the ones that showed the right pattern were sent for sequencing and confirmed to be correct. A test digestion using MluI (NEB) and SacI (NEB) was performed for 10 colonies of the SFG.LAG3, and the 2 colonies that showed the right pattern were confirmed to be correct via sequencing.

2.2.1.8. In vitro transcription of GFP, Cas9 and gRNAs

The *in vitro* transcription was performed using the mMESSAGE mMACHINE T7 Ultra Kit (ThermoFisher Scientific) following the manufacturer's instructions. At the end of the *in vitro* transcription, RNA was purified using the RNeasy Mini Kit (Qiagen) following the manufacturer's instructions. RNA was eluted in Cytoporation Medium T (BTX) at 1mg/mL and stored at -80ºC until needed for electroporation.

2.2.1.9. DNA isolation from cells

For genomic confirmation of gene editing, DNA was extracted from T cells using the DNeasy Blood & Tissue Kit (Qiagen; Cat #69504) following the manufacturer's instructions.

2.2.1.10. Genomic confirmation of gene editing

2.2.1.10.1 TIDE and ICE Analysis

DNA extracted from the edited TILs was sent for Sanger sequencing with primers flanking the location of the edit and the results were analysed using the TIDE (https://tide.deskgen.com/) and ICE (https://ice.synthego.com/) analysis software tools.

2.2.1.10.2 MiSeq Analysis

The edited-TILs DNA was sent to the Genomics and Genome Engineering Core Facility of the UCL Cancer Institute with the appropriate primers. Next-generation sequencing was performed on a MiSeq platform and the analysis of these results was carried out by the core facility.

2.2.2. Cell culture techniques

2.2.2.1. Transfection of adherent HEK293T cell line

For the transfection, HEK293T cells were seeded at ~30% confluency in a 100mm plate with 10mL of complete IMDM. The following day the transfection was performed with the reactions that were prepared as shown in Table 2.7.

Reagents	**Amounts for 100mm plate**
Plain RPMI	470μL
GeneJuice	30μL
Gently mix and incubate for 5 minutes at room temperature. Then add the DNA one by one:	
Envelope (pMONO.RD114env_wt.I.neo)	3.125μg
Gag-Pol (pEQ-Pam3-E)	4.6875μg
Retroviral Construct (either SFG.TIGIT or SFG.LAG3)	4.6875μg
Gently mix and incubate for 15 minutes at room temperature.	

Table 2.7. Reactions made for transfections of HEK293T cells. Volumes of reagents and amounts of DNA for a 100mm plate transfection are shown.

After the incubation, the mixture was added dropwise to the 100mm plate with the HEK293T cells and the plate was gently swirled to distribute evenly. The supernatant was harvested 48h and 72h after the transfection and mixed together.

2.2.2.2. Transduction of adherent HEK293T cell line

For the transduction, HEK293T cells were seeded at a density of $2x10^5$ cells in 3mL of complete IMDM/well of a 6-well plate. The transduction was performed the following day by adding 1.5mL of the supernatant mixture (48h + 72h) to each well + 0.5mL of complete IMDM/well + polybrene to a final concentration of 10µg/mL. The cells were collected 72h after transduction and tested for the expression of GFP and, later on, the transgene.

2.2.2.3. Human peripheral blood mononuclear cell isolation

Peripheral blood mononuclear cells (PBMCs) were isolated from whole blood of healthy donors by gradient centrifugation with Ficoll-Paque Plus (GE Healthcare; Cat #17-1440-03).

2.2.2.4. Activation of human T cells

PBMCs and TILs (that were not undergoing expansion) were activated 48-72 hours prior to electroporation by incubating them in plates coated with αCD3 antibody (10µg/mL) and adding soluble αCD28 antibody (1µg/mL) and IL-2 (100IU/mL). For the reactivation of PBMCs or TILs after electroporation, the cells were incubated in media with IL-2 for 4-6 hours prior to reactivating them in the same manner (for TILs edited while undergoing the REP, the reactivation was performed with 6000IU/mL of IL-2 instead of 100IU/mL).

Alternatively, where indicated in the text and figure legends, T cells were activated with ImmunoCult Human CD3/CD2/CD28 T Cell Activator (Stemcell Technologies; Cat #10970) and IL-2 (100IU/mL) following the manufacturer's instructions.

2.2.2.5. Expansion of human TILs using the pre-REP and Rapid Expansion Protocol (REP)

MX063 TILs were expanded from frozen either directly with the rapid expansion protocol (REP) (Dudley, Wunderlich, Shelton, Even, & Rosenberg, 2003) or with a modified version of the pre-REP followed by a REP. The modified version of the pre-REP consisted of setting up cultures of unexpanded TILs with irradiated (50Gy) autologous tumour cells in the presence of IL-2 (6000IU/mL) and IL-21 (25ng/mL) for two weeks prior to performing the REP. Briefly, the REP consists of incubating the TILs in the presence of irradiated (50Gy) allogeneic feeder cells at a 200:1 ratio (feeder cells:TILs) with αCD3 antibody (30ng/mL) and IL-2 (6000IU/mL) for two weeks.

LTX997 and LTX1000 TILs were expanded from fresh. This expansion consisted of an initial pre-REP phase in which small tumour fragments were grown in media containing IL-2 (6000IU/mL) and IL-21 (25ng/mL) for 3 weeks (IL-21 was given only at day 0, whereas IL-2 was continually replenished). Afterwards, a REP (described above) was performed.

2.2.2.6. Electroporation of primary T cells

2.2.2.6.1. BTX electroporator machine

Each electroporation was performed with at least $5x10^6$ cells as this electroporator machine is specifically engineered for large-volume application and as such this is the minimum number of cells that needs to be used. All electroporations were performed with *in vitro* transcribed mRNA, as it is known that electroporation of DNA into primary cells renders low efficiency and viability. Prior to electroporation the cells were washed and resuspended in 180µL of Cytoporation Medium T (BTX) per electroporation. The cells were transferred to a 0.4-cm cuvette and either 20µg of mRNA GFP, 15µg of mRNA Cas9 + 10µg of mRNA PD1e1 gRNA, or 3µM RNP complex (1:1 molar ratio of Cas9 protein and mRNA PD1e1 gRNA) was added to the cuvette. Electroporation of the T cells was performed using an Agile Pulse BTX system (Harvard Apparatus) allowing several square wave pulses as described in Table 2.8.

Parameters	Pulse 1	Pulse 2	Pulse 3-6
Voltage	1200 V	1200 V	130 V
Pulse Duration	0,1 ms	0,1 ms	0,2 ms
Pulse Intervals	0,2 ms	100 ms	2 ms
Number of Pulses	1	1	4

Table 2.8. Electrical variables for electroporation of primary T cells. Six square wave pulses were done with different voltages, durations, and duration of intervals between pulses.

After electroporation the cells were transferred to a 12-well plate containing 2mL of media + 1000IU/mL IL-2 per well (TILs and PBMCs) or 2mL of media alone (cell lines). The cells were left incubating at 32ºC for 24h. Afterwards the medium was changed for fresh medium + IL-2 (1000IU/mL) (TILs and PBMCs) or fresh media alone (cell lines) and the cells were left to incubate at 37ºC until needed for flow cytometry.

2.2.2.6.2. Amaxa 4D Nucleofector machine

Each electroporation was performed with either $1x10^6$ cells at the optimisation stage using the P3 Primary Cell 4D-Nucleofector X Kit S (Lonza; Cat #V4XP-3032), or with $5\text{-}10x10^6$ cells using the P3 Primary Cell 4D-Nucleofector X Kit L (Lonza; Cat #V4XP-3024), following the manufacturer's instructions. Cells were electroporated using program EH-115 on the Amaxa 4D-Nucleofector (Lonza).

2.2.3. CRISPR cRNAs design and Cas9 RNP complex production

The design of the crRNAs was performed with three online design tools (E-CRISP, CHOPCHOP, and WGE) (Heigwer, Kerr, & Boutros, 2014; Hodgkins et al., 2015; Montague, Cruz, Gagnon, Church, & Valen, 2014) as explained in more detail in Chapter 3.

The crRNAs and tracrRNA purchased from IDT were resuspended to 200µM. Single gRNAs (crRNA:tracrRNA duplexes) were produced by mixing the crRNA and tracrRNA (1:1 molar ratio), incubating them in a thermocycler at 95ºC for 5min and then letting them cool down to room temperature. Cas9 RNP complexes were generated by mixing 2.5µM of Cas9 protein with 5µM of the

crRNA:tracrRNA duplex and incubating them at room temperature for 10-20 minutes.

2.2.4. Flow cytometry staining and analysis

2.2.4.1. Staining protocol

Cells were resuspended in 20µL of Fc Receptor binding inhibitor polyclonal antibody (ThermoFisher Scientific; Cat #14-9161-73) and incubated at 4ºC for 20 minutes. Then, 50µL of FACS buffer (PBS with 2% FBS and 2mM EDTA) with a mix of surface antibodies (see Table 2.3) were directly added and cells were stained during 30 minutes at 4ºC protected from the light. Cells were washed twice with FACS buffer and either resuspended in 200µL of FACS buffer for data acquisition or the staining was continued for the intracellular antibodies.

For the intracellular staining, cells were then fixed and permeabilised with 100µL of the Fixation/Permeabilization solution (Fixation/Permeabilization Concentrate diluted in Fixation/Permeabilization Diluent) (ThermoFisher Scientific; Cat #00-5123-43 & 00-5223-56) during 20 minutes at 4ºC protected from the light. Cells were washed twice with Permeabilization buffer (ThermoFisher Scientific; Cat #00-8333-56) and stained in 50µL of a mix of Permeabilization buffer with intracellular antibodies (see Table 2.3) for 30 minutes at 4ºC in the dark. Cells were then washed twice with Permeabilization buffer and resuspended in 200µL of FACS Buffer prior to data acquisition.

'Unstained' controls (cells stained only with viability dye) were included in all the stainings and fluorescence minus one (FMO) controls were included in bigger panels. Data was acquired using an LSR-Fortessa X-20 analyser (BD Biosciences) and analysed with FlowJo v.10.6.0.

2.2.4.2. Compensation

Spillover of certain fluorophores into secondary channels can result in false positives. To correct for this spillover, compensation was performed by acquiring single-stained compensation beads (UltraComp eBeads) (ThermoFisher Scientific; Cat #01-2222-42) to record positive and negative populations of each fluorophore. This allowed the calculation of compensation matrixes using the FACS Diva (BD Biosciences) or FlowJo softwares.

2.2.4.3. Fluorescence cell sorting

Electronic cell sorting was performed with a FACSAria Fusion Class II Type A2 Biosafety Cabinet (BD Biosciences). The fluorescence cell sorting was carried out by the Flow Cytometry Core Facility (Flow Cytometry Translational Technology Platform) of the UCL Cancer Institute.

2.2.5. Statistical analysis

Data presented in this thesis was analysed using GraphPad Prism 8.0 statistical software package. The different statistical tests used to calculate significance between conditions are indicated in the figure legends.

2.2.6. *In vitro* functional assays

2.2.6.1. Recall assay

MX063 expanded and edited TILs were incubated with their autologous tumour cells in a 1:1 ratio for 16 hours in the presence of a protein transport inhibitor (Brefeldin A) (BD Biosciences; Cat #555029). For the condition were MHC blocks were included as controls, LEAF purified anti-human HLA-A,B,C antibody (Clone W6/32) (Biolegend; Cat #311423) and purified anti-human HLA-DR,DP,DQ antibody (Clone Tü39) (Biolegend; Cat #361702) were added at 20µg/mL. ImmunoCult Human CD3/CD2/CD28 T Cell Activator (Stemcell Technologies; Cat #10970) was added to the TILs as a positive control. After the incubation, the TILs were intracellularly stained for IFNγ and TNFα.

2.2.6.2. CFSE proliferation assay

MX063 expanded and edited TILs were washed twice with PBS and labelled with CellTrace CFSE (1µM) (ThermoFisher Scientific; Cat #C34554) for 10 minutes at room temperature. After this, FBS was added to stop the labelling (2 minutes incubation at room temperature). TILs were then washed and resuspended in TexMACS media (Miltenyi Biotec; Cat #130-097-196) with only IL-15 (0.1ng/mL) added. CFSE-labelled TILs were incubated with their autologous tumour cells at a 5:1 ratio (TILs:tumour) at 37ºC for 6-7 days prior to fluorescence cell sorting.

2.2.6.3. Killing assay

MX063 tumour cells were washed twice with PBS and labelled with CellTrace CFSE (2.5μM) (ThermoFisher Scientific; Cat #C34554) for 10 minutes at room temperature. After this, FBS was added to stop the labelling (2 minutes incubation at room temperature). Cells were then washed and resuspended in media for the assay (a 1:1 mixture of AIM-V + complete RPMI with 10% Human Serum). CFSE-labelled tumour cells were incubated for 16 hours with their autologous expanded TILs at the different ratios stated in the text and figure legends of Chapter 5. For the conditions were MHC blocks were included as controls, LEAF purified anti-human HLA-A,B,C antibody (Clone W6/32) (Biolegend; Cat #311423) and purified anti-human HLA-DR,DP,DQ antibody (Clone Tü39) (Biolegend; Cat #361702) were added at either 10 or 20μg/mL (as stated in the text and figure legends of Chapter 5). After the incubation period, the cells were stained with viability dye, washed, and resuspended in 150μL of FACS buffer. Counting beads (ThermoFisher Scientific; Cat #C16506) in 50μL PBS were added to each sample prior to data acquisition. The percentage of killing was calculated with the following formula:

$$\%\ of\ Killing = 100 - \left\{ \left[\frac{\left(\frac{Target\ Cells}{Counting\ Beads} \right)}{Mean\ Counting\ Beads\ for\ Control} \right] * 100 \right\}$$

2.2.6.4. Peptide screen

Lyophilised peptides were reconstituted in DMSO to 10nmols/μL. Pools of 5 or 20 peptides were generated (0.4-0.5nmols/peptide) and 100,000 TILs were added to each pool (in TexMACS media with no supplement added). TILs were incubated with the peptide pools for 16 hours in the presence of a protein transport inhibitor (Brefeldin A) (BD Biosciences; Cat #555029). After the incubation, the TILs were intracellularly stained for IFNγ and TNFα.

2.2.7. Single cell suspensions of tumours for flow cytometry analysis

Mice were euthanised at the end of the experiments and tumours were resected. Tumour samples were cut into small pieces (2-3mm) using sterile scalpels and digested with Collagenase (10U/mL, Gibco; Cat #17018029) and DNAse I (75µg/mL, Sigma-Aldrich; Cat #10104159001) at 37ºC for 1 hour, homogenised using a gentleMACS Octo Dissociator (Miltenyi Biotec) (program 37-h-TDK-2). The digested samples were then filtered through a 0.7µm cell strainer. Leukocytes were enriched by gradient centrifugation with Ficoll-Paque Plus (GE Healthcare; Cat #17-1440-03). Cells were analysed immediately for T cell profiling or frozen at -80ºC until analysis of tumour profiling.

Chapter 3. CRISPR/Cas9-mediated gene editing in cell lines, primary T cells and tumour infiltrating lymphocytes

3.1. Overview

The aim of this study was to develop a methodology that allowed efficient gene editing of tumour infiltrating lymphocytes (TILs) so as to render them resistant to the co-inhibitory signals that the tumour cells co-opt as a means to avoid immune attack. In this chapter, the different gRNAs tested for this purpose are discussed, as well as the different methods of delivery of the CRISPR/Cas9 components into the cells.

3.2. Introduction

3.2.1. CRISPR/Cas9 gRNAs design

The discovery of the CRISPR/Cas9 system and its emergence as one of the dominant technologies for genome engineering has generated a need for tools that facilitate the design of specific and effective gRNAs. As such, many different algorithms have been developed to rank the possible gRNAs for a specific genomic locus based on their predicted on-target activity, as well as their predicted specificity to reduce off-targets (Heigwer et al., 2014; Hodgkins et al., 2015; Montague et al., 2014). Each online tool has a different algorithm to calculate their efficacy and specificity scores; however, they all follow roughly the same workflow, as represented in Figure 3.1.

Regardless of the online tool of choice, the gRNA design will depend mainly on: a) the CRISPR approach that is being used (i.e. NHEJ-mediated knockouts, HDR-mutation, CRISPRa, CRISPRi) and b) the Cas9 chosen (i.e. SpCas9, SaCas9, Cpf1, etc). The CRISPR approach will define the gRNA's position relative to particular aspects of the gene. For example, if using CRISPRa, the gRNA should be -200bp to +1bp upstream of the transcription start site (TSS), however, if using CRISPRi, the gRNA should be -50bp to +300bp around the TSS (Konermann et al., 2015; Radzisheuskaya, Shlyueva, Müller, & Helin, 2016). If

the strategy is to generate a knockout via NHEJ, then the gRNA should be designed to target either a common coding exon (preferably as close to the 5' end of the coding region as possible) or known essential protein domain (Shalem et al., 2014; J. Shi et al., 2015; T. Wang, Wei, Sabatini, & Lander, 2014). In regard to the Cas9 chosen, the gRNA design will be restricted to the protospacer adjacent motif (PAM) sequence that the Cas9 needs. The PAM sequence serves as a binding signal for the Cas9 protein, but this sequence will vary depending on the type of Cas9 that is used. Hence, if using the SpCas9 the gRNA of choice will have to target a 20bp region of the genome that has a 3' NGG PAM sequence. Or, if using the SaCas9, the targeted sequence will have to have a 3' NNGRRT (most efficient) or NNGRRN PAM sequence. As such, the PAM restriction will continue to vary depending on the Cas9 of choice (Jinek et al., 2012; Ran et al., 2015).

Recently, it has been discovered that the targeting efficiency of the gRNAs is influenced by their GC content and specific bases at different positions of the gRNA sequence. In this regard, it has been shown that in *Drosophila*, gRNAs with three or fewer GCs in the six nucleotides closest to the PAM rarely reach a 60% mutation rate, but gRNAs with at least 4 GCs in that region nearly always have a mutation rate over 60% (X. Ren et al., 2014). Another study, based on a mammalian cell line, found that gRNAs with a total GC percentage within the range of 40%–60% are favoured for efficient on-target cleavage (X. Liu et al., 2016). In addition, it has been shown that a G nucleotide at position 1 greatly enhances targeting efficiency (Doench et al., 2014), whilst a G nucleotide is also strongly preferred at position 20, which is associated with the sequence preference in Cas9 loading (T. Wang et al., 2014).

Knowing the restrictions for the gRNA design means that, as long as there is a good annotated reference genome for the target organism, there isn't a need for the algorithms to design the gRNAs. There is the possibility to manually search the annotated genome for gRNAs that fit the criteria needed. However, the online design tools have the advantage that they give an *in silico* prediction of on-target efficiency and specificity. These predictions are useful, but one should be cautious not to rely too much on them as they are calculated solely based on the reference genome, and there may be sequence variations between the genome of the experimental cells/organism and the reference one.

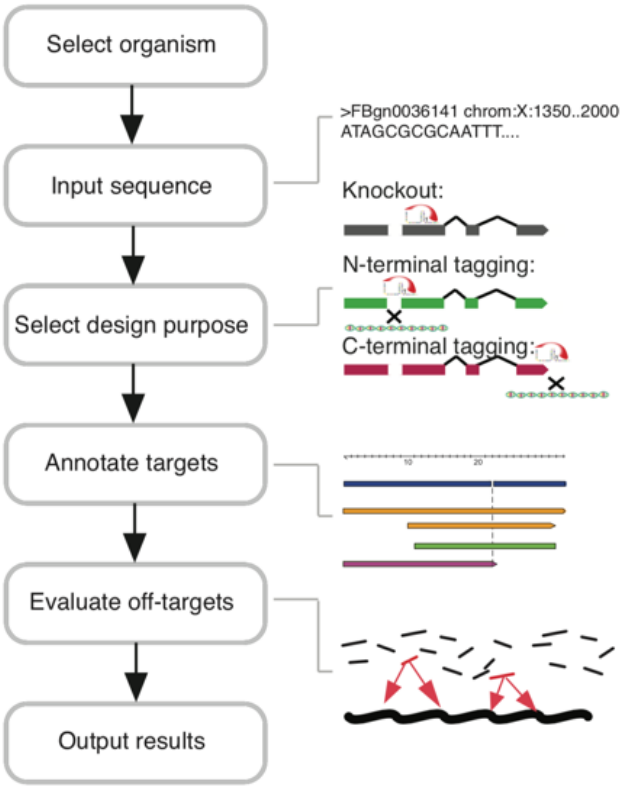

Figure 3.1. E-CRISP workflow. A representative example of the workflow that many of the online tools for gRNA design follow. Adapted from (Heigwer et al., 2014).

3.2.2. Delivery of CRISPR/Cas9 components

For efficient CRISPR/Cas9-mediated gene editing, the successful delivery of the gRNA and the Cas9 into the cells is essential. Vehicles used to deliver the CRISPR components into the cells can be divided in three groups: viral vectors, non-viral vectors, and physical delivery (Lino, Harper, Carney, & Timlin, 2018). Moreover, the CRISPR components can be delivered in DNA format, mRNA format, or as a ribonucleoprotein (RNP) complex. All of these delivery systems have advantages and limitations, which will vary depending on the experimental cells/organism of choice and the experimental aim. Here I will focus on the benefits and disadvantages of these delivery methods in the context of the gene editing of primary human cells in a translational/clinical setting.

3.2.2.1. Viral vectors

The most common viral vectors that have been used in the context of CRISPR are the lentivirus, the adenovirus, and the adeno-associated virus

(AAV). All of these viruses can infect both dividing and non-dividing cells, which makes them highly efficient delivery systems. Unlike adenoviruses and AAVs, lentiviruses integrate into the genome. This is a relative disadvantage for CRISPR delivery in a translational/clinical setting. This is because: a) integration can occur in unwanted locations, and b) the Cas9 delivery should be transient because of the potential for off-target activity. In contrast, adenoviruses have the safety advantage of not integrating into the genome, as well as having a bigger packaging capacity than that of AAVs (~8.5kb vs. ~4.5kb) (Wu, Yang, & Colosi, 2010). However, the strong disadvantage for adenoviruses (as well as for lentiviruses) in a clinical setting is that they both elicit strong immune responses (Ahi, Bangari, & Mittal, 2011; Follenzi, Santambrogio, & Annoni, 2007). AAVs have already been extensively used for gene therapy in a clinical setting (Daya & Berns, 2008). Moreover, late last year the first in-body CRISPR clinical trial with an AAV delivery system was given the go ahead (Sheridan, 2018), but unfortunately it is still too early to have any data from this trial. Some of the reasons why AAVs have been considered prime delivery vehicles for gene therapy are that: a) they are not known to cause any disease in humans (Hüser et al., 2017); b) there are many known AAV serotypes and it has been demonstrated that each serotype shows preferential delivery efficiency to specific cell types (Zincarelli, Soltys, Rengo, & Rabinowitz, 2008), and this can help improve targeted delivery to the cells or organ of interest; c) they can provide long-term expression of the delivered genomic material as exogenous DNA (Duan et al., 1998); and d) the infection of cells with this type of viral vehicle generates little to no immune response in the recipient (at least upon first infection) (Daya & Berns, 2008). However, it has been shown that AAVs will eventually elicit immune responses, generating capsid-specific antibodies (Chew et al., 2016), and sometimes even eliciting responses from $CD8^+$ cytotoxic T cells (Hauck et al., 2009). Furthermore, the advantage of providing long-term expression of the genomic material may not be a real advantage in the context of CRISPR. This is again because the Cas9 expression should be as transient as possible to reduce the risk of off-target activity. Because of this, research is being undertaken to generate an AAV-CRISPR system that either deletes or switches off the Cas9 after the editing has taken place (A. Li et al., 2019; Shen et al., 2018). Finally, one of the most significant disadvantages of AAV vectors is

their packaging capacity. These vectors only allow for ~4.5kb of genomic material to be packaged within them. This constraint in size makes the packaging of CRISPR components a challenge given that the SpCas9 (the most used type of Cas9) and gRNA alone are already ~4.2kb in size. Researchers have adopted different methods to circumvent this problem, such as using the SaCas9 instead of the SpCas9, given that it is considerably smaller (Ran et al., 2015); or using a dual AAV system, where one AAV construct delivers the SpCas9 and the other one delivers the gRNA (Yang et al., 2016). However, the dual AAV system adds more complexity than a single vector, as there is the need to validate co-infection of both AAVs in the same cell. Furthermore, the SaCas9 solution brings the complication of a longer PAM sequence and hence the greater limitation on sequences that are available for targeting.

3.2.2.2. Non-viral vectors

The non-viral vectors that have been most widely used as delivery vehicles are the cationic lipids nanoparticles and lipoplexes. The advantages of these vectors over the viral vehicles in a clinical setting is that they minimise safety risks and immunogenicity concerns, as well as reducing lot-to-lot variability. Furthermore, unlike viruses, these non-viral vectors are not limited to a size or type of genetic cargo they can carry. Hence, they can deliver the Cas9 and gRNA as plasmid DNA, as mRNA, or as an RNP complex. However, the transfection efficiency of these vehicles will vary depending on the nature and size of the genetic cargo, as well as on the target cell type. Regarding this, a study in 2015 investigated the efficient delivery of Cas9:gRNA complexes via lipid-mediated transfection and electroporation, in different mammalian cell lines including primary cells (Liang et al., 2015). In this study they found that in the eleven cell lines they tested (including human iPSCs, human keratinocytes, and human $CD34^+$ cord blood cells) electroporation consistently outperformed lipid-mediated transfection, and in many cases the lipid-mediated transfection efficiency was close to zero (Liang et al., 2015). Moreover, in hard-to-transfect primary T cells, it has been shown that the uptake of polyplexes (and hence, the transfection efficiency) is only ~10% (Olden, Cheng, Cheng, & Pun, 2019), and, even with the advancements made in the field of cationic polymers for the improvement of T

cell transfection, the best efficiency that has been achieved is only 25% (Olden, Cheng, Yu, & Pun, 2018). Finally, it has been shown that lipofection (i.e. lipid-based transfection) has a negative impact on viability of T cells, as it leads to TNFα secretion, apoptosis, and necrosis of lymphocytes (Ebert et al., 1997).

3.2.2.3. Physical delivery

The physical delivery methods work by using mild physical forces to temporarily open pores in the cell membranes so that the genetic cargo can reach its intended destination (Glass, Lee, Li, & Xu, 2018). These delivery methods can be divided into two widely used categories: microinjection and electroporation/nucleofection. The delivery of CRISPR components via microinjection has proven to be highly efficacious, with efficiencies approaching 100% (Horii et al., 2014). In this method of delivery, the Cas9:gRNA (in either DNA, mRNA, or RNP complex format) is directly injected into individual cells using a microscope and micron-scale needles. In addition to the high efficiency, this delivery method also has the added advantages of precisely controlled dosage and the assurance that the CRISPR components are delivered exactly to the intended site (i.e. pronucleus or cytoplasm) (Horii et al., 2014). However, there are some disadvantages to this form of delivery. The two main ones are: a) that it is a method that requires a high level of skill to perform, given that it induces damage to the cell membrane, and, if done incorrectly can cause apoptosis of the cells; and b) it is not a high-throughput system, as it has to be performed one cell at a time, which makes it an unsuitable delivery system in a clinical setting. On the contrary, the other main physical delivery method (i.e. electroporation/nucleofection) is a high-throughput delivery system. Electroporation uses high-voltage electrical currents to transiently permeabilise the cells allowing large biomolecules to pass through. A specific type of electroporation is the nucleofection, a method that allows the direct delivery of the genetic cargo into the cell nucleus by a combination of specific electric parameters and specific solutions (X. Zhang & Piedrahita, 2014). Nucleofection has been widely used as a delivery method in the CRISPR field, especially in hard-to-transfect primary cells, with impressive results (S. Kim, Kim, Cho, Kim, & Kim, 2014; Liang et al., 2015; Schumann et al., 2015; Seki & Rutz, 2018). This

delivery method can deliver the Cas9:gRNA as plasmid DNA, as mRNA, or as a RNP complex. However, so far the best efficiencies have been seen with the genetic cargo being delivered as a RNP complex (Liang et al., 2015). Some of the advantages of this delivery method are: a) it has the ability to transfect slow-proliferating cells or hard-to-transfect cells; b) unlike with some viral vectors, there is no concern about insertional mutagenesis caused by genomic integration; c) it provides a transient expression of the Cas9 protein (especially when delivered as a RNP complex), which decreases the potential for off-target activity (S. Kim et al., 2014; Liang et al., 2015); d) it is a high-throughput delivery system, with current nucleofector machines being able to perform large-scale transfections of up to $1x10^9$ cells (Dever et al., 2016). The main disadvantages of this system are: a) that it is costly; and b) that if the electrical current is not finely tuned for the cell of interest, it may generate irreversible changes to the physiology of its cell membrane and have a negative impact on the viability of the cell. However, many nucleofector companies have circumvented this limitation by generating optimised protocols for a variety of cells that favour high transfection efficiency and/or high viability of cells after transfection. The only disadvantage of these optimised protocols is that they are proprietary information, so there is no way of knowing their parameters, or indeed, of changing them.

There are three formats in which the CRISPR components can be delivered: a) as DNA (a plasmid encoding the Cas9 and the gRNA); b) as mRNA (both the Cas9 and the gRNA as RNA); or c) as a Cas9 RNP complex (Cas9 as protein and gRNA as RNA). Delivering the CRISPR components as DNA is a simple and low-cost strategy, and therefore it is widely used in laboratories. However, this format comes with the disadvantages of an accumulation of Cas9 protein in the transfected cells over time, as well as the risk of DNA-based cellular toxicity. This long persistence of Cas9 increases the probability of off-target effects (Liang et al., 2015), which is a key concern in the clinical setting. This probability of off-target effects is considerably reduced when using either mRNA or Cas9 RNP complexes for the delivery of the CRISPR components, as it has been shown that the expression of Cas9 in mRNA-transfected cells peaks at 4 hours post-transfection and diminishes after 48 hours. In Cas9 RNP-transfected

cells the level of Cas9 decreases even faster, with the protein being barely detectable at 48 hours post-transfection (S. Kim et al., 2014; Liang et al., 2015). A disadvantage when using mRNA to deliver the CRISPR components is that this type of molecule is less stable than DNA and highly susceptible to degradation by RNAses. Furthermore, for genome editing to take place, the Cas9 mRNA first needs to be translated into protein, while the gRNA may get degraded. Considering the above, it has been shown that the co-delivery of the Cas9 mRNA and the gRNA is very inefficient, but that delaying the delivery of the gRNA 4 to 8 hours post-delivery of the Cas9 mRNA restores the editing efficiency (Hendel et al., 2015). This suggests that the Cas9 protein protects the gRNA from degradation. In this sense, the Cas9 RNP has an advantage over the mRNA format, as delivering the Cas9 as a protein removes the need for translation to take place, and hence eliminates the possibility of gRNA degradation. Moreover, in a study performed in 2015, it was shown that the delivery of the CRISPR components as mRNA or as Cas9 RNP generated a higher editing efficiency compared to plasmid delivery in eleven different cell lines (this was in the context of electroporation-mediated delivery). Furthermore, it was also shown that in ten out of eleven cases Cas9 RNP outperformed mRNA, and in one case (in human $CD34^+$ cord blood cells) Cas9 RNP delivered via electroporation was the only format that produced a significant gene edit (Liang et al., 2015).

3.3. Aims

Although a number of clinical trials using CRISPR-edited autologous lymphocytes are already underway (NCT03399448, NCT03081715, NCT02793856), there is a lack of preclinical data in the field, especially regarding the CRISPR-mediated editing of TILs. In fact, two of the clinical trials previously mentioned are being performed with patients PBMCs, and the third one doesn't state where the autologous cells they are using come from (i.e. if they are peripheral or tumour infiltrating lymphocytes).

To date, regarding preclinical data, the editing of different genes using the CRISPR/Cas9 system has been successfully achieved in the field of CAR-T cells, as well as in healthy donors and patients PBMCs. However, there is a lack of information regarding gene editing of TILs via CRISPR. This could be due to the

limitations of obtaining patient samples, as well as the technical difficulties that arise when working with TILs.

Given this, in this study we aimed to develop a methodology for genomic engineering of primary human tumour infiltrating lymphocytes using the CRISPR/Cas9 technology. For this, the main objectives of the work presented in this chapter were the following:

- To design different crRNAs targeting PD1, TIM3, CTLA4, TIGIT, and LAG3.
- To generate cell lines that constitutively express the targets of interest to create a system to easily validate the gRNAs.
- To validate the gRNAs first in the generated cell lines, afterwards in healthy donors PBMCs, and finally in TILs from different patients.
- To ascertain the best method of delivery of the CRISPR components into the primary cells (i.e. mRNA vs RNP complexes, as well as different electroporator machines).
- To validate the efficient co-editing of two different targets edited at the same time.

3.4. Design of crRNAs and ligation into Cas9 vector

The first step in this project was to design the crRNAs (the targeting part of the gRNA) for the human targets of interest (PD1, TIM3, CTLA4, TIGIT, and LAG3). Importantly, one of the considerations when designing the crRNAs was that they targeted exons that were common to the different isoforms of the protein of interest. For this, three online design tools were used: E-CRISP, CHOPCHOP, and WGE. These online design tools were used in combination to increase their power. Hence, the crRNAs chosen were ranked within the top 20 of E-CRISP and, at the same time, had an efficiency of >50% according to CHOPCHOP (Heigwer et al., 2014; Montague et al., 2014). After choosing two crRNAs per target in this manner (except for PD1, for that target only 1 crRNA), their specificity was confirmed using the WGE online tool (Hodgkins et al., 2015). In regard to specificity, crRNAs that had 3 or more mismatches in other regions of the genome were accepted, however the majority of these regions were not exonic (i.e. they were intronic or intergenic). Both PD1 exon 1 (PD1e1) and TIM3

exon 3 (TIM3e3) gRNAs were validated sequences that were kindly provided to our laboratory by Professor Andy Sewell's laboratory from Cardiff University. For the first validation of the gRNAs (validation in cell lines with a Cas9+gRNA plasmid), a guanosine ('G') nucleotide at the 5' of the target sequence was added in two of the designed crRNAs (TIM3e3 and CTLA4e1) due to the transcription initiation requirement of a 'G' base for the human U6 promoter (S. Kim, Bae, Hwang, & Kim, 2017). Table 3.1 lists the designed crRNAs.

Name	Target Sequence	Target Gene	Exon	Strand	Genomic Location
PD1e1	GGGCGGTGCTACAACTGGGC TGG	*PD1*	1	-	chr2:241858782
TIM3e2	GGGCACGAGGTTCCCTGGGG CGG	*TIM3*	2	+	chr5:157106871
TIM3e3	GAGGTCACCCCTGCACCGACT CGG	*TIM3*	3	-	chr5:157104724
CTLA4e1	GTGGCTTGCCTTGGATTTCAG CGG	*CTLA4*	1	+	chr2:203867944
CTLA4e2	GGGACTCTACATCTGCAAGG TGG	*CTLA4*	2	+	chr2:203870848
TIGITe1	GCCCCTGGGCCCAGATCAGG AGG	*TIGIT*	1	-	chr3:114294076
TIGITe2	GGCCATTTGTAATGCTGACT TGG	*TIGIT*	2	+	chr3:114295681
LAG3e1	GACCATAGGAGAGATGTGGG AGG	*LAG3*	1	+	chr12:6772840
LAG3e2	GGGCTGAGGTCCCGGTGGTG TGG	*LAG3*	2	+	chr12:6773210

Table 3.1. Designed crRNAs. A table listing the gRNAs designed for this project and their location in the human genome. The PAM of each sequence is marked in red. Added nucleotides that weren't part of the original sequence are marked in blue.

Once the different gRNAs were designed, complimentary oligos were ordered and cloned into a human codon-optimised SpCas9 and chimeric guide RNA expression plasmid (plasmid pX330) (see materials and methods section for details on the cloning strategy). A schematic of the expression plasmid can be found on Figure 3.2A. Confirmation of proper cloning was performed via Sanger sequencing (Figure 3.2B-F) and this showed that the cloning of the crRNAs into the Cas9 expression plasmid had an efficiency of 100%.

Figure 3.2. Cloning of crRNAs into a human codon-optimised SpCas9 and chimeric guide RNA expression plasmid. (A) Schematic representation of Cas9 expression plasmid. Each crRNA was cloned into the region flanked by the BbsI restriction enzyme (after the U6 promoter and before the gRNA scaffold). Only one crRNA was cloned per plasmid. **(B-F)** Alignment of the

area of cloning with the reference map for **(B)** CTLA4, **(C)** TIM3, **(D)** TIGIT, **(E)** LAG3, and **(F)** PD1 crRNAs. Upper rows show the sequence of the reference maps that flank the region of cloning. Lower rows show the alignment of the experimental samples. A schematic representation of the area of cloning is also shown (white: part of the U6 promoter, blue: part of the gRNA scaffold, green: cloned crRNAs).

3.5. Generation of HEK293T cell lines constitutively expressing checkpoints of interest

Once the Cas9+gRNA expression plasmids were generated, the next objective was to produce a system to validate the gRNAs. The quickest way to test the efficiency of the gRNAs without adding confounding factors (such as methods of delivery, viability of primary cells, level of expression of targets, etc) is to use easy-to-transfect cell lines that have been engineered to constitutively express the targets of interest. However, it is important to note that this model of editing (i.e. editing a transgene) is an artificial one, as viral LTRs will open the chromatin at the target site. Hence, the gene locus will no longer be native and there may be multiple transgene copies per cell.

For the development of the system to validate gRNAs, HEK293T cells that had constitutive expression of PD1 and TIM3 (kindly provided by Professor Andy Sewell's laboratory from Cardiff University), and HEK293T cells that had constitutive expression of CTLA4 (kindly provided by Dr Martin Pule's laboratory from UCL Cancer Institute) were used (see materials and methods section for more information on these cell lines). Additionally, cell lines constitutively expressing TIGIT or LAG3 were generated.

For the generation of these cell lines, HEK293T cells were transfected and subsequently transduced with either the SFG.TIGIT plasmid (Figure 3.3A) or the SFG.LAG3 plasmid (Figure 3.4A). For the generation of these plasmids, a MMLV-derived retroviral vector with an eGFP cassette was used (the original vector was kindly provided by Dr Martin Pule's laboratory from UCL Cancer Institute), and the open reading frame of either TIGIT or LAG3 was added to this vector (see materials and methods for more details on the creation of these plasmids). After ligation of the insert (either TIGIT or LAG3) to the vector and transformation of competent bacteria with the plasmids, ten colonies from each were picked and

test digestions were performed to confirm the correct ligation of the backbone vector (SFG) with the insert (TIGIT or LAG3) (see material and methods section for more information). Seven out of 10 colonies gave the expected pattern of digestion for the SFG.TIGIT plasmid (Figure 3.3B), and only 2 out of 10 colonies had the correct pattern of digestion for the SFG.LAG3 plasmid (Figure 3.4B). Afterwards, 3 of the 7 correct SFG.TIGIT clones and both of the correct SFG.LAG3 clones were Sanger sequenced and this further validation confirmed that all of them had the correct ligation (Supplementary Figure 8.1).

HEK293T cells were transduce with the validated plasmids (see materials and methods for transfection and transduction strategy). Ten days after transduction of HEK293T cells (for SFG.TIGIT plasmid) and four days post-transduction (for SFG.LAG3 plasmid), cells were stained for either TIGIT or LAG3 and this confirmed that the overexpression of TIGIT was achieved at high efficiency (Figure 3.3C). The transduction efficiency for the SFG.LAG3 plasmid was also very high, although there were approximately 15% of cells that weren't successfully transduced. This was determined by calculating the percentage of LAG3 positive cells (Figure 3.4C), as well as the percentage of GFP positive cells (Supplementary Fig. 8.2) (given that the SFG.LAG3 has an eGFP cassette, the percentage of GFP^+ cells was an alternative way of validating the efficiency of transduction).

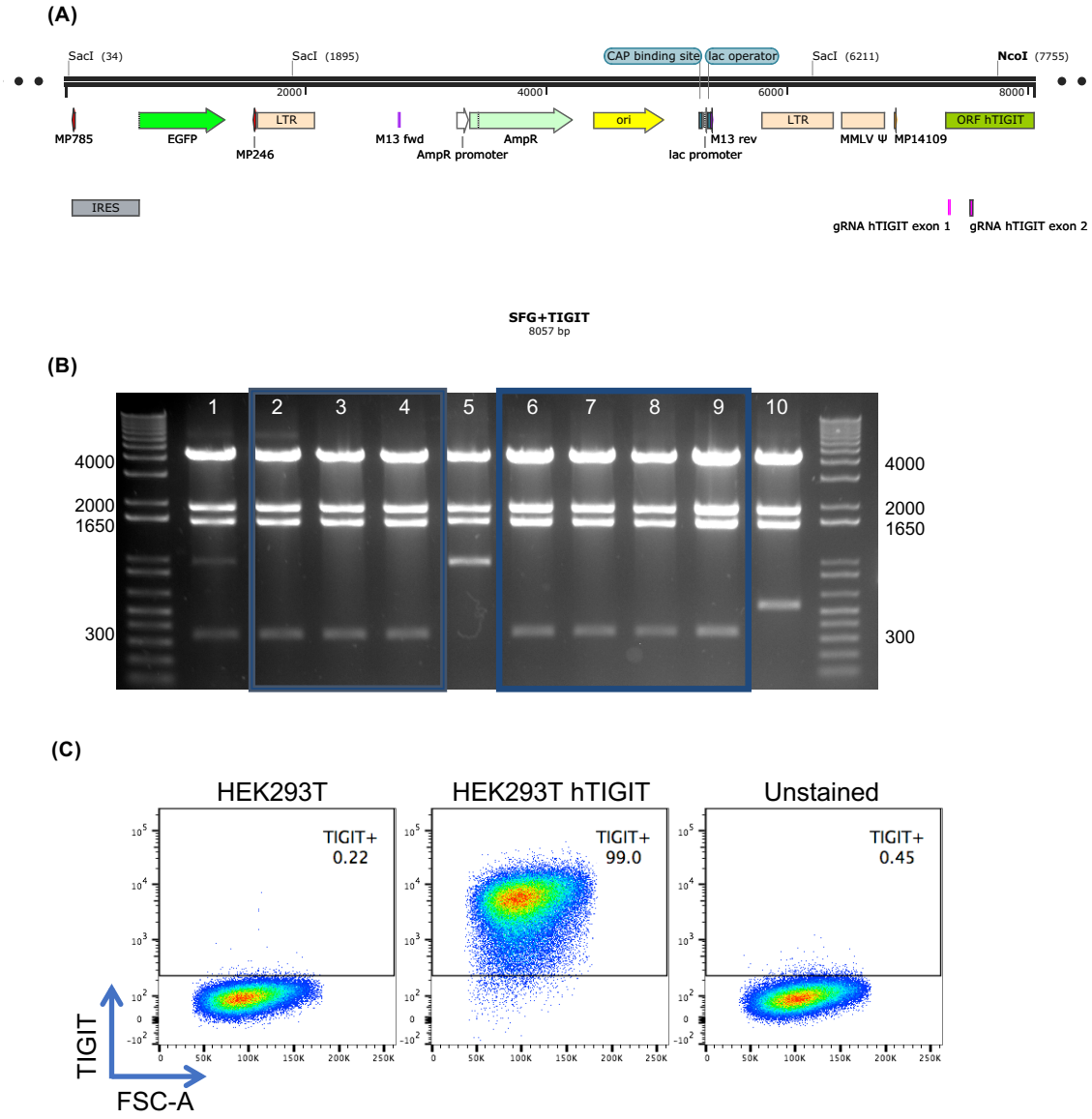

Figure 3.3. Generation of HEK293T cell line constitutively expressing TIGIT for validation of gRNAs. (A) Schematic representation of the plasmid used to transduce human TIGIT ORF (hTIGIT) into HEK293T cells. **(B)** Test digestion of SFG+TIGIT ligations using NcoI and SacI. Expected bands were: 4316bp, 1861bp, 1544bp, and 336bp. Clones with the correct digestion pattern are enclosed in blue. **(C)** TIGIT expression on HEK293T cells transduced to express hTIGIT constitutively, as well as of not transduced HEK293T cells as control (gated on live cells).

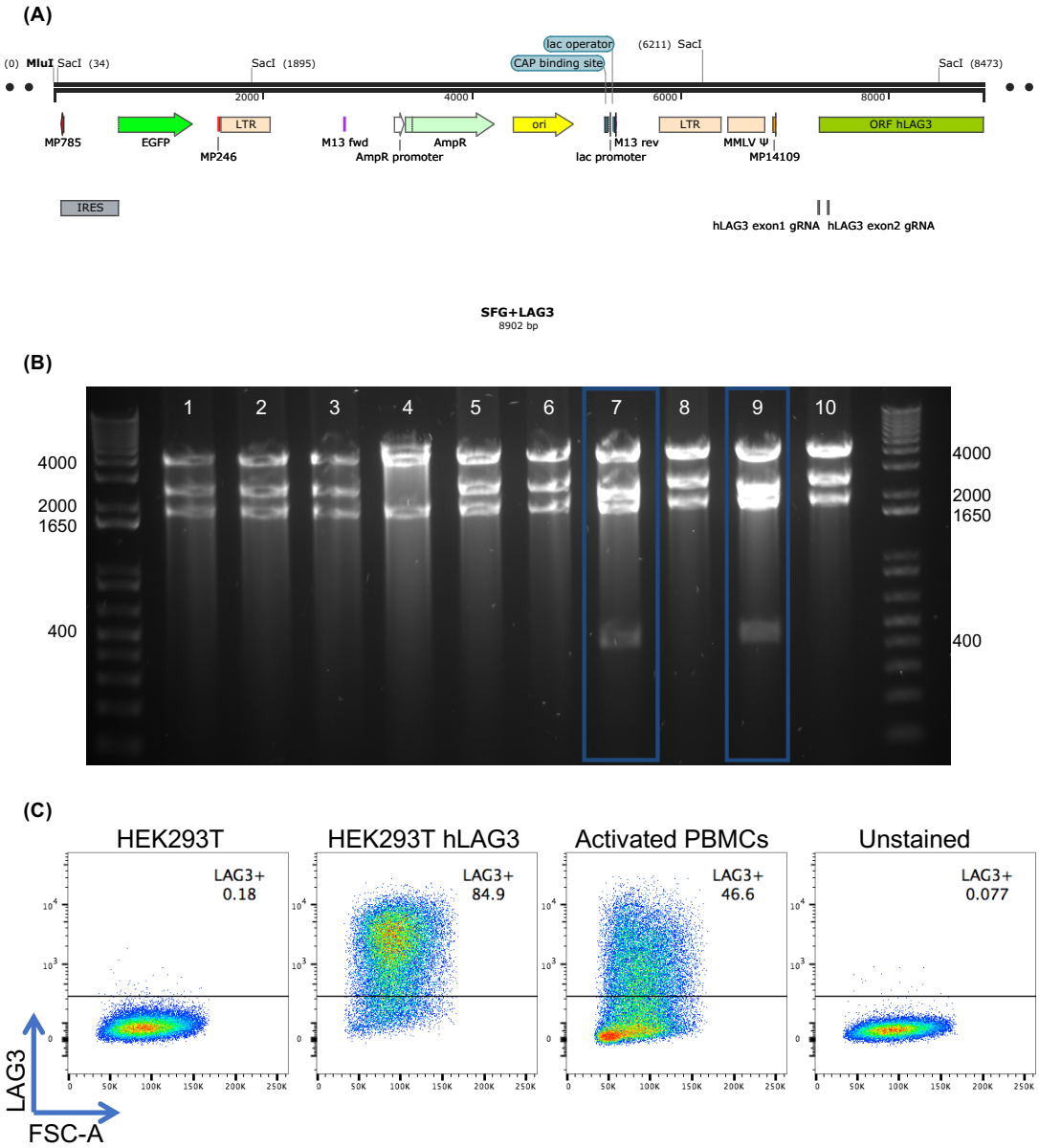

Figure 3.4. Generation of HEK293T cell line constitutively expressing LAG3 for validation of gRNAs. (A) Schematic representation of the plasmid used to transduce human LAG3 ORF (hLAG3) into HEK293T cells. **(B)** Test digestion of SFG+LAG3 ligations using MluI and SacI. Expected bands were: 4316bp, 2262bp, 1861bp, and 429bp (as well as a 34bp band that wouldn't be in the gel). Clones with the correct digestion pattern are enclosed in blue. **(C)** Flow cytometry plot of HEK293T cells transduced to express hLAG3 constitutively, as well as of not transduced HEK293T cells and of activated PBMCs as controls (all gated on live cells).

3.6. CRISPR/Cas9-mediated knockdown of targets via DNA transfection into cell lines constitutively expressing checkpoints of interest

HEK293T constitutively expressing PD1 and TIM3 (HEK293T PD1/TIM3) were transfected with plasmids encoding Cas9 and the different gRNAs (either PD1 exon 1 (PD1e1), TIM3 exon 2 (TIM3e2) or TIM3 exon 3 (TIM3e3)). Transfections were also performed with combinations of these plasmids, either Cas9PD1e1 + Cas9TIM3e2 or Cas9PD1e1 + Cas9TIM3e3. All of these transfections were performed in triplicate. Because of the cleavage kinetics of the CRISPR/Cas9 components (Liang et al., 2015), the cells were analysed via flow cytometry forty-eight and seventy-two hours post-transfection to test the level of expression of PD1 (Figure 3.5A and Figure 3.5C) and of TIM3 (Figure 3.6A and Figure 3.6B). The percentage of gene editing was determined by calculating the decrease in the percentage of $PD1^+$ or $TIM3^+$ cells compared to control. This calculation determined that a high editing efficiency was achieved (average of three experiments showed ~60% of gene editing for both targets when transfected individually). Moreover, quantification of the percentage of gene editing (corrected against the Cas9 control) was performed and statistical analysis confirmed that 72h post-transfection the percentage of edited cells was significant compared to Cas9 control for PD1-edited cells (61% $\pm$ 14%; $P<0.001$), for TIM3e2-edited cells (54% $\pm$ 9%; $P<0.001$), and for TIM3e3-edited cells (43% $\pm$ 11%; $P<0.01$). The editions proved to be successful to a lesser degree for the PD1+TIM3 combined conditions (Figure 3.5B and 3.6C). Of note, the cells that had been transfected only with the Cas9TIM3e2 plasmid showed ~15% of PD1 editing at 72h post-transfection (Figure 3.5B and 3.5C), however this proved not to be statistically significant. Importantly, all of the results retained statistical significance even when measuring percentage of PD1 positive cells or percentage of TIM3 positive cells without doing the correction against the Cas9 control (Supplementary Figure 8.3A and 8.3.C, respectively).

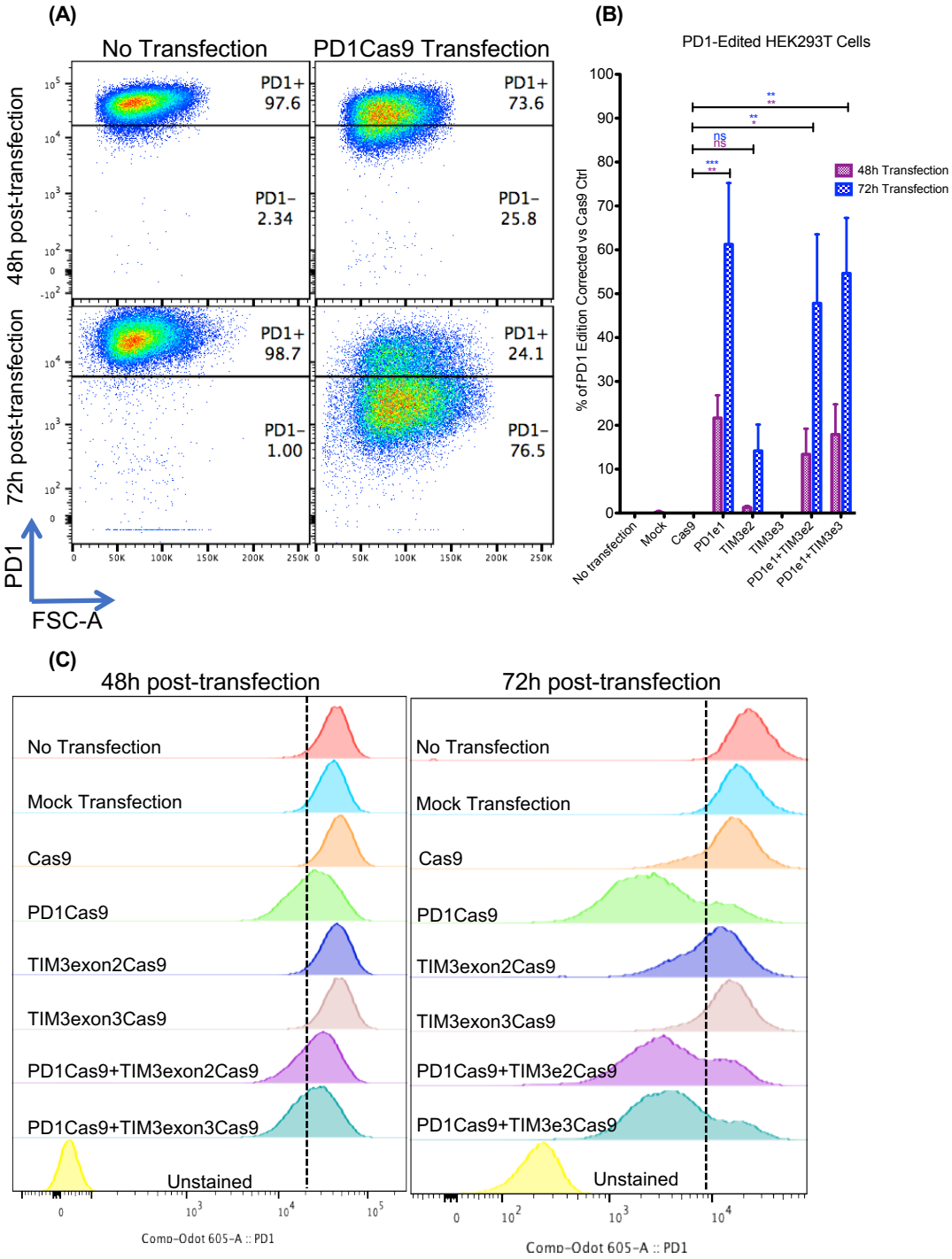

Figure 3.5. CRISPR/Cas9-mediated Knockdown of PD1. HEK293T PD1/TIM3 cells were transfected with Cas9PD1e1, Cas9TIM3e2 and Cas9TIM3e3 plasmids. **(A)** Flow cytometry plots showing PD1 expression 48h and 72h after transfection. Representatives from triplicates. **(B)** Percentage of PD1 edits corrected against Cas9 control at 48h and 72h post-transfection; n=3 (mean ± SEM). Percentage of edits was calculated with the following formula: 100*[(%PD1$^+$ cells in control (Cas9) - %PD1$^+$ cells in edited cells)/%PD1$^+$ cells in control (Cas9)]. One-way repeated measures ANOVA followed by Dunnett's Multiple Comparison was performed for each timepoint. **(C)** Histograms showing PD1 expression of all transfection conditions 48h and 72h after transfection. Representatives from triplicates.

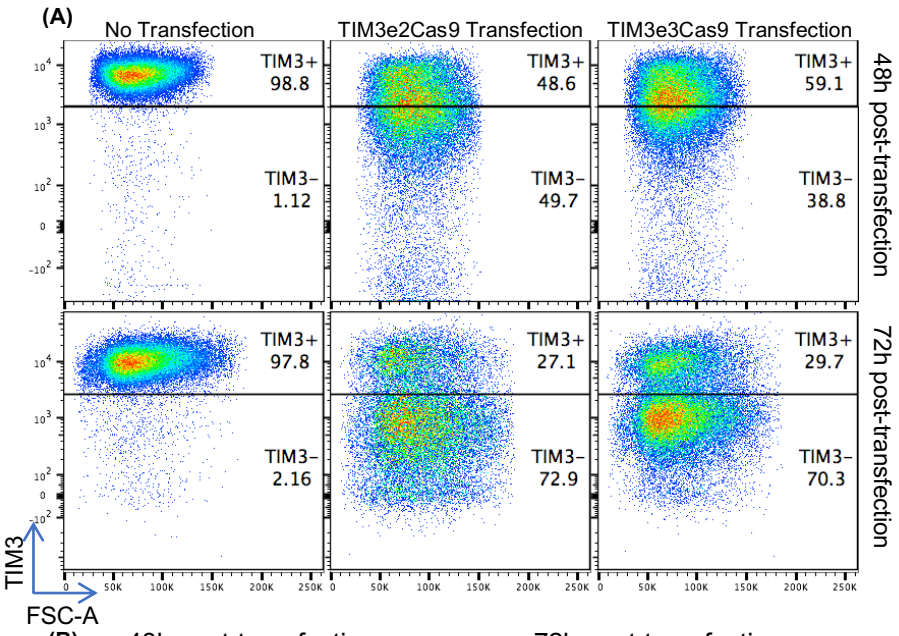
(A)
No Transfection
TIM3e2Cas9 Transfection
TIM3e3Cas9 Transfection
TIM3+ 98.8
TIM3- 1.12
TIM3+ 48.6
TIM3- 49.7
TIM3+ 59.1
TIM3- 38.8
48h post-transfection
TIM3+ 97.8
TIM3- 2.16
TIM3+ 27.1
TIM3- 72.9
TIM3+ 29.7
TIM3- 70.3
72h post-transfection
TIM3
FSC-A

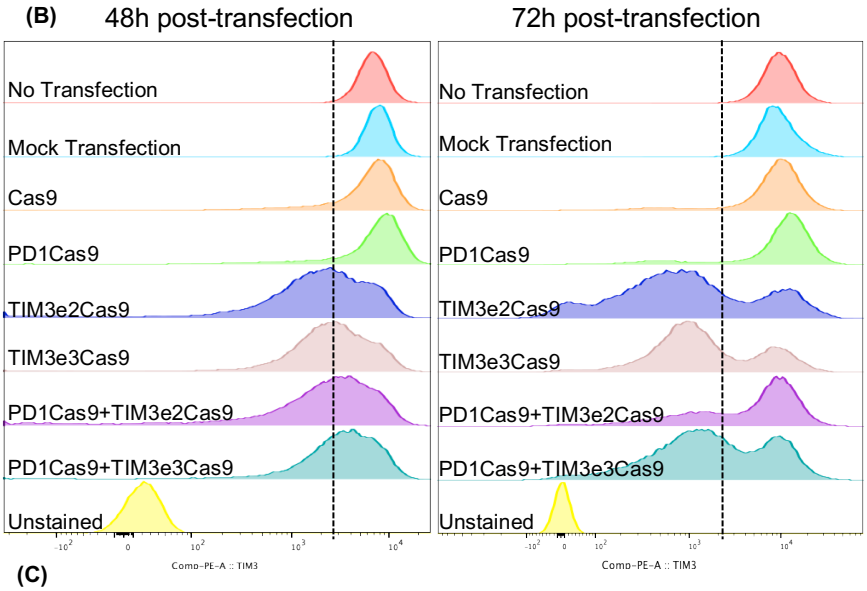
(B)
48h post-transfection
72h post-transfection
No Transfection
Mock Transfection
Cas9
PD1Cas9
TIM3e2Cas9
TIM3e3Cas9
PD1Cas9+TIM3e2Cas9
PD1Cas9+TIM3e3Cas9
Unstained
Comp-PE-A :: TIM3

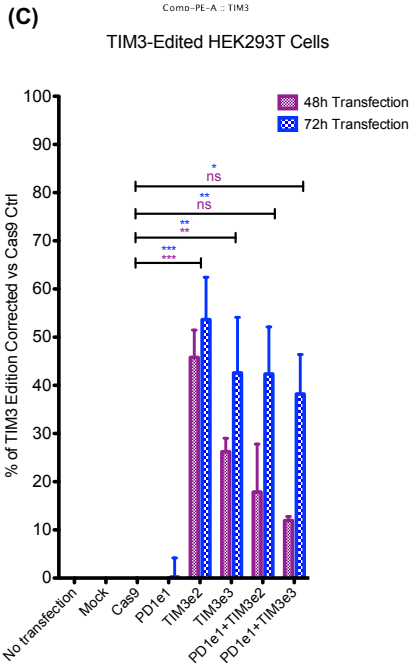
(C)
TIM3-Edited HEK293T Cells
48h Transfection
72h Transfection
% of TIM3 Edition Corrected vs Cas9 Ctrl
No transfection
Mock
Cas9
PD1e1
TIM3e2
TIM3e3
PD1e1+TIM3e2
PD1e1+TIM3e3
ns
ns

Figure 3.6. CRISPR/Cas9-mediated Knockdown of TIM3. HEK293T PD1/TIM3 cells were transfected with Cas9PD1e1, Cas9TIM3e2 and Cas9TIM3e3 plasmids. **(A)** Flow cytometry plots showing TIM3 expression 48h and 72h after transfection. Representatives from triplicates. **(B)** Histograms showing TIM3 expression of all transfection conditions 48h and 72h after transfection. Representatives from triplicates. **(C)** Percentage of TIM3 edits corrected against Cas9 control at 48h and 72h post-transfection; n=3 (mean ± SEM). Percentage of edits was calculated with the following formula: 100*[(%$TIM3^+$ cells in control (Cas9) - %$TIM3^+$ cells in edited cells)/%$TIM3^+$ cells in control (Cas9)]. One-way repeated measures ANOVA followed by Dunnett's Multiple Comparison was performed for each timepoint.

Following the same protocol, HEK293T constitutively expressing CTLA4 were transfected with plasmids encoding Cas9 and the different gRNAs (either CTLA4 exon 1 (CTLA4e1) or CTLA4 exon 2 (CTLA4e2)). Triplicates of these transfections were performed and expression of CTLA4 was tested by flow cytometry at 48h and 72h post-transfection (Figure 3.7A and 3.7B). The percentage of gene editing was determined by calculating the decrease in the percentage of $CTLA4^+$ cells compared to control. This calculation established that a significant editing efficiency was achieved (average of three experiments showed that ~40-45% of cells were edited for CTLA4). Furthermore, quantification of the percentage of gene editing (corrected against the Cas9 control) was performed and statistical analysis confirmed that 72h post-transfection the percentage of edited cells for cells transfected with either Cas9CTLA4e1 (36% ± 4%; $P<0.001$) or Cas9CTLA4e2 (46% ± 0.8%; $P<0.001$) plasmids was significant compared to Cas9 control (Figure 3.7C). Importantly, all of the results retained statistical significance even when measuring percentage of CTLA4 positive cells without performing the correction against the Cas9 control (Supplementary Figure 8.3B).

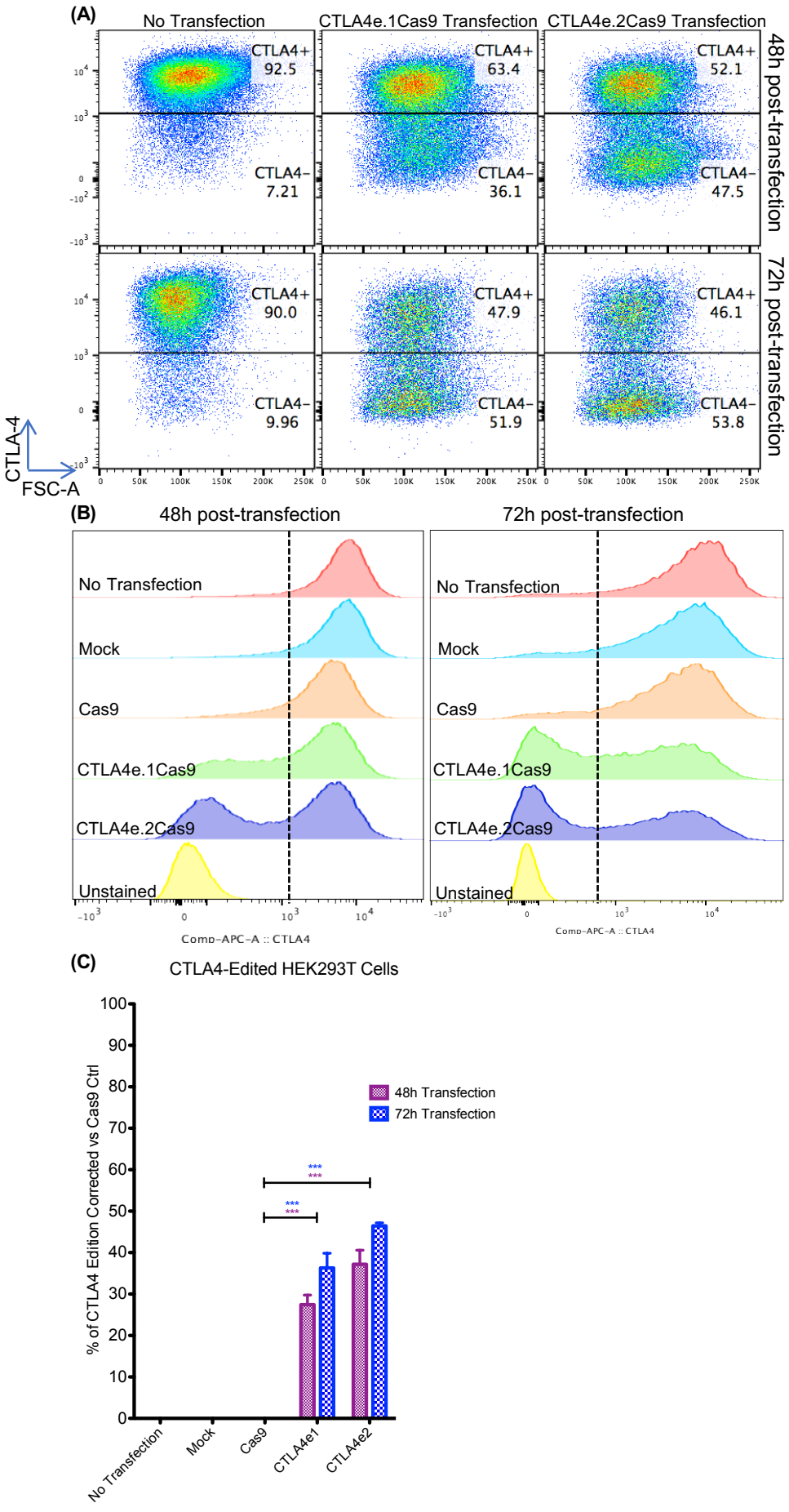
(A)
No Transfection
CTLA4e.1Cas9 Transfection
CTLA4e.2Cas9 Transfection
48h post-transfection
72h post-transfection
CTLA4+ 92.5
CTLA4- 7.21
CTLA4+ 63.4
CTLA4- 36.1
CTLA4+ 52.1
CTLA4- 47.5
CTLA4+ 90.0
CTLA4- 9.96
CTLA4+ 47.9
CTLA4- 51.9
CTLA4+ 46.1
CTLA4- 53.8
CTLA-4
FSC-A
(B)
48h post-transfection
72h post-transfection
No Transfection
Mock
Cas9
CTLA4e.1Cas9
CTLA4e.2Cas9
Unstained
Comp-APC-A :: CTLA4
(C)
CTLA4-Edited HEK293T Cells
% of CTLA4 Edition Corrected vs Cas9 Ctrl
48h Transfection
72h Transfection
***
***
***
***
No Transfection
Mock
Cas9
CTLA4e1
CTLA4e2

Figure 3.7. CRISPR/Cas9-mediated Knockdown of CTLA4. HEK293T cells constitutively expressing CTLA4 were transfected with Cas9CTLA4e1 and Cas9CTLA4e2 plasmids. **(A)** Flow cytometry plots showing CTLA4 expression 48h and 72h after transfection. Representatives from triplicates. **(B)** Histograms showing CTLA4 expression of all transfection conditions 48h and 72h after transfection. Representatives from triplicates. **(C)** Percentage of CTLA4 edits corrected against Cas9 control at 48h and 72h post-transfection; n=3 (mean ± SEM). Percentage of edits was calculated with the following formula: 100*[(%CTLA4$^+$ cells in control (Cas9) - %CTLA4$^+$ cells in edited cells)/%CTLA4$^+$ cells in control (Cas9)]. One-way repeated measures ANOVA followed by Dunnett's Multiple Comparison was performed for each timepoint.

HEK293T engineered to constitutively express TIGIT were transfected with plasmids encoding Cas9 and the different gRNAs (either TIGIT exon 1 (TIGITe1) or TIGIT exon 2 (TIGITe2)). Triplicates of these transfections were performed and expression of TIGIT was tested by flow cytometry at 48h and 72h post-transfection (Figure 3.8A and 3.8B). Furthermore, the percentage of gene editing was determined by calculating the decrease in the percentage of TIGIT$^+$ cells compared to control. With this calculation we were able to ascertain that the editing efficiency that was achieved was of ~25% for both plasmids (average of three experiments). It is worth noting that both gRNAs showed the same editing efficiency, even though during the *in silico* design the E-CRISP algorithm ranked them as #3 (TIGITe1) and #20 (TIGITe2), so a significant difference of efficiency between them was expected. This discrepancy could be due to the algorithm using a reference genome that is a slightly different build than the one used for the construction of the SFG.TIGIT plasmid (the E-CRISP tool states that it uses the GRCh38 human reference genome but at the moment Ensembl is already at GRCh38.p12), so there may be slight sequence variations between the two reference genomes used. Furthermore, quantification of the percentage of edits (corrected against the Cas9 control) was performed and the statistical analysis confirmed that 72h post-transfection the percentage of edited cells for cells transfected with either Cas9TIGITe1 (26% ± 3%; $P<0.001$) or Cas9TIGITe2 (26% ± 4%; $P<0.001$) plasmids was significant compared to Cas9 control (Figure 3.8C). Importantly, all of the results retained statistical significance even when measuring percentage of TIGIT positive cells without doing the correction against the Cas9 control (Supplementary Figure 8.3D). Even though the editing efficiency was not as high as with the gRNAs targeting the other checkpoints of interest, we

decided to proceed with these TIGIT gRNAs for the following experiments and to test their editing efficiency in the primary T cells.

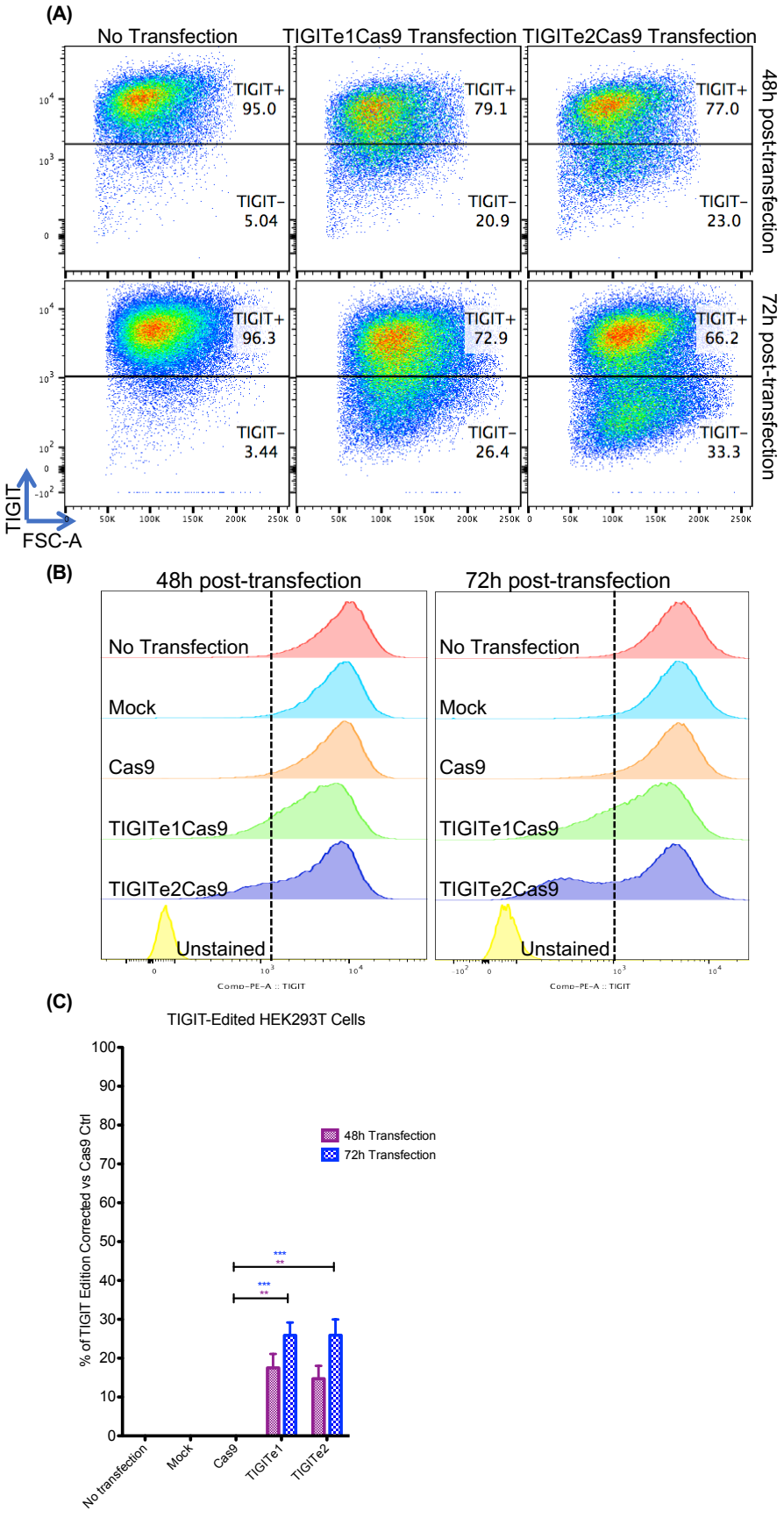

Figure 3.8. CRISPR/Cas9-mediated Knockdown of TIGIT. HEK293T cells constitutively expressing TIGIT were transfected with Cas9TIGITe1 and Cas9TIGITe2 plasmids. **(A)** Flow cytometry plots showing TIGIT expression 48h and 72h after transfection. Representatives from triplicates. **(B)** Histograms showing TIGIT expression of all transfection conditions 48h and 72h after transfection. Representatives from triplicates. **(C)** Percentage of TIGIT edits corrected against Cas9 control at 48h and 72h post-transfection; n=3 (mean ± SEM). Percentage of edits was calculated with the following formula: 100*[(%$TIGIT^+$ cells in control (Cas9) - %$TIGIT^+$ cells in edited cells)/%$TIGIT^+$ cells in control (Cas9)]. One-way repeated measures ANOVA followed by Dunnett's Multiple Comparison was performed for each timepoint.

Finally, the last gRNAs to be tested were the ones targeting LAG3. For this, HEK293T engineered to constitutively express LAG3 were transfected with plasmids encoding Cas9 and the different gRNAs (either LAG3 exon 1 (LAG3e1) or LAG3 exon 2 (LAG3e2)). Expression of LAG3 was tested by flow cytometry at 48h and 72h post-transfection (Figure 3.9A and 3.9B), and the percentage of gene editing was determined by calculating the decrease in the percentage of $LAG3^+$ cells compared to control. This determined that a ~25% of edits was achieved by 72h post-transfection for both gRNAs. It is worth noting that at 72h post-transfection the HEK293T cells that hadn't been transfected, the ones that were 'mock' transfected (transfected with no plasmid), and the ones that had been transfected with a plasmid encoding for Cas9 only with no gRNA seemed to be downregulating LAG3. This experiment was done only once (no triplicates), so no statistical analysis could be performed. However, by the time this experiment was performed, the validation of these gRNAs on primary T cells was already underway and this had led to the observation that the editing efficiency varied from the HEK293T cell lines to the actual cells of interest (i.e. some of the gRNAs that had the worst efficiency in the HEK293T cells performed the best on the primary T cells, or vice versa). This phenomenon of varying efficacy between cell types has been previously reported (Mandal et al., 2014). Because of this, it was decided that it was not worth repeating this experiment on the HEK293T cells.

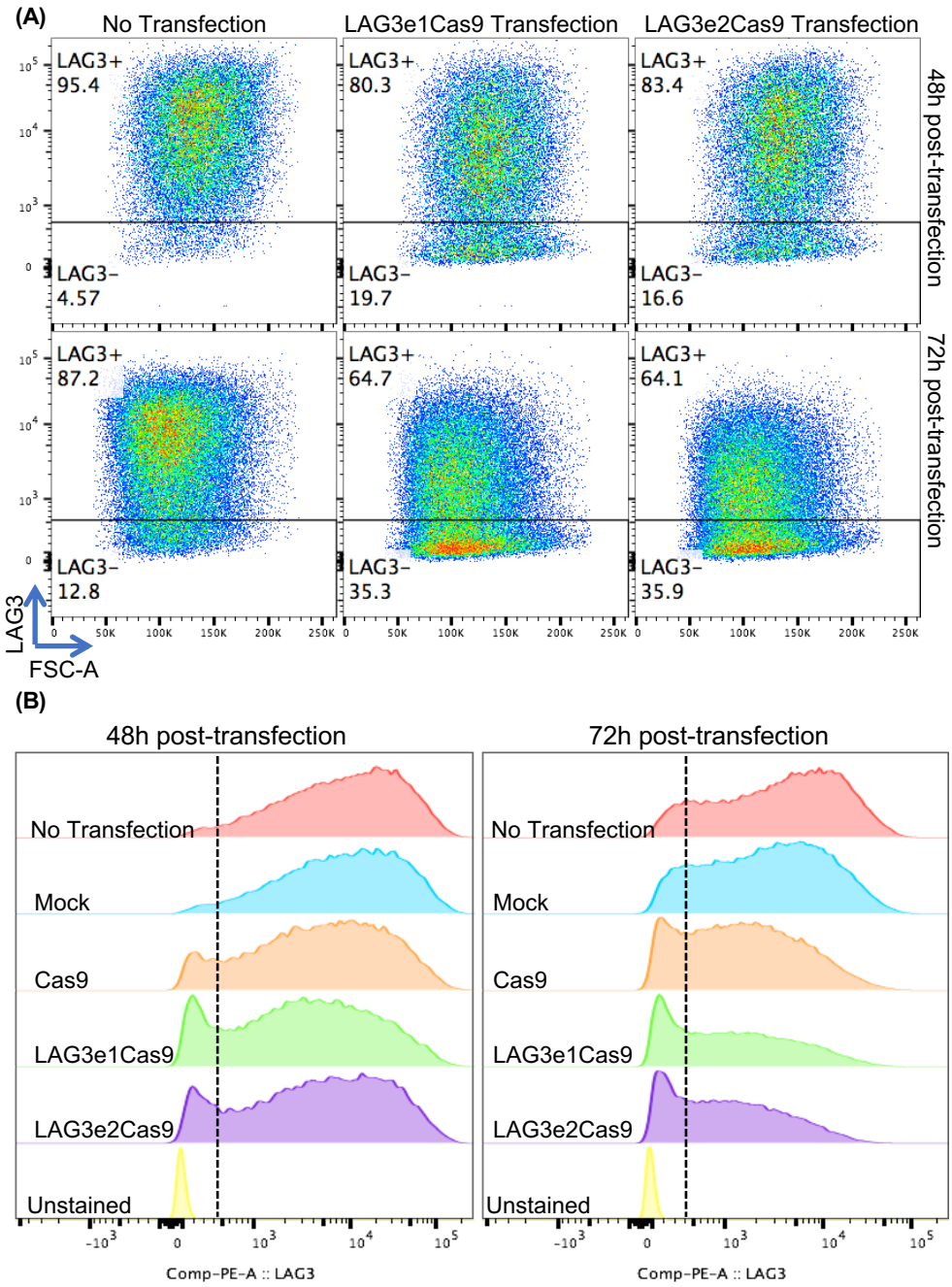

Figure 3.9. CRISPR/Cas9-mediated Knockdown of LAG3. HEK293T cells constitutively expressing LAG3 were transfected with Cas9LAG3e1 and Cas9LAG3e2 plasmids. **(A)** Flow cytometry plots showing LAG3 expression 48h and 72h after transfection. **(B)** Histograms showing LAG3 expression of all transfection conditions 48h and 72h after transfection.

3.7. Electroporation of Cell Line and Primary T cells (BTX electroporator)

After confirming the efficacy of the gRNAs in the engineered cell lines, the method of delivery of the CRISPR components into the cells needed to be

validated. Given that primary T cells are categorised as hard-to-transfect cells (Ebert et al., 1997), and because it has been shown that transfection of the CRISPR components as DNA into these cells is very inefficient (Mandal et al., 2014), it was decided to use electroporation as the delivery method, as well as trying mRNA or RNP complexes as the format of the CRISPR components. For this, at first, an "AgilePulse Max" BTX Electroporator (Harvard Apparatus) was employed. This electroporator had been used previously for two projects of TALEN-mediated editing of primary T cells (Menger et al., 2015, 2016), and as such it had already an optimised program of voltages that had been set up (see materials and methods sections for more information). However, at that point in time, this electroporator hadn't been used in any of the publications in the CRISPR field. There was a marked preference in the field for the Amaxa Nucleofector (Lonza) and the Neon Transfection System (Thermo Fisher Scientific), but there wasn't any literature comparing the efficiency of the different systems. Hence, as a first approach, this electroporator was tried with the optimised settings for delivery of TALENs into human primary T cells.

The HEK293T cells that constitutively expressed PD1 and TIM3 (HEK293T PD1/TIM3) were electroporated with the Cas9 (mRNA) and the PD1e1 gRNA (mRNA). As a control, these cells were also electroporated with GFP (mRNA). It has been shown that co-delivery of the Cas9 mRNA and the gRNA is very inefficient (Hendel et al., 2015). This can be explained by the fact that the gRNA may begin to degrade before the Cas9 mRNA has been translated (Glass et al., 2018). It has also been shown that delaying the delivery of the gRNA by 4 to 8 hours after the delivery of the Cas9 mRNA restores the editing efficiency (Hendel et al., 2015). Because of this, both conditions (co-delivery of Cas9 mRNA and gRNA, and delivery of Cas9 mRNA 8h prior to delivery of gRNA) were tested. Hence, the Cas9, gRNA, and GFP were *in vitro* transcribed (see materials and methods sections for more information) and these mRNA were electroporated into the cells (the 'Mock' control was electroporated twice without any mRNA, 8h apart). Seventy-two hours post-electroporation, the PD1 (Figure 3.10A, top row) and the GFP (Figure 3.10A, bottom row) expression of the cells were evaluated via flow cytometry. It is worth noting that the viability of the cells that were electroporated twice with a difference of 8h ('Mock' condition and 'Cas9+PD1 8h apart' condition) was greatly reduced compared to the other conditions ('No

Electroporation': 94% of viable cells, 'Mock': 43% of viable cells, 'GFP': 82% of viable cells, 'Cas9+PD1' codelivery: 80% of viable cells, and 'Cas9+PD1 8h apart' condition: 20% of viable cells; data not shown). This was to be expected as the electroporation generates pores on the cellular membrane and doing this twice in a very brief period of time was too much stress for the cells. It was hypothesised that it was because of this change in morphology of the cells that the PD1 expression was observed to be higher in these two conditions. The flow cytometry analysis showed no knockdown in the expression of PD1 for any of the conditions, and given that the gRNA had been validated with the same cell line, it was concluded that the problem was either the delivery method (the electroporation) or the format of the Cas9:gRNA (delivered as mRNA).

It is known that the optimal electroporation setup changes depending on the cell type (Potter & Heller, 2018), so it was hypothesised that the problem was that the setup used was for primary T cells and not for an adherent cell line like HEK293T cells. However, the cells that had been transfected with GFP mRNA showed a transfection efficiency of ~60% (measured by the percentage of GFP^+ cells), so the electroporation conditions used did generate pores that were sufficient for the GFP mRNA to pass through the membrane of the cells. Nonetheless, it is known that the electrical parameters used to electroporate cells need to be adjusted according to the size of the molecule that is being transfected. In this sense, it is worth considering that the GFP molecule is only ~700bp, and that the Cas9 and gRNA are ~4000bp and 100bp, respectively. This could explain why the GFP transfection is showing high efficiency but the Cas9+PD1e1 gRNA transfection is not.

The other possibility for lack of gene editing was that the delivery of the CRISPR components as mRNA was not working. This could be because of a) the quality of the *in vitro* transcribed mRNA (given that a quality control check was not performed to confirm proper poly(A) tailing, with only a quantitation by UV light absorbance being performed as confirmation of successful *in vitro* transcription); or because of b) the condition that is supposed to generate high editing efficiency ('Cas9+PD1 8h apart' condition) was too toxic for the cells, so any possible knockdown was masked by the lethality of the double electroporation. To test the latter possibility, HEK293T PD1/TIM3 cells were electroporated with a Cas9 RNP complex (Cas9 protein + *in vitro* transcribed

PD1e1 gRNA in a 1:1 molar ratio). Then, 72 hours post-electroporation the PD1 expression was measured via flow cytometry (Figure 3.10B). The PD1 expression remained unchanged in the Cas9 RNP complex transfection compared to controls. The Mock electroporation (electroporated once without any mRNA or protein) again showed poor viability (30% of viable cells; data not shown). Surprisingly, the viability of the Cas9 RNP electroporated cells was very similar to the no electroporation control ('No Electroporation': 90% of viable cells, 'Cas9 RNP': 82% of viable cells; data not shown).

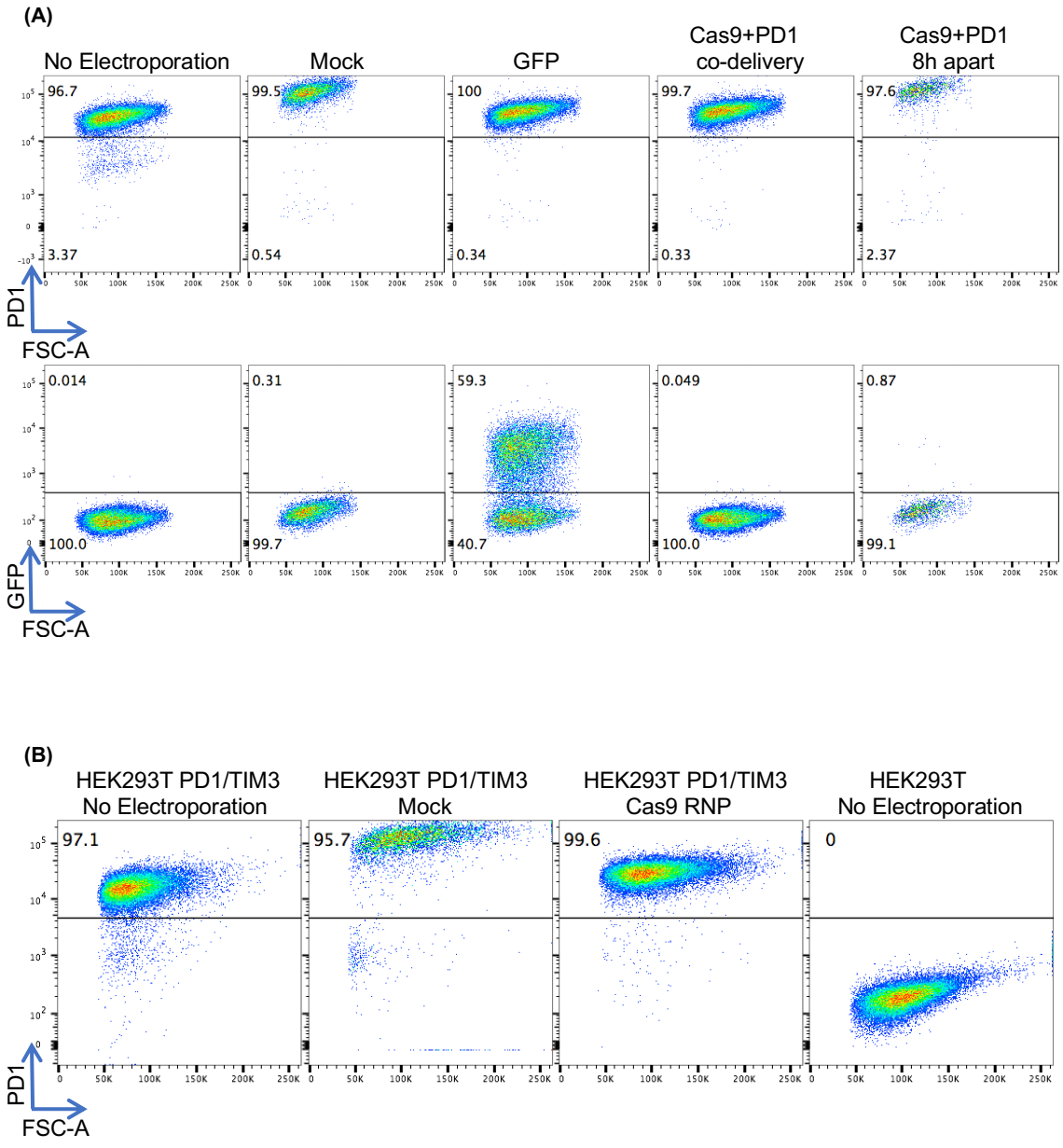

Figure 3.10. Electroporation of HEK293T PD1/TIM3 cells with Cas9:gRNA mRNA and with Cas9 RNP complex. (A) PD1 (top row) and GFP (bottom row) expression of HEK293T PD1/TIM3

cells electroporated with *in vitro* transcribed Cas9 and PD1e1 gRNA (either co-delivery or 8h apart (first the Cas9)) or with *in vitro* transcribed GFP. PD1 and GFP expression of the 'No electroporation' and 'Mock' controls are shown for comparison. Gated on live cells. **(B)** PD1 expression of HEK293T PD1/TIM3 cells electroporated with a Cas9 RNP complex (Cas9 protein + *in vitro* transcribed PD1e1 gRNA). PD1 expression of the 'No electroporation' and 'Mock' controls are shown for comparison, as well as of HEK293T cells that do not express PD1. Gated on live cells.

As the electroporation conditions were set up for primary T cells, and because these were the cells of interest, it was decided to continue the optimisation on the primary T cells. The efficiency of transfection and the viability of the cells post-electroporation was tested by electroporating activated PBMCs from a healthy donor with *in vitro* transcribed GFP. One day after electroporation, the viability of the electroporated cells and the level of expression of GFP was analysed via flow cytometry (Figure 3.11A). This showed a transfection efficiency of 74%; however, the viability of the electroporated cells was reduced compared to control (~50% vs. ~90%). Of these 47% live cells, the percentage that were $CD3^+$ cells was only ~70%, compared to almost 100% on the 'No Electroporation' control. The viability of the cells of interest (TILs) post-electroporation was also tested. TILs from a lung TRACERx patient (LTX11 TILs) were activated with αCD3, αCD28 and IL-2 (see materials and methods for more information) for 3 days prior to the electroporation. Most of these TILs did not survive the activation, so only one electroporation with *in vitro* transcribed GFP could be performed (a 'Mock' electroporation control could not be performed). The viability of the electroporated cells and the level of expression of GFP was analysed via flow cytometry one day after electroporation (Figure 3.11B). This showed a ~60% of transfection efficiency (measured by the percentage of GFP^+ cells) but it also revealed that most of the cells were dead. However, the viability of the cells was the same for the 'No Electroporation' condition, proving that the death of the cells was not caused by the electroporation, but most likely by the freezing/thawing and the activation. This experiment was repeated with LTX11 TILs that had been sorted for live cells prior to activating them, and the efficiency of transfection remained high (~45% of $CD8^+$ GFP^+ cells) (Figure 3.11C). These cells showed a

reduction on their viability of ~50% compared to the 'No Electroporation' control (Figure 3.11C).

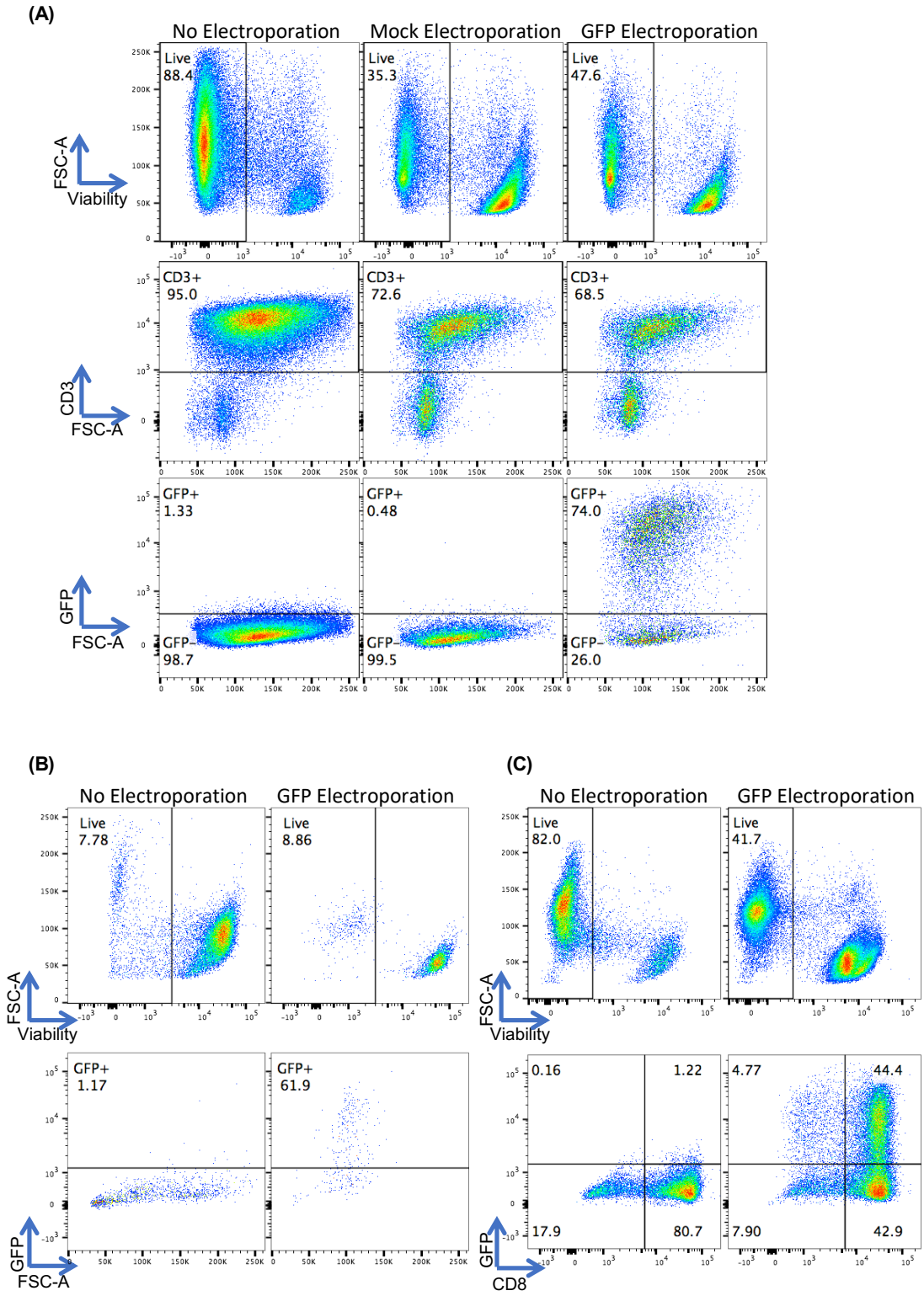

Figure 3.11. Electroporation of healthy donor PBMCs and of TILs with *in vitro* transcribed GFP. (A) Viability of electroporated and non-electroporated PBMCs, percentage of $CD3^+$ cells (gated on live cells) and of GFP^+ cells (gated on $CD3^+$ cells) are shown. **(B)** Viability of electroporated and non-electroporated TILs and level of GFP expression (gated on live cells) in

both conditions is shown. **(C)** Viability of electroporated and non-electroporated TILs and level of GFP expression (gated on live cells) in both conditions is shown.

To avoid the added complication of the viability of the TILs prior to electroporation, it was decided to continue to use healthy donors PBMCs for the optimisation of the delivery system. PBMCs that had been activated for 3 days were electroporated with either Cas9 mRNA and gRNA (co-delivery or 8h apart), Cas9 mRNA alone, GFP mRNA, or with nothing ('Mock' control). Three days post-electroporation, the viability of the cells and the level of PD1 expression was analysed via flow cytometry (Figure 3.12A). As with the HEK293T PD1/TIM3 cells, the PBMCs that had been electroporated twice within 8 hours ('Mock' condition and 'Cas9+PD1 8h apart' condition) showed a reduced viability compared to the 'No Electroporation' control and even to the co-delivery condition. Even though the GFP mRNA electroporation showed a high efficiency of transfection (60% of $CD3^+$ GFP^+ cells) (Figure 3.12B), the PD1 expression of the cells that had the CRISPR components co-delivered remained the same compared to the Cas9 alone control (this control was electroporated only once). The percentage of $PD1^+$ $CD3^+$ cells seemed to decrease in the condition of 'Cas9+PD1 8h apart' compared to the 'Mock' control (this control was electroporated twice in 8 hours). However, this decrease was due to the increase of the $CD3^-$ compartment, hence, the percentage of the $CD3^+$ $PD1^-$ cells remained unchanged when compared to the 'Mock' control (Figure 3.12A, red arrows). Taken together, these results show that the PD1 editing was unsuccessful.

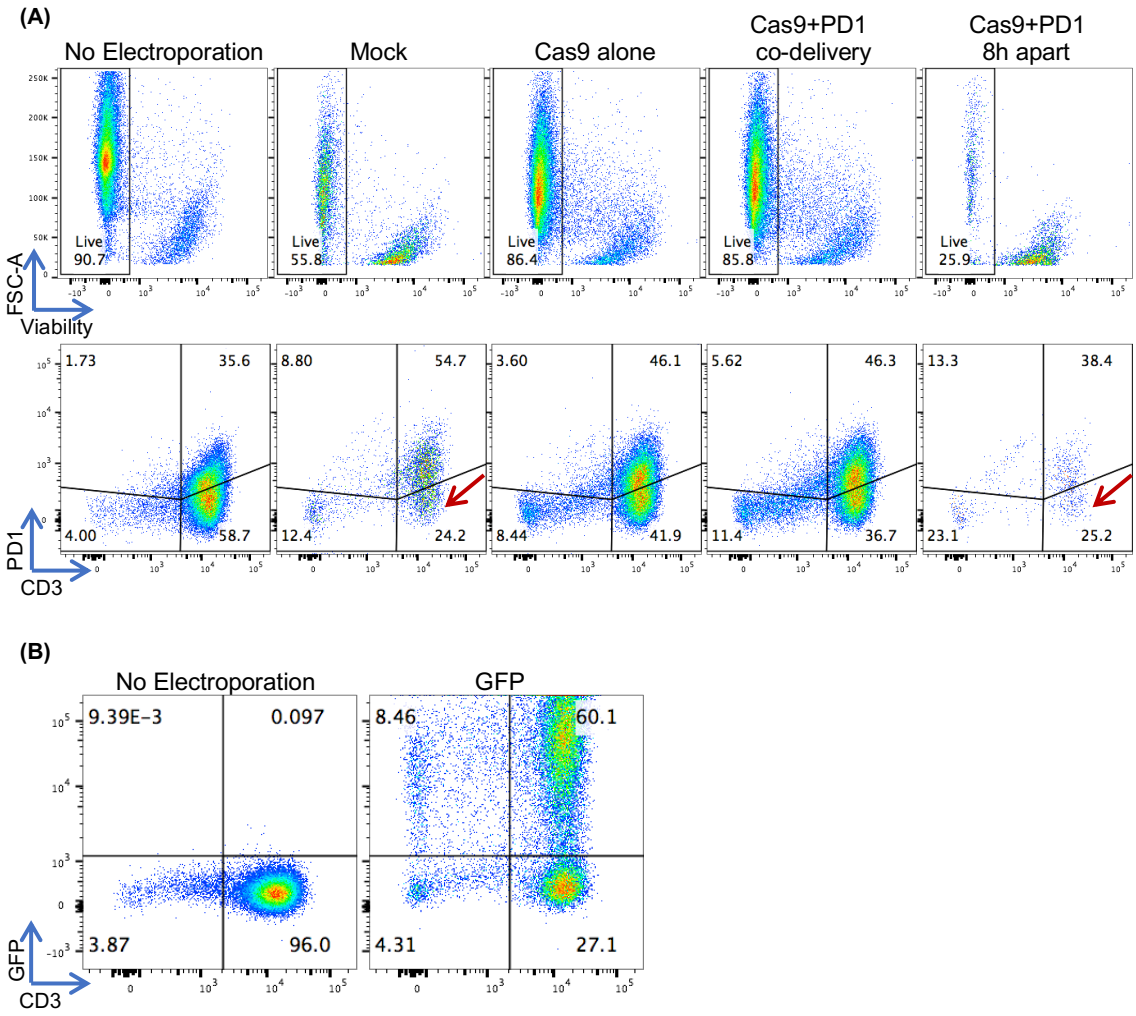

Figure 3.12. Electroporation of healthy donor PBMCs with *in vitro* transcribed Cas9 and gRNA or with *in vitro* transcribed GFP. (A) Flow cytometry plots showing the viability of the cells post-electroporation (top row) and the percentage of $CD3^+$ $PD1^+$ cells (bottom row) (gated on live cells) for the different conditions. Red arrows point to comparison of the $CD3^+$ $PD1^-$ compartment between mock control and 'Cas9+PD1 8h apart' condition. **(B)** Flow cytometry plots showing $CD3^+$ GFP^+ cells (gated on live cells) for the 'No Electroporation' and 'GFP' conditions.

To determine whether the problem was associated with the CRISPR components, healthy donor PBMCs were electroporated with a Cas9 RNP complex (Cas9 protein + *in vitro* transcribed PD1e1 gRNA in a 1:1 molar ratio). Seventy-two hours post-electroporation the PD1 expression and the viability of the cells were measured via flow cytometry (Figure 3.13). There was no significant decrease in the viability of the electroporated PBMCs compared to the 'No Electroporation' control, however the morphology of the cells did change (as seen by the difference in forward scatter between the electroporated cells and

the ‘No Electroporation’ control). It was hypothesised that this change in morphology was the reason behind the PD1 expression being higher in the electroporated cells (both the ‘Mock’ control and the ‘Cas9 RNP condition) compared to the ‘No Electroporation’ control. There was no difference of PD1 expression between the ‘Cas9 RNP’ condition and the ‘Mock’ control. Hence, the gene editing was unsuccessful.

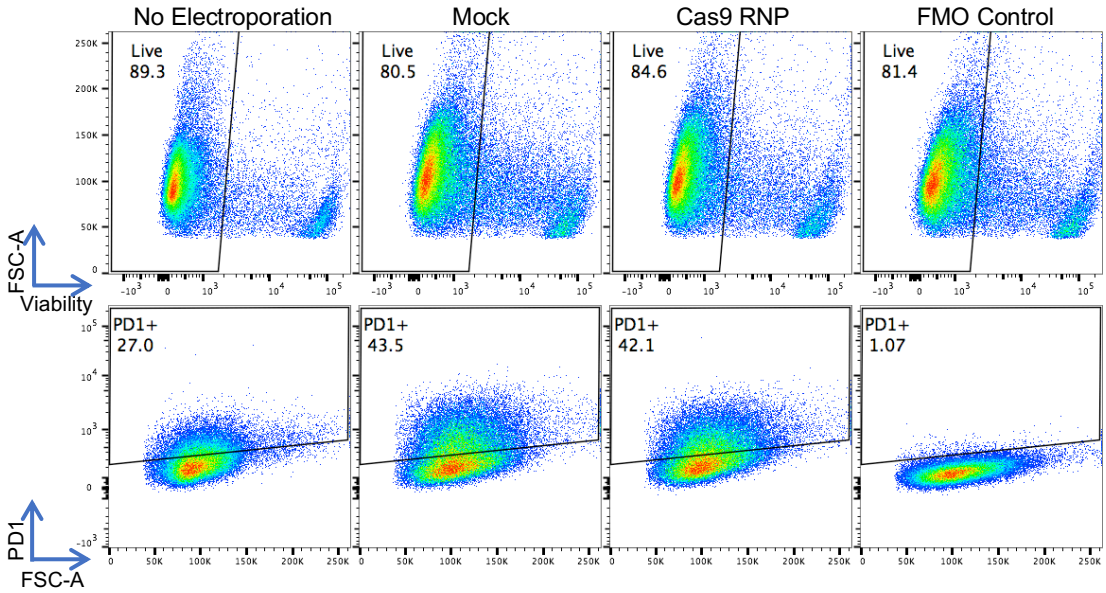

Figure 3.13. Electroporation of healthy donor PBMCs with Cas9 RNP complex. Flow cytometry plots that show the viability (top row) and the PD1 expression (bottom row, gated on live cells) of the healthy donor PBMCs that were electroporated with a Cas9 RNP complex (Cas9 protein + *in vitro* transcribed PD1e1 gRNA). Viability and PD1 expression of ‘No electroporation’ and ‘Mock’ controls are shown for comparison, as well as a fluorescence-minus-one (FMO) control of PD1 to show how the gating was established.

To rule out the possibility that the problem was related to the electroporation machine being utilised, it was decided to use the Amaxa 4D nucleofector as this machine had been shown to successfully deliver the CRISPR components into primary human T cells (Hultquist et al., 2016). Additionally, it was decided that further electroporations with Cas9 RNP complexes would be performed with commercially synthesised gRNAs (crRNA:tracRNA duplexes; see materials and methods section for more information) to avoid batch-to-batch variations of the *in vitro* transcribed gRNAs. In regard to this, it was later shown that *in vitro* transcribed gRNAs trigger a potent innate immune response that

leads to cytotoxicity in many cell types, including human primary T cells (S. Kim et al., 2018; Wienert, Shin, Zelin, Pestal, & Corn, 2018). In contrast, commercially synthesised crRNA:tracRNA duplexes contain chemical modifications that protect them from innate immune response activation as well as from degradation by cellular RNases.

3.8. Cas9 RNP complex electroporation of primary T cells and of TILs (Amaxa 4D Nucleofector)

3.8.1. Healthy donors PBMCs

The Amaxa 4D nucleofector (Lonza) has built-in setups (programs) for a broad range of cell types (i.e. the protocols have been optimised but they do not share the information about the voltages used). Hence, the programs are already set and the user only has to decide which program to use depending on the cell type and depending on if highest viability or highest efficiency is preferred. Hence, two different programs that were already optimised to give good viability and high efficiency of electroporation in human primary T cells were tested (FI-115 and EH-115). It is worth noting that the EH-115 program was already being used in the context of CRISPR-mediated editing of primary T cells by other groups (Hultquist et al., 2016; Rupp et al., 2017). The Amaxa 4D Nucleofector is supposed to be able to efficiently transfect both stimulated and unstimulated human T cells (which are even harder to transfect) (Aksoy, Aksoy, Czech, & Hammerbacher, 2018). To test this, unstimulated PBMCs from a healthy donor were electroporated with the pmaxGFP vector (the positive control that comes with the Lonza kits) using the two programs previously chosen (FI-115 and EH-115). A ‘No Pulse’ control (cells that are added to the electroporation cuvette with the pmaxGFP vector but that do not receive a pulse) and a ‘No DNA’ control (cells without any pmaxGFP added to them receive the pulse settings from the FI-115 program) were added. One day post-electroporation, the viability and the GFP expression of the cells were analysed via flow cytometry (Figure 3.14). There was a high percentage of viable cells when using either program, with only a ~20% decrease from the ‘No Pulse’ condition. Moreover, the transfection efficiency was very high for both programs (~70% GFP^+ cells). As both programs performed the same in terms of viability and efficiency, program EH-115 was chosen for all of

the following experiments, as it was the one that had been used the most in the field of CRISPR electroporation into primary T cells.

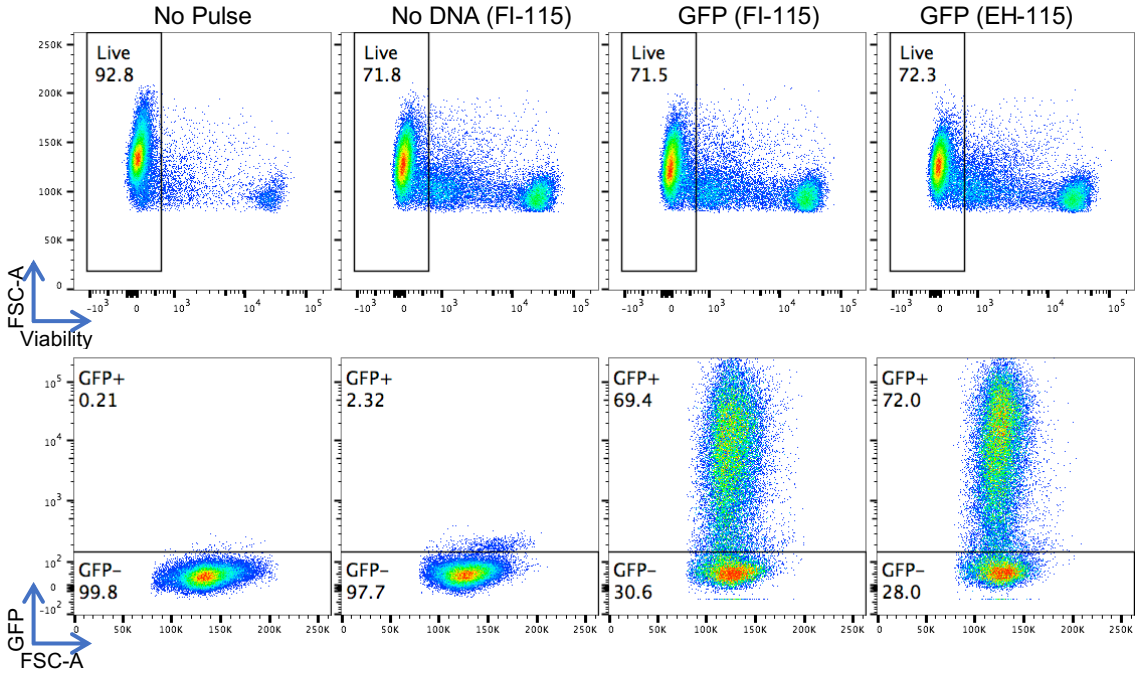

Figure 3.14. Electroporation of unstimulated healthy donor PBMCs with pmaxGFP vector. Flow cytometry plots that show the viability (top row) and the GFP expression (bottom row, gated on live cells) of the healthy donor PBMCs that were electroporated with a pmaxGFP vector using two different programs from the Amaxa nucleofector.

To test the efficiency of delivery of the CRISPR components using this machine, activated PBMCs were electroporated with either Cas9 protein alone (control), a Cas9 RNP complex with the previously validated PD1 gRNA targeting exon 1 (Cas9:PD1e1 RNP1), or a Cas9 RNP complex with a different PD1 gRNA also targeting exon 1 that had been previously shown to have a high editing efficiency on CAR T cells (Cas9:PD1e1 RNP2) (J. Ren, Liu, et al., 2017) (see materials and methods section for gRNA sequence). Both of these Cas9 RNP complexes were done in a 1:1 molar ratio of gRNA:Cas9. Three days post-electroporation, the expression of PD1 was measured via flow cytometry. This experiment was repeated 4 times and in 2 of those times the edited cells were reactivated post-electroporation (see materials and methods section for more information) as a further validation of the knockdown (i.e. if the knockdown is real then even with the reactivation of the cells there should be a population of cells

that remains PD1 negative). Representative flow plots of both the non-reactivated and reactivated edited cells are shown in Figure 3.15A. Quantification of the percentage of gene editing (corrected against the Cas9 control) was performed and statistical analysis confirmed that the percentage of edited cells for the cells electroporated with either Cas9:PD1e1 RNP1 (Non-Reactivated: 32% ± 4%; $P<0.0001$) (Reactivated: 28% ± 6%; $P<0.001$) or Cas9:PD1e1 RNP2 (Non-Reactivated: 21% ± 2%; $P<0.001$) (Reactivated: 13% ± 0.3%; $P<0.05$) was significant compared to Cas9 protein control (Figure 3.15B). Importantly, all of the results retained statistical significance even when measuring percentage of PD1 positive cells without performing the correction against the Cas9 control (Supplementary Figure 8.4). Even though both PD1e1 gRNAs tested here had a significant knockdown efficiency, the PD1e1 gRNA that had been validated on the HEK293T PD1/TIM3 cell line outperformed the other PD1e1 gRNA in all of the experiments performed. Hence, it was decided to use this gRNA for all further experiments. It is worth noting that the viability of the electroporated cells in all of the 'non-reactivated' conditions was between 60%-85% (data not shown).

As the conditions tested here produced a significant knockdown of PD1 in primary T cells (~30% editing efficiency), we decided to continue all future electroporations with the Amaxa nucleofector, as well as with the Cas9 RNP complexes using the commercially synthesised crRNA and tracrRNA. Additionally, the control for all future edits was improved from a 'Cas9 protein alone' control to a commercially synthesised crRNA that is non-targeting to the human genome ('scrambled gRNA'). This scrambled gRNA was complexed with the Cas9 protein to create a control Cas9 RNP complex for each experiment.

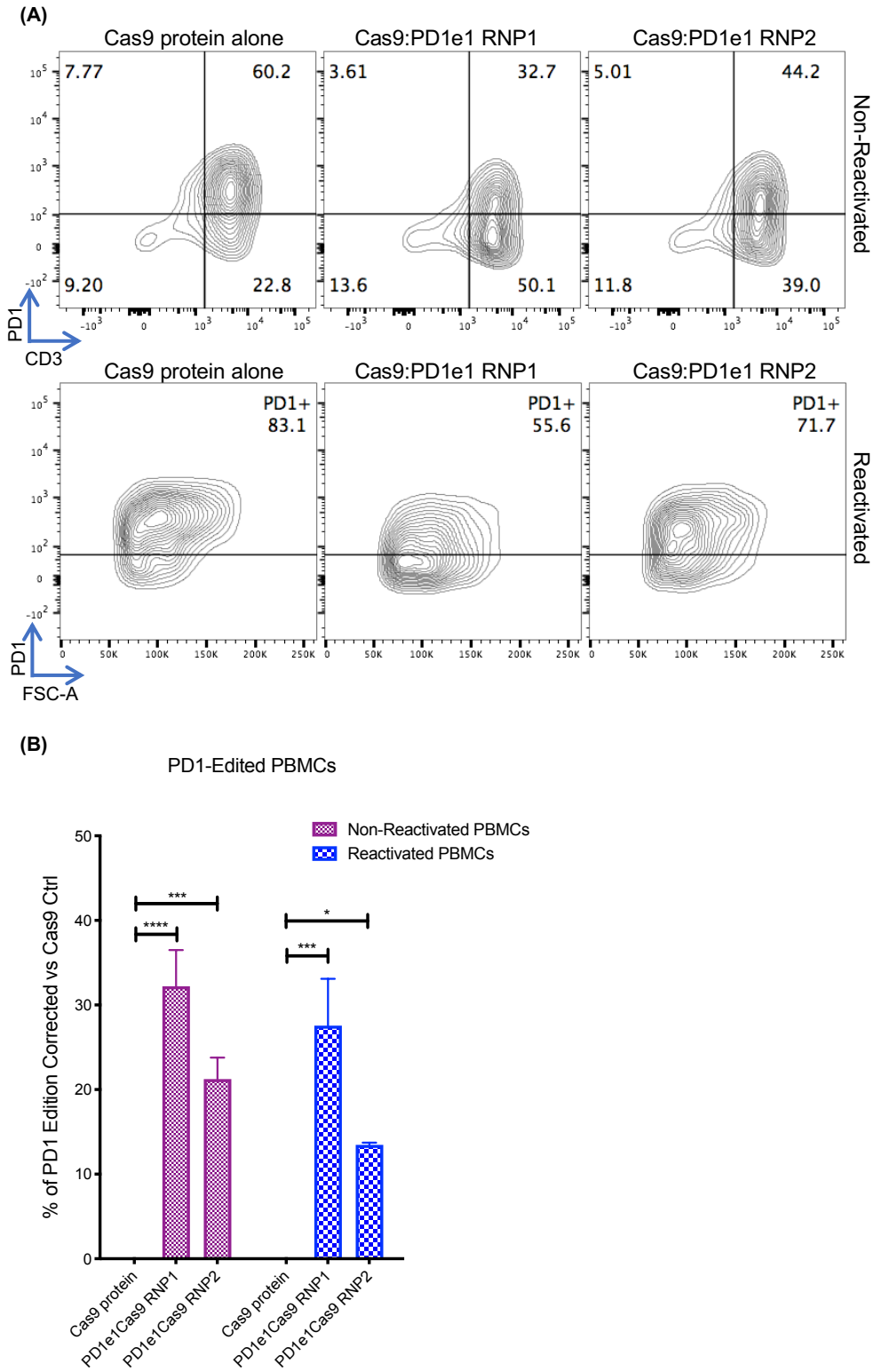

Figure 3.15. Amaxa electroporation of healthy donor PBMCs with Cas9 RNP complexes. **(A)** PD1 expression (gated on live cells) measured by flow cytometry. Representative flow plots of 4 experiments for the 'Non-Reactivated' condition and of 2 experiments for the 'Reactivated' condition. **(B)** Percentage of PD1 edits corrected against Cas9 control for Non-Reactivated (n=4 (mean ± SEM)) and Reactivated PBMCs (n=2 (mean ± SEM)). Percentage of edits was calculated with the following formula: 100*[(%PD1$^+$ cells in control (Cas9 protein) - %PD1$^+$ cells in edited

cells)/% PD1$^+$ cells in control (Cas9 protein)]. Two-way repeated measures ANOVA followed by Dunnett's Multiple Comparison was performed.

It had been previously reported that using two gRNAs directed against the same locus promoted an improved targeting efficacy on CD4$^+$ T cells (Mandal et al., 2014). Hence, to try to improve the editing efficiency, both PD1e1 gRNAs that were previously tested were co-delivered into activated PBMCs. Cas9 RNP complexes that had either a scrambled gRNA (control) or the 2 PD1e1 gRNAs were electroporated into the cells. These conditions were performed in duplicate and after electroporation all of the samples were divided into 'Non-Reactivation' (cells left with IL-2 only) and 'Reactivation' (cells left with αCD3, αCD28, and IL-2) conditions. Three days post-electroporation, the PD1 expression of both the Non-Reactivated and Reactivated cells was measured via flow cytometry (Figure 3.16A and 3.16C, respectively). The percentage of gene editing was determined by calculating the decrease in the percentage of PD1$^+$ cells compared to control. This calculation determined that a high editing efficiency was achieved when targeting PD1 with two different gRNAs (~60% editing efficiency in CD3$^+$ cells). Moreover, it was of interest to see that the gene editing was equally efficacious on CD8$^+$ cells (70% $\pm$ 3%) and CD4$^+$ cells (72% $\pm$ 3%) (Figure 3.16B), and that this percentage of gene editing was maintained (albeit, decreased by 10-15%) even after reactivating the cells (CD8$^+$: 56% $\pm$ 0.1%; CD4$^+$: 60% $\pm$ 0.5%) (Figure 3.16D). However, in this experiment we lacked the controls for the single PD1 gRNAs, and without them we cannot make any conclusions regarding the improved editing efficiency that the dual gRNA approach may confer. Of note, in this experiment the viability of the electroporated 'non-reactivated' PBMCs was ~45% (data not shown).

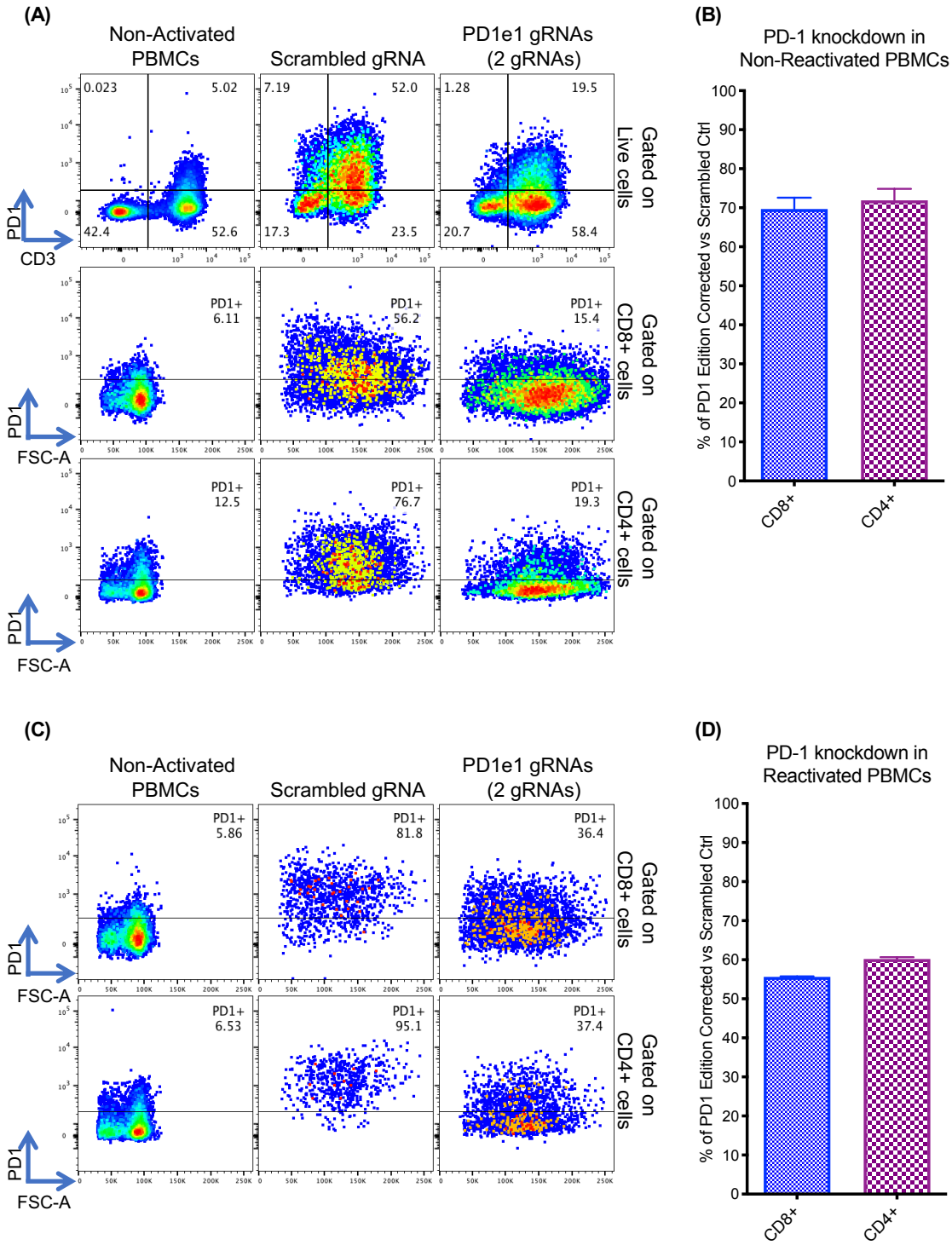

Figure 3.16. Dual gRNA electroporation targeting PD1 exon 1. (A) Flow cytometry plots of 'Non-Reactivated' cells showing expression of PD1 in the whole population of live cells (top row), and in $CD8^+$ and $CD4^+$ cells (middle row and bottom row, respectively). Representative from duplicates. **(B)** Percentage of PD1 edits corrected against scrambled ctrl in 'Non-Reactivated' $CD8^+$ and $CD4^+$ cells; n=2 (mean ± SEM). Percentage of edits was calculated with the following formula: 100*[(%$PD1^+$ cells in control (Scrambled gRNA) - %$PD1^+$ cells in edited cells)/%$PD1^+$ cells in control (Scrambled gRNA)]. **(C)** Flow cytometry plots of 'Reactivated' cells showing expression of PD1 in $CD8^+$ and $CD4^+$ cells (top row and bottom row, respectively). Representative

from duplicates. **(D)** Percentage of PD1 edits corrected against scrambled ctrl in 'Reactivated' $CD8^+$ and $CD4^+$ cells; n=2 (mean ± SEM). Percentage of edits was calculated with the following formula: 100*[(%$PD1^+$ cells in control (Scrambled gRNA) - %$PD1^+$ cells in edited cells)/%$PD1^+$ cells in control (Scrambled gRNA)].

By comparing the editing efficiency of the cells targeted with 2 PD1 gRNAs (~60%) against the editing efficiency of the cells from the last experiment that were targeted with only 1 PD1 gRNA (~30%), it was concluded that the dual gRNA approach definitely increases the editing efficiency in primary T cells. Albeit, this is with the caveat that the comparison was done between experiments. However, even though the editing efficiency improves two-fold when using a dual gRNA approach, this entails the disadvantage of an increase in the possibility of off-target effects, which would be detrimental in a clinical setting. Moreover, the dual gRNA approach of this experiment was performed with a total 2:1 molar ratio (gRNA:Cas9), whilst the single gRNA approach done previously was performed with a 1:1 molar ratio. Hence, the increase in the editing efficiency could be due to the synergistic effect of the two gRNAs or to the excess of gRNA. Indeed, it has been recently shown that providing the gRNA in a 2:1 or even in a 3:1 excess molar ratio dramatically increases the editing efficiency (Seki & Rutz, 2018). To test if this was the case, activated PBMCs were electroporated with Cas9 RNP complexes that had either scrambled gRNA in a 2:1 molar ratio (control), the previously validated PD1e1 (in a 1:1 molar ratio and in a 2:1 ratio), and the previously validated PD1e1 + the PD1e1 from the literature (J. Ren, Liu, et al., 2017) (2:1 molar ratio total). Three days post-electroporation the viability of the cells (Figure 3.17A, top row) and the PD1 expression (Figure 3.17A, bottom row) was analysed via flow cytometry. Quantification of the percentage of gene editing corrected against the scrambled control for both $CD4^+$ and $CD8^+$ cells was performed (Figure 3.17B). This showed that the viability of the cells was similar between conditions (~60% for the 1:1 molar ratio and ~54% for the 2:1 molar ratio conditions), and that increasing the gRNA concentration had a positive effect in the editing efficiency of both $CD8^+$ and $CD4^+$ cells (there was a ~1.8 fold improvement in the editing efficiency from the 1:1 molar ratio condition to the 2:1 molar ratio). It also showed that the use of two different gRNAs achieved the best editing efficiency in both $CD8^+$ and $CD4^+$ cells (there was a ~1.3 fold improvement

in the editing efficiency compared to the 2:1 molar ratio condition, and a ~2.4 fold improvement compared to the 1:1 molar ratio).

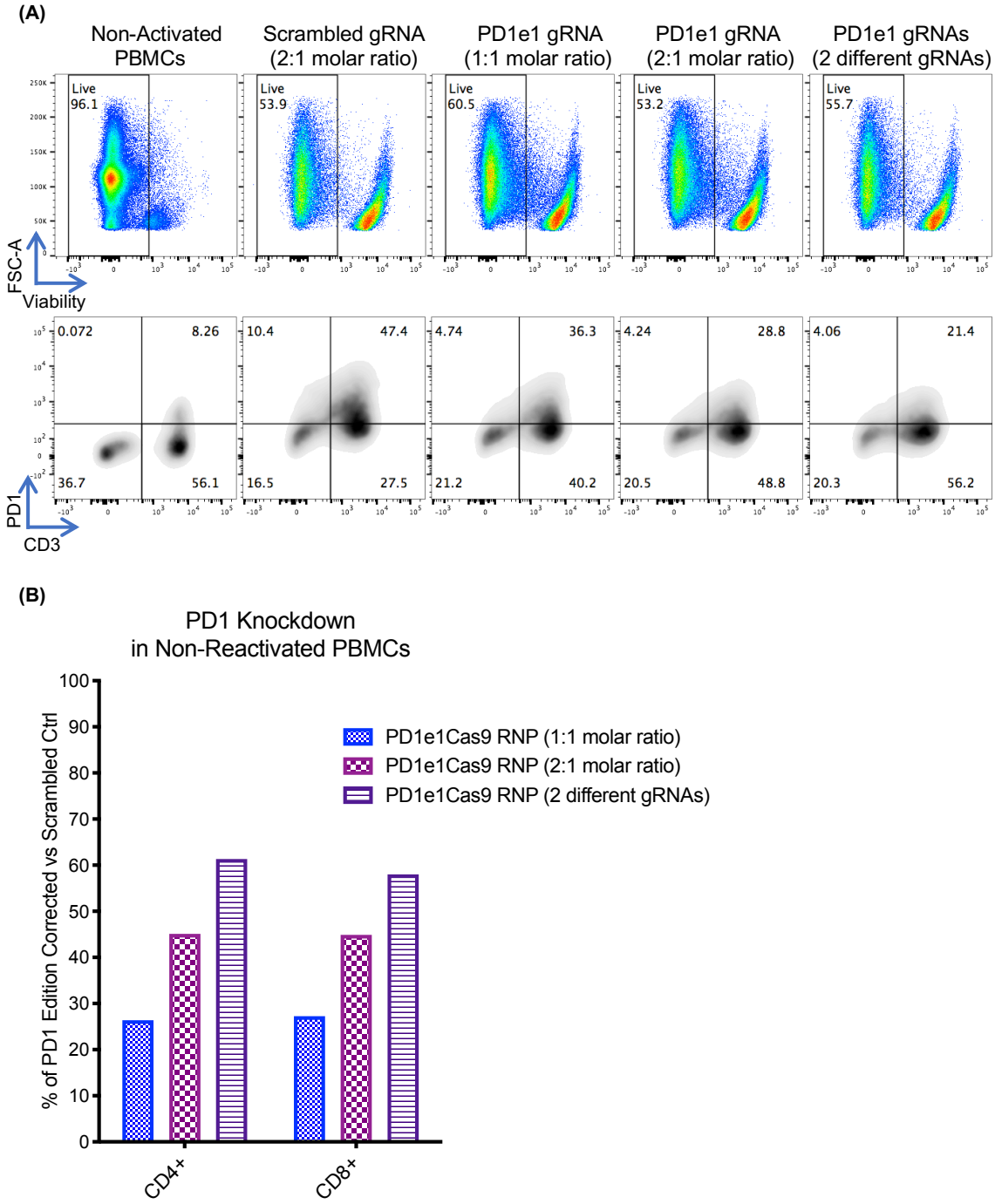

Figure 3.17. PD1 editing of healthy donor PBMCs with Cas9 RNP complexes with different molar ratios and with combination of PD1 gRNAs. (A) Flow cytometry plots showing viability of cells (top row) and percentage of $PD1^+$ $CD3^+$ cells (bottom row, gated on live cells) for all conditions. Non-activated PBMCs shown as comparison. **(B)** Quantification of PD1 gene editing in $CD4^+$ and $CD8^+$ cells corrected against the scrambled control; n=1. Percentage of editing was calculated with the following formula: 100*[(%$PD1^+$ cells in control (Scrambled gRNA) - %$PD1^+$ cells in edited cells)/%$PD1^+$ cells in control (Scrambled gRNA)].

Together with the results from the previous experiments, this data shows that the best efficiency was achieved with a combination of two different gRNAs that target the same locus. However, it has been previously stated that the SpCas9 tolerates mismatches between the gRNA and the target DNA at different positions of the guide RNA sequence (Hsu et al., 2013), hence there is a possibility of off-target effects with any gRNA used. This possibility increases with the employment of more gRNAs, and, as the future objective for this project was to perform multiplex gene editing by using gRNAs that target different checkpoints of interest at the same time, it was decided to keep to one gRNA per target. Henceforward, it was decided to use a 2:1 molar ratio (gRNA:Cas9 protein) when generating the Cas9 RNP complexes, as this condition also showed an increase in the editing efficiency.

The validation for the other targets of interest was performed in parallel in both PBMCs and TILs, hence, for some of the gRNAs the validation took place on TILs and not on PBMCs (see next section for TILs results). Furthermore, it was decided not to continue with the optimisation of TIM3, as it was shown that the two previously validated gRNAs had an editing efficiency of less than 10% in PBMCs (Supplementary Figure 8.5A) as well as in TILs (see next section). Likewise, it was decided not to pursue the validation of the CTLA4 gRNAs. Even though on PBMCs CTLA4e1 showed a good editing efficiency (Supplementary Figure 8.5B and 8.5C), the decision to stop working on this target was due to the fact that CLTA4 has been intensely studied in the clinical setting in the context of antibodies and, in this context, it has been proven to be more toxic and less efficient than PD1 in clinical trials (Larkin et al., 2015).

As a final optimisation in healthy donor PBMCs, Cas9 RNP complexes were generated with previously validated PD1, TIGIT, and LAG3 gRNAs that targeted exon 1 of each of these proteins. These Cas9 RNP complexes (2:1 molar ratio of gRNA:Cas9) were electroporated into activated PBMCs from 4 different healthy donors. Only the gRNAs targeting exon 1 of these proteins were tested as a comparison performed on TILs showed that the editing efficiency for both TIGIT and LAG3 was best for the gRNAs targeting the first exon (see next section for results on TILs). After the electroporation, the samples were divided into ‘Non-Reactivated’ (cells left with IL-2 only) and ‘Reactivated’ (cells left with

αCD3, αCD28, and IL-2) conditions. Three days post-electroporation, the expression of PD1, TIGIT, and LAG3 on both the non-reactivated and the reactivated cells was measured via flow cytometry. Representative flow cytometry plots are shown in Figure 3.18A and 3.18C, respectively. Quantification of the percentage of gene editing corrected against the scrambled control was performed for both the 'Non-Reactivated' condition (Figure 3.18B) and the 'Reactivated' condition (Figure 3.18D). This analysis showed that the percentage of PD1 gene editing was significant on both the 'Non-Reactivated' (40% ± 1%; P<0.001) and 'Reactivated' (42% ± 2%; P<0.001) cells that had been targeted with the PD1 gRNA, but not on the ones targeted with either TIGIT or LAG3 gRNA, and the same applied to the TIGIT-edited (Non-Reactivated: 87% ± 5%; P<0.001) (Reactivated: 76% ± 8%; P<0.001) and the LAG3-edited cells (Non-Reactivated: 79% ± 6%; P<0.001) (Reactivated: 73% ± 5%; P<0.001). Furthermore, the results retained statistical significance even when measuring the percentage of PD1, TIGIT, or LAG3 positive cells without correcting against the scrambled control (Supplementary Figure 8.6). These results showed a very high editing efficiency for the TIGITe1 gRNA and LAG3e1 gRNA, as well as a high editing efficiency for the PD1e1 gRNA. It is worth noting that, as expected, the electroporation of the Cas9 RNP complexes decreased the viability of the cells (~45-50% viable cells depending on donor) (data not shown).

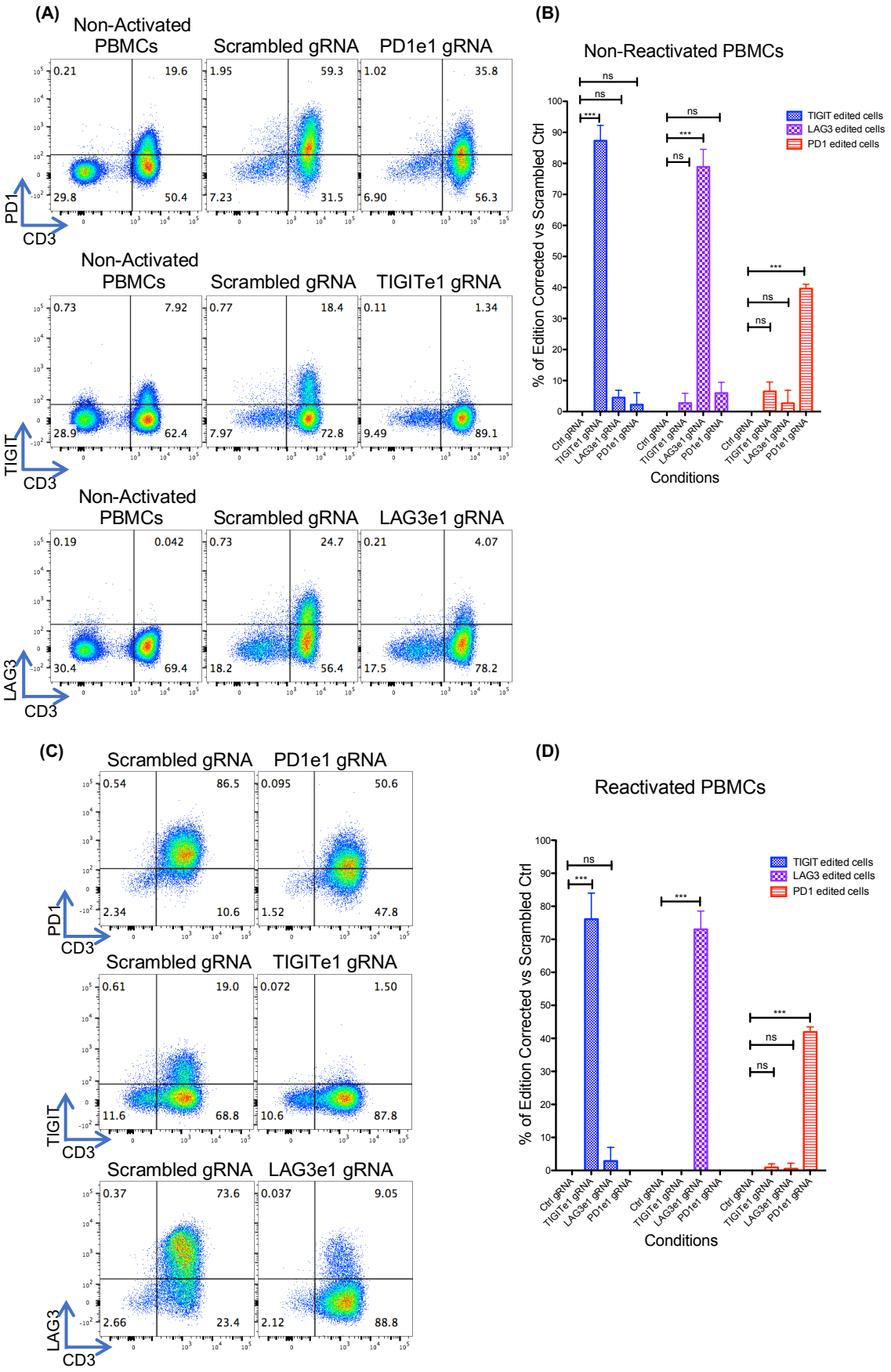

Figure 3.18. Gene editing of four different healthy donors PBMCs with either PD1, TIGIT, or LAG3 gRNA. (A and C) Flow cytometry plots showing the expression of $PD1^{+}$ $CD3^{+}$ cells (top

row), TIGIT$^+$ CD3$^+$ cells (middle row), or LAG3$^+$ CD3$^+$ cells (bottom row) (all gated on live cells) on either **(A)** 'Non-Reactivated' PBMCs (non-activated PBMCs shown for comparison) or **(C)** 'Reactivated' PBMCs. **(B and D)** Quantification of gene editing in CD3$^+$ cells corrected against the scrambled control of either **(B)** 'Non-Reactivated' PBMCs or **(D)** 'Reactivated' PBMCs; n=4 (mean ± SEM). Percentage of gene editing was calculated with the following formula: 100*[(%Target$^+$ cells in control (Scrambled gRNA) - %Target$^+$ cells in edited cells)/%Target$^+$ cells in control (Scrambled gRNA)]. One-way repeated measures ANOVA followed by Dunnett's Multiple Comparison was performed for each group of cells.

3.8.2. Melanoma and Non-Small-Cell Lung Carcinoma (NSCLC) Patient's TILs

After validating the gRNAs and the delivery method in healthy donors primary T cells, the gene editing was performed on the cells of interest (patient's TILs). The data shown in this section is a combination of experiments performed on 3 different patient samples. Most of the optimisation and validation performed at the beginning was carried out with melanoma TILs from patient MX063. Afterwards, gene editing of the targets of interest were performed on two other TILs samples from NSCLC patients (patients LTX997 and LTX1000).

As previously stated, at the same time as certain gRNAs were being validated on PBMCs, validation of these was being performed on TILs as well. Hence, the first gRNAs that were tested on MX063 TILs were the ones targeting TIM3 and TIGIT. For this, TILs that had been previously expanded using the rapid expansion protocol (see materials and methods section) and subsequently frozen, were thawed and activated for 48 hours (same activation protocol as with healthy donor PBMCs, see materials and methods for more information). After activation, the melanoma TILs were electroporated using program EH-115 and Cas9 RNP complexes (2:1 molar ratio) that had either scrambled gRNA (control), TIM3 gRNA targeting exon 2 (TIM3e2), TIM3 gRNA targeting exon 3 (TIM3e3) or a combination of these two guide RNAs. Three days post-electroporation the TIM3 expression was analysed via flow cytometry. This experiment was repeated 5 times with different batches of MX063 expanded TILs (these 5 different experiments can be counted as biological replicates since expansions are stochastic processes by nature and the population of TILs is heterogeneous, hence, each round of REP will generate a different pool of expanded TILs).

Representative flow cytometry plots are shown in Figure 3.19A and they show that there was a very slight decrease of TIM3 expression on the cells targeted with the TIM3e2 gRNA, and no decrease when targeted with the TIM3e3 gRNA. Moreover, the combination of both guides did not improve the knockdown efficiency. Furthermore, the quantification of the percentage of gene editing showed that all of the conditions gave less than 10% of edits and that the difference against the scrambled control was not statistically significant (Figure 3.19B). This result was maintained even when measuring TIM3 expression without correcting against the scrambled control (Supplementary Figure 8.7). Of note, the viability of the TILs from these experiments was greatly decreased after electroporation (~50-60% of viable cells for no electroporation control vs. ~5-20% of viable cells for the electroporated conditions) (data not shown).

TIGIT gRNA targeting exon 1 (TIGITe1) and the one targeting exon 2 (TIGITe2) were tested in one of the TIM3 gRNAs replicate experiments. Both of these Cas9 RNP complexes were generated at a 2:1 molar ratio and three days post-electroporation the expression of TIGIT was measured via flow cytometry. The results of this experiment clearly showed that the gRNA targeting exon 1 achieved a better knockdown of TIGIT compared to the gRNA targeting exon 2 (Figure 3.19C). Hence, all of the following TIGIT edits were performed with TIGITe1. Of note, in this particular experiment the viability of the no electroporated TILs was 56% and this viability dropped to ~20% on the electroporated conditions (data not shown).

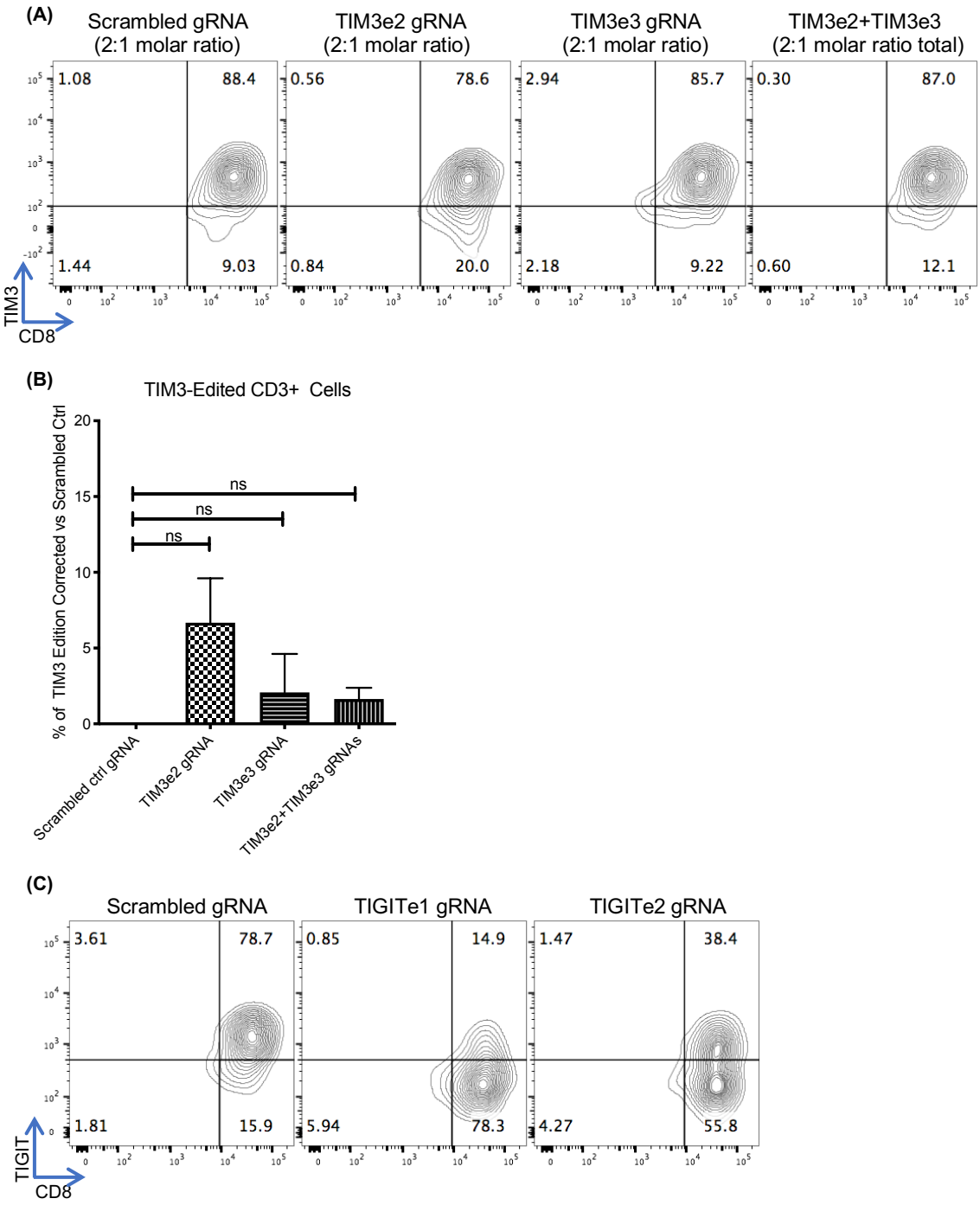

Figure 3.19. Gene editing of MX063 TILs with gRNAs targeting TIM3 or TIGIT. (A) Representative flow plots (gated on $CD3^+$ cells) from 5 different experiments targeting TIM3 with different gRNAs. **(B)** Quantification of gene editing in $CD3^+$ cells corrected against the scrambled control; n=5 (mean ± SEM). Percentage of gene editing was calculated with the following formula: 100*[(%$TIM3^+$ cells in control (Scrambled gRNA) - %$TIM3^+$ cells in edited cells)/%$TIM3^+$ cells in control (Scrambled gRNA)]. One-way repeated measures ANOVA followed by Dunnett's Multiple Comparison was performed. **(C)** Flow plots (gated on $CD3^+$ cells) of MX063 TILs edited with different Cas9 RNP complexes targeting TIGIT.

A considerable decrease in the viability of the MX063 TILs post-electroporation was consistently observed. It was hypothesised that this could be because the TILs were already only 60% or less viable prior to the electroporation due to the freeze/thaw cycle. To try to increase the viability of the MX063 TILs post-editing, the electroporation was performed with TILs that had just undergone a round of rapid expansion (the electroporation was performed prior to the freeze/thaw cycle). These expanded MX063 TILs were electroporated with Cas9 RNP complexes with the gRNAs targeting LAG3 exon 1 (LAG3e1) or exon 2 (LAG3e2). Both of these Cas9 RNP complexes were given at a 2:1 molar ratio and three days post-electroporation the expression of LAG3 was measured via flow cytometry. Even though this was only one experiment, it distinctly showed that the gRNA targeting exon 1 achieved a high knockdown of LAG3 whilst the gRNA targeting exon 2 did not achieve any significant knockdown (Figure 3.20A). Hence, all of the following LAG3 edits were performed with LAG3e1. It is interesting that even though the viability of the TILs prior to electroporation was ~80%, the viability of the electroporated samples still dropped to ~30% (data not shown). Additionally, as a further confirmation of gene editing, DNA was extracted from the LAG3e1-edited TILs as well as from the scrambled control and the area flanking the gene editing site was amplified via PCR. These samples were Sanger sequenced and the LAG3 editing was analysed at a genomic level using TIDE (data not shown) and ICE analysis (Brinkman, Chen, Amendola, & Van Steensel, 2014; Hsiau et al., 2018). These online tools work under the same principle of a decomposition algorithm that identifies the indels generated via CRISPR editing. Indeed, the ICE algorithm is based on the TIDE method (Hsiau et al., 2018), hence the results of both analyses were very similar (data not shown). The analysis of the ICE algorithm showed that there was indeed a difference between the control sequence (scrambled gRNA) and the LAG3e1-edited sequence. Importantly, this difference was observed only after the expected cut site (Figure 3.20B and 3.20D), and it showed that there was an editing efficiency of 25% (Figure 3.20C).

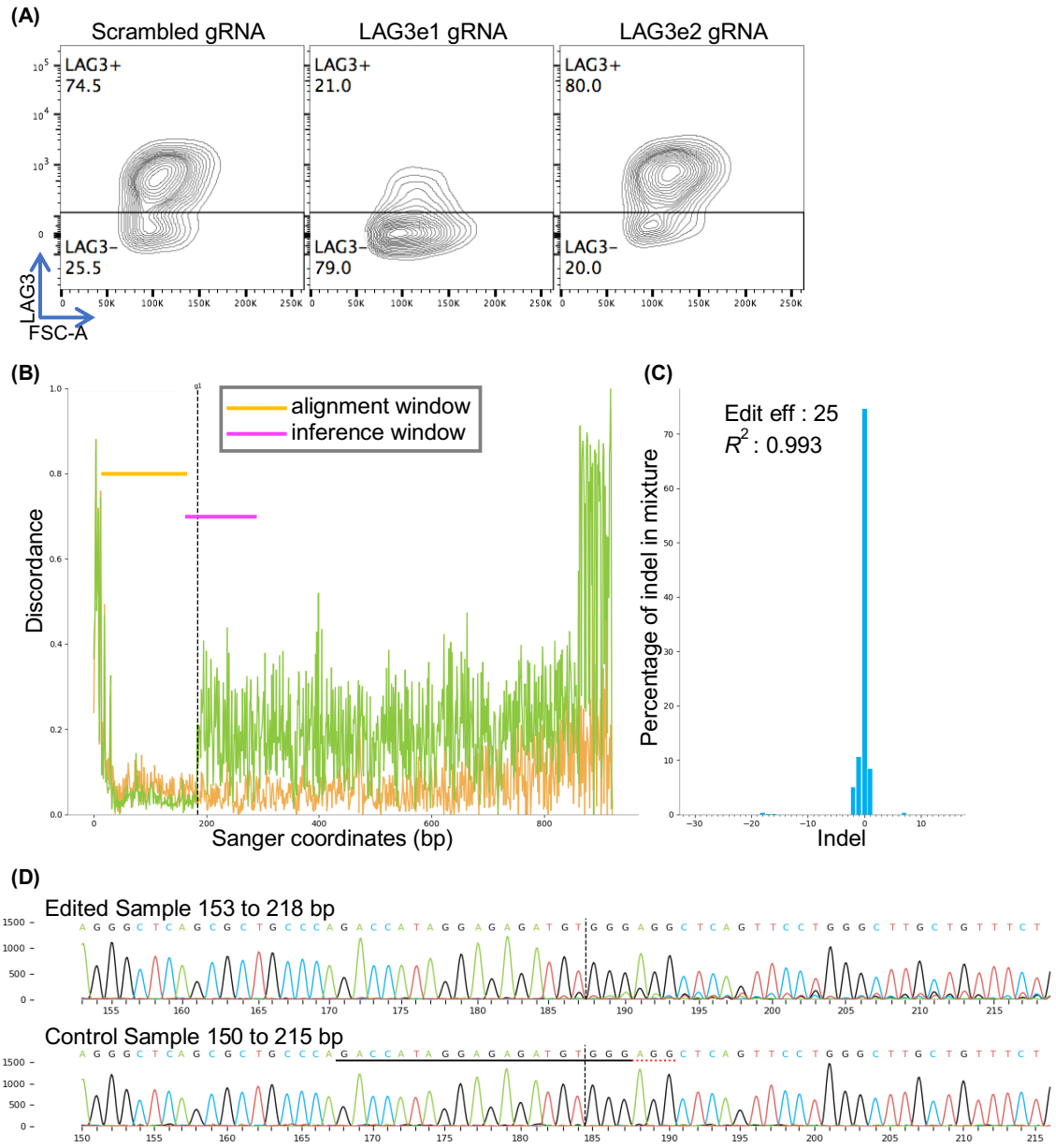

Figure 3.20. Gene editing of MX063 TILs with gRNAs targeting LAG3. (A) Flow plots (gated on CD3⁺ cells) of MX063 TILs edited with different Cas9 RNP complexes targeting LAG3. **(B)** Visualisation of the difference between the scrambled control sequence (orange) and the LAG3e1-edited sequence (green). The expected cut site is denoted by the vertical dotted line (analysis performed with ICE by Synthego). **(C)** Percentage of indels generated with the LAG3e1 gRNA, as well as the percentage of editing efficiency (analysis performed with ICE by Synthego). **(D)** Sequences spanning the cut site from the LAG3e1-edited TILs (top row) and the scrambled control (bottom row). The gRNA is underlined in black and the PAM is underlined in red, the expected cut site is denoted by the vertical dotted lines (analysis performed with ICE by Synthego).

After verifying that the editing efficiency seen on PBMCs was maintained on TILs (at least for the TIGITe1 and LAG3e1 gRNAs), the next stage of the

optimisation was to increase the viability of the TILs post-electroporation. Hence, TILs were electroporated whilst they were undergoing a rapid expansion, as it was hypothesised that this would be the time when the cells would be healthiest and proliferative. Indeed, it had already been shown that editing TILs during the REP showed high efficiency and only a small impact on fold expansion (this was done in the context of ZFN-mediated editing) (Beane et al., 2015). Hence, for the following experiments on TILs the gene editing was performed on day 7-12 of the rapid expansion protocol depending on initial number of cells and quality of the expansion. Performing the gene editing at this time made a positive impact on the viability of the cells 3 days post-editing, with viabilities now ranging from ~65% to 90% (Supplementary Figure 8.8). Moreover, after an initial drop in viability and number of cells post-editing, the cells continued to expand to great numbers (data not shown).

The gene editing of TIGIT, LAG3, and PD1 were performed on different patients' TILs that were undergoing rapid expansion. These edits were done in different experiments during different rapid expansions and constantly achieved high editing efficiency. For TIGIT, the gene editing was performed on MX063 (n=7) and LTX997 (n=1) TILs. For LAG3, the gene editing was carried out on MX063 (n=3), LTX997 (n=1), and LTX1000 (n=1) TILs. For PD1 the gene editing was done on MX063 (n=2), LTX997 (n=1), and LTX1000 (n=1) TILs. Additionally, in some of the experiments (n=4 for each target) the edited TILs were divided into 'Non-Reactivated' (left with the same high dose of IL-2 (6000 IU/mL) as they were before) and 'Reactivated' (left with high dose IL-2, αCD3, and αCD28) conditions. Representative flow plots of the different edits are shown in Figure 3.21A ('Non-Reactivated') and Figure 3.21B ('Reactivated'). Furthermore, when combining all of the different experiments, the quantification of the percentage of gene editing for each target (corrected against the scrambled control) showed that the TIGITe1 gRNA (79% $\pm$ 5%; P<0.0001) and the LAG3e1 gRNA (79% $\pm$ 4%; P<0.0001) had a high editing efficiency, and that the PD1e1 gRNA (45 $\pm$ 9%; P<0.05) had a lower editing efficiency when the TILs were not reactivated (Figure 3.21C). However, the editing efficiency of PD1 increased when the TILs were reactivated (65% $\pm$ 6%; P<0.01) (Figure 3.21D). This is due to the fact that PD1

expression needs to be upregulated for the effect of the gene editing to properly show.

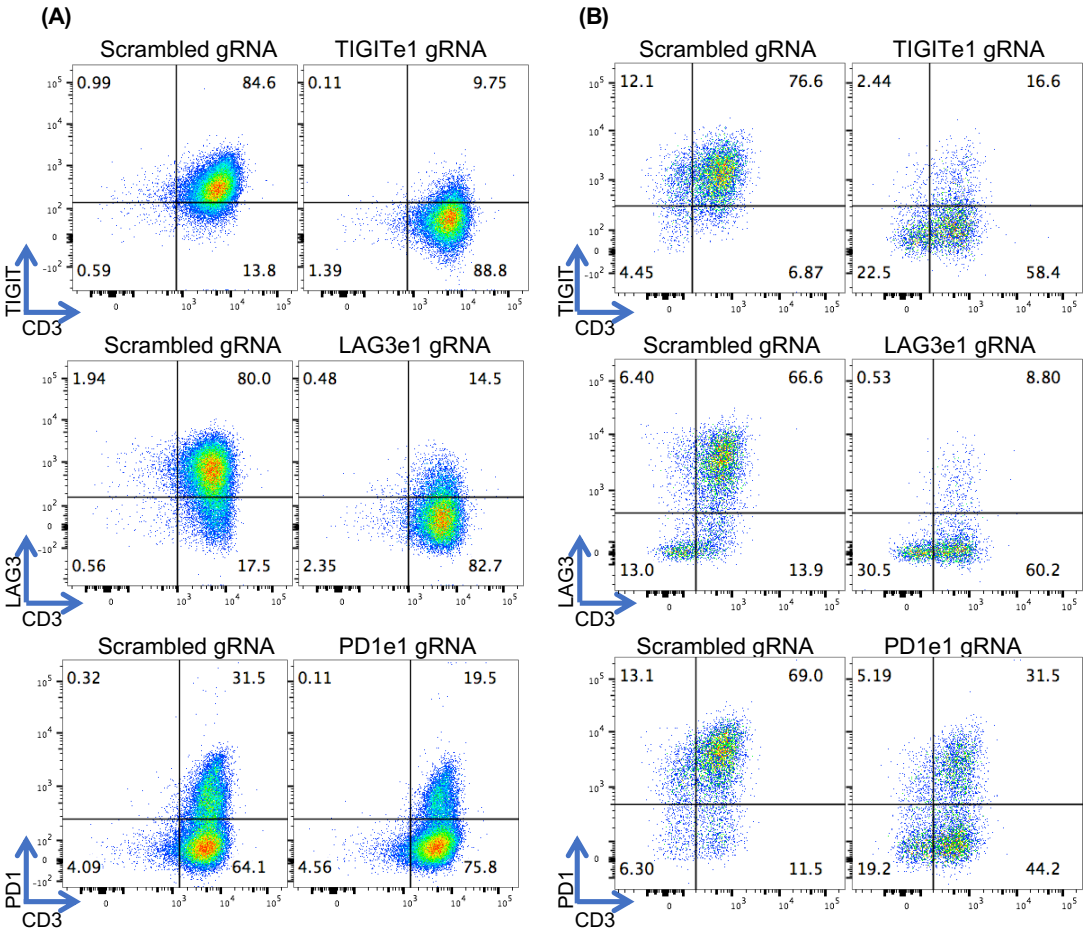

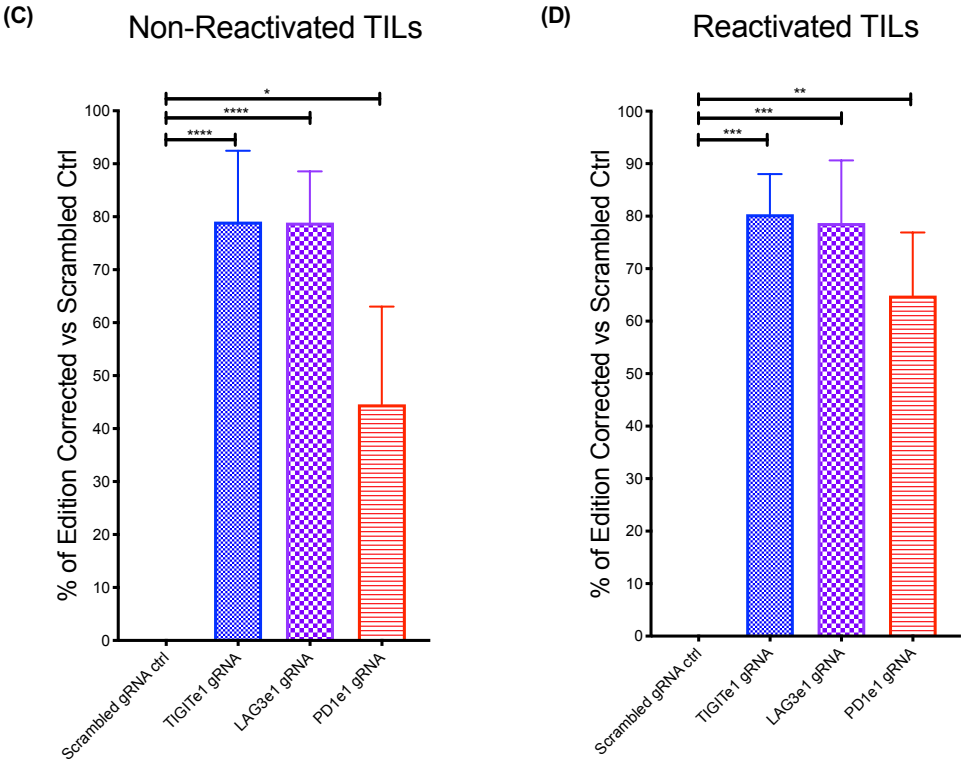

Figure 3.21. Gene editing of TILs during REP. TILs from different patients were edited whilst they were undergoing rapid expansion. **(A and B)** Representative flow plots of expression of TIGIT, LAG3, and PD1 three days post-editing (gated on live cells) for the **(A)** 'Non-Reactivated' and the **(B)** 'Reactivated' conditions. **(C and D)** Percentage of gene editing corrected against the scrambled gRNA for the **(C)** 'Non-Reactivated' and the **(D)** 'Reactivated' conditions. Percentage of gene editing was calculated with the following formula: 100*[(%Target$^+$ cells in control (Scrambled gRNA) - %Target$^+$ cells in edited cells)/%Target$^+$ cells in control (Scrambled gRNA)]. For 'Non-Reactivated' TILs: TIGIT: n=8 (mean ± SEM), LAG3: n=5 (mean ± SEM), PD1: n=4 (mean ± SEM). For 'Reactivated' TILs: n=4 (mean ± SEM) for each target. For each target and each activation condition paired t-tests were performed (against their paired scrambled gRNA control).

Furthermore, statistical analyses were performed on each target compared to the scrambled control. These analyses showed that the percentage of gene editing for all of the targets in both 'Non-Reactivated' and 'Reactivated' conditions was statistically significant. Of note, the gene editing retained statistical significance even when measuring the expression of the targets without correcting against the scrambled control (Supplementary Figure 8.9). Importantly, the viability of the edited TILs was ~76-85% in all of the experiments (data not shown).

DNA was extracted from the TILs used in one of these experiments (editing of LTX997) to analyse the gene editing at the genomic level. The sequencing of the samples was performed via Sanger sequencing, as well as via next generation sequencing (NGS). A comparison was carried out between the Sanger sequencing results (analysed via the ICE platform) and the NGS analysis of the samples (the NGS was performed on a MiSeq platform by the Genomics and Genome Engineering Core Facility of the UCL Cancer Institute). Both analyses were performed for TIGIT gRNA vs Scrambled gRNA (Figure 3.22.A and 3.22B), for LAG3 gRNA vs Scrambled gRNA (Figure 3.22C and 3.22D), and for PD1 gRNA vs Scrambled gRNA (Figure 3.22E and 3.22F). The comparison between these analyses showed a similar editing efficiency for TIGIT (35% from ICE vs. 28.2% from MiSeq). However, for both LAG3 and PD1 edits the MiSeq showed double the editing efficiency that ICE showed (17% vs. 33.3% for LAG3 and 14% vs. 29.6% for PD1). It was hypothesised that these differences could be due because of the higher sensitivity of the NGS compared to Sanger

sequencing. Hence, future experiments where the gene editing was analysed at the genomic level were performed with NGS analysis.

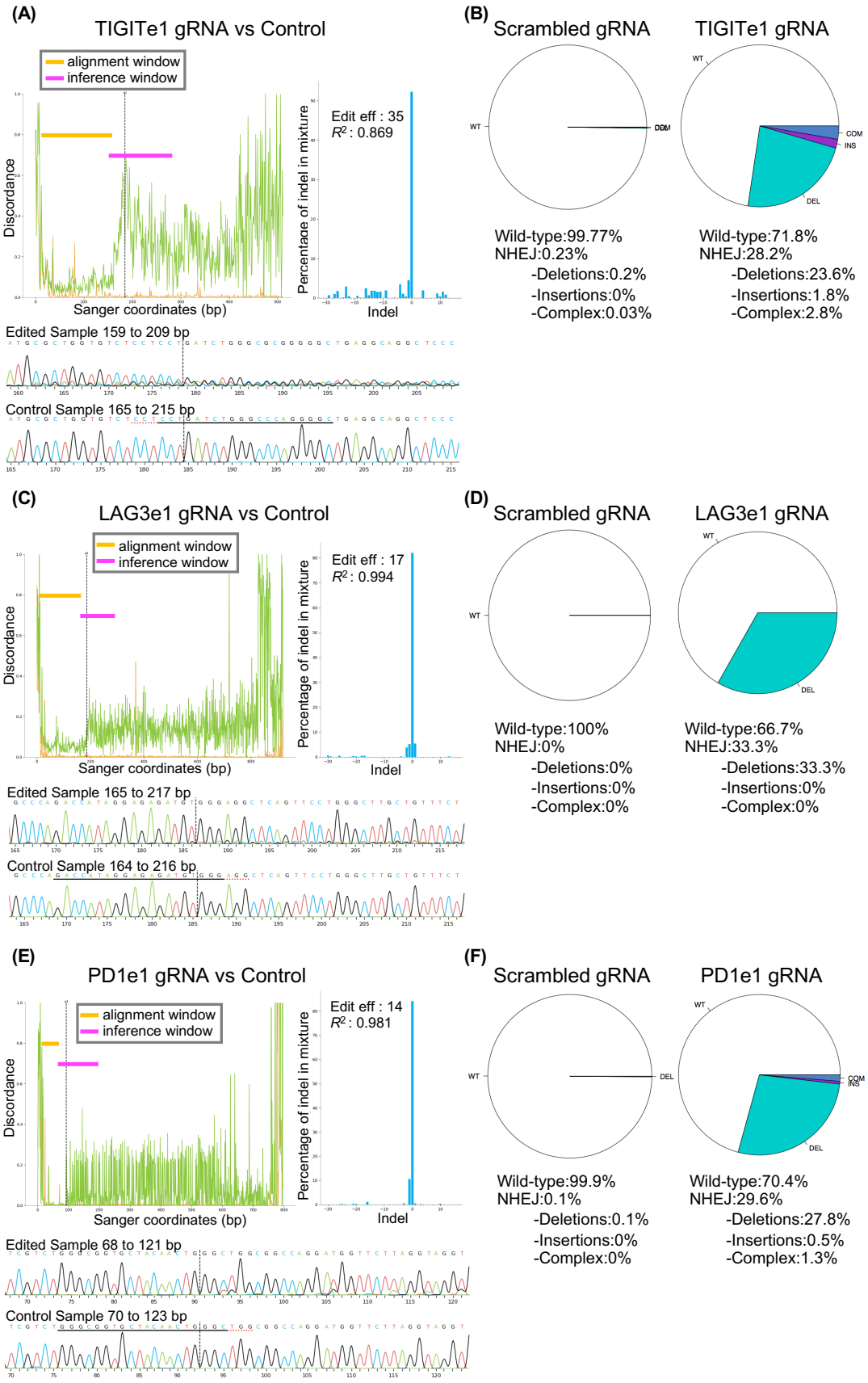

Figure 3.22. Genomic confirmation of gene editing on LTX997 edited TILs. (A, C, and E) The three different outputs of ICE are shown for **(A)** TIGIT-edited TILs, **(C)** LAG3-edited TILs, and **(E)** PD1-edited TILs. **(B, D, and F)** Results of MiSeq are shown for **(B)** TIGIT-edited TILs, **(D)** LAG3-edited TILs, and **(F)** PD1-edited TILs.

Finally, it was of interest to test if the co-delivery of two different gRNAs into TILs could be achieved with equal efficiency as the single delivery. Given that there is evidence showing that LAG3 and PD1 synergistically regulate T cell function in the context of cancer (R.-Y. Huang et al., 2015; Woo et al., 2012), it was decided that it would be a good combination of targets to try to edit at the same time. Hence, MX063 TILs that were undergoing rapid expansion were electroporated with Cas9 RNP complexes that had either scrambled gRNA, PD1e1 gRNA, LAG3e1 gRNA, or a combination of PD1e1 and LAG3e1 gRNAs (all of them at a 2:1 molar ratio of gRNA:Cas9). For the co-delivery condition, two different Cas9 RNP complexes were generated and delivered at the same time (one for PD1e1 and one for LAG3e1, both at a 2:1 molar ratio of gRNA:Cas9). The expression of PD1 and LAG3 was analysed on the TILs prior to the electroporation via flow cytometry as a baseline value. After the electroporation, the cells were divided into the 'Non-Reactivated' and the 'Reactivated' conditions, and three days post-editing the expression of PD1 and LAG3 was analysed via flow cytometry (data not shown). After the gene editing, the cells were maintained expanding in culture for longer than usual, as it was of interest to test if the edits could be maintained in a mixed population of cells without generating clones or sorting the edited cells. Hence, aliquots of 'Non-Reactivated' (data not shown) and 'Reactivated' TILs were taken to test the gene editing of the TILs via flow cytometry on day 3 (data not shown) (viability of edited TILs was ~75-85%; data not shown), day 15 (data not shown), and day 27 post-electroporation (Figure 3.23A) (reactivation was done 48h prior to flow cytometry) (viability of edited TILs was ~93-95%; data not shown). It was observed that the editing of both PD1 and LAG3 was maintained on all of these timepoints. The percentage of $LAG3^+$ and $PD1^+$ cells (gated on $CD3^+$ cells) on the edited TILs was quantified for all of the timepoints and the percentage of these cells was compared to the scrambled gRNA control on each timepoint. This showed that the difference was statistically significant for the LAG3-edited TILs ($P<0.001$) (Figure 3.23.B) as well as for the

PD1-edited TILs ($P<0.001$) (Figure 3.23C). Finally, 56 days post-editing, DNA was extracted from the edited TILs and sent to the UCL Cancer Institute Genomics and Genome Engineering Core Facility for MiSeq analysis. This analysis showed a high editing efficiency at the genomic level for the TILs edited with the single targets or with the combination of them (Figure 3.23D). As an internal control, it was observed that when analysing LAG3 editing, the cells edited with PD1 gRNA showed no editing whatsoever. The same was true for the cells edited with LAG3 gRNA when analysing PD1 editing.

As a validation of these results, the same gene editing conditions were repeated on LTX1000 TILs, and at the protein level these edits showed similar editing efficiencies to the MX063 edited TILs on day 3 and day 27 post-editing (day 15 was not sampled) (Supplementary Figure 8.10). The LTX1000 edited TILs were not sent for MiSeq analysis so a comparison of gene editing could not be made at the genomic level.

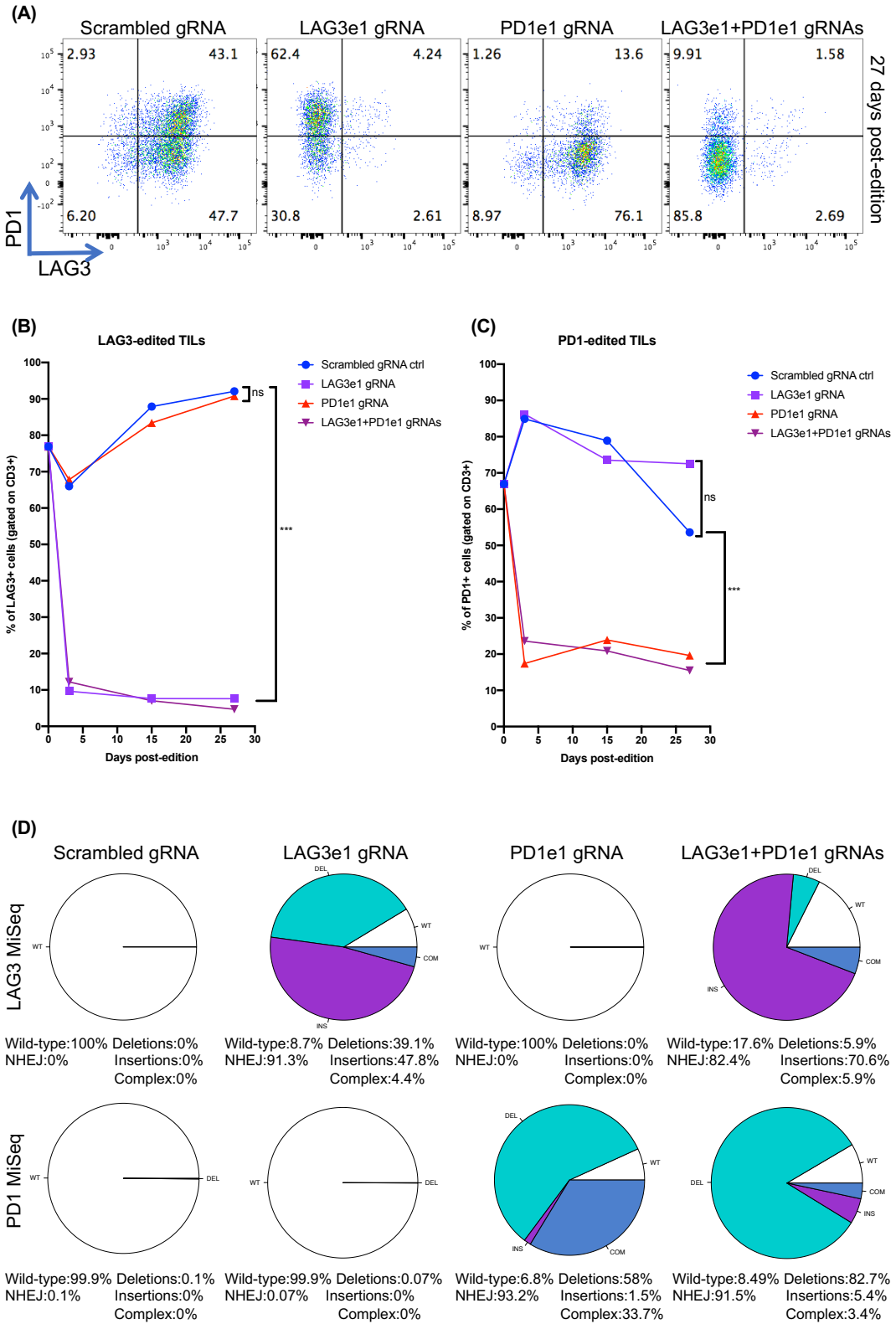

Figure 3.23. Efficient and persistent co-editing of PD1 and LAG3 on MX063 TILs. (A) Flow cytometry plots showing expression of PD1 and TIM3 in 'Reactivated' TILs that had been edited 27 days prior (gated on $CD3^+$ cells). **(B and C)** Quantification of percentage of **(B)** $LAG3^+$ cells or **(C)** $PD1^+$ cells in 'Reactivated TILs' at day 0 (prior to editing), day 3, day 15, and day 27 post-editing (gated on $CD3^+$ cells). One-way repeated measures ANOVA followed by Dunnett's

Multiple Comparison was performed for each graph (day 0 values were excluded from statistical analysis). **(D)** Results of MiSeq are shown (LAG3 top row and PD1 bottom row) for 'Non-Reactivated' TILs at day 56 post-editing.

3.9. Discussion

In this chapter I have shown the work performed to optimise a methodology for the genomic engineering of primary human tumour infiltrating lymphocytes using the CRISPR/Cas9 technology. In short, this methodology consists of electroporating the TILs with an Amaxa 4D nucleofector (Lonza) whilst they are undergoing a rapid expansion. Performing the electroporation of the CRISPR components in this way and with Cas9 RNP complexes achieved a high editing efficiency, as well as maintaining a high viability of the cells post-editing (65% to 90% of viable TILs three days post-editing).

The methodology that was utilised for the design of the crRNAs proved successful, as at least one of the two gRNAs for each target designed in this manner conveyed a high editing efficiency in the cells of interest. The only exception to this were the gRNAs for TIM3. This could be because the gRNAs designed for TIM3 targeted exon 2 or 3, and it was observed that the gRNAs that achieved the greatest knockdown of protein were the ones that targeted exon 1 of the genes of interest. Further work will be needed to test if redesigning the TIM3 gRNAs to target exon 1 of the protein improves their editing efficiency.

The use of HEK293T cells as a system to easily validate the gRNAs proved not to be useful, as it was later shown that the editing efficiencies were not maintained between the cell line and the cells of interest. These results are consistent with previous reports showing that a gRNA exhibiting high editing efficiency in HEK293T cells showed little activity in $CD4^+$ T cells (Mandal et al., 2014). It was interesting that the editing efficiencies of certain gRNAs were higher in the cells of interest than in the HEK293T cells, as it is usually the case that primary cells have lower editing efficiencies compared to easy-to-transfect cell lines (S. Kim et al., 2014; Mandal et al., 2014). Further studies would be necessary to understand the factors that make a gRNA more efficacious in one cell type compared to another. These factors will likely be related to chromatin states and other epigenetic influences (Verkuijl & Rots, 2019).

Electroporation was chosen as the delivery method of the CRISPR components into the cells of interest because of the many advantages that electroporation/nucleofection has over the other delivery systems. The main benefits that this method confers is the ability to transfect slow-proliferating cells or hard-to-transfect cells, as well as being a high-throughput delivery system. Moreover, electroporation is already accepted as a delivery method of CRISPR components in several clinical trials (NCT03399448 and NCT03166878).

For this project, the Amaxa 4D Nucleofector (Lonza) was chosen as we were not able to successfully edit the cells using the AgilePulse Max BTX Electroporator (Harvard Apparatus). A side-to-side comparison using these two electroporator machines was not performed as the editing programs set up by Lonza are proprietary information, and as such there is no way of comparing the same protocols against a different electroporator. However, the Amaxa 4D Nucleofector can also be adapted to edit greater numbers of cells with ease (i.e. it can perform large-scale transfections of up to $1x10^9$ cells). This consideration was taken into account since the work performed in this PhD project was always done with the view to generate a translational method that could be later applied in a clinical setting.

The final improvement made to this editing methodology was to incorporate the targeting of two different genes of interest at the same time. In this sense, the combination chosen for this proof-of-concept was to target LAG3 and PD1 as there is evidence showing that LAG3 and PD1 synergistically regulate T cell function in the context of cancer (R.-Y. Huang et al., 2015; Woo et al., 2012). The successful co-editing of two different targets in TILs is of great clinical relevance, as it has been shown that in certain cancers, treatment with an anti-CTLA4 antibody in combination with an anti-PD1 antibody improves the progression-free survival of patients compared to the treatment of either anti-CTLA4 or anti-PD1 alone (Larkin et al., 2015). Furthermore, there are currently different clinical trials exploring the efficacy of the combination treatment with anti-LAG3 and anti-PD1 antibodies in the context of different cancers, such as glioblastoma (NCT02658981), B cell malignancies (NCT02061761), and different solid tumours (NCT01968109), amongst others. Data from these clinical trials is not available yet, but the results of these trials will be of great importance to the

immunotherapy field, especially because there are still many patients that do not benefit from anti-CTLA4 or anti-PD1 treatment.

Finally, it is worth noting that in the experiments where the gene editing was analysed as late as 27 days (or, in one case, 56 days) post-editing, it was shown that the gene editing was successfully maintained in the population of TILs without having to sort the cells or generate clones. These results generated the hypothesis that these edits (PD1, LAG3, or the combination of both) were not harmful to the cells *in vitro* given that the proportion of edited TILs remained constant. We hypothesise that in an *in vivo* setting the edits will prove to be advantageous to the TILs.

In sum, the work presented in this chapter established a platform for the genomic engineering of primary human TILs using the CRISPR/Cas9 technology. The hypothesis set forth is that knocking down the expression of some of the prevalent immune-checkpoints in these cells using the established platform will render them resistant to the negative regulation exerted by cancerous cells and their surrounding microenvironment. Furthermore, by genetically engineering only the T cells that are tumour reactive, the toxicities associated with systemic blockade of immune checkpoints (as the ones seen in the clinic with the immune checkpoint inhibitors) will be minimised if not completely prevented. In the next chapters the work performed to try to prove these hypotheses will be discussed.

Chapter 4. Expansion and characterisation of melanoma-reactive T cells

4.1. Overview

The aim of this study was to efficiently perform gene editing of tumour infiltrating lymphocytes (TILs) for the generation of a powerful adoptive cellular therapy (ACT) against cancer. However, it is known that TILs are a heterogeneous population of tumour-reactive and bystander T cells (Duhen et al., 2018; Gros et al., 2014; Scheper et al., 2019; Simoni et al., 2018), and prospective clinical studies have suggested that enrichment of tumour-reactive cells could enhance clinical efficacy (Dudley et al., 2013; Schwartzentruber et al., 1994). Because of this, this chapter will discuss the work performed to try to selectively expand tumour-reactive T cells from a melanoma patient sample. The work presented in this chapter was done in parallel to the optimisation of gene editing presented in the previous chapter of this thesis.

4.2. Introduction

4.2.1. *Ex vivo* expansion of tumour infiltrating lymphocytes for adoptive cellular therapies

In 1988, the first TILs pilot study was carried out. In this study two partial responses were observed, one in a metastatic melanoma patient and the other in a renal cell carcinoma patient (S. L. Topalian et al., 1988). Later that year, a bigger study showed that the use of autologous TILs in combination with IL-2 was a powerful adoptive cellular therapy in patients with metastatic melanoma that had undergone a regimen of cyclophosphamide (Rosenberg et al., 1988). This study achieved responses in 9 out of 15 patients who had not been treated previously with IL-2, as well as in 2 out of 5 patients in whom treatment with IL-2 had previously failed (Rosenberg et al., 1988). Since then, many phase I/II clinical trials have confirmed that the treatment of TILs combined with high-dose IL-2 and lymphodepleting preconditioning can mediate objective responses in patients

with metastatic melanoma (Dudley et al., 2002, 2005, 2008; Rosenberg et al., 2011).

Initially the protocol for the expansion of these TILs consisted in the excision of deposits of metastatic melanoma that were subsequently fragmented into microcultures in the presence of high-dose IL-2 (6000 IU/mL). Once several million TILs were grown from these cultures (usually 2-4 weeks), the TILs were screened for recognition of autologous tumour cells, and if not available, reactivity to a panel of human leukocyte antigen (HLA)-matched allogeneic melanoma cell lines was evaluated. The independent TIL cultures with the highest cytokine secretion (i.e. highest tumour-reactivity) were further grown until a cell number of $5x10^7$ was achieved (usually achieved 3-6 weeks after tumour excision). These TILs were then rapidly expanded by stimulation with soluble αCD3 (OKT3) monoclonal antibody, high-dose IL-2 (6000 IU/mL), and irradiated allogeneic feeder cells. This rapid expansion protocol typically achieved 1000-fold expansions of cells in a 14-day time period, after which the cells were concentrated and infused (Dudley et al., 2002).

This first version of the *ex vivo* expansion of TILs for clinical use had some limitations. First, the selection of tumour-reactive T cells required the generation of an autologous melanoma cell line. With only a 50% success rate for growing these autologous tumour cell lines, half of the patients could not undergo this selection step (Dudley et al., 2003). Secondly, the total culture time of the TILs prior to patient treatment was long (6-8 weeks), and this increased the probability of these melanoma patients to progress to a stage where TIL therapy would no longer be considered beneficial. Thirdly, because of the long culture time, the TILs generated had a more terminally differentiated phenotype, which negatively impacted on their survival and persistence following ACT (J. Huang et al., 2005; Powell, Dudley, Robbins, & Rosenberg, 2005).

Because of these limitations, the “standard” TILs production process was simplified to generate “young” TILs for therapy. This approach changed the microcultures of TILs to bulk lymphocyte cultures and it eliminated the *in vitro* tumour-recognition assay. These two changes shortened the pre-REP culture time to only 10-18 days, bringing the total culture time prior to infusion to 3-4 weeks. It was shown that the frequency of tumour-reactive TILs in these “young”

TILs was similar to the frequency in the “standard” TILs (M. Donia et al., 2012; K. Q. Tran et al., 2008). Furthermore, these “young” TILs benefitted from a significantly higher expression of CD27 and CD28, as well as longer telomeres compared to the “standard” TILs (M. Donia et al., 2012; K. Q. Tran et al., 2008), giving them an advantage in *in vivo* persistence and survival after ACT (J. Huang et al., 2006, 2005; Zhou et al., 2005). A phase II study demonstrated that these “young” TILs cultures could be generated for 90% of the metastatic melanoma patients and that 50% of the treated patients achieved an objective clinical response (Besser et al., 2010; Itzhaki et al., 2011).

The first clinical trial in which the “young” TILs were used also included an enrichment step for $CD8^+$ cells prior to rapid expansion. This was performed to eliminate non-specific $CD4^+$ T cells and deplete $CD4^+FoxP3^+$ regulatory T cells. Of the 33 metastatic melanoma patients treated in this trial, 18 exhibited an objective response (55%), demonstrating that $CD8^+$ TILs alone were sufficient to mediate tumour regression (Dudley et al., 2010). However, the role of CD4 lymphocytes in the infused TILs is controversial, as there have been reports of clinical tumour regression associated with $CD4^+$ lymphocytes (Friedman et al., 2012; Hunder et al., 2008). Conversely, it has also been shown that reconstitution of $CD4^+FoxP3^+$ regulatory T cells in patient peripheral blood after ACT is inversely correlated with clinical response to therapy (Yao et al., 2012).

To address the question of the relevance of $CD4^+$ lymphocytes in the context of ACT, a randomised, single-institution phase II clinical trial in metastatic melanoma was designed. In this trial, 34 patients were treated with unselected “young” TILs containing $CD4^+$ and $CD8^+$ lymphocytes and 35 patients with CD8-enriched “young” TILs. The results of this trial showed that there were no significant differences in objective response, overall survival, or toxicity between the two treatments. Additionally, although the difference was not statistically significant, there were more responses in the unselected “young” TILs group compared to the CD8-enriched “young” TILs (35% vs. 20%). Given these results, as well as the simpler manufacturing process of the unselected “young” TILs, this randomised trial advocated for the use of unselected “young” TILs for future ACT trials (Dudley et al., 2013).

4.2.2. Detection and expansion of neoantigen reactive T cells

It is known that cancer arises as a result of the accumulation of somatic mutations (Alexandrov et al., 2013). These mutations can lead to the expression of mutated proteins that are recognised by the immune system as being foreign (i.e. tumour antigens) (Lu et al., 2014; Robbins et al., 2013). Tumour antigens can be divided into three general categories: self-antigens that possess an aberrant expression in cancer, such as overexpressed antigens or cancer/testis (C/T) antigens; differentiation antigens, which are tissue-specific; and antigens derived from tumour-specific somatically mutated genes (i.e. neoantigens).

Adoptive cellular therapies that target neoantigens have possible advantages over those that target either of the other two groups of tumour antigens. One of these advantages is that T cell responses against neoantigens are not expected to result in autoimmunity as the antigens are only present in the tumour cells. In this regard, targeting either differentiation antigens or overexpressed self-antigens with potent effector T cells has been known to associate with autoimmune toxicities against healthy tissues (Johnson et al., 2009; Parkhurst et al., 2011). Additionally, another advantage is that T cells that recognise neoantigens are not exposed to central tolerance, and therefore possibly express higher-affinity T cell receptors (TCRs) compared to those that recognise self-antigens (Heemskerk et al., 2013).

Until recently, the role of neoantigens in tumour rejection had been largely ignored as these mutations are patient specific and rare. However, with whole exome sequencing of tumour DNA becoming feasible in recent years, the field of neoantigens has progressed. This is because the identification of potential neoepitopes is based on the alignment of whole exome DNA from tumour and matching healthy cells in order to detect tumour-specific mutations. After identifying expressed somatic mutations in this way, *in silico* approaches are used to prioritise candidate neoepitopes. The best established algorithms for this purpose are the ones designed to predict MHC/HLA binding affinity (Jurtz et al., 2017; M. Nielsen & Andreatta, 2016). *In silico* predicted and prioritised peptides are then synthesised, and *in vitro* assays are performed to assess if there is a population of T cells that is able to recognise and respond to these mutated antigens. It is worth noting that predicting affinities for MHC class II molecules

has proved more difficult and not as reliable as predicting affinities for MHC class I molecules (M. Nielsen, Lund, Buus, & Lundegaard, 2010). This is partly due to MHC class II molecules presenting longer sequences of amino acids than MHC class I molecules (11-20 amino acids, or even longer, compared to 8-11 amino acids).

There are three main *in vitro* immunological screening methods that have been used to evaluate neoantigen recognition: 1) cDNA libraries; 2) peptide-HLA multimers; and 3) tandem minigenes or peptide pools. The advantage of cDNA libraries is that they interrogate all of the transcribed sequences without the *in silico* prediction bias. However, these libraries are laborious, time-consuming, and biased towards highly transcribed genes. Moreover, given that these libraries interrogate both mutated and non-mutated antigens, there is a frequent identification of self-antigens rather than neoantigens (Garcia-Garijo, Fajardo, & Gros, 2019). The screening of T cells using peptide-HLA multimers has the advantage of overcoming the need of autologous or HLA-matched APCs. Furthermore, it allows for the isolation of antigen-specific T cells via flow cytometry (Altman et al., 1996). However, peptide-HLA multimers are only available for a limited number of HLA allotypes. Furthermore, it is worth noting that the majority of screens performed using these multimers are focused on identifying neoepitopes presented on MHC class I molecules, as technical issues in the production of MHC class II multimers have hindered the use of this approach for the identification of neoantigen-specific $CD4^+$ T cells (Vollers & Stern, 2008). Finally, the use of tandem minigenes or peptide pools provides an unbiased screening of all the candidate neoantigens identified by the tumour whole exome sequencing. The main advantage of this approach is that it mimics the natural antigen processing and presentation of neoepitopes. However, the requirement of large numbers of autologous APCs and effector cells to perform these screens can be a limitation (Garcia-Garijo et al., 2019).

In the clinical setting, neoantigen-reactive T cells have been identified and isolated from both TILs and peripheral blood of different cancer patients (Cafri et al., 2019; Cohen et al., 2015; Deniger et al., 2018; Gros et al., 2016; Lennerz et al., 2005; Lu et al., 2014; Robbins et al., 2013; E. Tran et al., 2015). Moreover, it has been shown that neoantigen-reactive T cells can drive tumour rejection of different cancer types (Prickett et al., 2016; E. Tran et al., 2016, 2014; Zacharakis

et al., 2018). Together, these studies provide support for the central role of neoantigen-reactive lymphocytes in the clinical activity of cancer immunotherapies. Hence, enriching for neoantigen-specific T cells in adoptive cellular therapies is a promising approach to increase the response rate.

4.3. Aims

The efficacy of TIL therapy is dependent on T cells recognising and eradicating tumour cells. Furthermore, it has been shown that tumour regression is associated with a higher absolute number of infused tumour-reactive T cells (R. Andersen et al., 2016). Hence, to generate powerful adoptive cellular therapies, it is paramount that the TIL product that is infused contains a high number of tumour-reactive T cells. To try to achieve the selection and preferential expansion of tumour-reactive T cells (or, if possible, of neoantigen-reactive T cells), the main objectives of the work presented in this chapter were the following:

- Characterisation of expanded melanoma TILs.
- Characterisation of a primary melanoma cell line.
- Detection and selection of tumour-reactive T cells post-expansion.

4.4 Characterisation of expanded MX063 tumour infiltrating lymphocytes and of autologous primary tumour cell line

Expanded TILs from patient MX063 were characterised early in this project as they were the main sample used for the optimisation of gene editing. For this, TILs that had been expanded using the REP and frozen were thawed and stimulated with ImmunoCult Human CD3/CD2/CD28 T Cell Activator (Stemcell Technologies) and IL-2 (see materials and methods for more information). It was of interest to this project to see the kinetics of the targets for gene editing (i.e. PD1, TIGIT, LAG3, and, at that point in time, TIM3). Hence, TILs were left in culture for 6 days with the αCD3/CD2/CD28 T cell activator (Stemcell Technologies) and every day aliquots were taken to stain for the targets of interest. This showed that, after providing the required primary and co-stimulatory

signals for T cell activation, the TILs started to express PD1 and TIM3 as early as day 1. Moreover, a majority of the cells (~82%) became $TIM3^+$ by day 3, and by day 5 most of the cells were expressing TIM3 (~93%) (Figure 4.1A). The kinetics of PD1 were different, with ~60% of cells expressing PD1 as soon as day 2. Afterwards, the percentage of $PD1^+$ cells steadily decreased until there were only ~30% of cells expressing PD1 by day 6 (Figure 4.1A). Additionally, these TILs already expressed a considerable amount of TIGIT (~54%) and LAG3 (~20%) prior to stimulation with αCD3/CD2/CD28 (however, it is worth noting that these TILs had already been expanded prior to freezing). Expression of TIGIT and LAG3 increased rapidly, with ~86% of cells expressing TIGIT and ~88% of cells expressing LAG3 as early as day 1 post-stimulation. Furthermore, most of the cells (~97%) were expressing TIGIT by days 2 and 3 post-stimulation, and this high expression of TIGIT (~94% of cells were $TIGIT^+$) persisted on days 4-6 post-stimulation (Figure 4.1B), albeit with a slightly lower MFI (data not shown). LAG3 expression steadily increased from ~95% of cells expressing LAG3 on day 2 to almost 100% of cells expressing it at day 6 (Figure 4.1B). It is worth noting that the expression of these targets was evaluated only on $CD8^+$ cells as the batch of expanded TILs used for this experiment consisted primarily of $CD8^+$ T cells (>90%, data not shown).

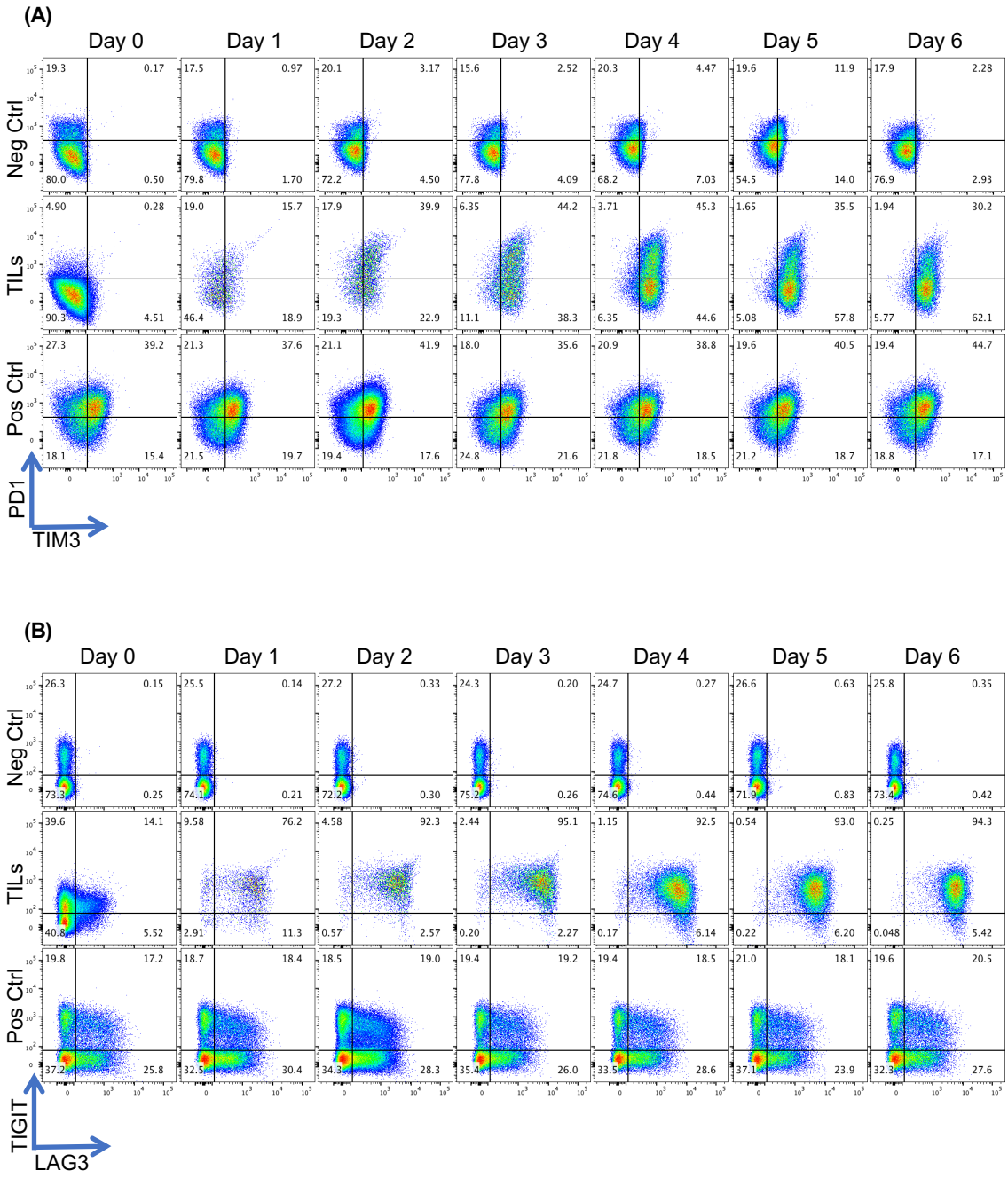

Figure 1 Checkpoint expression in expanded MX063 TILs after stimulation. Expanded MX063 TILs were thawed and stimulated with αCD3/CD2/CD28 + IL-2 for 6 days. Each day aliquots were taken and stained for **(A)** PD1 and TIM3 expression and **(B)** TIGIT and LAG3 expression. Negative control are non-activated healthy donor PBMCs. Positive control are healthy donor PBMCs activated for 3 days with αCD3+αCD28+IL-2. All gated on $CD8^+$ T cells.

Furthermore, a primary tumour cell line for patient MX063 was established in our laboratory (this work was performed by Sophia Wong). The establishment of this primary cell line allowed this project to have an autologous system to test

the expanded TILs (edited vs. non-edited) in a variety of functional assays. Hence, it was important to first characterise the MX063 tumour cell line. For this, expression of the major histocompatibility complex (MHC) class I (HLA-ABC) and MHC class II (HLA-DR) was evaluated by flow cytometry in MX063 tumour cells that had been grown in culture for eleven passages (Figure 4.2). Moreover, the expression of ligands of interest on these cells was also evaluated by flow cytometry (Figure 4.2). Fluorescence minus one (FMO) controls were used to determine where to set the gates (Supplementary Figure 8.11).

This evaluation showed that all of the MX063 tumour cells expressed MHC class I molecules and that the majority of the cells also expressed MHC class II molecules (the canonical ligand for LAG3). In addition, ~30% of the tumour cells expressed CD155 (the ligand that TIGIT binds to with high affinity) and all of the cells also expressed CD112 (the ligand that TIGIT binds to with a lower affinity). There was also a high expression of B7-H3 in all of the tumour cells. This is of interest as B7-H3 has been shown to be overexpressed in many types of cancer, and this overexpression has been associated with a poor clinical prognosis (Ingebrigtsen et al., 2012; Jinhua Wang et al., 2013), hence it has become an attractive target for cancer immunotherapy. Furthermore, the tumour cells were evaluated for CD45 expression as there have been rare cases of tumours expressing this haematopoietic marker (Nandedkar, M. A., Palazzo, J., Abbondanzo, S. L., Lasota, J., & Miettinen, 1998; Ngo, Patel, Isaacson, & Naresh, 2007). This evaluation showed that there was no expression of CD45 in this primary tumour cell line.

These tumour cells did not express either of the PD1 ligands (PD-L1 and PD-L2), nor the ligand for TIM3 (Galectin-9). However, it has been shown that IFNγ can regulate expression of PD-L1 and of Galectin-9 (Imaizumi et al., 2002; Mimura et al., 2018). To test if this was the case with these cells, MX063 tumour cells were cultured for 24 hours in the presence or absence of human IFNγ and evaluated via flow cytometry (Figure 4.3). This evaluation showed that IFNγ upregulated the expression of PD-L1 but not of Galectin-9 on these cells.

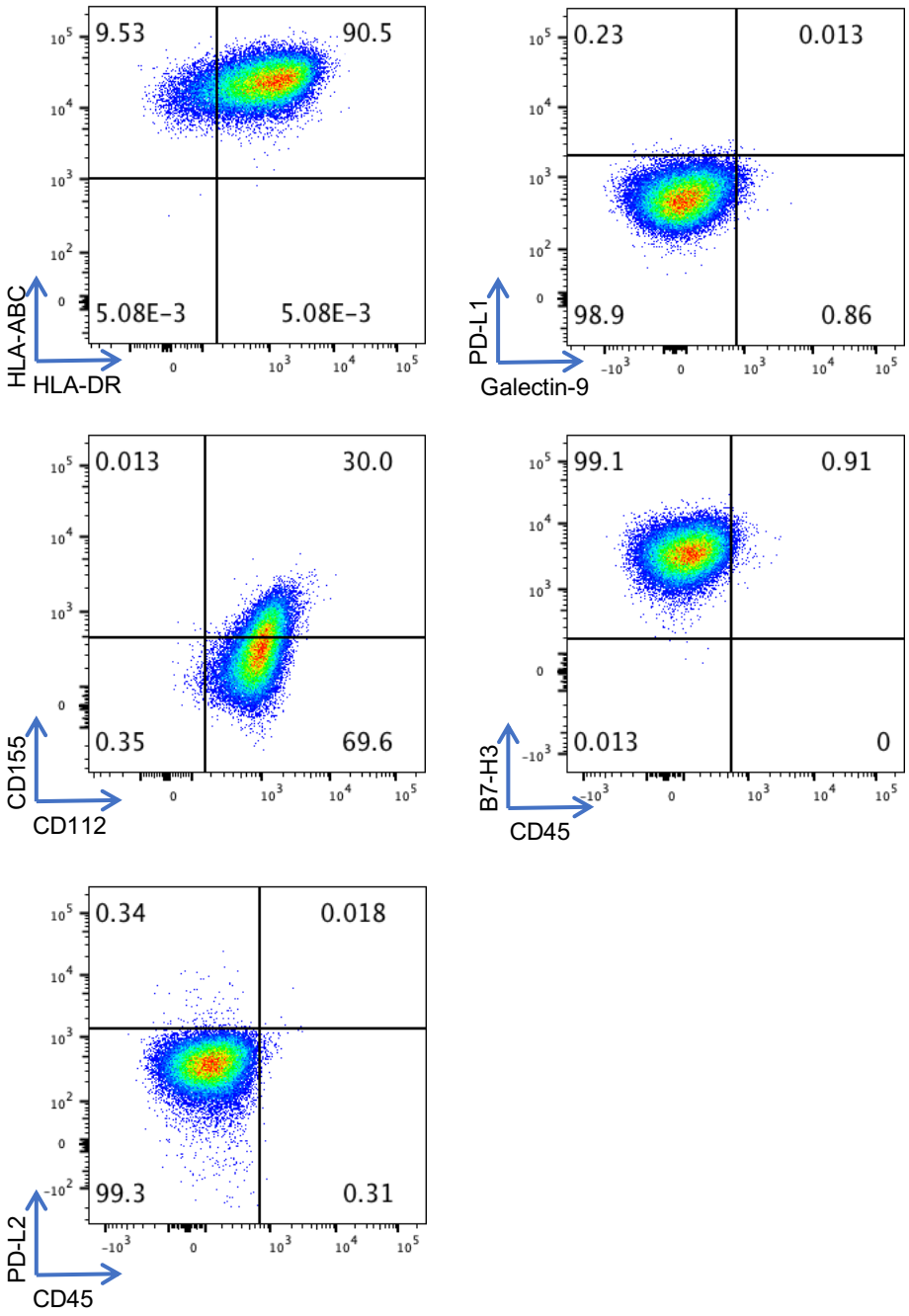

Figure 4.2. Characterisation of MX063 primary tumour cell line. A primary tumour cell line grown from patient MX063 was stained for ligands of interest as well as for MHC class I and class II expression. All gated on live cells.

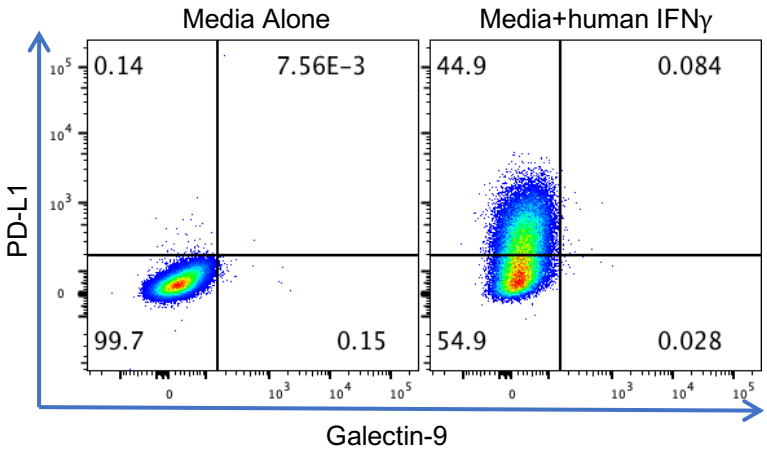

Figure 4.3. Upregulation of PD-L1 by IFNγ in MX063 primary tumour cell line. A primary tumour cell line grown from patient MX063 was stained for PD-L1 and Galectin-9 in the absence or presence of human IFNγ (50ng/mL), and this showed an upregulation of PD-L1 mediated by IFNγ. Gated on live cells.

4.5. Expansion and selection of tumour-reactive T cells

After confirming the ability of the MX063 TILs to upregulate the targets of interest and corroborating the expression of the ligands for these targets in the tumour cell line, the next aim was to test if the expanded MX063 TILs were reactive to the autologous tumour cell line. For this, MX063 TILs that had been previously frozen were expanded in one of two ways, either using the rapid expansion protocol (REP) or using a modified version of the 'pre-REP' followed by a REP (see materials and methods section for more information). Briefly, this modified version of the pre-REP protocol consists of setting up cultures of unexpanded TILs with irradiated autologous cell line in the presence of 6000IU/mL of IL-2 and 25ng/mL of IL-21 for two weeks prior to performing the REP. After expanding the cells in these ways, recall assays were performed against the autologous cell line to test tumour reactivity of the expanded TILs (see materials and methods section for more information). This showed that TILs expanded using the 'REP' were $CD8^+$ cells and, that when incubated with the autologous cell line, the majority of them secreted IFNγ (there was ~60% of IFNγ expression) (Figure 4.4A). In contrast, the TILs expanded using the 'pre-REP+REP' were a mixture of $CD4^+$ and $CD8^+$ cells, with the majority of them being $CD4^+$ cells. Moreover, when incubated with the autologous cell line, ~40%

of the CD8$^+$ cells secreted both IFNγ and TNFα, whilst the CD4$^+$ cells did not secrete either (Figure 4.4B).

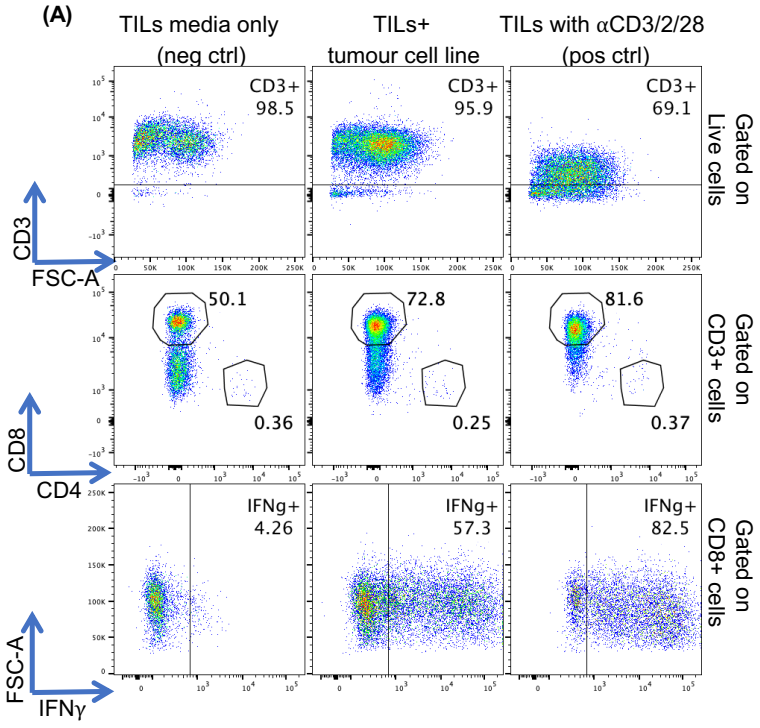

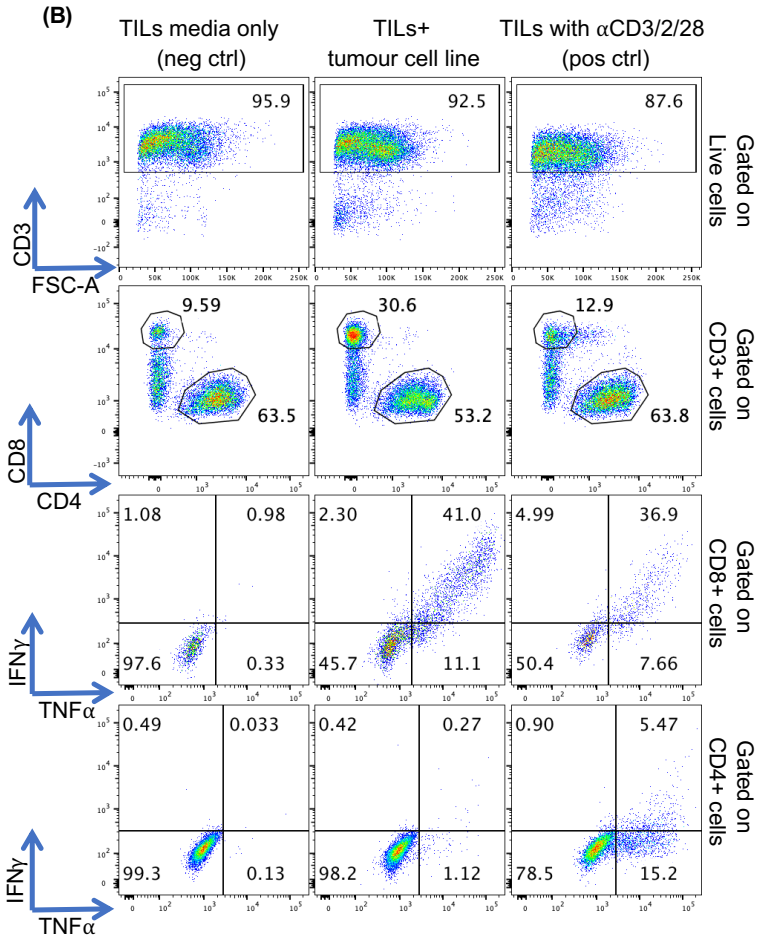

Figure 4.4. Recall assay for expanded TILs against autologous tumour cell line. MX063 TILs that were expanded using either **(A)** the REP or **(B)** the pre-REP followed by a REP, were incubated against the MX063 tumour cell line for 16 hours in the presence of a protein transport inhibitor (Brefeldin A). 'REP' cells were later stained for IFNγ and 'pre-REP+REP' cells were stained for IFNγ and TNFα. TILs left in media alone are shown as a negative control and TILs stimulated with ImmunoCult Human CD3/CD2/CD28 T Cell Activator (Stemcell Technologies) are shown as a positive control.

Although there was a substantial percentage of expanded TILs that had reactivity against the tumour cell line in both the 'REP' and the 'pre-REP+REP' conditions, there were still ~40-60% of cells that expanded but did not show reactivity against the tumour. To achieve a pure population of tumour-reactive TILs, the expanded TILs were CFSE-labelled and incubated with the autologous tumour cells for 6 days. After incubation with the tumour cells the TILs that had divided (i.e. the tumour-reactive TILs), and hence diluted their CFSE staining, were sorted via flow cytometry. This sorting showed a 5.65% of dividing $CD8^+$ cells in the 'REP' TILs (Figure 4.5A), and a 6.39% of dividing $CD8^+$ and 5.94% of dividing $CD4^+$ cells in the 'pre-REP+REP' TILs (Figure 4.5B). The sorted TILs were then left to recover in media with 1000IU/mL of IL-2 for 48 hours before rapidly expanding them again. Unfortunately, the cells did not survive the sorting and subsequent rapid expansion, as the viability of the cells post-sorting was ~30%, and this viability worsened during the REP. With cells dying instead of expanding, the viability declined to less than 10%.

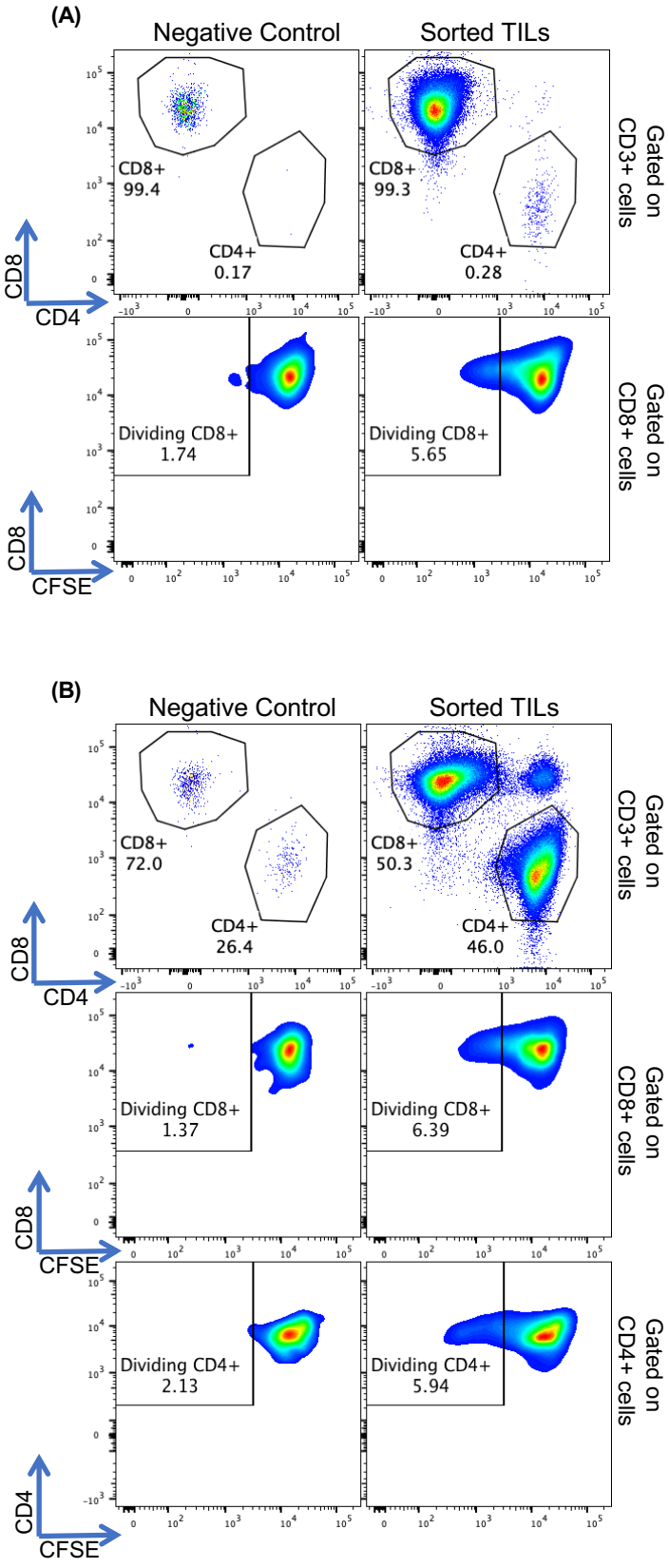

Figure 4.5. Sorting of tumour-reactive MX063 TILs. Expanded MX063 TILs using the **(A)** 'REP' or **(B)** the 'pre-REP+REP' method were CFSE-labelled and incubated with the autologous tumour cell line for 6 days prior to sorting. The negative controls are expanded TILs using the **(A)** 'REP'

or **(B)** the 'pre-REP+REP' method that were CFSE-labelled and left in media without the tumour cell line for 6 days.

It was hypothesised that incubating the sorted TILs for 48 hours with only a high dose of IL-2 may have been detrimental to the viability of the cells. To test this, tumour-reactive TILs were sorted again, however this time they were expanded immediately after sorting. Hence, TILs that has been expanded via the 'REP' were thawed, CFSE-labelled and incubated with the autologous tumour cells for a week. After incubation with the tumour cells the TILs that had divided (i.e. the tumour-reactive TILs), and the ones that had not (i.e. non tumour-reactive TILs) were sorted via flow cytometry. This sort showed that the viability of the cells prior to the sorting was ~74%. Moreover, 99% of these viable cells were $CD8^+$ cells and 42.5% of these were tumour-reactive (they had undergone at least 4 rounds of division). This was in comparison to the negative control (expanded TILs left in media alone for a week), where there were only 0.53% of tumour-reactive $CD8^+$ cells (Figure 4.6). Immediately after sorting, the tumour-reactive and the non tumour-reactive TILs were expanded using the rapid expansion protocol. Five days into the rapid expansion protocol, aliquots of the TILs were taken to count the cells and it was discovered that the viability of the cells was less than 5%. Furthermore, by the end of the REP the cells had not expanded and their viability had only increased to ~10%. Of note, this was the case for both the tumour-reactive and the non tumour-reactive TILs. Hence, we hypothesised that technical issues with the sorting were compromising the viability of the cells, as both tumour-reactive and non-tumour reactive TILs failed to expand post-sorting even though they were previously able to proliferate normally when incubated with their autologous tumour cells.

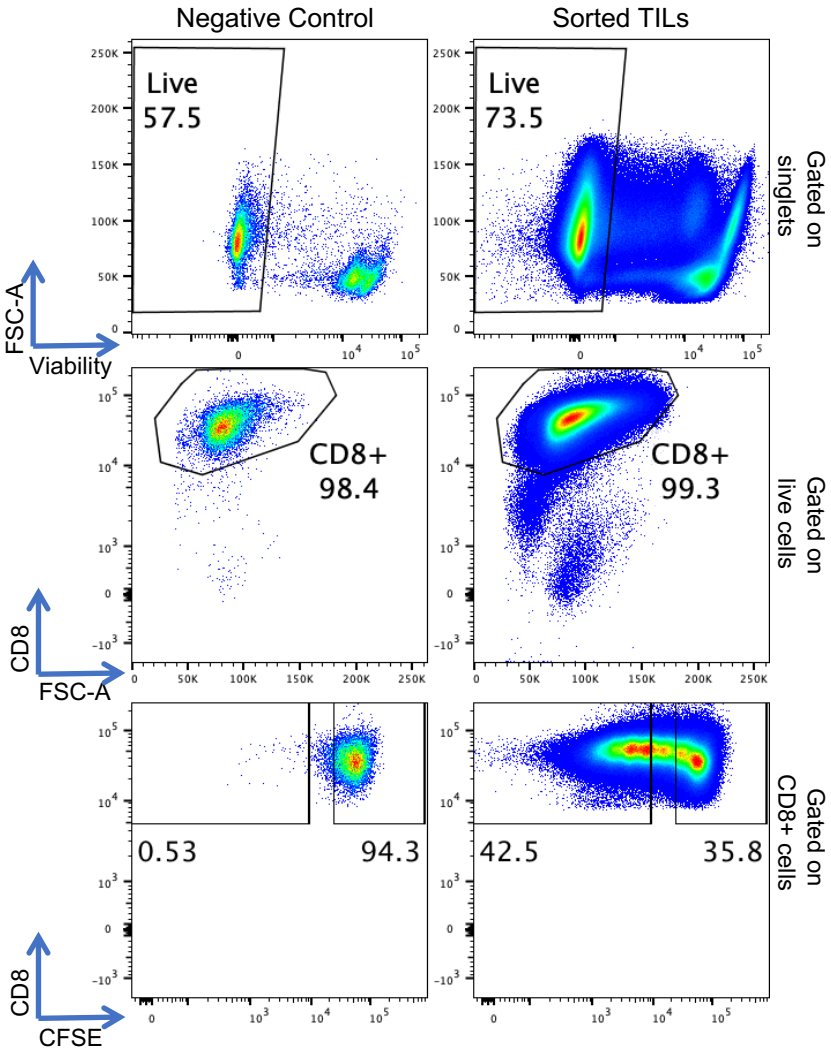

Figure 4.6. Sorting of tumour-reactive TILs from MX063 TILs expanded using the 'REP'. Expanded MX063 TILs using the 'REP' were CFSE-labelled and incubated with the autologous tumour cell line for one week prior to sorting. The negative control is expanded MX063 TILs using the 'REP' that were CFSE-labelled and left in media without the tumour cell line for a week.

4.6. Peptide screening of MX063 tumour infiltrating lymphocytes in search of neoantigen reactive T cells

Given that the expanded TILs did not survive the sorting (regardless if they were tumour-reactive or not), it was concluded that this was not a viable option for selection and further expansion of tumour-reactive T cells. As an alternative, another approach to select tumour-reactive TILs would be to screen the TILs for reactivity against neoantigens and preferentially expand those neoantigen-reactive T cells with the corresponding peptide. To achieve this, the MX063

primary cell line was sequenced by our collaborators at the Francis Crick Institute and single nucleotide variants (SNVs) as well as short insertions and deletions (indels) were detected (sequencing and bioinformatics analysis performed by Samra Turajlic's lab). It is important to note that there is the possibility that some of the detected indels could lead to nonsense mediated decay and hence not be expressed at the protein level. To quantify this, RNA-seq with allelic skewing could be added as part of the peptide-detection pipeline.

Afterwards, the SNVs and indels peptides were commercially synthesised by Pepscan (373 peptides in total). Upon receiving these peptides, three screenings were performed with different stocks of expanded MX063 TILs (all of the peptide screenings were performed in conjunction with Emine Hatipoglu).

The first screening was performed with the indels peptides as it was hypothesised that the indels would have a higher probability of inducing a response on the MX063 TILs. The indels were divided into seventeen pools of 5 peptides and one pool of 2 peptides (0.4nmols/peptide). For this screening, we made use of a new batch of MX063 TILs that had been expanded using the REP (these TILs will be named 'REP*' to differentiate them from the previous stock of 'REP' TILs). We decided on using these TILs as they expanded to great numbers; however, they had not been previously assessed for tumour reactivity. Since the peptide screen performed made use of T cell-T cell interactions, TILs were thawed and plated, and the pools of peptides directly added to them. A recall assay was performed to screen for peptide reactivity on the $CD8^+$ cells (see materials and methods section for more information). This showed that the 'REP*' TILs were not as tumour-reactive as the previous stocks, with only ~6% of them secreting both IFNγ and TNFα when stimulated with their autologous tumour cell line (Figure 4.7A). Moreover, none of the indels peptide pools elicited a response (Figure 4.7A). This peptide screening was performed in triplicates and quantification was performed. This quantification showed that the percentage of double positives for IFNγ and TNFα was statistically significant for the TILs stimulated with αCD3/CD2/CD28 (21% $\pm$ 1%; $P<0.0001$) and with their autologous tumour cell line (5% $\pm$ 0.5%; $P<0.0001$) compared to control (media alone). This statistical significance was lost on the TILs stimulated with the tumour cell line when the MHC blocking agent was added (0.4% $\pm$ 0.03%; P=ns).

Furthermore, there was no significant difference between the control (media alone) and any of the peptide pools (Figure 4.7B).

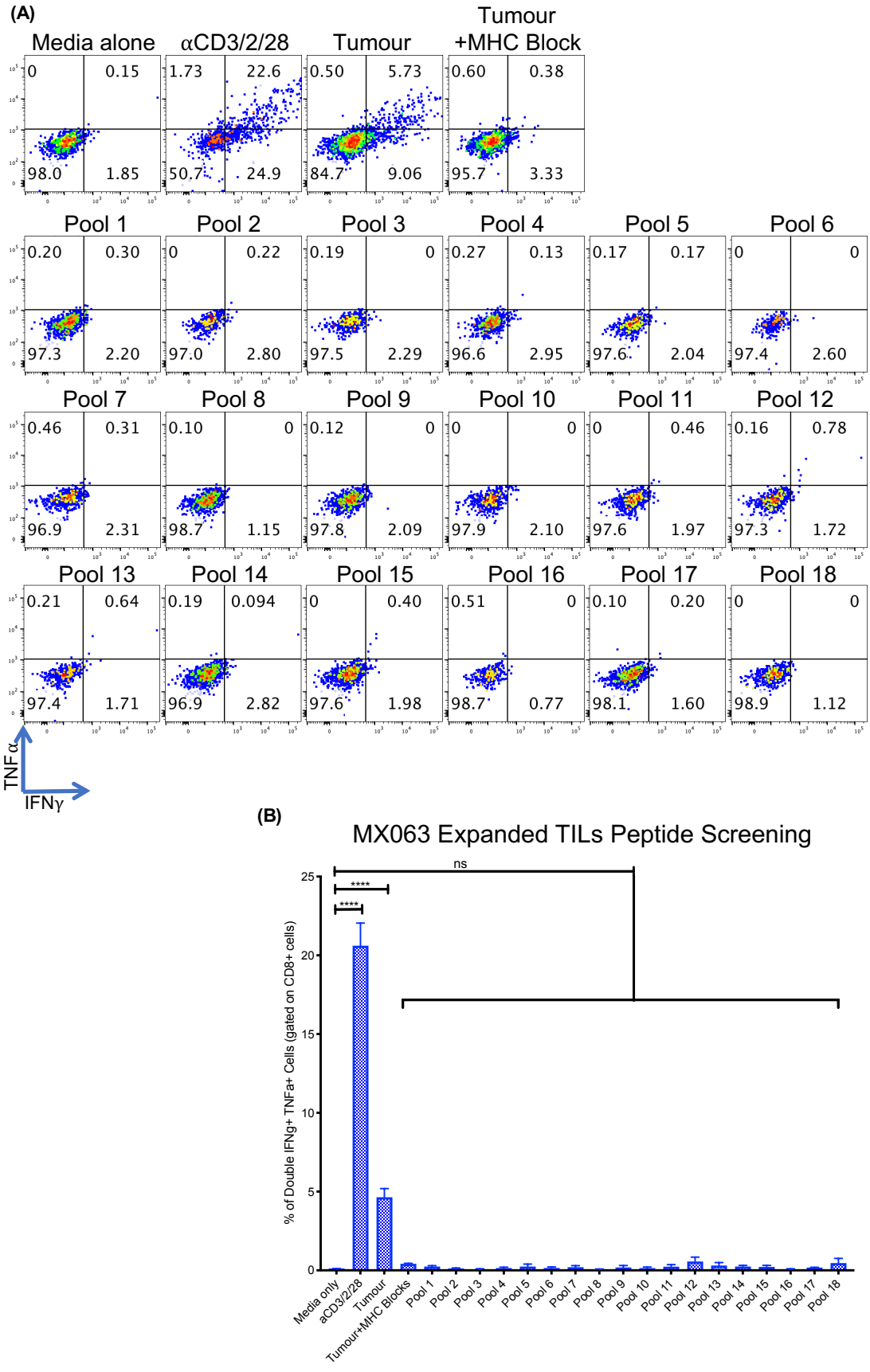

Figure 4.7. Indels peptide screening of MX063 'REP*' TILs. MX063 TILs that were expanded using the REP (MX063 'REP*' TILs) were thawed and incubated with pools of indels peptides for 16 hours in the presence of a protein transport inhibitor (Brefeldin A). 'REP*' cells were later stained for IFNγ and TNFα. TILs left in media alone are shown as a negative control and TILs stimulated with ImmunoCult Human CD3/CD2/CD28 T Cell Activator (Stemcell Technologies) are shown as a positive control, as well as TILs stimulated with their autologous tumour cell line +/- an MHC blocking agent. All of the analysis was performed on $CD8^+$ cells. **(A)** Representative flow cytometry plots from triplicates. **(B)** Quantification and statistical analysis of the triplicates of this screen. One-way ANOVA followed by Dunnett's Multiple Comparison was performed.

As we observed that there was only a ~6% of $IFN\gamma^+$ and $TNF\alpha^+$ double positives when these expanded TILs were stimulated with their autologous tumour cell line (i.e. there was a very small proportion of tumour-reactive T cells), it was concluded that this stock of TILs was not the most suitable to test the reactivity against the peptides. Hence, the indel peptide screen was repeated with the stock of 'pre-REP+REP' TILs that had previously shown ~40% of $IFN\gamma^+$ $TNF\alpha^+$ double positives when stimulated with the autologous tumour cell line. Given the number of cells available from this stock, this screen was performed with bigger pools of peptides. Therefore, four pools of 20 indel peptides and one pool of 7 indel peptides (0.5nmols/peptide) were generated. A recall assay was performed to screen for peptide reactivity on the $CD8^+$ cells (see materials and methods section for more information). This peptide screen showed that the 'pre-REP+REP' TILs secreted both IFNγ and TNFα when stimulated with their autologous tumour cell line (26% ± 1%), and that this was an MHC-mediated response, as it was suppressed when an MHC blocking agent was added (2%) (Figure 4.8A). Moreover, the 'pre-REP+REP' TILs showed a strong response when stimulated with either CD3/CD2/CD28 (74% ± 2%) or a superantigen (Staphylococcus aureus Enterotoxin Type B; SEB) (31% ± 3%). However, as with the previous peptide screening, none of the indels peptide pools elicited a response (Figure 4.8A). Furthermore, a quantification of the $IFN\gamma^+$ $TNF\alpha^+$ double positives was performed (Figure 4.8B), however, because of the low number of cells only the positive controls were performed in duplicate, so no statistical analysis could be carried out.

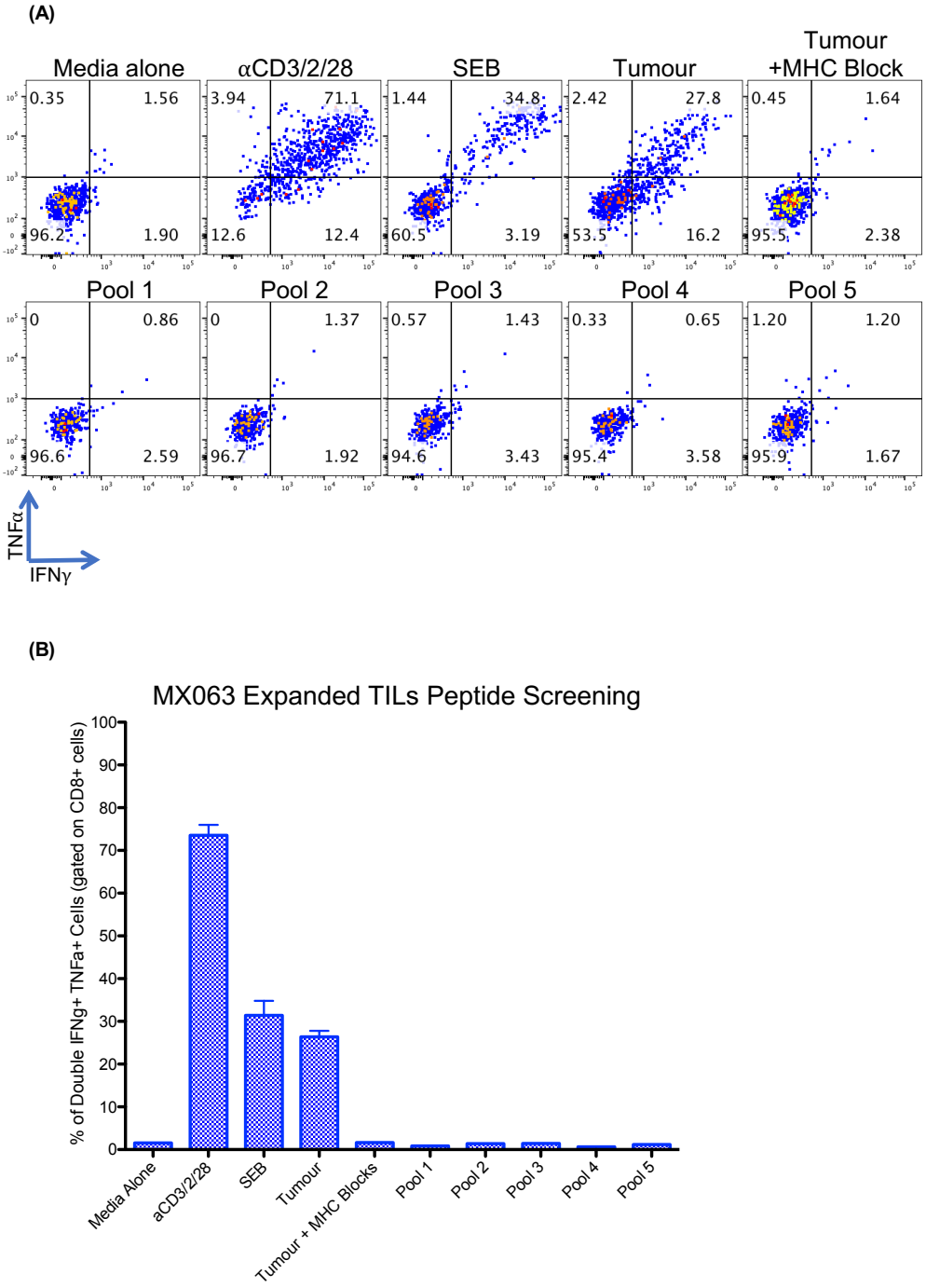

Figure 4.8. Indels peptide screening of MX063 'pre-REP+REP' TILs. MX063 TILs that were expanded using a pre-REP+REP method (MX063 'pre-REP+REP' TILs) were thawed and incubated with pools of indels peptides for 16 hours in the presence of a protein transport inhibitor (Brefeldin A). 'Pre-REP+REP' cells were later stained for IFNγ and TNFα. TILs left in media alone are shown as a negative control and TILs stimulated with either ImmunoCult Human CD3/CD2/CD28 T Cell Activator (Stemcell Technologies) or a superantigen (Staphylococcus aureus Enterotoxin Type B; SEB) are shown as positive controls. TILs stimulated with their autologous tumour cell line +/- an MHC blocking agent are also shown as controls. All of the analysis was performed on $CD8^+$ cells. **(A)** Representative flow cytometry plots (duplicates

performed only for positive controls). **(B)** Quantification of the IFNγ and TNFα double positives on $CD8^+$ cells.

As it was shown that the 'pre-REP+REP' expanded TILs did not react to any of the indels peptide pools but did react to the autologous tumour cell line, the next step was to test if the SNV peptides could elicit a response on these TILs. For this, the 286 SNV peptides were divided into fifteen pools (fourteen pools of 20 peptides and one pool of 6 peptides; 0.5nmols/peptide) and plated with the 'pre-REP+REP' expanded TILs. A recall assay was performed to screen for peptide reactivity on the $CD8^+$ cells (see materials and methods section for more information). This screen showed that ~73% of the 'pre-REP+REP' TILs secreted both IFNγ and TNFα when stimulated with their autologous tumour cell line, and that this was an MHC-mediated response, as it was suppressed when an MHC blocking agent was added (Figure 4.9). This is in contrast with the last screen, where this positive control only showed a ~28% of double positive $IFN\gamma^+$ $TNF\alpha^+$ secretion. This could be explained by a difference in the tumour cells used between these screens. In both of the previous screens freshly thawed MX063 passage 7 tumour cell line was employed, while in this screen tumour cells that had been thawed and grown for two passages were used (MX063 tumour cell line passage 9). Additionally, as with the previous peptide screening, the 'pre-REP+REP' TILs showed a strong response when stimulated with either CD3/CD2/CD28 or a superantigen (SEB). However, none of the SNV peptide pools elicited a response (Figure 4.9).

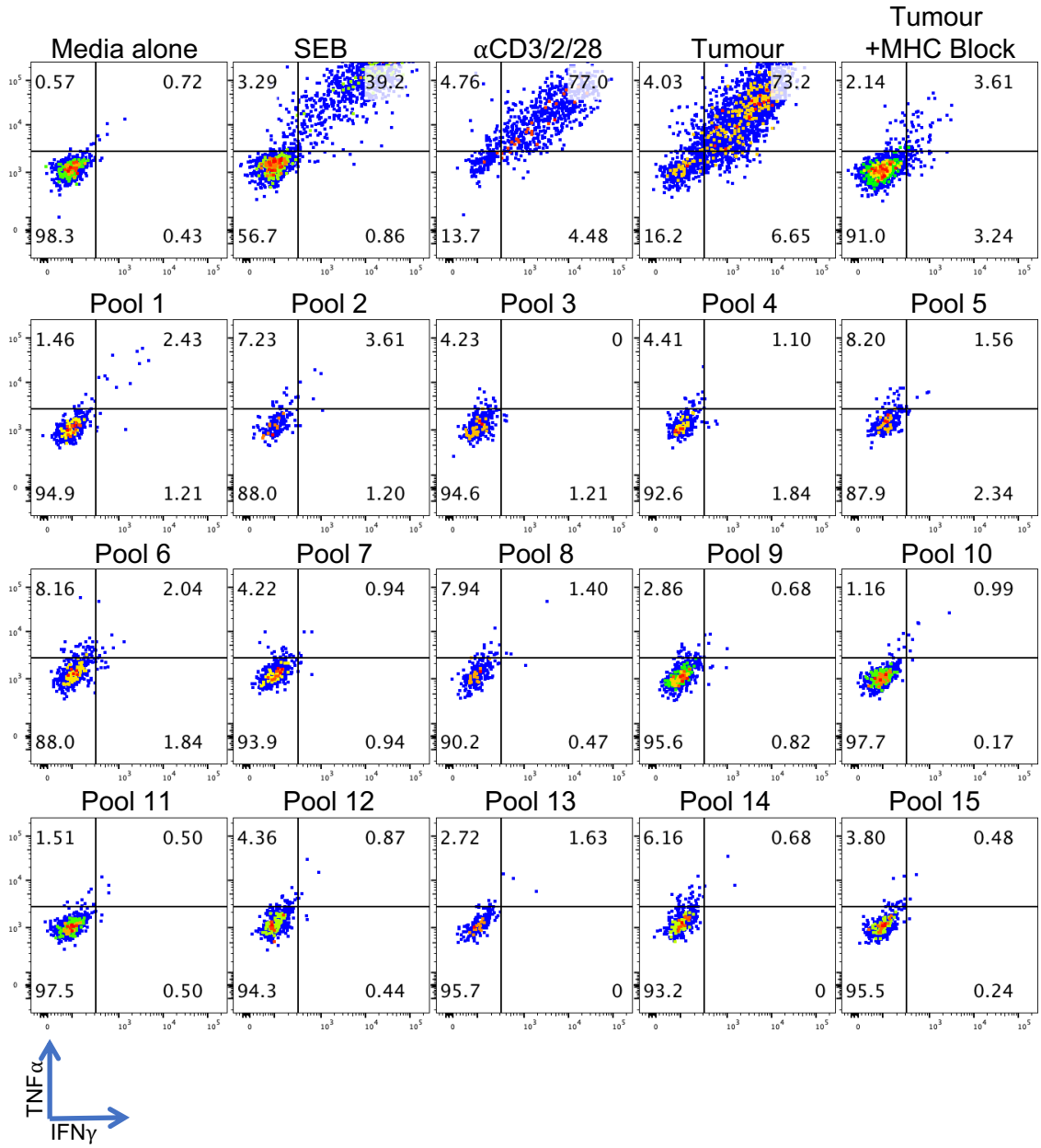

Figure 4.9. SNV peptide screening of MX063 'pre-REP+REP' TILs. MX063 TILs that were expanded using a pre-REP+REP method (MX063 'pre-REP+REP' TILs) were thawed and incubated with pools of SNV peptides for 16 hours in the presence of a protein transport inhibitor (Brefeldin A). 'Pre-REP+REP' cells were later stained for IFNγ and TNFα. TILs left in media alone are shown as a negative control and TILs stimulated with either ImmunoCult Human CD3/CD2/CD28 T Cell Activator (Stemcell Technologies) or a superantigen (Staphylococcus aureus Enterotoxin Type B; SEB) are shown as positive controls. TILs stimulated with their autologous tumour cell line +/- an MHC blocking agent are also shown as controls. All of the analysis was performed on $CD8^+$ cells.

4.7. Discussion

This chapter has shown the work performed to characterise the expanded TILs and the primary tumour cell line from patient MX063. Additionally, in this chapter it was also shown that the identification of tumour-reactive T cells within the expanded MX063 TIL population was achieved. However, a selection and further expansion of these tumour-reactive T cells was not possible. It was hypothesised that this was not successful because of the fragility of these heavily expanded cells combined with the roughness of the selection method (i.e. sorting of the cells via flow cytometry). Furthermore, work presented here also showed that neoantigen-reactive T cells were not detectable in the expanded MX063 TIL populations that were screened.

The characterisation of the expanded MX063 TILs showed that upon stimulation, the immune-checkpoints of interest were upregulated, making them good targets for editing in these cells. Interestingly, although >90% of the $CD8^+$ TILs were able to express LAG3, TIGIT, and TIM3 upon stimulation, only ~60% of these cells expressed PD1. The characterisation performed on the MX063 tumour cell line further demonstrated that the immune-checkpoints chosen were relevant for this patient's cells, as this primary cell line expressed the ligands for two of the immune-checkpoints of interest (i.e. TIGIT and LAG3) at high levels. Expression of Galectin-9 (TIM3 ligand) was not detected in these cells, even after stimulation with IFNγ (Imaizumi et al., 2002). In contrast, these cells were shown to express PD-L1 (PD1 ligand), but only after stimulation with IFNγ (Mimura et al., 2018).

The main aim of the research discussed in this chapter was to detect and preferentially expand tumour-reactive T cells or, if possible, neoantigen-reactive T cells. In this regard, the detection of tumour-reactive T cells was achieved, as incubating different stocks of expanded TILs against the autologous tumour cell line achieved a response from a portion of these expanded cells. The response upon stimulation with the autologous tumour cells was measured in two ways: 1) by secretion of cytokines (i.e. IFNγ and TNFα); and 2) by proliferation of TILs (measured by CFSE-dilution). Furthermore, the TILs that had proliferated when stimulated with their autologous tumour cell line (i.e. the tumour-reactive T cells) were isolated using flow cytometry sorting. These cells did not recover well after

sorting and this resulted in failed expansions. Although CFSE-labelling has been shown to be toxic for cells (Lašťovička, Budinský, Špíšek, & Bartůňková, 2009), this was not the cause of the low viability of the TILs. Given that the cells proliferated normally when incubated with their autologous tumour cells, and that they were alive prior to the sorting (cells that were sorted were also labelled with a fixable viability dye and this showed that the viability of the cells prior to sorting was ~95% on the first two sorts (data not shown) and ~74% on the last sort), we concluded that the problem lay with the sorting via flow cytometry. Hence, the current hypothesis is that technical issues with the sorting are compromising the viability of the cells, and changes that have been shown to improve cell viability and yield, such as dividing the sort into shorter intervals and adjusting the flow rate to maintain the lowest possible pressure (Basu, Campbell, Dittel, & Ray, 2010; Cossarizza et al., 2017), will be implemented in future sorts.

As a further attempt to select and expand tumour-reactive T cells, a neoantigen peptide screen was performed with two stocks of expanded MX063 TILs. The first stock of expanded TILs used for this peptide screen (MX063 'REP*' TILs) proved to have a lower proportion of tumour-reactive T cells than the previous stocks. This was visible in the low percentage of cytokine secretion when incubated with its autologous tumour cell line (~6%). Hence, even though no neoantigen-reactive T cells were detected in this screen, it was concluded that this was because of the low proportion of tumour-reactive T cells that had expanded. To improve the probability of finding neoantigen-reactive T cells, a previous batch of expanded TILs was used (MX063 'pre-REP+REP' TILs). This stock of TILs had previously shown to contain a high proportion of tumour-reactive T cells (~40%), however neither the indels nor the SNVs peptides elicited a response in these expanded cells. One of the positive controls for these screens was the stimulation of the 'pre-REP+REP' TILs with the autologous tumour cell line, and this showed a high proportion of TILs secreting both IFNγ and TNFα (~28% in the indels screen and ~73% in the SNVs screen). This disconnect between the lack of detectable neoantigen-reactive T cells and the high proportion of tumour-reactive T cells could be explained in the following ways:

1) *T cell to T cell interactions are not sufficient to efficiently present the peptides.* It is known that the efficiency of this screening approach is

influenced by the APC chosen (Garcia-Garijo et al., 2019) and that usually this peptide pool approach is performed with autologous APCs such as immature dendritic cells and *ex vivo* stimulated B cells (Garcia-Garijo et al., 2019). Hence, it could be hypothesised that by using T cell-T cell interactions, the mutated proteins are not being properly processed to generate MHC class I binding epitopes. However, colleagues in the lab have detected neoantigen-reactive T cells in other patients' TILs using this type of peptide screening with T cell-T cell interactions (data not shown), so this hypothesis is not currently favoured.

2) *The cells used could be suboptimal for this assay.* It is known that the choice of effector population screened can greatly impact on neoantigen identification (Garcia-Garijo et al., 2019). In this regard, given that frequencies of neoantigen-reactive T cells are very low (usually <1%) (McGranahan et al., 2016; Yossef et al., 2018), and that rapid expansion has been shown to decrease the frequency of tumour-specific T cells (R. S. Andersen et al., 2012), it may be that to detect neoantigen-reactive T cells unexpanded TILs are needed.
3) *The tumour-reactive T cells that are seen in high proportion in these expanded TILs are not neoantigen-reactive T cells.* There is the possibility that the tumour-reactive T cells are recognising tumour-associated antigens. Indeed, it is known that tumour-reactive T cells in melanoma frequently recognise melanocyte differentiation antigens such as MART-1 and gp100 (Kvistborg et al., 2012). It could also be that the neoantigen(s) that would drive a response were not screened as only the peptides that were predicted as strong binders were synthesised and screened. To investigate these hypotheses further, the immunopeptidome of this tumour cell line will be analysed using mass spectrometry (Bassani-Sternberg, 2018). The results from this immunopeptidomics assay will be used to prioritise new candidate neoantigens for screening.

In conclusion, the work presented in this chapter allowed for the characterisation of a melanoma patient expanded TILs as well as of the

autologous tumour cell line generated. Moreover, it was shown that tumour-reactive T cells were detectable in expanded TILs to high numbers, but that the proportion of these cells varied between expansions. At this moment, the selection of these tumour-reactive T cells and further expansion of them is still under optimisation, and different methods for achieving this are under investigation. Finally, neoantigen-reactive T cells were not detected in these expanded TILs, and more work will be needed to decipher if this was due to technical limitations of the assay, if the TILs selected for the assay were suboptimal (i.e. expanded TILs vs. unexpanded), or if the majority of the tumour-reactive T cells that are in this patient TILs are tumour-associated antigens (i.e. overexpressed antigens, C/T antigens, or differentiation antigens) instead of tumour-specific antigens (i.e. neoantigens).

Chapter 5. Development of *in vitro* and *in vivo* functional assays for the characterisation of tumour infiltrating lymphocytes

5.1. Overview

As the overall goal of this study was to generate novel and powerful adoptive cellular therapies by gene editing of tumour infiltrating lymphocytes (TILs), it was critical to develop assays that allowed functional evaluation of such new therapies. The work presented in this chapter aims to determine whether the gene editing of different immune checkpoints in human TILs grants them functional advantages *in vitro* and *in vivo*.

5.2. Introduction

5.2.1. Patient derived xenografts as a model for adoptive cellular therapies

Current *in vitro* assays that measure the tumour-recognition by immune cells via cytokine secretion and the anti-tumour efficacy of the T cells via tumour-killing have been established as rapid and economical methods of screening for tumour-reactive T cells that can be used for adoptive cellular therapies (Dudley et al., 2003; Lee et al., 2017; Muul, Spiess, Director, & Rosenberg, 1987; Vánky et al., 1986). However, these *in vitro* systems do not take into account the influences of the tumour microenvironment upon the immune response. As it is known that the tumour microenvironment has an important role in cancer progression and resistance to therapy (Chang et al., 2015; Quail & Joyce, 2013; Sun, 2016), *in vivo* models that can recreate the three-dimensional structure of the tumour with its microenvironment are better suited for preclinical studies of adoptive cellular therapies.

In a preclinical setting, the *in vivo* mouse models that are used for the study of adoptive cellular therapies are the cell line-derived xenografts (CDX) and

the patient-derived xenografts (PDX). The main difference between these two models is that the CDX are human tumour samples that have been cultured as cell lines and implanted into immunodeficient mice, while the PDX are fresh human tumour tissue or cells that are not grown in plastic or propagated as cell cultures but injected directly into immunodeficient mice following surgical resection.

It has been demonstrated that CDX models lose key genetic signatures of the original tumours (Daniel et al., 2009). In contrast, PDX models have been shown to retain the main characteristics of the original tumours (Bertotti et al., 2011; Derose et al., 2011). Because of this, PDX models can offer predictive insights into clinical outcomes when evaluating the efficacy of cancer therapies (Einarsdottir et al., 2014; Gao et al., 2015; Izumchenko et al., 2017; Quintana et al., 2012). The first reported PDX model (reported in 1969) was a primary colonic adenocarcinoma implanted into nude mice (Rygaard & Poulsen, 1969). Since then, most of the preclinical studies that have used PDX as a model for translational research have applied them for drug testing, for the modelling of drug resistance, and for biomarker development (Ambrogio et al., 2016; Bertotti et al., 2011; X. Dong et al., 2010; Fichtner et al., 2008; Gao et al., 2015; Judde et al., 2007; Kemper et al., 2016; Kortmann et al., 2011; Krumbach et al., 2011; Rajeshkumar et al., 2017). However, a key limitation of conventional PDX models is that, given their necessity to be generated in immunodeficient mice, they lack immune cells and hence cannot reproduce the interaction that exists between tumour cells and the immune system in patients' tumours.

In the context of adoptive cellular therapies (ACT) using autologous tumour infiltrating lymphocytes, PDX models have not been as extensively used. This could be due to the technical difficulties of generating a patient-matched system of PDX model and TILs for adoptive cellular therapy. In this regard, a study published in 2017 showed that rapidly expanded tumour infiltrating lymphocytes (TILs) from breast cancer patients could delay tumour growth in autologous PDX models. However, even though the researchers were able to successfully expand TILs from over 100 breast cancer samples, they could only test the ACT in two PDX models because of a low PDX implantation rate (Lee et al., 2017). Moreover, another study published on the same year showed the development of a melanoma PDXv2.0 model. The difference of this new PDX

model was that it was performed in human interleukin-2 (IL-2) transgenic NOG (*hIL2*-NOG) mice instead of the normally used NOD/Shi-scid IL-2Rγ(null) (NOG) or NOD-scid IL-2Rγ(null) (NSG) mice. This study showed that normal PDX models that were treated with autologous tumour infiltrating lymphocytes could only achieve tumour regression when the ACT was given alongside a daily injection of recombinant human IL-2 for 16 days. However, contrary to the PDXv2.0 model (i.e. the *hIL2*-NOG mouse model), the response was not durable when injections of IL-2 were stopped and only one mouse out of three was cured (Jespersen et al., 2017). The results from this study showed that the continuous presence of IL-2 was crucial to obtain a full response following ACT in an *in vivo* mouse model (this mirrors what is observed in the clinic). Furthermore, this study showed that tumours that grow in the PDXv2.0 model were eradicated if the autologous TILs came from patients that exhibited an objective response to ACT in the clinic, but not if the autologous TILs came from patients that were non-responders to ACT.

Finally, a study published in 2019 that used ACT based on autologous T cells derived from PBMCs, offered a proof-of-concept that ovarian cancer PDX models can be used for neoantigen research (Want et al., 2019). In this study it was demonstrated that PDXs generated from an ovarian cancer tumour retained neoantigens from the primary tumour and that these were recognised by autologous T cells. Adoptive cellular therapy was conducted in these PDXs with either autologous PBMCs stimulated with the pool of immunogenic neoantigens or with no peptides. This showed that tumour growth was significantly delayed in mice that received ACT with the neoantigen-pulsed PBMCs.

Together, these studies provide evidence supporting the use of PDX models as a relevant preclinical platform in the context of adoptive cellular therapies. Moreover, given that PDX models retain the main characteristics of their original tumours, the use of these *in vivo* models should lead to a higher rate of success in identifying new translational cancer treatments compared to other *in vitro* and *in vivo* models (Hutchinson & Kirk, 2011).

5.3. Aims

The main aim of the work presented in this chapter was to test the hypothesis that the gene editing of immune checkpoints renders the TILs resistant to negative regulation exerted by cancerous cells and their surrounding microenvironment, and that this confers an advantage to the cytotoxic functions of these TILs. To assess if this was the case, the two objectives of the work presented in this chapter were the following:

- To optimise *in vitro* functional assays to test if the gene editing of immune checkpoints on TILs confers an improvement in their cytotoxicity against tumour cells.
- To optimise an *in vivo* system of adoptive cellular therapy with melanoma TILs and autologous tumour cells to test if the ACT with the edited TILs improves tumour rejection and survival.

5.4. Functional *in vitro* assays of MX063 tumour infiltrating lymphocytes (edited and non-edited) vs. autologous primary cell line

After achieving the optimisation of gene editing of TILs using the CRISPR/Cas9 technology, it was of interest to test if the knockdown of LAG3, PD1, and/or TIGIT yielded a functional advantage in these cells. To assess if this was the case, unexpanded TILs from patient MX063 were subjected to a modified version of the 'pre-REP' followed by a REP (see materials and methods section for more information) and while expanding they were edited using the CRISPR/Cas9 technology to knockdown either LAG3, PD1, or TIGIT. After confirming the successful editing of these targets (TIGIT editing: 82%, LAG3 editing: 79%, PD1 editing: 53%) (Figure 3.21), the edited and control TILs were incubated against the autologous tumour cell line, which had previously been CFSE-labelled. After 16 hours, cells were analysed alongside counting beads via flow cytometry and percentage of killing was quantified (see materials and methods for more information). To optimise the best effector to target (E:T) ratio for this killing assay, different ratios were used (1:1, 2:1, and 5:1 E:T ratio). Additionally, MHC class I and class II blocks were added as a control in the 5:1

E:T ratio. The quantification of the percentage of killing showed that in the 1:1 E:T ratio a trend of improved killing could be observed with the edited TILs compared to the non-edited control (scrambled gRNA). The statistical analysis revealed that this higher percentage of killing (compared to control) was not statistically significant for the TIGIT-edited nor for the LAG3-edited TILs. However, the percentage of killing performed by the PD1-edited TILs was significantly higher (64% ± 10%; $P<0.05$) than the killing performed by the control TILs (Figure 5.1). It is important to note that only the 1:1 ratio showed any significant difference between the edited TILs and control. Additionally, the trend of improved killing with the edited TILs disappeared in the 2:1 and 5:1 E:T ratios. Of interest, the condition of the 5:1 E:T ratio that contained the MHC blocks (10μg/mL) did not show a decrease in the percentage of killing, which would suggest an MHC-independent killing or insufficient blocking of MHC. Moreover, although there appears to be an increase in the percentage of killing in the condition of the 5:1 ratio + MHC blocks (10μg/mL), these percentages were not significantly different from the ones on the 5:1 ratio (data not shown).

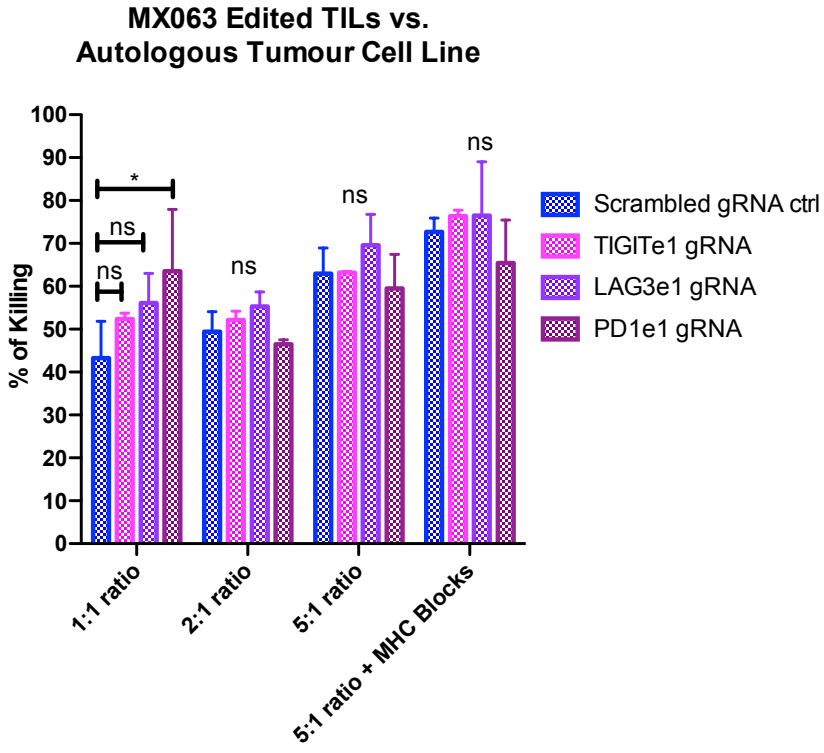

Figure 5.1. Killing assay of MX063 edited TILs against autologous tumour cell line. CFSE-labelled MX063 primary tumour cells were incubated with edited and control TILs (1:1, 2:1, 5:1 E:T ratios) for 16 hours prior to analysis via flow cytometry in the presence of counting beads.

Percentage of killing was quantified; n=2 (mean ± SEM). For the statistical analysis two-way ANOVA followed by Dunnett's Multiple Comparison was performed.

Given that it was observed that on a 1:1 E:T ratio the LAG3 editing generated an increase in killing of autologous tumour cells compared to control TILs (albeit, not significant) and that on this E:T ratio the PD1 editing achieved a statistically significant increase in killing of autologous tumour cells compared to control TILs, it was of interest to test if the double editing of LAG3+PD1 could produce a significant improvement in the killing potential of these TILs. To assess if this was the case, unexpanded TILs from patient MX063 were subjected to a REP (see materials and methods section for more information) and while expanding they were gene edited using the CRISPR/Cas9 technology to knockdown either LAG3, PD1, or a combination of both. After confirming the successful gene editing of these targets (Figure 3.23), the edited and control TILs were employed as the effector cells in a killing assay against their autologous tumour cells (see materials and methods section for more information). It had been previously observed that the E:T ratio in which a difference in killing percentage could be detected between control and edited TILs was 1:1, and that there was no significant difference between the killing capacity between the 1:1 ratio and either the 2:1 or the 5:1 ratio conditions (data not shown). Given this, it was decided to test the killing efficiency of these edited TILs in two extreme ratios (1:2 and 5:1 E:T ratios). Additionally, MHC class I and class II blocks were added as controls in both ratios (20μg/mL of each). The statistical analysis of the quantification of the percentage of killing showed no significant differences between the edited TILs and the non-edited control (scrambled gRNA) in either of the ratios tested (Figure 5.2). Furthermore, it was observed that increasing the dose of MHC blocking agents (20μg/mL compared to 10μg/mL from the previous experiment) resulted in a partial decrease of the killing capacity in the 5:1 E:T ratio and in a complete elimination of the killing ability in 3 out of the 4 conditions in the 1:2 E:T ratio. Of note, it was observed that the TILs employed for this experiment maintained a high killing efficiency of their autologous tumour cells even after undergoing a rapid expansion for 38 days.

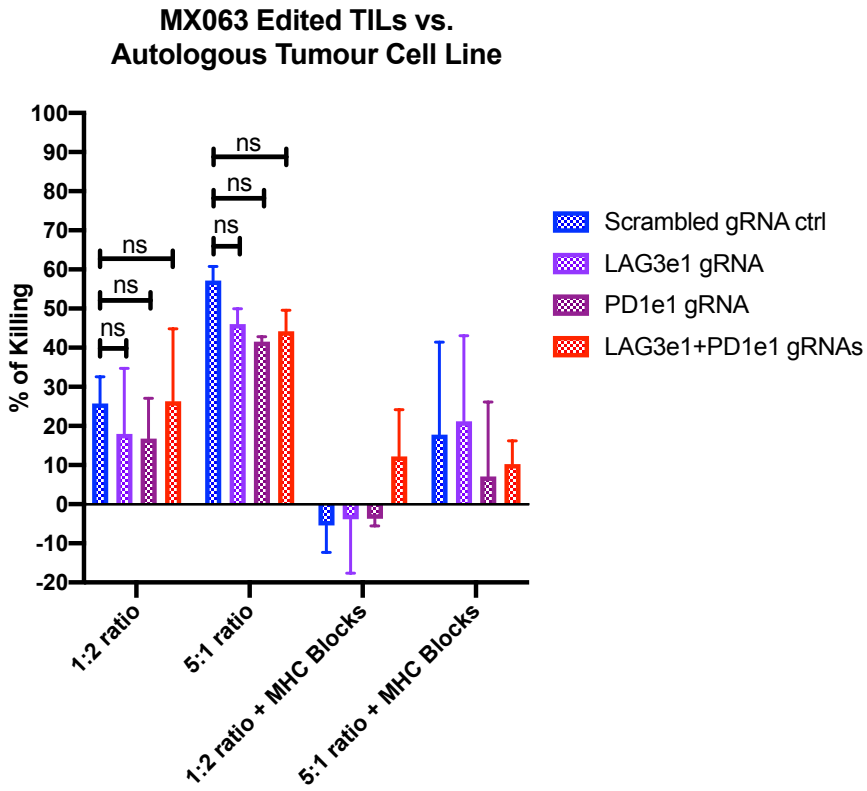

Figure 5.2. Killing assay of MX063 edited TILs (single and double edited) against autologous tumour cell line. CFSE-labelled MX063 primary tumour cells were incubated with edited and control TILs (1:2 and 5:1 E:T ratios) for 16 hours prior to analysis via flow cytometry in the presence of counting beads. Percentage of killing was quantified; n=3 (mean ± SEM). For the statistical analysis two-way ANOVA followed by Dunnett's Multiple Comparison was performed.

As no statistical difference of killing efficiency was observed between the single-target edited, double-target edited, and non-edited control TILs, it was of interest to test if there was at least a discernible difference in the secretion of cytokines of the edited TILs against the non-edited ones when they were incubated with the autologous tumour cells. To assess this, triplicates of a recall assay were performed against the autologous tumour cells (see materials and methods section for more information). As these expanded TILs had ~80% of $CD8^+$ cells and ~20% of $CD4^+$ cells (Supplementary Figure 8.12) and given that the tumour expresses both MHC class I and class II, the analysis of this recall assays was performed in separate for each population of cells. Representative flow plots of the IFNγ and TNFα secretion on $CD8^+$ TILs can be seen on Figure 5.3A. Quantification of the IFNγ^+TNFα^+ double positives showed that all of the $CD8^+$ TILs (edited and non-edited) secreted less than 10% of both these

cytokines (Figure 5.3B) and that this secretion was MHC-dependant, as adding MHC blocking agents caused the TILs to not secrete them. Comparing this to previous expansions where the TILs had secreted ~40-60% of these cytokines, generated the hypothesis that there was a smaller population of tumour-reactive T cells in this expanded TILs compared to previous expansions. Even though the percentage of $IFN\gamma^{+}TNF\alpha^{+}$ double positives was small for all of the conditions, statistical analysis showed that both the PD1-edited (2% $\pm$ 0.06; $P<0.01$) and the LAG3+PD1-edited (3% $\pm$ 0.2%; $P<0.05$) TILs secreted significantly less of these cytokines than the non-edited control TILs (7% $\pm$ 0.5%) (Figure 5.3B). Furthermore, the representative flow plots of the IFNγ and TNFα secretion on $CD4^{+}$ TILs (Figure 5.3C) show that even though the tumour expresses MHC class II, the $CD4^{+}$ cells are showing almost no reactivity against it (seen by the very low percentages of IFNγ and TNFα). Quantification of the $IFN\gamma^{+}TNF\alpha^{+}$ double positives on the $CD4^{+}$ TILs (Figure 5.3D) showed that the non-edited control TILs had only a 0.3% of secreted cytokines, while the edited TILs had a ~1.3%, but this difference was not statistically significant. Furthermore, the difference of cytokine secretion between the media alone control and the TILs incubated against the tumour was not statistically significant (data not shown).

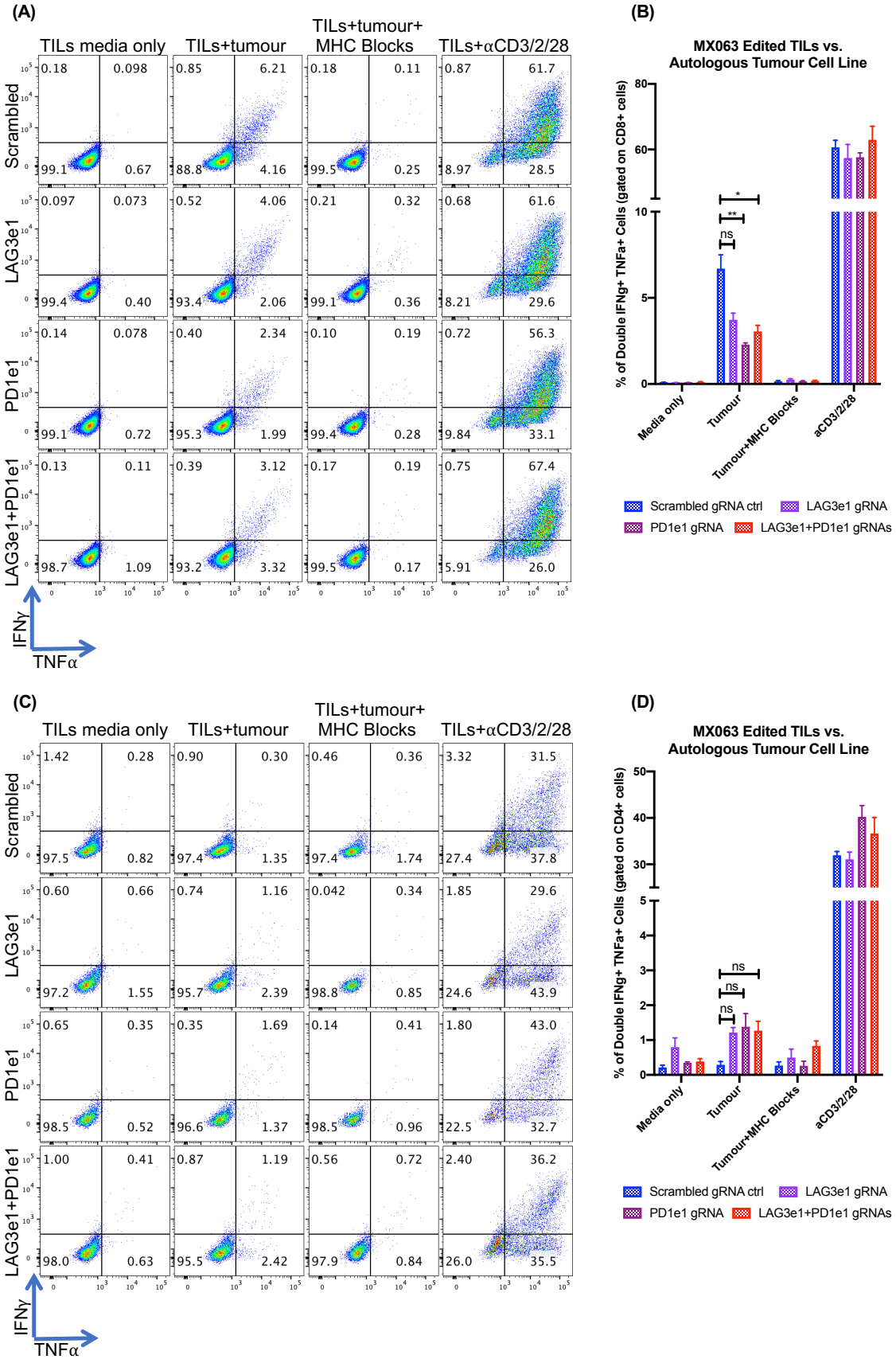

Figure 5.3. Recall assay of MX063 edited TILs (single and double edited) against autologous tumour cell line. MX063 TILs that were expanded and edited during the REP were

incubated with their autologous tumour cell line +/- MHC blocking agents for 16 hours in the presence of a protein transport inhibitor (Brefeldin A). These TILs were later stained for IFNγ and TNFα. TILs left in media alone are shown as a negative control and TILs stimulated with ImmunoCult Human CD3/CD2/CD28 T Cell Activator (Stemcell Technologies) are shown as positive controls. This experiment was performed in triplicates. **(A and C)** Representative flow cytometry plots for **(A)** $CD8^+$ cells and **(C)** $CD4^+$ cells. **(B and D)** Quantification of the IFNγ and TNFα double positives on **(B)** $CD8^+$ cells and **(D)** $CD4^+$ cells; n=3 (mean ± SEM). For the statistical analysis two-way ANOVA followed by Dunnett's Multiple Comparison was performed.

As previously stated, it was hypothesised that there was a smaller population of tumour-reactive T cells in the last expanded TILs compared to previous expansions (seen by the difference in percentage of secreted cytokines when incubated with their autologous tumour cells). It was of interest to edit a higher proportion of tumour-reactive T cells, as these would have a better tumour-killing capacity. However, the work performed previously to try to selectively expand tumour-reactive T cells from a melanoma patient sample (Chapter 4) had proven unsuccessful. Hence, it was decided to re-expand MX063 TILs that had been expanded using the REP ('REP' TILs) and that had previously shown to secrete ~60% of IFNγ when stimulated with their autologous tumour cells, as it was hypothesised that by starting with a higher proportion of tumour-reactive TILs there would be a better probability of expanding these cells to great numbers. The previously expanded MX063 TILs ('REP' TILs) were expanded again using the REP (see materials and methods section for more information) (these expanded TILs will be named 'REP 2' to differentiate them from the previous stock of 'REP' TILs) and while expanding they were edited using the CRISPR/Cas9 technology to knockdown either LAG3, PD1, a combination of both, or TIGIT. It is worth noting that the editing had to be delayed to day 16 of the REP because of the viability of the cells. After confirming the successful editing of these targets (Supplementary Figure 8.13), triplicates of a recall assay were performed against the autologous tumour cells with both the edited and non-edited TILs as controls (see materials and methods section for more information). The secretion of IFNγ and TNFα on the $CD8^+$ cells was higher than on the previous expansion (Figure 5.4A vs Figure 5.3A), however, it was still suboptimal compared to the secretion of IFNγ that had been observed on the

$CD8^+$ 'REP TILs' (Figure 4.4A). Additionally, quantification of the $IFN\gamma^+TNF\alpha^+$ double positives on the $CD8^+$ TILs showed that all of the TILs (edited and non-edited) secreted ~15% of both these cytokines (Figure 5.4B) and that this secretion was MHC-dependant, as adding MHC blocking agents diminished the secretion of the cytokines. Statistical analysis confirmed that there was no significant difference in the percentage of $IFN\gamma^+TNF\alpha^+$ double positives between the edited TILs and the non-edited control TILs (Figure 5.4B). Furthermore, the representative flow plots of the IFNγ and TNFα secretion on $CD4^+$ TILs (Figure 5.4C) show a ~9% of $IFN\gamma^+TNF\alpha^+$ double positives, and a higher percentage of TNFα positive IFNγ negative (~25%). Additionally, quantification and statistical analysis of the $IFN\gamma^+TNF\alpha^+$ double positives on the $CD4^+$ TILs (Figure 5.4D) showed that there was no significant difference between the amount of cytokines secreted by the non-edited TILs and the LAG3-edited, PD1-edited, or LAG3+PD1-edited TILs. However, the percentage of $IFN\gamma^+TNF\alpha^+$ double positives was significantly reduced in the TIGIT-edited TILs (6% ± 0.7%; $P<0.05$) compared to the non-edited control (10% ± 1%) (Figure 5.4D). Furthermore, it was observed that the percentage of $IFN\gamma^+TNF\alpha^+$ double positives was marginally reduced on the $CD4^+$ TILs when the MHC blocking agents were added, however this reduction was only significant in the PD1-edited and PD1+LAG3-edited TILs (data not shown). Moreover, the secretion of TNFα by the $CD4^+$ TILs was observed to be an MHC-independent process, as the addition of the MHC blocking agents did not reduce the percentage of TNFα that was secreted by these cells (data not shown).

With these optimised assays we were able to observe specific killing and cytokine secretion of the TILs in response to their autologous tumour cells. Interestingly, although the addition of MHC class I diminished or even completely ablated these responses in $CD8^+$ T cells, we observed that the addition of MHC class II did not have this effect on $CD4^+$ T cells. This would suggest an MHC class II-independent secretion of cytokines or insufficient blocking of MHC class II. Importantly, neither of these assays (killing assay and recall assay) showed consistently a functional advantage for the edited TILs suggesting that perhaps these assays are not the best suited to see those differences.

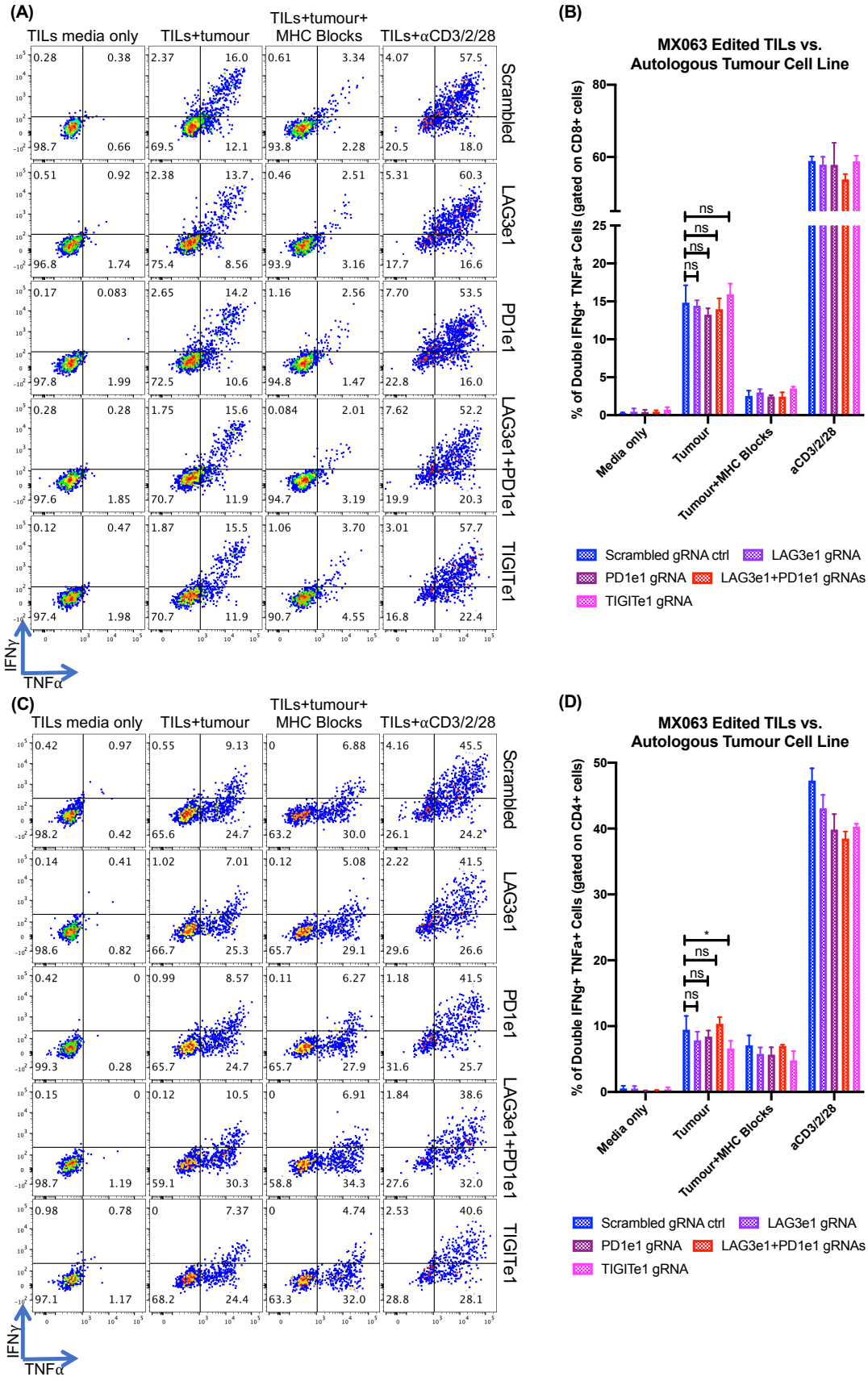

Figure 5.4. Recall assay of MX063 'REP' edited TILs (single and double edited) against autologous tumour cell line. MX063 TILs that were expanded and edited during the REP were

incubated with their autologous tumour cell line +/- MHC blocking agents for 16 hours in the presence of a protein transport inhibitor (Brefeldin A). These TILs were later stained for IFNγ and TNFα. TILs left in media alone are shown as a negative control and TILs stimulated with ImmunoCult Human CD3/CD2/CD28 T Cell Activator (Stemcell Technologies) are shown as positive controls. This experiment was performed in triplicates. **(A and C)** Representative flow cytometry plots for **(A)** $CD8^+$ cells and **(C)** $CD4^+$ cells. **(B and D)** Quantification of the IFNγ and TNFα double positives on **(B)** $CD8^+$ cells and **(D)** $CD4^+$ cells; n=3 (mean ± SEM). For the statistical analysis two-way ANOVA followed by Dunnett's Multiple Comparison was performed.

5.5. Optimisation of an *in vivo* model to test adoptive cellular therapies

It is known that tumours are composed of more than just neoplastic cells, and that this tumour microenvironment (i.e. stromal and inflammatory cells, extracellular matrix proteins, as well as blood and lymphatic vascular networks) has a role in cancer progression and in resistance to therapy (Quail & Joyce, 2013; Sun, 2016). Moreover, the *in vitro* functional studies previously performed did not preserve the three-dimensional tumour structure and thus lacked the component of the tumour microenvironment. Given this, *in vivo* tumour models are preferable as preclinical systems to study adoptive cellular therapies.

As a first step to optimise an *in vivo* model to test the edited vs. non-edited TILs, MX063 primary tumour cells were co-injected (intradermal injection) with autologous non-edited TILs ('pre-REP+REP' TILs that were previously shown to contain at least 40% of tumour-reactive T cells; Figure 4.4B) into NSG mice. This was to test if the autologous non-edited TILs could control the tumour growth and improve survival of tumour-bearing mice. Hence, $2x10^6$ tumour cells were injected alone or co-injected with autologous TILs in a 1:1 or 1:2 E:T ratio. Tumours were monitored and 41 days after injection the tumours were excised and processed. A schematic of this *in vivo* experiment can be found on Figure 5.5A. Prior to the co-injection of these cells, an aliquot of the 'pre-REP+REP' TILs was analysed via flow cytometry (Figure 5.5B). This showed that all of the cells were $CD3^+$, and that a fraction of them expressed CD56. CD56 (also known as neural cell adhesion molecule (NCAM)) is the classic phenotypic marker of natural killer (NK) cells, but it has been shown that this marker can also be

expressed by other immune cells (i.e. αβ T cells, γδ T cells, dendritic cells, and monocytes), and that these CD56-expressing cells have strong immunostimulatory effector functions, such as cytokine production and an efficient cytotoxic capacity (Correia, Costa, Uhrberg, Cardoso, & Arosa, 2011; Pittet, Speiser, Valmori, Cerottini, & Romero, 2000; Van Acker, Capsomidis, Smits, & Van Tendeloo, 2017). Moreover, it was observed that the $CD56^+$ fraction of the $CD3^+$ TILs was composed of ~80% of $CD8^+$ cells and ~20% of $CD4^+$ cells. The $CD56^-$ fraction contained ~96% of $CD4^+$ cells and only ~3% of $CD8^+$ cells (Figure 5.5B). The tumours were measured on average every 3 days from the day the tumours became visible until the end of the experiment. These measurements showed that the mice that had been injected with the tumour cells and no TILs had tumours growing in them as early as day 7. Additionally, by the last day of the experiment, two of these tumours had ulcerated, so they were eliminated from the last measurement (Figure 5.5C, asterisks on left panel). In contrast, the mice co-injected with a 1:1 ratio of TILs:tumour were able to control tumour growth until day 20, when one of the tumours started to grow. By day 27 all but one of the tumours in this group were growing, and by day 33 there was no tumour control left in this group (Figure 5.5C, middle panel). Furthermore, it was observed that in the group that had been co-injected with a 1:2 ratio of TILs:tumour there was a partial tumour control, with 2 out of 5 tumours starting to grow as early as day 7 (however, at a slower rate than the 'No TILs' group). By day 19 only two mice from this group were tumour-free, and by day 33 all of the mice had tumours on them (Figure 5.5C, right panel).

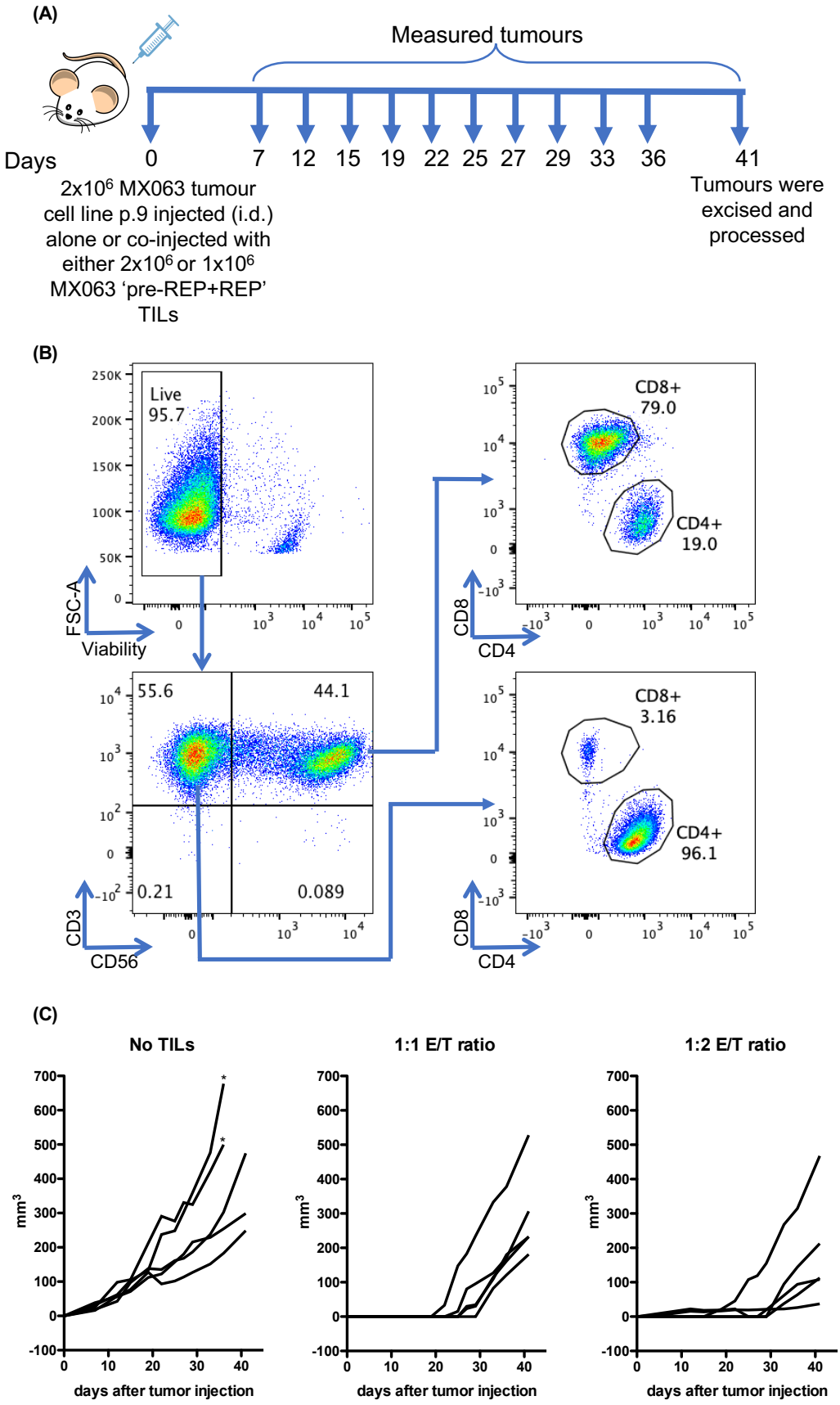

Figure 5.5. Co-injection of MX063 tumour primary cell line and non-edited autologous tumour infiltrating lymphocytes into NSG mice. (A) Schematic of *in vivo* experiment. **(B)** Flow

cytometry analysis of the 'pre-REP+REP' TILs prior to the co-injection of these cells with their autologous tumour cells. **(C)** Tumour growth curves for the three experimental groups; n=5 mice per group. *Tumours were eliminated from final measurement because of ulceration.

Forty-one days after the tumour cells and TILs were injected, the tumours were excised and processed (see materials and methods section for more information). Flow cytometry analysis showed that both groups of tumours that had been co-injected with TILs did not have any $CD3^+$ cells left at the end of the experiment (Figure 5.6A), and that the majority of the cells were $CD56^+$. As it has been shown that upon activation the CD3 expression is downregulated (Valitutti, Müller, Salio, & Lanzavecchia, 1997), CD8 and CD4 expression were likewise analysed. This analysis confirmed that both groups of tumours that had been co-injected with TILs did not contain any $CD8^+$ nor $CD4^+$ cells at the end of the experiment (Figure 5.6B). Furthermore, as it is known that one of the mechanisms of immune evasion employed by the tumour cells is HLA loss (Ferrone & Marincola, 1995; Gettinger et al., 2017; McGranahan et al., 2017), expression of HLA class I (HLA-ABC) and class II (HLA-DR) was analysed. We observed that tumours in all experimental groups lost the expression of HLA class II, however, they maintained a high expression of HLA class I (Figure 5.6C).

This first *in vivo* experiment showed that the non-edited TILs were able to control the tumour growth at the beginning, but that ultimately the tumours escaped. Taken together, these results suggest that the loss of tumour-growth control was due to the T cells dying. However, there is the possibility that it was a consequence of loss of function of the T cells followed by their death. Nonetheless, to conclude if either of these hypotheses are correct, tumours would need to be analysed at an earlier timepoint before the tumour-control is lost. However, given the artificial design of the experiment (i.e. the co-injection of the effector cells at the same time as the target cells are delivered), the analysis at an earlier timepoint is not possible as there are no visible tumours before the tumours escape control.

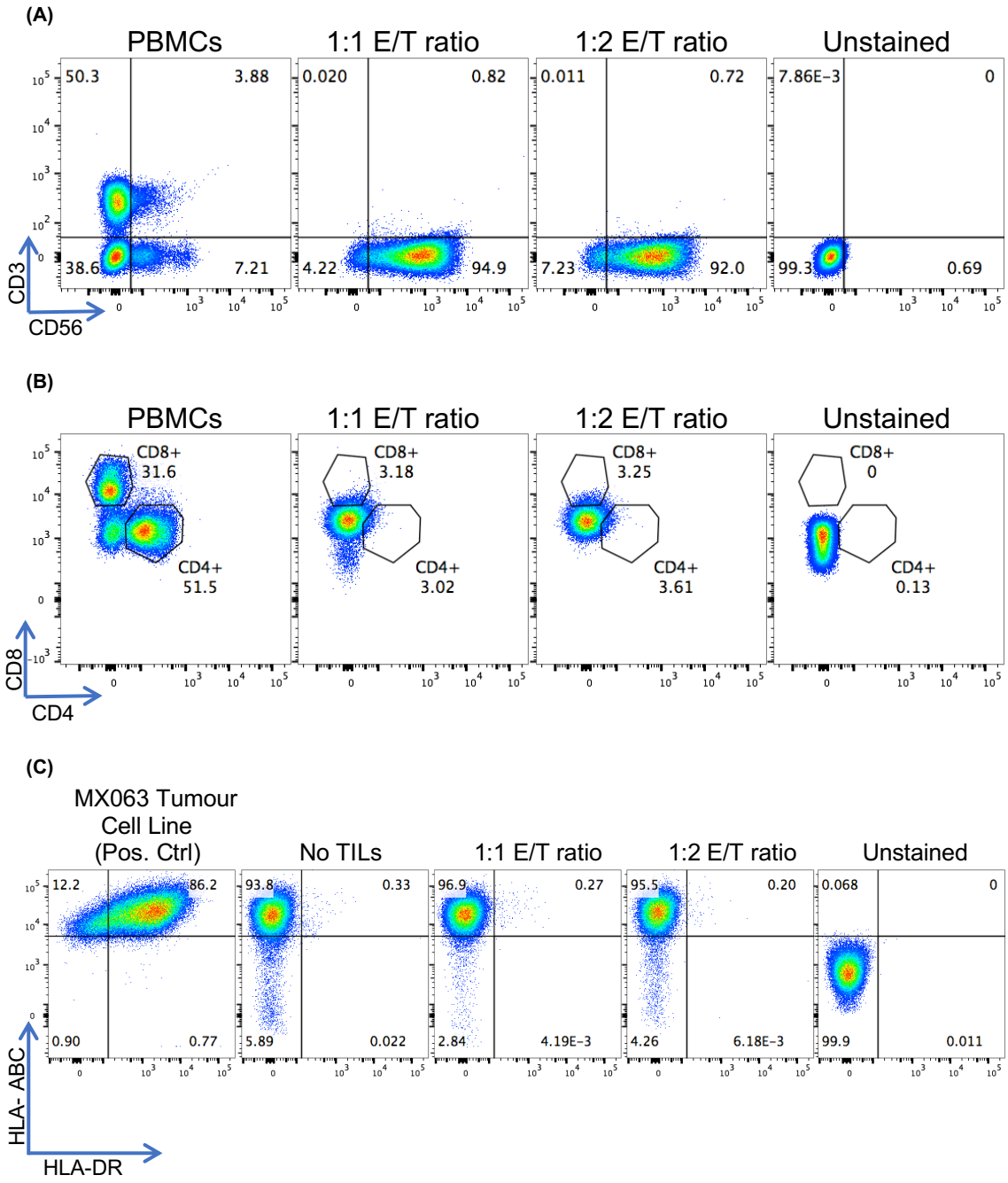

Figure 5.6. Flow cytometry analysis of tumours 41 days post-injection of cells. (A and B) Representative flow plots showing expression of either **(A)** CD3 and CD56 or **(B)** CD8 and CD4 in the groups that were co-injected with 1:1 and 1:2 TILs:tumour ratios. Healthy human PBMCs are shown as a positive control. All gated on live cells. **(C)** Representative flow plots showing expression of HLA-ABC and HLA-DR in all of the experimental groups. MX063 tumour cell line is shown as a positive control. Gated on live cells.

It was important to optimise an *in vivo* model that more closely resembled tumour progression and adoptive cellular therapy in patients, as we wanted to test systemic expansion of T cells, followed by engraftment and tumour

infiltration (this model was set up in conjunction with Dr Pablo Becker). To achieve this, $2x10^6$ MX063 tumour cells were injected intradermally into NSG mice (intradermal injections performed by Dr Pablo Becker). Once the tumours were palpable (approximate volume was $50mm^3$), either $2x10^6$ (1:1 E:T ratio) or $1x10^7$ (5:1 E:T ratio) of autologous expanded TILs ('Scrambled-edited' TILs that were previously shown to contain ~6% of tumour-reactive T cells; Figure 5.3) were injected intravenously (intravenous injections performed by Dr Pablo Becker). Moreover, a high-dose of IL-2 (200,000IU) was continually injected (intraperitoneally) to these mice during the course of the experiment. A schematic of this *in vivo* experiment can be found on Figure 5.7A. Furthermore, the 'Scrambled-edited' TILs were analysed via flow cytometry before injecting them. This analysis showed that these TILs had a high viability, and that they were composed of 67% of $CD8^+$ cells and of 32% of $CD4^+$ cells (Figure 5.7B). The tumours were measured every two to three days until the end of the experiment. These measurements showed a slower tumour progression in the group treated with 1:1 E:T ratio TILs compared to the untreated group, but this prove to be not significant when the means of both groups were compared (data not shown). This was due to the high variability seen in the untreated group, with one of the tumours growing slower than any of the tumours in the treatment groups. Moreover, the tumours treated with TILs at a 5:1 E:T ratio did not show any decrease in the tumour-growth rate compared to the untreated group (Figure 5.7C).

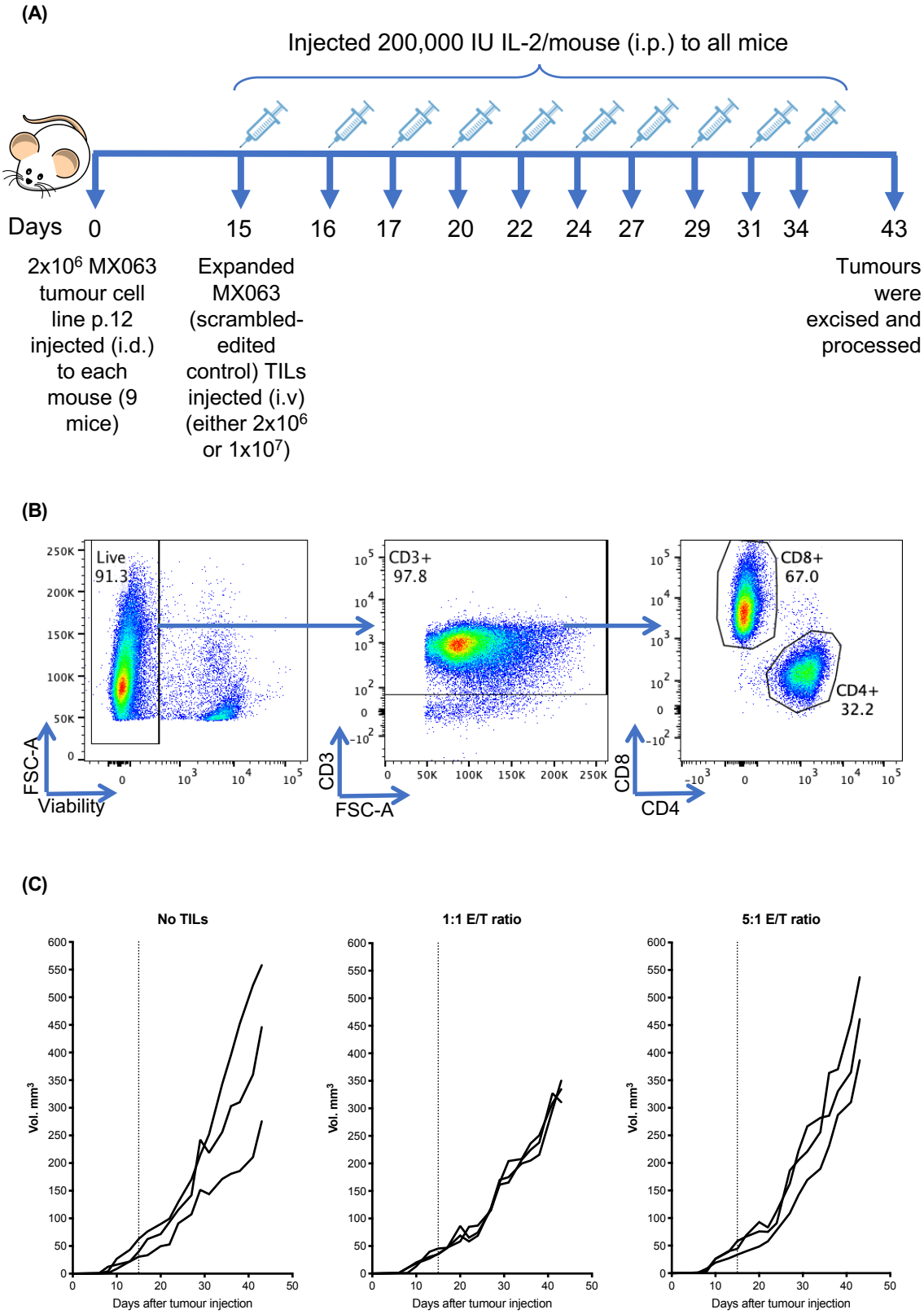

Figure 5.7. Treatment of MX063 tumour-bearing NSG mice with autologous tumour infiltrating lymphocytes. (A) Schematic of *in vivo* experiment. **(B)** Flow cytometry analysis of the expanded 'Scrambled-edited' TILs prior to the intravenous injection of these cells. **(C)** Tumour growth curves for the three experimental groups; n=3 mice per group. Dotted vertical line indicates the injection of the TILs.

Forty-three days after the tumour cells were injected and 28 days post-injection of TILs, the tumours were excised and processed (see materials and methods section for more information). The expression of HLA class I (HLA-ABC) and of HLA class II (HLA-DR) on the tumours was analysed via flow cytometry and this showed that all of the tumours (treated and untreated) lost the expression of HLA class II but retained the expression of HLA class I (Figure 5.8).

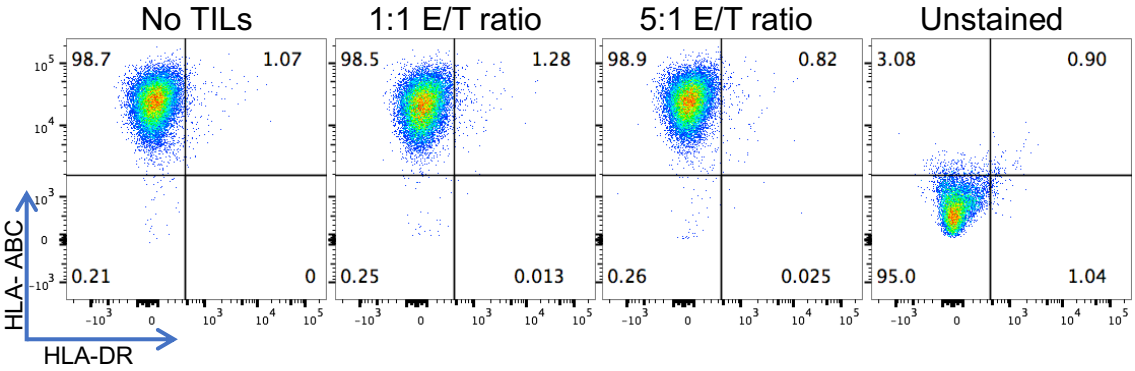

Figure 5.8. Flow cytometry analysis of tumours 43 days post-injection of cells. Representative flow plots showing expression of HLA-ABC and HLA-DR on all of the experimental groups. Gated on live cells.

Flow cytometry analysis of the single-cell suspension obtained from the processed tumours also showed that 2 out of the 3 tumours treated with TILs at a 1:1 E:T ratio (tumours "1:1 E/T ratio" #1 and #3) still contained a small but distinct population of TILs (identified by expression of human CD45 (hCD45) and an absence of expression of mouse CD45 (mCD45)) (Figure 5.9). These populations of $hCD45^+$ $mCD45^-$ cells were further analysed and this showed that ~46% were CD3 positive. The $CD3^+$ population of cells consisted of ~38% of $CD8^+$ and ~47% of $CD4^+$ cells in one of the tumours, and of ~78% of $CD8^+$ and ~22% of $CD4^+$ cells in the other tumour. It is worth noting that these $hCD45^+$ $mCD45^-$ populations constituted only 0.081% and 0.015% of the whole population of live cells in these two tumours.

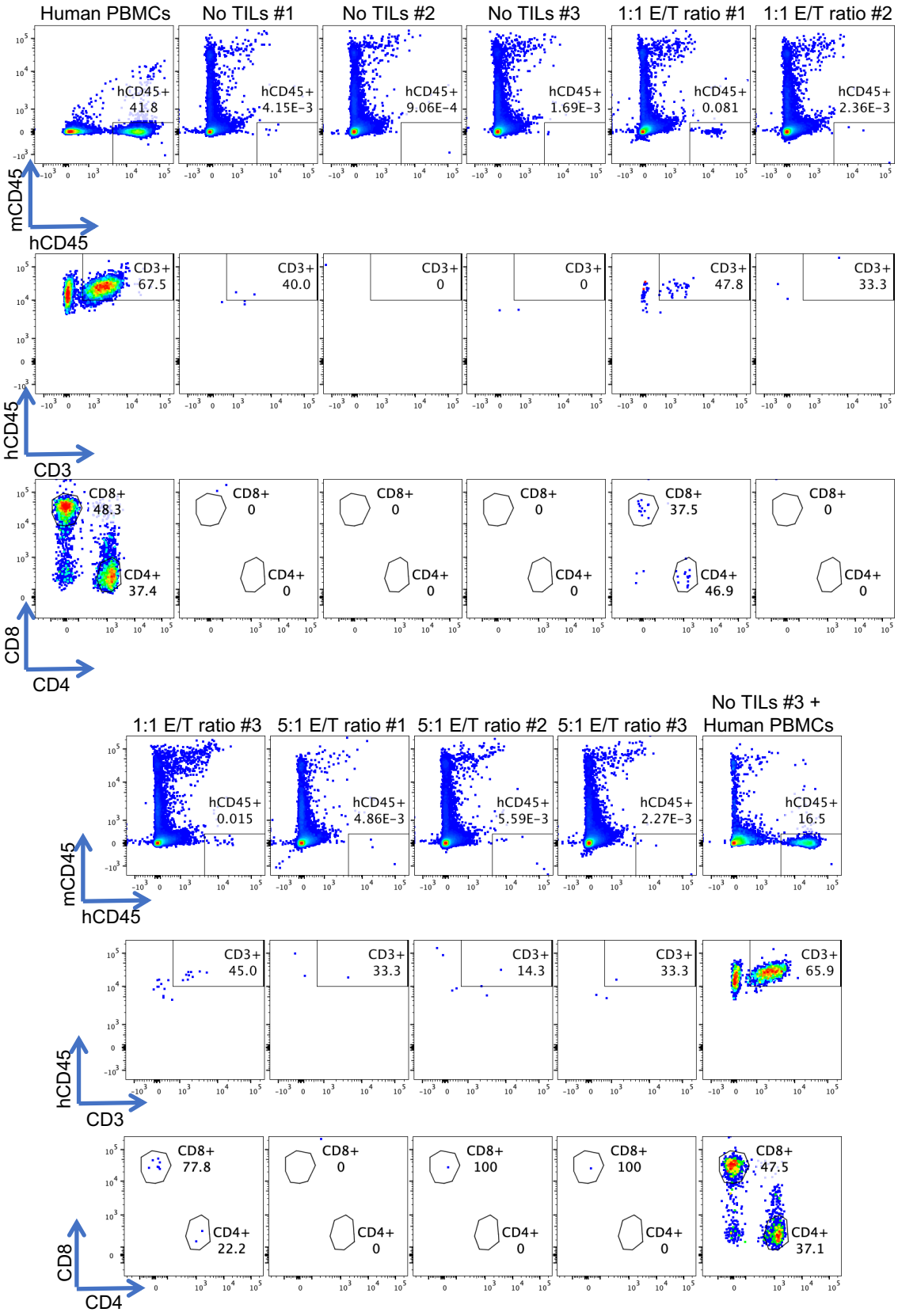

Figure 5.9. T cell infiltration of tumours 28 days post-injection of TILs. Flow cytometry analysis of the single-cell suspension of processed tumours. Human T cells were identified by expression of human CD45 (hCD45), CD3, and either CD8 or CD4, and by the lack of expression

of mouse CD45 (mCD45). Human PBMCs and a sample of one of the untreated tumours (no TILs) combined with human PBMCs are shown as positive controls.

We observed that the population of $hCD45^+$ $mCD45^-$ cells in both the untreated tumours and the tumours that were treated with TILs at a 5:1 E:T ratio was negligible, as further analysis of CD3, CD8, and CD4 expression showed that there weren't any CD8 nor CD4 positive cells in the untreated group (Figure 5.9). One of the three tumours of the group treated with TILs at a 5:1 E:T ratio had no CD8 nor CD4 positive cells, while the other two tumours of this group had only one $CD8^+$ cell each (Figure 5.9). Finally, it is worth noting that as one of the positive controls, a tumour from the untreated group was combined with human PBMCs prior to staining. This showed that the division between human CD45 and mouse CD45 staining was very effective, and this allowed us to verify that the human $CD45^+$ populations seen in the two tumour samples were not false positives.

It is worth noting that the percentage of tumour-reactive T cells in the TILs used for this assay was only ~6.7% (measured via recall assay). Hence, even though the number of TILs injected in each group was $2x10^6$ and $1x10^7$, the ratio of tumour-reactive T cells:tumour cells was in reality 1:15 and 1:3, respectively. We hypothesise that the lack of tumour control could be partially explained by the low frequency of tumour-reactive T cells. Future optimisation of this ACT model will require higher frequencies of tumour-reactive T cells.

5.6. Discussion

In this chapter, we presented the results of the functional *in vitro* assays performed with the MX063 edited TILs, as well as the optimisation that was carried out to generate an *in vivo* model to test if the editing of PD1, LAG3, PD1+LAG3, and/or TIGIT conferred a functional advantage to the MX063 TILs.

The first *in vitro* killing assay of the MX063 tumour cells was performed with MX063 expanded TILs that had not been previously assessed for tumour-reactivity. These expanded TILs proved to have at least a fraction of tumour-reactive T cells as the non-edited control TILs were shown to achieve a ~40% of tumour killing in a 1:1 E:T ratio. This percentage of tumour killing increased to

~50% in the 2:1 E:T ratio and to ~60% in the 5:1 E:T ratio. Although this killing did not decrease when MHC class I and MHC class II blocking agents were added, we hypothesised that it was because of the concentration being too low to fully block all of the MHC-TCR interactions. Moreover, we observed that in the 1:1 E:T ratio, the PD1 editing significantly improve the killing capacity of the TILs, whilst the LAG3 and TIGIT editing did not. However, when this experiment was repeated with a different stock of expanded TILs, we observed that in this case the PD1 editing did not improve the killing capacity of the TILs. It is important to note that this second killing assay was performed with a 1:2 E:T ratio and a 5:1 E:T ratio, and that the comparison between the 5:1 E:T ratio from the two experiments showed a different pattern of killing between the conditions.

As the results of the *in vitro* killing assays were not consistent, we also performed recall assays to test if the editing consistently conferred an advantage in the secretion of cytokines when the TILs were incubated with their autologous tumour cells. These assays again showed a lot of variability between experiments with one experiment showing that the PD1-edited and PD1+LAG3-edited $CD8^+$ TILs had a decreased secretion of cytokines compared to the non-edited control, and the other experiment showing that there was no significant difference between the cytokine secretion of the edited and non-edited TILs. Moreover, one of these experiments showed an MHC-independent secretion of TNFα in the $CD4^+$ TILs but not in the $CD8^+$ TILs, which could be explained by a Toll-like receptor (TLR)-dependent secretion of cytokines (Caron et al., 2005).

We hypothesise that the variability in the results between experiments of both the killing and recall assays was due to the difference in percentage of tumour-reactive T cells that were expanded in each REP. More work comparing different stocks of expanded TILs will be needed to assess if this was the case. Moreover, optimisation of the selective expansion of tumour-reactive T cells is still needed to be able to have a consistent preferential expansion and editing of tumour-reactive T cells (see Chapter 4 for the methods that were tried for the selective expansion of tumour-reactive T cells during the course of this project).

As it is known that 2D-*in vitro* assays disregard the influences of the tumour microenvironment upon the immune response, models that can recreate the three-dimensional structure of the tumour are better suited for research on

immune-mediated therapies. Because of this, we decided to optimise an *in vivo* model with the MX063 tumour cells and autologous TILs. It is important to note that this model was not a conventional PDX, as the cells did undergo a phase of *in vitro* growth. However, these cells were still early passage primary tumour cells, in contrast to some of the immortalised cell lines used for CDX. Although it has been shown that long periods of *in vitro* culture of tumour cells cause a loss of key genetic signatures of the original tumours (Daniel et al., 2009), it has also been demonstrated that generating an *in vivo* model with melanoma tumour cells that were briefly cultured *in vitro* can still recreate the results of the same patients' cells that underwent ACT in the clinic (Jespersen et al., 2017).

We first sought to test if the non-edited expanded TILs were capable of slowing or preventing tumour growth when co-injected with the tumour cells, as this experimental setup would avoid the confounding factor of the necessity of T cell homing to the tumour. We observed that tumours treated with TILs at a 1:1 and at a 1:2 E:T ratio had a delayed growth compared to the untreated control. Flow cytometry analysis of the processed tumours at the end of the experiment showed that there were no $CD3^+$ cells left in any of the conditions. The results from this experiment made us conclude that these expanded TILs were able to slow the tumour growth *in vivo* and we hypothesised that the tumour control was lost due to T cell death.

To test if the TILs were able to control tumour growth in an *in vivo* model that more closely resembled tumour progression and adoptive cellular therapy in patients, we did an intravenous injection of the autologous TILs into the mice once there was a palpable tumour. Tumours treated with TILs at a 1:1 E:T ratio, but not with a 5:1 E:T ratio, showed a slower tumour progression compared to the untreated group, however this was not significant due to the high variability of the untreated group. Of note, although the number of TILs injected in each group was $2x10^6$ and $1x10^7$, the percentage of tumour-reactive T cells was only ~6.7% (measured via recall assay). Hence, the ratio of tumour-reactive T cells:tumour cells was in reality 1:15 and 1:3, respectively.

In sum, the *in vitro* functional assays shown here will need to be repeated and optimised to be able to conclusively prove or disprove our hypothesis stating that the edited TILs will have a functional advantage compared to their non-edited counterpart. Moreover, as there is the possibility that this functional advantage is

not observed *in vitro* given that the tumour microenvironment is missing, an *in vivo* model will need to be further optimised to test our hypothesis. In this regard, more experiments will be needed with a higher number of tumour-bearing mice to test different timings of TILs treatment, as well as daily application of different doses of IL-2, as these two factors have been shown to be critical in the immune-mediated tumour response (Jespersen et al., 2017; Oflazoglu et al., 2007).

Chapter 6. Conclusion and Future Work

6.1. Concluding remarks

Adoptive cellular therapies (ACT) and immune checkpoint blockade (ICB) have proven to be two effective immune-based treatment modalities for cancer, resulting in long lasting responses in a fraction of patients (R. Andersen et al., 2016; Frank Stephen Hodi et al., 2018; McDermott et al., 2013; Rosenberg et al., 2011). Although results from clinical trials using either of these treatment modalities are encouraging, to date, only a small percentage of patients with advanced malignancies can benefit from ACT or ICB. Hence, there is a need to develop therapies that can achieve complete responses in a higher proportion of patients.

There is a strong rationale for combining ACT with ICB, as it has been shown that the tumour-reactive portion of TILs can be identified by the expression of certain immune checkpoints (i.e. PD1, LAG3, and TIM3) (Gros et al., 2014). Moreover, it has been demonstrated that tumour-reactive $CD8^+$ T cells that persist in patient peripheral blood for up to 1 year after ACT are mostly polyfunctional; however they express high levels of PD1, rendering them sensitive to PD-L1 (Marco Donia et al., 2017). Hence, impaired T cell activity via the different immune checkpoint signalling pathways may be responsible for relapses observed in some patients treated with ACT. Furthermore, the success of ICB treatment is reliant on the presence of a pre-existing population of tumour-reactive T cells in sufficient numbers. Hence, the *ex vivo* expansion and transfer of the tumour-reactive T cells that occurs in ACT could increase the number of patients that benefit from ICB therapy.

In this regard, it has been observed that the combination of ACT with ICB improves T cell cytotoxicity and promotes tumour regression in different mouse models (Blake et al., 2015; John et al., 2013; L. Z. Shi et al., 2018). Furthermore, ACT of tumour antigen-specific cytotoxic T cells in combination with CTLA4 systemic blockade has shown promising clinical results with toxicities comparable to that of CTLA4 blockade monotherapy (Chapuis, Lee, et al., 2016; Chapuis, Roberts, et al., 2016).

It has been reported that toxicities generated by treatment with ICB (i.e. immune-related adverse events (irAEs)) are frequent, with irAEs occurring in up to 90% of patients treated with an anti-CTLA4 antibody (F. Stephen Hodi et al., 2010) and in 70% of patients treated with an anti-PD1 antibody (Suzanne L. Topalian et al., 2012). These irAEs are a direct consequence of the systemic loss of T cell inhibition, as this results in impaired self-tolerance that can be fatal in some cases (F. Stephen Hodi et al., 2010; Robert et al., 2015). As these irAEs occur because of the systemic blockade of the immune checkpoints, it would be preferable to deliver a more selective therapy that could stop the T cell inhibition exclusively on the T cells that are tumour-reactive.

The aim of this project was to generate a proof-of-concept for the combination of adoptive cellular therapy of tumour infiltrating lymphocytes (TILs) with immune checkpoint inhibition via gene engineering of the TILs. We hypothesised that by genetically engineering TILs to knockdown the expression of immune checkpoints in their surface, we would render them resistant to checkpoint inhibition. This in turn would render the transferred T cells resistant to negative regulation exerted by cancerous cells and their surrounding microenvironment, giving them a functional advantage against the tumour cells. Moreover, a further aim was to selectively expand and genetically engineer only the tumour-reactive T cells (or, if possible, the neoantigen-reactive T cells); as we hypothesised that this selective editing would be able to prevent or at least reduce toxicities associated with systemic blockade of immune checkpoints as the ones seen in the clinic with the immune checkpoint inhibitors.

The majority of the work presented in this thesis consisted in the optimisation of a methodology for the genomic engineering of primary human tumour infiltrating lymphocytes using the CRISPR/Cas9 technology. In regard to this, we succeeded in generating a protocol that was able to achieve a high editing efficiency, whilst maintaining a high viability of the cells post-editing. However, to be able to make this into a clinical-grade protocol the following factors would need to be improved upon:

1) *The batch-to-batch variability of TILs would need to be addressed:* Selective expansion of tumour-reactive T cells would need to be consistently achieved and a bank of these tumour-reactive T cells

would need to be created for each patient so as to have the same reactivities between batches of TILs from the same patient.

2) *Cell numbers:* The number of cells that are lost or that die after the electroporation would need to be minimised. In addition, further experiments would need to test if the number of edited cells at the end of the protocol would be enough to reinfuse into patients (would need to compare the number of edited T cells with the number of non-edited T cells that are currently given to patients in adoptive cellular therapies).
3) *Assessment of off-target activity:* To be able to convert the current protocol into a clinical-grade one it will be paramount to assess the possible off-target effects of the gRNAs used via whole-genome sequencing.

More work will be needed to achieve a selective expansion and editing of tumour-reactive (or neoantigen-reactive) T cells. Further experiments will also be needed to be able to conclusively prove or disprove the hypothesis that the knockdown of these immune-checkpoints will grant a functional advantage to the tumour-reactive T cells. The future work that still needs to be performed will be discussed in the next section.

6.2. Outlook for future work

6.2.1. Selective expansion of tumour-reactive or neoantigen-reactive T cells

As it was discussed in Chapter 4, a selective expansion of tumour-reactive T cells was not achieved. We hypothesised that there were technical issues with the sorting via flow cytometry of the tumour-reactive T cells that compromised the viability of the cells. Hence, for all future sorts we will implement changes that have been shown to improve cell viability and yield, such as dividing the sort into shorter intervals and adjusting the flow rate to maintain the lowest possible pressure (Basu et al., 2010; Cossarizza et al., 2017). It is worth noting that the TILs that were sorted via flow cytometry had already undergone a round of rapid expansion, and that they were then CFSE-labelled and incubated with their

autologous tumour cells to select the tumour-reactive T cell population (i.e. the cells that divided in the presence of the tumour cells). Hence, there is the possibility that the prior expansion and CFSE-labelling of the TILs contributed to the decrease in viability.

In addition to sorting of proliferating cells, future work could focus on other methods of selection of tumour-reactive T cells prior to their expansion and editing. In this regard, future experiments will need to focus on the following:

1. Sorting unexpanded $CD8^+$ TILs that have co-expression of CD103 and CD39, as it has been shown that $CD103^+$ $CD39^+$ $CD8^+$ TILs are enriched for tumour-reactive cells both in primary and metastatic tumours (Duhen et al., 2018).
2. Sorting unexpanded $CD8^+$ TILs that have a high expression of PD1, as it has been demonstrated that these cells have an intrinsically high capacity for tumour recognition (Ahmadzadeh et al., 2009; Gros et al., 2014; Thommen et al., 2018).
3. Utilising commercially available IFNγ or TNFα secretion detection kits to sort unexpanded or expanded $CD8^+$ and $CD4^+$ TILs that secrete cytokines when incubated with their autologous tumour cells (i.e. tumour-reactive T cells).
4. Using unexpanded MX063 TILs to repeat the peptide screen shown in Chapter 4. As rapid expansion has been shown to decrease the frequency of tumour-specific T cells (R. S. Andersen et al., 2012), there is the possibility that neoantigen-reactive T cells were not detected because of the TILs used.
5. Generating the immunopeptidome of the MX063 primary tumour cell line. The results of this immunopeptidomics assay would need to be used to prioritise new candidate neoantigens for screening with the unexpanded MX063 TILs.

6.2.2. Generation of *in vitro* and *in vivo* models to test adoptive cellular therapies

In Chapter 5 we showed the work performed to generate reliable *in vitro* assays and *in vivo* models to test the adoptive cellular therapies with edited vs

non-edited TILs. The *in vitro* assays showed variability due to the stochastic expansion of TILs, which generated stocks of expanded TILs that varied in their proportion of tumour-reactive T cells. This variability would be addressed by the selective expansion of tumour-reactive T cells (see previous section). We hypothesise that once the selective expansion is achieved, the *in vitro* assays would become reliable and conclusive. In this regard, a further improvement that should be consider for future functional assays would be performing the killing assay using real-time cell analysis. This would allow for the analysis of T cell killing of autologous tumour cells without the need to detach the tumour cells (the detachment and further washing of the tumour cells prior to analysis via flow cytometry can generate a loss of cells). Moreover, the real-time cell analysis has the added advantage of allowing the analysis of longer timepoints. Hence it would be useful for optimising the best timepoint to observe the lysis of the tumour cells.

It is known that 2D assays do not take into account the influences of the tumour microenvironment on the immune response. Because of this, we were interested in generating a model that could recreate the three-dimensional structure of the tumour. To this end, we started the optimisation of an *in vivo* model with the MX063 tumour cells and autologous TILs. This model will need to be further optimised to be able to achieve a partial tumour control or complete tumour regression. Further work will be needed to test different ratios of E:T, as well as different timings of TILs treatment and IL-2 application, and different doses of IL-2. In this regard, it may be useful to consider using *hIL2*-NOG transgenic mice (these mice overexpress IL-2 by virtue of a CMV-driven human *IL2* transgene), as it has been shown that IL-2 needs to be supplied continuously for the transplantation of autologous T cells into tumour-bearing NOG mice to achieve tumour eradication (Jespersen et al., 2017). If the use of normal NOG or NSG mice is preferred, then a daily injection of high dose IL-2 would need to be performed for the first 16 days after TILs transplantation, as this has been shown to result in tumour regressions. However, it is worth noting that these tumour regressions were not durable, contrary to the ones observed using the *hIL2*-NOG mouse model (Jespersen et al., 2017). Moreover, other primary tumour cell lines from melanoma and NSCLC patients (patient MX076 and patient LTX1000) have been established in the laboratory by Sophia Wong and Assma

Ben Aissa, respectively. It would therefore be of interest to also optimise *in vivo* ACT models with these primary tumour cell lines and their autologous TILs.

It is important to note that these *in vivo* models are not conventional PDXs, as the tumour cells first undergo a phase of *in vitro* growth prior to injection into mice. As it has been shown that *in vitro* growth can lead to changes in the cancer cells that differ from the host-derived entity (Daniel et al., 2009), future work would also need to focus on the generation of conventional PDX models to test the ACT of edited vs non-edited autologous TILs. In regard to this, Rob Hynds (collaborator in Professor Charlie Swanton's laboratory) has already started the generation of these PDX models as part of the TRACERx (TRAcking Cancer Evolution through therapy (Rx)) lung study. Hence, these PDXs could be used with their autologous TILs to test tumour control once the optimisation of the ACT in an *in vivo* model is achieved.

Although PDX models maintain most of the characteristics of the primary tumours, the human tumour-derived stroma is substituted by murine stroma throughout the tumour growth in mice (Maykel et al., 2014). Hence, after 3-5 passages the stroma (including the extracellular matrix, cancer associated fibroblasts, and blood vessels) is in essence murine. This new murine stroma may impair T cell homing and infiltration to the tumour. Therefore, future work should also focus on the generation of *in vitro* 3D tumouroid systems or explant cultures (Karekla et al., 2017; Neal et al., 2018; Thommen et al., 2019).

6.2.3. Targets for future work

The methodology used in this project for the gene editing of human TILs can be further utilised for the knockdown of other targets of interest. In this regard, targets that could be pursued in future work are negative regulators of the TCR signal transduction pathway, transcription factors that promote T cell exhaustion, as well as negative regulators of T cell responsiveness (i.e. promoters of T cell anergy), amongst others (Thommen et al., 2018; Tirosh et al., 2016; Zheng et al., 2017).

7. References

Abate-Daga, D., & Davila, M. L. (2016). CAR models: Next-generation CAR modifications for enhanced T-cell function. *Molecular Therapy - Oncolytics*, *3*, 16014. https://doi.org/10.1038/mto.2016.14

Abbas, Abul K, Lichtman, Andrew H. and Pillai, S. (2015). Basic Immunology: Functions and Disorders of the Immune System, Fifth Edition. In *Elsevier Health Sciences*.

Agata, Y., Kawasaki, A., Nishimura, H., Ishida, Y., Tsubata, T., Yagita, H., & Honjo, T. (1996). Expression of the PD-1 antigen on the surface of stimulated mouse T and B lymphocytes. *International Immunology*, *8*(5), 765–772. https://doi.org/10.1093/intimm/8.5.765

Ahi, Y. S., Bangari, D. S., & Mittal, S. K. (2011). Adenoviral vector immunity: its implications and circumvention strategies. *Current Gene Therapy*, *11*(4), 307–320. https://doi.org/10.2174/156652311796150372

Ahmadzadeh, M., Johnson, L. A., Heemskerk, B., Wunderlich, J. R., Dudley, M. E., White, D. E., & Rosenberg, S. A. (2009). Tumor antigen-specific CD8 T cells infiltrating the tumor express high levels of PD-1 and are functionally impaired. *Blood*, *114*(8), 1537–1544. https://doi.org/10.1182/blood-2008-12-195792

Aksoy, P., Aksoy, B. A., Czech, E., & Hammerbacher, J. (2018). Electroporation characteristics of human primary T cells. *BioRxiv*, 466243. https://doi.org/10.1101/466243

Alexandrov, L. B., Nik-Zainal, S., Wedge, D. C., Aparicio, S. A. J. R., Behjati, S., Biankin, A. V., … Stratton, M. R. (2013). Signatures of mutational processes in human cancer. *Nature*, *500*(7463), 415–421. https://doi.org/10.1038/nature12477

Algarra, I., García-Lora, A., Cabrera, T., Ruiz-Cabello, F., & Garrido, F. (2004). The selection of tumor variants with altered expression of classical and nonclassical MHC class I molecules: Implications for tumor immune escape. *Cancer Immunology, Immunotherapy*, *53*(10), 904–910. https://doi.org/10.1007/s00262-004-0517-9

Altman, J. D., Moss, P. A. H., Goulder, P. J. R., Barouch, D. H., McHeyzer-Williams, M. G., Bell, J. I., … Davis, M. M. (1996). Phenotypic analysis of

antigen-specific T lymphocytes. *Science*, *274*(5284), 94–96. https://doi.org/10.1126/science.274.5284.94

Ambrogio, C., Gómez-López, G., Falcone, M., Vidal, A., Nadal, E., Crosetto, N., … Barbacid, M. (2016). Combined inhibition of DDR1 and Notch signaling is a therapeutic strategy for KRAS-driven lung adenocarcinoma. *Nature Medicine*, *22*(3), 270–277. https://doi.org/10.1038/nm.4041

Andersen, R., Donia, M., Ellebaek, E., Borch, T. H., Kongsted, P., Iversen, T. Z., … Svane, I. M. (2016). Long-lasting complete responses in patients with metastatic melanoma after adoptive cell therapy with tumor-infiltrating lymphocytes and an attenuated IL-2 regimen. *Clinical Cancer Research*, *22*(15), 3734–3745. https://doi.org/10.1158/1078-0432.CCR-15-1879

Andersen, R. S., Thrue, C. A., Junker, N., Lyngaa, R., Donia, M., Ellebæk, E., … Hadrup, S. R. (2012). Dissection of T-cell antigen specificity in human melanoma. *Cancer Research*, *72*(7), 1642–1650. https://doi.org/10.1158/0008-5472.CAN-11-2614

Anderson, A. C., Joller, N., & Kuchroo, V. K. (2016). Lag-3, Tim-3, and TIGIT: Co-inhibitory Receptors with Specialized Functions in Immune Regulation. *Immunity*, *44*(5), 989–1004. https://doi.org/10.1016/j.immuni.2016.05.001

Anzalone, A. V., Randolph, P. B., Davis, J. R., Sousa, A. A., Koblan, L. W., Levy, J. M., … Liu, D. R. (2019). Search-and-replace genome editing without double-strand breaks or donor DNA. *Nature*. https://doi.org/doi:10.1038/s41586-019-1711-4

Azuma, M., Ito, D., Yagita, H., Okumura, K., Phillips, J. H., Lanier, L. L., & Somoza, C. (1993). B70 antigen is a second ligand for CTLA-4 and CD28. *Nature*, *366*(6450), 76–79. https://doi.org/10.1038/366076a0

Bassani-Sternberg, M. (2018). Mass spectrometry based immunopeptidomics for the discovery of cancer neoantigens. In *Peptidomics. Methods in Molecular Biology* (pp. 209–221). https://doi.org/10.1007/978-1-4939-7537-2_14

Basu, S., Campbell, H. M., Dittel, B. N., & Ray, A. (2010). Purification of Specific Cell Population by Fluorescence Activated Cell Sorting (FACS). *Journal of Visualized Experiments*, *41*, e1546. https://doi.org/10.3791/1546

Beane, J. D., Lee, G., Zheng, Z., Mendel, M., Abate-Daga, D., Bharathan, M., … Feldman, S. A. (2015). Clinical Scale Zinc Finger Nuclease-mediated Gene Editing of PD-1 in Tumor Infiltrating Lymphocytes for the Treatment of

Metastatic Melanoma. *Molecular Therapy*, *23*(8), 1380–1390. https://doi.org/10.1038/mt.2015.71

Bertotti, A., Migliardi, G., Galimi, F., Sassi, F., Torti, D., Isella, C., … Trusolino, L. (2011). A molecularly annotated platform of patient-derived xenografts ("xenopatients") identifies HER2 as an effective therapeutic target in cetuximab-resistant colorectal cancer. *Cancer Discovery*, *1*(6), 508–523. https://doi.org/10.1158/2159-8290.CD-11-0109

Besser, M. J., Shapira-Frommer, R., Itzhaki, O., Treves, A. J., Zippel, D. B., Levy, D., … Schachter, J. (2013). Adoptive transfer of tumor-infiltrating lymphocytes in patients with metastatic melanoma: Intent-to-treat analysis and efficacy after failure to prior immunotherapies. *Clinical Cancer Research*, *19*(17), 4792–4800. https://doi.org/10.1158/1078-0432.CCR-13-0380

Besser, M. J., Shapira-Frommer, R., Treves, A. J., Zippel, D., Itzhaki, O., Hershkovitz, L., … Schachter, J. (2010). Clinical responses in a phase II study using adoptive transfer of short-term cultured tumor infiltration lymphocytes in metastatic melanoma patients. *Clinical Cancer Research*, *16*(9), 2646–2655. https://doi.org/10.1158/1078-0432.CCR-10-0041

Bibikova, M., Carroll, D., Segal, D. J., Trautman, J. K., Smith, J., Kim, Y.-G., & Chandrasegaran, S. (2001). Stimulation of Homologous Recombination through Targeted Cleavage by Chimeric Nucleases. *Molecular and Cellular Biology*, *21*(1), 289–297. https://doi.org/10.1128/mcb.21.1.289-297.2001

Bikard, D., Jiang, W., Samai, P., Hochschild, A., Zhang, F., & Marraffini, L. A. (2013). Programmable repression and activation of bacterial gene expression using an engineered CRISPR-Cas system. *Nucleic Acids Research*, *41*(15), 7429–7437. https://doi.org/10.1093/nar/gkt520

Blake, S. J. P., Ching, A. L. H., Kenna, T. J., Galea, R., Large, J., Yagita, H., & Steptoe, R. J. (2015). Blockade of PD-1/PD-L1 promotes adoptive T-Cell immunotherapy in a tolerogenic environment. *PLoS ONE*, *10*(3), e0119483. https://doi.org/10.1371/journal.pone.0119483

Boch, J., Scholze, H., Schornack, S., Landgraf, A., Hahn, S., Kay, S., … Bonas, U. (2009). Breaking the code of DNA binding specificity of TAL-type III effectors. *Science*, *326*(5959), 1509–1512. https://doi.org/10.1126/science.1178811

Boles, K. S., Vermi, W., Facchetti, F., Fuchs, A., Wilson, T. J., Diacovo, T. G., … Colonna, M. (2009). A novel molecular interaction for the adhesion of follicular CD4 T cells to follicular dendritic cells. *European Journal of Immunology*, *39*(3), 695–703. https://doi.org/10.1002/eji.200839116

Bonifant, C. L., Jackson, H. J., Brentjens, R. J., & Curran, K. J. (2016). Toxicity and management in CAR T-cell therapy. *Molecular Therapy - Oncolytics*, *3*, 16011. https://doi.org/10.1038/mto.2016.11

Bretscher, P. A. (1999). A two-step, two-signal model for the primary activation of precursor helper T cells. *Proceedings of the National Academy of Sciences*, *96*(1), 185–190. https://doi.org/10.1073/pnas.96.1.185

Bretscher, P., & Cohn, M. (1970). A theory of self-nonself discrimination. *Science*, *169*(3950), 1042–1049. https://doi.org/10.1126/science.169.3950.1042

Brinkman, E. K., Chen, T., Amendola, M., & Van Steensel, B. (2014). Easy quantitative assessment of genome editing by sequence trace decomposition. *Nucleic Acids Research*, *42*(22), e168. https://doi.org/10.1093/nar/gku936

Brudno, J. N., & Kochenderfer, J. N. (2016). Toxicities of chimeric antigen receptor T cells: Recognition and management. *Blood*, *127*(26), 3321–3330. https://doi.org/10.1182/blood-2016-04-703751

Brunet, J. F., Denizot, F., Luciani, M. F., Roux-Dosseto, M., Suzan, M., Mattei, M. G., & Golstein, P. (1987). A new member of the immunoglobulin superfamily-CTLA-4. *Nature*, *328*(6127), 267–270. https://doi.org/10.1038/328267a0

Cafri, G., Yossef, R., Pasetto, A., Deniger, D. C., Lu, Y. C., Parkhurst, M., … Rosenberg, S. A. (2019). Memory T cells targeting oncogenic mutations detected in peripheral blood of epithelial cancer patients. *Nature Communications*, *10*(1), 449. https://doi.org/10.1038/s41467-019-08304-z

Cao, E., Zang, X., Ramagopal, U. A., Mukhopadhaya, A., Fedorov, A., Fedorov, E., … Almo, S. C. (2007). T Cell Immunoglobulin Mucin-3 Crystal Structure Reveals a Galectin-9-Independent Ligand-Binding Surface. *Immunity*, *26*(3), 311–321. https://doi.org/10.1016/j.immuni.2007.01.016

Caron, G., Duluc, D., Frémaux, I., Jeannin, P., David, C., Gascan, H., & Delneste, Y. (2005). Direct Stimulation of Human T Cells via TLR5 and TLR7/8: Flagellin and R-848 Up-Regulate Proliferation and IFN-γ Production by

Memory CD4 + T Cells. *The Journal of Immunology*, *175*(3), 1551–1557. https://doi.org/10.4049/jimmunol.175.3.1551

Chang, C. H., Qiu, J., O'Sullivan, D., Buck, M. D., Noguchi, T., Curtis, J. D., … Pearce, E. L. (2015). Metabolic Competition in the Tumor Microenvironment Is a Driver of Cancer Progression. *Cell*, *162*(6), 1229–1241. https://doi.org/10.1016/j.cell.2015.08.016

Chapuis, A. G., Lee, S. M., Thompson, J. A., Roberts, I. M., Margolin, K. A., Bhatia, S., … Yee, C. (2016). Combined IL-21-primed polyclonal CTL plus CTLA4 blockade controls refractory metastatic melanoma in a patient. *Journal of Experimental Medicine*, *213*(7), 1133–1139. https://doi.org/10.1084/jem.20152021

Chapuis, A. G., Roberts, I. M., Thompson, J. A., Margolin, K. A., Bhatia, S., Lee, S. M., … Yee, C. (2016). T-cell therapy using interleukin-21-primed cytotoxic T-cell lymphocytes combined with cytotoxic T-cell lymphocyte antigen-4 blockade results in long-term cell persistence and durable tumor regression. *Journal of Clinical Oncology*, *34*(31), 3787–3795. https://doi.org/10.1200/JCO.2015.65.5142

Chemnitz, J. M., Parry, R. V., Nichols, K. E., June, C. H., & Riley, J. L. (2004). SHP-1 and SHP-2 Associate with Immunoreceptor Tyrosine-Based Switch Motif of Programmed Death 1 upon Primary Human T Cell Stimulation, but Only Receptor Ligation Prevents T Cell Activation. *The Journal of Immunology*, *173*(2), 945–954. https://doi.org/10.4049/jimmunol.173.2.945

Chen, L., & Flies, D. B. (2013). Molecular mechanisms of T cell co-stimulation and co-inhibition. *Nature Reviews Immunology*, *13*(4), 227–242. https://doi.org/10.1038/nri3405

Chew, W. L., Tabebordbar, M., Cheng, J. K. W., Mali, P., Wu, E. Y., Ng, A. H. M., … Church, G. M. (2016). A multifunctional AAV-CRISPR-Cas9 and its host response. *Nature Methods*, *13*(10), 868–874. https://doi.org/10.1038/nmeth.3993

Christian, M., Cermak, T., Doyle, E. L., Schmidt, C., Zhang, F., Hummel, A., … Voytas, D. F. (2010). Targeting DNA double-strand breaks with TAL effector nucleases. *Genetics*, *186*(2), 757–761. https://doi.org/10.1534/genetics.110.120717

Chuang, E., Fisher, T. S., Morgan, R. W., Robbins, M. D., Duerr, J. M., Vander

Heiden, M. G., … Thompson, C. B. (2000). The CD28 and CTLA-4 receptors associate with the serine/threonine phosphatase PP2A. *Immunity*, *13*(3), 313–322. https://doi.org/10.1016/S1074-7613(00)00031-5

Cohen, C. J., Gartner, J. J., Horovitz-Fried, M., Shamalov, K., Trebska-McGowan, K., Bliskovsky, V. V., … Robbins, P. F. (2015). Isolation of neoantigen-specific T cells from tumor and peripheral lymphocytes. *The Journal of Clinical Investigation*, *125*(10), 3981–3991. https://doi.org/10.1172/JCI82416

Cong, L., Ran, F. A., Cox, D., Lin, S., Barretto, R., Habib, N., … Zhang, F. (2013). Multiplex genome engineering using CRISPR/Cas systems. *Science*, *339*(6121), 819–823. https://doi.org/10.1126/science.1231143

Cooper, M. L., Choi, J., Staser, K., Ritchey, J. K., Devenport, J. M., Eckardt, K., … DiPersio, J. F. (2018). An “off-the-shelf” fratricide-resistant CAR-T for the treatment of T cell hematologic malignancies. *Leukemia*, *32*(9), 1970–1983. https://doi.org/10.1038/s41375-018-0065-5

Cornu, T. I., Thibodeau-Beganny, S., Guhl, E., Alwin, S., Eichtinger, M., Joung, J. K., & Cathomen, T. (2008). DNA-binding specificity is a major determinant of the activity and toxicity of zinc-finger nucleases. *Molecular Therapy*, *16*(2), 352–358. https://doi.org/10.1038/sj.mt.6300357

Correia, M. P., Costa, A. V., Uhrberg, M., Cardoso, E. M., & Arosa, F. A. (2011). IL-15 induces CD8+ T cells to acquire functional NK receptors capable of modulating cytotoxicity and cytokine secretion. *Immunobiology*, *216*(5), 604–612. https://doi.org/10.1016/j.imbio.2010.09.012

Cossarizza, A., Chang, H. D., Radbruch, A., Akdis, M., Andrä, I., Annunziato, F., … Zimmermann, J. (2017). Guidelines for the use of flow cytometry and cell sorting in immunological studies. *European Journal of Immunology*, *47*(10), 1584–1797. https://doi.org/10.1002/eji.201646632

Daniel, V. C., Marchionni, L., Hierman, J. S., Rhodes, J. T., Devereux, W. L., Rudin, C. M., … Watkins, D. N. (2009). A primary xenograft model of small-cell lung cancer reveals irreversible changes in gene expression imposed by culture in vitro. *Cancer Research*, *69*(8), 3364–3373. https://doi.org/10.1158/0008-5472.CAN-08-4210

Daya, S., & Berns, K. I. (2008). Gene therapy using adeno-associated virus vectors. *Clinical Microbiology Reviews*, *21*(4), 583–593.

https://doi.org/10.1128/CMR.00008-08

Deniger, D. C., Pasetto, A., Robbins, P. F., Gartner, J. J., Prickett, T. D., Paria, B. C., … Rosenberg, S. A. (2018). T-cell responses to TP53 “Hotspot” mutations and unique neoantigens expressed by human ovarian cancers. *Clinical Cancer Research*, *24*(22), 5562–5573. https://doi.org/10.1158/1078-0432.CCR-18-0573

Derose, Y. S., Wang, G., Lin, Y. C., Bernard, P. S., Buys, S. S., Ebbert, M. T. W., … Welm, A. L. (2011). Tumor grafts derived from women with breast cancer authentically reflect tumor pathology, growth, metastasis and disease outcomes. *Nature Medicine*, *17*(11), 1514–1520. https://doi.org/10.1038/nm.2454

Dever, D. P., Bak, R. O., Reinisch, A., Camarena, J., Washington, G., Nicolas, C. E., … Porteus, M. H. (2016). CRISPR/Cas9 β-globin gene targeting in human haematopoietic stem cells. *Nature*, *539*(7629), 384–389. https://doi.org/10.1038/nature20134

Doench, J. G., Hartenian, E., Graham, D. B., Tothova, Z., Hegde, M., Smith, I., … Root, D. E. (2014). Rational design of highly active sgRNAs for CRISPR-Cas9-mediated gene inactivation. *Nature Biotechnology*, *32*, 1262–1267. https://doi.org/10.1038/nbt.3026

Dong, H., Strome, S. E., Salomao, D. R., Tamura, H., Hirano, F., Flies, D. B., … Chen, L. (2002). Tumor-associated B7-H1 promotes T-cell apoptosis: A potential mechanism of immune evasion. *Nature Medicine*, *8*(8), 793–800. https://doi.org/10.1038/nm730

Dong, X., Guan, J., English, J. C., Flint, J., Yee, J., Evans, K., … Wang, Y. (2010). Patient-derived first generation xenografts of non-small cell lung cancers: Promising tools for predicting drug responses for personalized chemotherapy. *Clinical Cancer Research*, *16*(5), 1442–1451. https://doi.org/10.1158/1078-0432.CCR-09-2878

Donia, M., Junker, N., Ellebaek, E., Andersen, M. H., Straten, P. T., & Svane, I. M. (2012). Characterization and comparison of “standard” and “young” tumour-infiltrating lymphocytes for adoptive cell therapy at a Danish translational research institution. *Scandinavian Journal of Immunology*, *75*(2), 157–167. https://doi.org/10.1111/j.1365-3083.2011.02640.x

Donia, Marco, Kjeldsen, J. W., Andersen, R., Westergaard, M. C. W., Bianchi, V.,

Legut, M., … Svane, I. M. (2017). PD-1+ polyfunctional T cells dominate the periphery after tumor-infiltrating lymphocyte therapy for cancer. *Clinical Cancer Research*, *23*(19), 5779–5788. https://doi.org/10.1158/1078-0432.CCR-16-1692

Duan, D., Sharma, P., Yang, J., Yue, Y., Dudus, L., Zhang, Y., … Engelhardt, J. F. (1998). Circular intermediates of recombinant adeno-associated virus have defined structural characteristics responsible for long-term episomal persistence in muscle tissue. *Journal of Virology*, *72*(11), 8568–8577.

Dudley, M. E., Gross, C. A., Langhan, M. M., Garcia, M. R., Sherry, R. M., Yang, J. C., … Rosenberg, S. A. (2010). CD8+ enriched "young" tumor infiltrating lymphocytes can mediate regression of metastatic melanoma. *Clinical Cancer Research*, *16*(24), 6122–6131. https://doi.org/10.1158/1078-0432.CCR-10-1297

Dudley, M. E., Gross, C. A., Somerville, R. P. T., Hong, Y., Schaub, N. P., Rosati, S. F., … Rosenberg, S. A. (2013). Randomized selection design trial evaluating CD8+-enriched versus unselected tumor-infiltrating lymphocytes for adoptive cell therapy for patients with melanoma. *Journal of Clinical Oncology*, *31*(17), 2152–2159. https://doi.org/10.1200/JCO.2012.46.6441

Dudley, M. E., Wunderlich, J. R., Robbins, P. F., Yang, J. C., Hwu, P., Schwartzentruber, D. J., … Rosenberg, S. A. (2002). Cancer regression and autoimmunity in patients after clonal repopulation with antitumor lymphocytes. *Science*, *298*(5594), 850–854. https://doi.org/10.1126/science.1076514

Dudley, M. E., Wunderlich, J. R., Shelton, T. E., Even, J., & Rosenberg, S. A. (2003). Generation of tumor-infiltrating lymphocyte cultures for use in adoptive transfer therapy for melanoma patients. *Journal of Immunotherapy*, *26*(4), 332. https://doi.org/10.1097/00002371-200307000-00005

Dudley, M. E., Wunderlich, J. R., Yang, J. C., Sherry, R. M., Topalian, S. L., Restifo, N. P., … Rosenberg, S. A. (2005). Adoptive cell transfer therapy following non-myeloablative but lymphodepleting chemotherapy for the treatment of patients with refractory metastatic melanoma. *Journal of Clinical Oncology*, *23*(10), 2346–2357. https://doi.org/10.1200/JCO.2005.00.240

Dudley, M. E., Yang, J. C., Sherry, R., Hughes, M. S., Royal, R., Kammula, U., … Rosenberg, S. A. (2008). Adoptive cell therapy for patients with metastatic

melanoma: Evaluation of intensive myeloablative chemoradiation preparative regimens. *Journal of Clinical Oncology*, *26*(32), 5233–5239. https://doi.org/10.1200/JCO.2008.16.5449

Duhen, T., Duhen, R., Montler, R., Moses, J., Moudgil, T., De Miranda, N. F., … Weinberg, A. D. (2018). Co-expression of CD39 and CD103 identifies tumor-reactive CD8 T cells in human solid tumors. *Nature Communications*, *9*(1), 2724. https://doi.org/10.1038/s41467-018-05072-0

Dunn, G. P., Old, L. J., & Schreiber, R. D. (2004). The Immunobiology of Cancer Immunosurveillance and Immunoediting. *Immunity*, *21*(2), 137–148. https://doi.org/10.1016/j.immuni.2004.07.017

Ebert, O., Finke, S., Salahi, A., Herrmann, M., Trojaneck, B., Lefterova, P., … Schmidt-Wolf, I. G. H. (1997). Lymphocyte apoptosis: Induction by gene transfer techniques. *Gene Therapy*, *4*(4), 296–302. https://doi.org/10.1038/sj.gt.3300394

Einarsdottir, B. O., Bagge, R. O., Bhadury, J., Jespersen, H., Mattsson, J., Nilsson, L. M., … Nilsson, J. A. (2014). Melanoma patient-derived xenografts accurately model the disease and develop fast enough to guide treatment decisions. *Oncotarget*, *5*(20), 9609–9618. https://doi.org/10.18632/oncotarget.2445

Ettinghausen, S. E., & Rosenberg, S. A. (1986). Immunotherapy of Murine Sarcomas Using Lymphokine Activated Killer Cells: Optimization of the Schedule and Route of Administration of Recombinant Interleukin-2. *Cancer Research*, *46*(6), 2784–2792.

Ferrone, S., & Marincola, F. M. (1995). Loss of HLA class I antigens by melanoma cells: molecular mechanisms, functional significance and clinial relevance. *Immunology Today*, *16*(10), 487–494. https://doi.org/10.1016/0167-5699(95)80033-6

Fichtner, I., Rolff, J., Soong, R., Hoffmann, J., Hammer, S., Sommer, A., … Merk, J. (2008). Establishment of patient-derived non-small cell lung cancer xenografts as models for the identification of predictive biomarkers. *Clinical Cancer Research*, *14*(20), 6456–6468. https://doi.org/10.1158/1078-0432.CCR-08-0138

Fisher, R. I., Rosenberg, S. A., & Fyfe, G. (2000). Long-term survival update for high-dose recombinant interleukin-2 in patients with renal cell carcinoma.

Cancer Journal from Scientific American, *6*(Supplement 1), S55–S57.

Follenzi, A., Santambrogio, L., & Annoni, A. (2007). Immune Responses to Lentiviral Vectors. *Current Gene Therapy*, *7*(5), 306–315. https://doi.org/10.2174/156652307782151515

Freeman, G. J., Long, A. J., Iwai, Y., Bourque, K., Chernova, T., Nishimura, H., … Honjo, T. (2000). Engagement of the PD-1 immunoinhibitory receptor by a novel B7 family member leads to negative regulation of lymphocyte activation. *Journal of Experimental Medicine*, *192*(7), 1027–1034. https://doi.org/10.1084/jem.192.7.1027

Friedman, K. M., Prieto, P. A., Devillier, L. E., Gross, C. A., Yang, J. C., Wunderlich, J. R., … Dudley, M. E. (2012). Tumor-specific CD4+ melanoma tumor-infiltrating lymphocytes. *Journal of Immunotherapy*, *35*(5), 400–408. https://doi.org/10.1097/CJI.0b013e31825898c5

Fu, Y., Sander, J. D., Reyon, D., Cascio, V. M., & Joung, J. K. (2014). Improving CRISPR-Cas nuclease specificity using truncated guide RNAs. *Nature Biotechnology*, *32*(3), 279–284. https://doi.org/10.1038/nbt.2808

Gao, H., Korn, J. M., Ferretti, S., Monahan, J. E., Wang, Y., Singh, M., … Sellers, W. R. (2015). High-throughput screening using patient-derived tumor xenografts to predict clinical trial drug response. *Nature Medicine*, *21*(11), 1318–1325. https://doi.org/10.1038/nm.3954

Garcia-Garijo, A., Fajardo, C. A., & Gros, A. (2019). Determinants for Neoantigen Identification. *Frontiers in Immunology*, *10*, 1392. https://doi.org/10.3389/fimmu.2019.01392

Gérard, A., Khan, O., Beemiller, P., Oswald, E., Hu, J., Matloubian, M., & Krummel, M. F. (2013). Secondary T cell-T cell synaptic interactions drive the differentiation of protective CD8+ T cells. *Nature Immunology*, *14*(4), 356–363. https://doi.org/10.1038/ni.2547

Gettinger, S., Choi, J., Hastings, K., Truini, A., Datar, I., Sowell, R., … Politi, K. (2017). Impaired HLA class I antigen processing and presentation as a mechanism of acquired resistance to immune checkpoint inhibitors in lung cancer. *Cancer Discovery*, *7*(12), 1420–1435. https://doi.org/10.1158/2159-8290.CD-17-0593

Gilbert, L. A., Larson, M. H., Morsut, L., Liu, Z., Brar, G. A., Torres, S. E., … Qi, L. S. (2013). CRISPR-mediated modular RNA-guided regulation of

transcription in eukaryotes. *Cell*, *154*(2), 442–451. https://doi.org/10.1016/j.cell.2013.06.044

Glass, Z., Lee, M., Li, Y., & Xu, Q. (2018). Engineering the Delivery System for CRISPR-Based Genome Editing. *Trends in Biotechnology*, *36*(2), 173–185. https://doi.org/10.1016/j.tibtech.2017.11.006

Goff, S. L., Dudley, M. E., Citrin, D. E., Somerville, R. P., Wunderlich, J. R., Danforth, D. N., … Rosenberg, S. A. (2016). Randomized, prospective evaluation comparing intensity of lymphodepletion before adoptive transfer of tumor-infiltrating lymphocytes for patients with metastatic melanoma. *Journal of Clinical Oncology*, *34*(20), 2389–2397. https://doi.org/10.1200/JCO.2016.66.7220

Greene, J. A. L., Leytze, G. M., Emswiler, J., Peach, R., Bajorath, J., Cosand, W., & Linsley, P. S. (1996). Covalent dimerization of CD28/CTLA-4 and oligomerization of CD80/CD86 regulate T cell costimulatory interactions. *Journal of Biological Chemistry*, *271*(43), 26762–26771. https://doi.org/10.1074/jbc.271.43.26762

Gros, A., Parkhurst, M. R., Tran, E., Pasetto, A., Robbins, P. F., Ilyas, S., … Rosenberg, S. A. (2016). Prospective identification of neoantigen-specific lymphocytes in the peripheral blood of melanoma patients. *Nature Medicine*, *22*(4), 433–438. https://doi.org/10.1038/nm.4051

Gros, A., Robbins, P. F., Yao, X., Li, Y. F., Turcotte, S., Tran, E., … Rosenberg, S. A. (2014). PD-1 identifies the patient-specific CD8+ tumor-reactive repertoire infiltrating human tumors. *Journal of Clinical Investigation*, *124*(5), 2246–2259. https://doi.org/10.1172/JCI73639

Hannier, S., Tournier, M., Bismuth, G., & Triebel, F. (1998). CD3/TCR complex-associated lymphocyte activation gene-3 molecules inhibit CD3/TCR signaling. *Journal of Immunology*, *161*(8), 4058–4065.

Hauck, B., Murphy, S. L., Smith, P. H., Qu, G., Liu, X., Zelenaia, O., … Wright, J. F. (2009). Undetectable transcription of cap in a clinical AAV vector: Implications for preformed capsid in immune responses. *Molecular Therapy*, *17*(1), 144–152. https://doi.org/10.1038/mt.2008.227

Heemskerk, B., Kvistborg, P., & Schumacher, T. N. M. (2013). The cancer antigenome. *The EMBO Journal*, *32*(2), 194–203. https://doi.org/10.1038/emboj.2012.333

Heigwer, F., Kerr, G., & Boutros, M. (2014). E-CRISP: fast CRISPR target site identification. *Nature Methods*, *11*(2), 122–123. https://doi.org/10.1038/nmeth.2812

Hendel, A., Bak, R. O., Clark, J. T., Kennedy, A. B., Ryan, D. E., Roy, S., … Porteus, M. H. (2015). Chemically modified guide RNAs enhance CRISPR-Cas genome editing in human primary cells. *Nature Biotechnology*, *33*(9), 985–989. https://doi.org/10.1038/nbt.3290

Hilton, I. B., D'Ippolito, A. M., Vockley, C. M., Thakore, P. I., Crawford, G. E., Reddy, T. E., & Gersbach, C. A. (2015). Epigenome editing by a CRISPR-Cas9-based acetyltransferase activates genes from promoters and enhancers. *Nature Biotechnology*, *33*(5), 510–517. https://doi.org/10.1038/nbt.3199

Hodgkins, A., Farne, A., Perera, S., Grego, T., Parry-Smith, D. J., Skarnes, W. C., & Iyer, V. (2015). WGE: A CRISPR database for genome engineering. *Bioinformatics*, *31*(18), 3078–3080. https://doi.org/10.1093/bioinformatics/btv308

Hodi, F. Stephen, O'Day, S. J., McDermott, D. F., Weber, R. W., Sosman, J. A., Haanen, J. B., … Urba, W. J. (2010). Improved survival with ipilimumab in patients with metastatic melanoma. *New England Journal of Medicine*, *363*(8), 711–723. https://doi.org/10.1056/NEJMoa1003466

Hodi, Frank Stephen, Chiarion-Sileni, V., Gonzalez, R., Grob, J. J., Rutkowski, P., Cowey, C. L., … Wolchok, J. D. (2018). Nivolumab plus ipilimumab or nivolumab alone versus ipilimumab alone in advanced melanoma (CheckMate 067): 4-year outcomes of a multicentre, randomised, phase 3 trial. *The Lancet Oncology*, *19*(11), 1480–1492. https://doi.org/10.1016/S1470-2045(18)30700-9

Holkers, M., Maggio, I., Liu, J., Janssen, J. M., Miselli, F., Mussolino, C., … Gonçalves, M. A. F. V. (2013). Differential integrity of TALE nuclease genes following adenoviral and lentiviral vector gene transfer into human cells. *Nucleic Acids Research*, *41*(5), e63. https://doi.org/10.1093/nar/gks1446

Horii, T., Arai, Y., Yamazaki, M., Morita, S., Kimura, M., Itoh, M., … Hatada, I. (2014). Validation of microinjection methods for generating knockout mice by CRISPR/Cas-mediated genome engineering. *Scientific Reports*, *4*, 4513. https://doi.org/10.1038/srep04513

Hsiau, T., Conant, D., Maures, T., Waite, K., Yang, J., Kelso, R., … Stoner, R. (2018). Inference of CRISPR Edits from Sanger Trace Data. *BioRxiv*, 251082. https://doi.org/10.1101/251082

Hsu, P. D., Scott, D. A., Weinstein, J. A., Ran, F. A., Konermann, S., Agarwala, V., … Zhang, F. (2013). DNA targeting specificity of RNA-guided Cas9 nucleases. *Nature Biotechnology*, *31*(9), 827–832. https://doi.org/10.1038/nbt.2647

Huang, C. T., Workman, C. J., Flies, D., Pan, X., Marson, A. L., Zhou, G., … Vignali, D. A. A. (2004). Role of LAG-3 in regulatory T cells. *Immunity*, *21*(4), 503–513. https://doi.org/10.1016/j.immuni.2004.08.010

Huang, J., Kerstann, K. W., Ahmadzadeh, M., Li, Y. F., El-Gamil, M., Rosenberg, S. A., & Robbins, P. F. (2006). Modulation by IL-2 of CD70 and CD27 Expression on CD8+ T Cells: Importance for the Therapeutic Effectiveness of Cell Transfer Immunotherapy. *The Journal of Immunology*, *176*(12), 7726–7735. https://doi.org/10.4049/jimmunol.176.12.7726

Huang, J., Khong, H. T., Dudley, M. E., El-Gamil, M., Li, Y. F., Rosenberg, S. A., & Robbins, P. F. (2005). Survival, persistence, and progressive differentiation of adoptively transferred tumor-reactive T cells associated with tumor regression. *Journal of Immunotherapy*, *28*(3), 258–267. https://doi.org/10.1097/01.cji.0000158855.92792.7a

Huang, R.-Y., Eppolito, C., Lele, S., Shrikant, P., Matsuzaki, J., & Odunsi, K. (2015). LAG3 and PD1 co-inhibitory molecules collaborate to limit CD8+ T cell signaling and dampen antitumor immunity in a murine ovarian cancer model. *Oncotarget*, *6*(29), 27359–27377. https://doi.org/10.18632/oncotarget.4751

Huang, Y. H., Zhu, C., Kondo, Y., Anderson, A. C., Gandhi, A., Russell, A., … Blumberg, R. S. (2015). CEACAM1 regulates TIM-3-mediated tolerance and exhaustion. *Nature*, *517*(7534), 386–390. https://doi.org/10.1038/nature13848

Huard, B., Prigent, P., Tournier, M., Bruniquel, D., & Triebel, F. (1995). CD4/major histocompatibility complex class II interaction analyzed with CD4- and lymphocyte activation gene-3 (LAG-3)-Ig fusion proteins. *European Journal of Immunology*, *25*(9), 2718–2721. https://doi.org/10.1002/eji.1830250949

Hultquist, J. F., Schumann, K., Woo, J. M., Manganaro, L., McGregor, M. J.,

Doudna, J., … Marson, A. (2016). A Cas9 Ribonucleoprotein Platform for Functional Genetic Studies of HIV-Host Interactions in Primary Human T Cells. *Cell Reports*, *17*(5), 1438–1452. https://doi.org/10.1016/j.celrep.2016.09.080

Hunder, N. N., Wallen, H., Cao, J., Hendricks, D. W., Reilly, J. Z., Rodmyre, R., … Yee, C. (2008). Treatment of Metastatic Melanoma with Autologous CD4+ T Cells against NY-ESO-1. *New England Journal of Medicine*, *358*(25), 2698–2703. https://doi.org/10.1056/nejmoa0800251

Hüser, D., Khalid, D., Lutter, T., Hammer, E.-M., Weger, S., Heßler, M., … Heilbronn, R. (2017). High Prevalence of Infectious Adeno-associated Virus (AAV) in Human Peripheral Blood Mononuclear Cells Indicative of T Lymphocytes as Sites of AAV Persistence. *Journal of Virology*, *91*(4), e02137-16. https://doi.org/10.1128/jvi.02137-16

Hutchinson, L., & Kirk, R. (2011). High drug attrition rates - Where are we going wrong? *Nature Reviews Clinical Oncology*, *8*, 189–190. https://doi.org/10.1038/nrclinonc.2011.34

Imaizumi, T., Kumagai, M., Sasaki, N., Kurotaki, H., Mori, F., Seki, M., … Satoh, K. (2002). Interferon-gamma stimulates the expression of Galectin-9 in cultured human endothelial cells. *Journal of Leukocyte Biology*, *72*(3), 486–491. https://doi.org/10.1189/jlb.72.3.486

Ingebrigtsen, V. A., Boye, K., Tekle, C., Nesland, J. M., Flatmark, K., & Fodstad, O. (2012). B7-H3 expression in colorectal cancer: Nuclear localization strongly predicts poor outcome in colon cancer. *International Journal of Cancer*, *131*(11), 2528–2536. https://doi.org/10.1002/ijc.27566

Irving, B. A., & Weiss, A. (1991). The cytoplasmic domain of the T cell receptor ζ chain is sufficient to couple to receptor-associated signal transduction pathways. *Cell*, *64*(5), 891–901. https://doi.org/10.1016/0092-8674(91)90314-O

Ishida, Y., Agata, Y., Shibahara, K., & Honjo, T. (1992). Induced expression of PD-1, a novel member of the immunoglobulin gene superfamily, upon programmed cell death. *The EMBO Journal*, *11*(11), 3887–3895. https://doi.org/10.1002/j.1460-2075.1992.tb05481.x

Itzhaki, O., Hovav, E., Ziporen, Y., Levy, D., Kubi, A., Zikich, D., … Besser, M. J. (2011). Establishment and large-scale expansion of minimally cultured

"young" tumor infiltrating lymphocytes for adoptive transfer therapy. *Journal of Immunotherapy*, *34*(2), 212–220. https://doi.org/10.1097/CJI.0b013e318209c94c

Izumchenko, E., Paz, K., Ciznadija, D., Sloma, I., Katz, A., Vasquez-Dunddel, D., … Sidransky, D. (2017). Patient-derived xenografts effectively capture responses to oncology therapy in a heterogeneous cohort of patients with solid tumors. *Annals of Oncology*, *28*(10), 2595–2605. https://doi.org/10.1093/annonc/mdx416

Jamieson, A. C., Kim, S. H., & Wells, J. A. (1994). In Vitro Selection of Zinc Fingers with Altered DNA-Binding Specificity. *Biochemistry*, *33*(19), 5689–5695. https://doi.org/10.1021/bi00185a004

Jamieson, A. C., Wang, H., & Kim, S. H. (1996). A zinc finger directory for high-affinity DNA recognition. *Proceedings of the National Academy of Sciences*, *93*(23), 12834–12839. https://doi.org/10.1073/pnas.93.23.12834

Jespersen, H., Lindberg, M. F., Donia, M., Söderberg, E. M. V., Andersen, R., Keller, U., … Nilsson, J. A. (2017). Clinical responses to adoptive T-cell transfer can be modeled in an autologous immune-humanized mouse model. *Nature Communications*, *8*(1), 707. https://doi.org/10.1038/s41467-017-00786-z

Jinek, M., Chylinski, K., Fonfara, I., Hauer, M., Doudna, J. A., & Charpentier, E. (2012). A programmable dual-RNA-guided DNA endonuclease in adaptive bacterial immunity. *Science*, *337*(6096), 816–821. https://doi.org/10.1126/science.1225829

John, L. B., Devaud, C., Duong, C. P. M., Yong, C. S., Beavis, P. A., Haynes, N. M., … Darcy, P. K. (2013). Anti-PD-1 antibody therapy potently enhances the eradication of established tumors by gene-modified T cells. *Clinical Cancer Research*, *19*(20), 5636–5646. https://doi.org/10.1158/1078-0432.CCR-13-0458

Johnson, L. A., Morgan, R. A., Dudley, M. E., Cassard, L., Yang, J. C., Hughes, M. S., … Rosenberg, S. A. (2009). Gene therapy with human and mouse T-cell receptors mediates cancer regression and targets normal tissues expressing cognate antigen. *Blood*, *114*(3), 535–546. https://doi.org/10.1182/blood-2009-03-211714

Joller, N., Hafler, J. P., Brynedal, B., Kassam, N., Spoerl, S., Levin, S. D., …

Kuchroo, V. K. (2011). Cutting Edge: TIGIT Has T Cell-Intrinsic Inhibitory Functions. *The Journal of Immunology*, *186*(3), 1338–1342. https://doi.org/10.4049/jimmunol.1003081

Judde, J. G., Rebucci, M., Vogt, N., De Cremoux, P., Livartowski, A., Chapelier, A., … Bras-Gonçalves, R. A. (2007). Gefitinib and chemotherapy combination studies in five novel human non small cell lung cancer xenografts. Evidence linking EGFR signaling to gefitinib antitumor response. *International Journal of Cancer*, *120*(7), 1579–1590. https://doi.org/10.1002/ijc.22364

June, C. H., Ledbetter, J. A., Gillespie, M. M., Lindsten, T., & Thompson, C. B. (1987). T-cell proliferation involving the CD28 pathway is associated with cyclosporine-resistant interleukin 2 gene expression. *Molecular and Cellular Biology*, *7*(12), 4472–4481. https://doi.org/10.1128/mcb.7.12.4472

Jurtz, V., Paul, S., Andreatta, M., Marcatili, P., Peters, B., & Nielsen, M. (2017). NetMHCpan-4.0: Improved Peptide–MHC Class I Interaction Predictions Integrating Eluted Ligand and Peptide Binding Affinity Data. *The Journal of Immunology*, *199*(9), 3360–3368. https://doi.org/10.4049/jimmunol.1700893

Karekla, E., Liao, W. J., Sharp, B., Pugh, J., Reid, H., Le Quesne, J., … Pringle, J. H. (2017). Ex Vivo explant cultures of non-small cell lung carcinoma enable evaluation of primary tumor responses to anticancer therapy. *Cancer Research*, *77*(8), 2029–2039. https://doi.org/10.1158/0008-5472.CAN-16-1121

Kemper, K., Krijgsman, O., Kong, X., Cornelissen-Steijger, P., Shahrabi, A., Weeber, F., … Peeper, D. S. (2016). BRAF V600E Kinase Domain Duplication Identified in Therapy-Refractory Melanoma Patient-Derived Xenografts. *Cell Reports*, *16*(1), 263–277. https://doi.org/10.1016/j.celrep.2016.05.064

Kim, S., Bae, T., Hwang, J., & Kim, J. S. (2017). Rescue of high-specificity Cas9 variants using sgRNAs with matched 5’ nucleotides. *Genome Biology*, *18*(1), 218. https://doi.org/10.1186/s13059-017-1355-3

Kim, S., Kim, D., Cho, S. W., Kim, J., & Kim, J. S. (2014). Highly efficient RNA-guided genome editing in human cells via delivery of purified Cas9 ribonucleoproteins. *Genome Research*, *24*(6), 1012–1019. https://doi.org/10.1101/gr.171322.113

Kim, S., Koo, T., Jee, H. G., Cho, H. Y., Lee, G., Lim, D. G., … Kim, J. S. (2018). CRISPR RNAs trigger innate immune responses in human cells. *Genome Research*, *28*(3), 367–373. https://doi.org/10.1101/gr.231936.117

Kim, Y. G., Cha, J., & Chandrasegaran, S. (1996). Hybrid restriction enzymes: Zinc finger fusions to Fok I cleavage domain. *Proceedings of the National Academy of Sciences*, *93*(3), 1156–1160. https://doi.org/10.1073/pnas.93.3.1156

Kinter, A. L., Godbout, E. J., McNally, J. P., Sereti, I., Roby, G. A., O'Shea, M. A., & Fauci, A. S. (2008). The Common γ-Chain Cytokines IL-2, IL-7, IL-15, and IL-21 Induce the Expression of Programmed Death-1 and Its Ligands. *The Journal of Immunology*, *181*(10), 6738–6746. https://doi.org/10.4049/jimmunol.181.10.6738

Kleinstiver, B. P., Pattanayak, V., Prew, M. S., Tsai, S. Q., Nguyen, N. T., Zheng, Z., & Joung, J. K. (2016). High-fidelity CRISPR-Cas9 nucleases with no detectable genome-wide off-target effects. *Nature*, *529*(7587), 490–495. https://doi.org/10.1038/nature16526

Kobayashi, K. S., & Van Den Elsen, P. J. (2012). NLRC5: A key regulator of MHC class I-dependent immune responses. *Nature Reviews Immunology*, *12*, 813–820. https://doi.org/10.1038/nri3339

Konermann, S., Brigham, M. D., Trevino, A. E., Joung, J., Abudayyeh, O. O., Barcena, C., … Zhang, F. (2015). Genome-scale transcriptional activation by an engineered CRISPR-Cas9 complex. *Nature*, *517*(7536), 583–588. https://doi.org/10.1038/nature14136

Konermann, S., Lotfy, P., Brideau, N. J., Oki, J., Shokhirev, M. N., & Hsu, P. D. (2018). Transcriptome Engineering with RNA-Targeting Type VI-D CRISPR Effectors. *Cell*, *173*(3), 665–676. https://doi.org/10.1016/j.cell.2018.02.033

Kortmann, U., McAlpine, J. N., Xue, H., Guan, J., Ha, G., Tully, S., … Gilks, C. B. (2011). Tumor growth inhibition by olaparib in BRCA2 germline-mutated patient-derived ovarian cancer tissue xenografts. *Clinical Cancer Research*, *17*(4), 783–791. https://doi.org/10.1158/1078-0432.CCR-10-1382

Krumbach, R., Schüler, J., Hofmann, M., Giesemann, T., Fiebig, H. H., & Beckers, T. (2011). Primary resistance to cetuximab in a panel of patient-derived tumour xenograft models: Activation of MET as one mechanism for drug resistance. *European Journal of Cancer*, *47*(8), 1231–1243.

https://doi.org/10.1016/j.ejca.2010.12.019

Kvistborg, P., Shu, C. J., Heemskerk, B., Fankhauser, M., Thrue, C. A., Toebes, M., … Schumacher, T. N. M. (2012). TIL therapy broadens the tumor-reactive CD8+ T cell compartment in melanoma patients. *Oncoimmunology*, *1*(4), 409–418. https://doi.org/10.4161/onci.18851

Larkin, J., Chiarion-Sileni, V., Gonzalez, R., Grob, J. J., Cowey, C. L., Lao, C. D., … Wolchok, J. D. (2015). Combined Nivolumab and Ipilimumab or Monotherapy in Untreated Melanoma. *The New England Journal of Medicine*, *373*(1), 23–34. https://doi.org/10.1056/NEJMoa1504030

Lašťovička, J., Budinský, V., Špíšek, R., & Bartůňková, J. (2009). Assessment of lymphocyte proliferation: CFSE kills dividing cells and modulates expression of activation markers. *Cellular Immunology*, *256*(1–2), 79–85. https://doi.org/10.1016/j.cellimm.2009.01.007

Latchman, Y. E., Liang, S. C., Wu, Y., Chernova, T., Sobel, R. A., Klemm, M., … Sharpe, A. H. (2004). PD-L1-deficient mice show that PD-L1 on T cells, antigen-presenting cells, and host tissues negatively regulates T cells. *Proceedings of the National Academy of Sciences of the United States of America*, *101*(29), 10691–10696. https://doi.org/10.1073/pnas.0307252101

Leach, D. R., Krummel, M. F., & Allison, J. P. (1996). Enhancement of antitumor immunity by CTLA-4 blockade. *Science*, *271*(5256), 1734–1736. https://doi.org/10.1126/science.271.5256.1734

Lee, H. J., Kim, Y.-A., Sim, C. K., Heo, S.-H., Song, I. H., Park, H. S., … Gong, G. (2017). Expansion of tumor-infiltrating lymphocytes and their potential for application as adoptive cell transfer therapy in human breast cancer. *Oncotarget*, *8*(69), 113345–113359. https://doi.org/10.18632/oncotarget.23007

Lennerz, V., Fatho, M., Gentilini, C., Frye, R. A., Lifke, A., Ferel, D., … Wolfel, T. (2005). The response of autologous T cells to a human melanoma is dominated by mutated neoantigens. *Proceedings of the National Academy of Sciences*, *102*(44), 16013–16018. https://doi.org/10.1073/pnas.0500090102

Levin, S. D., Taft, D. W., Brandt, C. S., Bucher, C., Howard, E. D., Chadwick, E. M., … Lewis, K. E. (2011). Vstm3 is a member of the CD28 family and an important modulator of T-cell function. *European Journal of Immunology*,

41(4), 902–915. https://doi.org/10.1002/eji.201041136

Li, A., Lee, C. M., Hurley, A. E., Jarrett, K. E., De Giorgi, M., Lu, W., … Lagor, W. R. (2019). A Self-Deleting AAV-CRISPR System for In Vivo Genome Editing. *Molecular Therapy - Methods and Clinical Development*, *12*, 111–122. https://doi.org/10.1016/j.omtm.2018.11.009

Li, M., Xia, P., Du, Y., Liu, S., Huang, G., Chen, J., … Fan, Z. (2014). T-cell immunoglobulin and ITIM domain (TIGIT) receptor/poliovirus receptor (PVR) ligand engagement suppresses interferon-γ production of natural killer cells via β-arrestin 2-mediated negative signaling. *Journal of Biological Chemistry*, *289*(25), 17647–17657. https://doi.org/10.1074/jbc.M114.572420

Li, T., Huang, S., Jiang, W. Z., Wright, D., Spalding, M. H., Weeks, D. P., & Yang, B. (2011). TAL nucleases (TALNs): Hybrid proteins composed of TAL effectors and FokI DNA-cleavage domain. *Nucleic Acids Research*, *39*(1), 359–372. https://doi.org/10.1093/nar/gkq704

Liang, X., Potter, J., Kumar, S., Zou, Y., Quintanilla, R., Sridharan, M., … Chesnut, J. D. (2015). Rapid and highly efficient mammalian cell engineering via Cas9 protein transfection. *Journal of Biotechnology*, *208*, 44–53. https://doi.org/10.1016/j.jbiotec.2015.04.024

Liechtenstein, T., Dufait, I., Lanna, A., Breckpot, K., & Escors, D. (2012). Modulating Co-Stimulation During Antigen Presentation to Enhance Cancer Immunotherapy. *Immunology Endocrine & Metabolic Agents - Medicinal Chemistry*, *12*(3), 224–235. https://doi.org/10.2174/187152212802001875

Lino, C. A., Harper, J. C., Carney, J. P., & Timlin, J. A. (2018). Delivering CRISPR: A review of the challenges and approaches. *Drug Delivery*, *25*(1), 1234–1257. https://doi.org/10.1080/10717544.2018.1474964

Linsley, P. S., Brady, W., Urnes, M., Grosmaire, L. S., Damle, N. K., & Ledbetter, J. A. (1991). CTLA4 is a second receptor for the b cell activation antigen B7. *Journal of Experimental Medicine*, *174*(3), 561–569. https://doi.org/10.1084/jem.174.3.561

Linsley, P. S., Clark, E. A., & Ledbetter, J. A. (1990). T-cell antigen CD28 mediates adhesion with B cells by interacting with activation antigen B7/BB-1. *Proceedings of the National Academy of Sciences*, *87*(13), 5031–5035. https://doi.org/10.1073/pnas.87.13.5031

Liu, S., Zhang, H., Li, M., Hu, D., Li, C., Ge, B., … Fan, Z. (2013). Recruitment of

Grb2 and SHIP1 by the ITT-like motif of TIGIT suppresses granule polarization and cytotoxicity of NK cells. *Cell Death and Differentiation*, *20*(3), 456–464. https://doi.org/10.1038/cdd.2012.141

Liu, X., Homma, A., Sayadi, J., Yang, S., Ohashi, J., & Takumi, T. (2016). Sequence features associated with the cleavage efficiency of CRISPR/Cas9 system. *Scientific Reports*, *6*, 19675. https://doi.org/10.1038/srep19675

Liu, X. S., Wu, H., Ji, X., Stelzer, Y., Wu, X., Czauderna, S., … Jaenisch, R. (2016). Editing DNA Methylation in the Mammalian Genome. *Cell*, *167*(1), 233–247. https://doi.org/10.1016/j.cell.2016.08.056

Lu, Y. C., Yao, X., Crystal, J. S., Li, Y. F., El-Gamil, M., Gross, C., … Robbins, P. F. (2014). Efficient identification of mutated cancer antigens recognized by T cells associated with durable tumor regressions. *Clinical Cancer Research*, *20*(13), 3401–3410. https://doi.org/10.1158/1078-0432.CCR-14-0433

Mali, P., Yang, L., Esvelt, K. M., Aach, J., Guell, M., DiCarlo, J. E., … Church, G. M. (2013). RNA-guided human genome engineering via Cas9. *Science*, *339*(6121), 823–826. https://doi.org/10.1126/science.1232033

Mandal, P. K., Ferreira, L. M. R., Collins, R., Meissner, T. B., Boutwell, C. L., Friesen, M., … Cowan, C. A. (2014). Efficient ablation of genes in human hematopoietic stem and effector cells using CRISPR/Cas9. *Cell Stem Cell*, *15*(5), 643–652. https://doi.org/10.1016/j.stem.2014.10.004

Maude, S. L., Frey, N., Shaw, P. A., Aplenc, R., Barrett, D. M., Bunin, N. J., … Grupp, S. A. (2014). Chimeric antigen receptor T cells for sustained remissions in leukemia. *New England Journal of Medicine*, *371*(16), 1507–1517. https://doi.org/10.1056/NEJMoa1407222

Maykel, J., Liu, J. H., Li, H., Shultz, L. D., Greiner, D. L., & Houghton, J. (2014). NOD-scidIl2rg (tm1Wjl) and NOD-Rag1 (null) Il2rg (tm1Wjl): A model for stromal cell-tumor cell interaction for human colon cancer. *Digestive Diseases and Sciences*, *59*(6), 1169–1179. https://doi.org/10.1007/s10620-014-3168-5

McDermott, D., Haanen, J., Chen, T. T., Lorigan, P., & O'Day, S. (2013). Efficacy and safety of ipilimumab in metastatic melanoma patients surviving more than 2 years following treatment in a phase III trial (MDX010-20). *Annals of Oncology*, *24*(10), 2694–2698. https://doi.org/10.1093/annonc/mdt291

McGranahan, N., Furness, A. J. S., Rosenthal, R., Ramskov, S., Lyngaa, R.,

Saini, S. K., … Swanton, C. (2016). Clonal neoantigens elicit T cell immunoreactivity and sensitivity to immune checkpoint blockade. *Science*, *351*(6280), 1463–1469. https://doi.org/10.1126/science.aaf1490

McGranahan, N., Rosenthal, R., Hiley, C. T., Rowan, A. J., Watkins, T. B. K., Wilson, G. A., … Dessimoz, C. (2017). Allele-Specific HLA Loss and Immune Escape in Lung Cancer Evolution. *Cell*, *171*(6), 1259–1271. https://doi.org/10.1016/j.cell.2017.10.001

Menger, L., Gouble, A., Marzolini, M. A. V., Pachnio, A., Bergerhoff, K., Henry, J. Y., … Peggs, K. S. (2015). TALEN-mediated genetic inactivation of the glucocorticoid receptor in cytomegalovirus-specific T cells. *Blood*, *126*(26), 2781–2789. https://doi.org/10.1182/blood-2015-08-664755

Menger, L., Sledzinska, A., Bergerhoff, K., Varga, F. A., Smith, J., Poirot, L., … Quezada, S. A. (2016). TALEN-Mediated Inactivation of PD-1 in Tumor-Reactive Lymphocytes Promotes Intratumoral T-cell Persistence and Rejection of Established Tumors. *Cancer Research*, *76*(8), 2087–2093. https://doi.org/10.1158/0008-5472.CAN-15-3352

Miller, J. C., Holmes, M. C., Wang, J., Guschin, D. Y., Lee, Y. L., Rupniewski, I., … Rebar, E. J. (2007). An improved zinc-finger nuclease architecture for highly specific genome editing. *Nature Biotechnology*, *25*(7), 778–785. https://doi.org/10.1038/nbt1319

Miller, J. C., Tan, S., Qiao, G., Barlow, K. A., Wang, J., Xia, D. F., … Rebar, E. J. (2011). A TALE nuclease architecture for efficient genome editing. *Nature Biotechnology*, *29*(2), 143–148. https://doi.org/10.1038/nbt.1755

Mimura, K., Teh, J. L., Okayama, H., Shiraishi, K., Kua, L. F., Koh, V., … Kono, K. (2018). PD-L1 expression is mainly regulated by interferon gamma associated with JAK-STAT pathway in gastric cancer. *Cancer Science*, *109*(1), 43–53. https://doi.org/10.1111/cas.13424

Montague, T. G., Cruz, J. M., Gagnon, J. A., Church, G. M., & Valen, E. (2014). CHOPCHOP: A CRISPR/Cas9 and TALEN web tool for genome editing. *Nucleic Acids Research*, *42*(W1), W401–W407. https://doi.org/10.1093/nar/gku410

Murphy, K., Weaver, C., Mowat, A., Berg, L., & Chaplin, D. (2017). Janeway's Immunobiology 9th Edition. In *New York: Garland Science*.

Muul, L. M., Spiess, P. J., Director, E. P., & Rosenberg, S. A. (1987). Identification

of specific cytolytic immune responses against autologous tumor in humans bearing malignant melanoma. *The Journal of Immunology*, *138*(3), 989–995.

Nandedkar, M. A., Palazzo, J., Abbondanzo, S. L., Lasota, J., & Miettinen, M. (1998). CD45 (leukocyte common antigen) immunoreactivity in metastatic undifferentiated and neuroendocrine carcinoma: a potential diagnostic pitfall. *Modern Pathology: An Official Journal of the United States and Canadian Academy of Pathology, Inc*, *11*(12), 1204–1210.

Nardelli, J., Gibson, T., & Charnay, P. (1992). Zinc finger-DNA recognition: Analysis of base specificity by site-directed mutagenesis. *Nucleic Acids Research*, *20*(16), 4137–4144. https://doi.org/10.1093/nar/20.16.4137

Neal, J. T., Li, X., Zhu, J., Giangarra, V., Grzeskowiak, C. L., Ju, J., … Kuo, C. J. (2018). Organoid Modeling of the Tumor Immune Microenvironment. *Cell*, *175*(7), 1972–1988. https://doi.org/10.1016/j.cell.2018.11.021

Ngo, N., Patel, K., Isaacson, P. G., & Naresh, K. N. (2007). Leucocyte common antigen (CD45) and CD5 positivity in an “undifferentiated” carcinoma: A potential diagnostic pitfall. *Journal of Clinical Pathology*, *60*(8), 936–938. https://doi.org/10.1136/jcp.2006.044750

Nielsen, C., Ohm-Laursen, L., Barington, T., Husby, S., & Lillevang, S. T. (2005). Alternative splice variants of the human PD-1 gene. *Cellular Immunology*, *235*(2), 109–116. https://doi.org/10.1016/j.cellimm.2005.07.007

Nielsen, M., & Andreatta, M. (2016). NetMHCpan-3.0; improved prediction of binding to MHC class I molecules integrating information from multiple receptor and peptide length datasets. *Genome Medicine*, *8*(1), 33. https://doi.org/10.1186/s13073-016-0288-x

Nielsen, M., Lund, O., Buus, S., & Lundegaard, C. (2010). MHC Class II epitope predictive algorithms. *Immunology*, *130*(3), 319–328. https://doi.org/10.1111/j.1365-2567.2010.03268.x

Nishimura, H., Nose, M., Hiai, H., Minato, N., & Honjo, T. (1999). Development of lupus-like autoimmune diseases by disruption of the PD-1 gene encoding an ITIM motif-carrying immunoreceptor. *Immunity*, *11*(2), 141–151. https://doi.org/10.1016/S1074-7613(00)80089-8

Nurieva, R., Thomas, S., Nguyen, T., Martin-Orozco, N., Wang, Y., Kaja, M. K., … Dong, C. (2006). T-cell tolerance or function is determined by combinatorial costimulatory signals. *EMBO Journal*, *25*(11), 2623–2633.

https://doi.org/10.1038/sj.emboj.7601146

Oflazoglu, E., Elliott, M., Takita, H., Ferrone, S., Henderson, R. a., & Repasky, E. a. (2007). Adoptively transferred human lung tumor specific cytotoxic T cells can control autologous tumor growth and shape tumor phenotype in a SCID mouse xenograft model. *Journal of Translational Medicine*, *5*(1), 29. https://doi.org/10.1186/1479-5876-5-29

Okazaki, T., Maeda, A., Nishimura, H., Kurosaki, T., & Honjo, T. (2001). PD-1 immunoreceptor inhibits B cell receptor-mediated signaling by recruiting src homology 2-domain-containing tyrosine phosphatase 2 to phosphotyrosine. *Proceedings of the National Academy of Sciences of the United States of America*, *98*(24), 13866–13871. https://doi.org/10.1073/pnas.231486598

Olden, B. R., Cheng, E., Cheng, Y., & Pun, S. H. (2019). Identifying key barriers in cationic polymer gene delivery to human T cells. *Biomaterials Science*, *7*(3), 789–797. https://doi.org/10.1039/c8bm01262h

Olden, B. R., Cheng, Y., Yu, J. L., & Pun, S. H. (2018). Cationic polymers for non-viral gene delivery to human T cells. *Journal of Controlled Release*, *282*, 140–147. https://doi.org/10.1016/j.jconrel.2018.02.043

Pardoll, D. M. (2012). The blockade of immune checkpoints in cancer immunotherapy. *Nature Reviews Cancer*, *12*(4), 252–264. https://doi.org/10.1038/nrc3239

Parkhurst, M. R., Yang, J. C., Langan, R. C., Dudley, M. E., Nathan, D. A. N., Feldman, S. A., … Rosenberg, S. A. (2011). T cells targeting carcinoembryonic antigen can mediate regression of metastatic colorectal cancer but induce severe transient colitis. *Molecular Therapy*, *19*(3), 620–626. https://doi.org/10.1038/mt.2010.272

Patsoukis, N., Brown, J., Petkova, V., Liu, F., Li, L., & Boussiotis, V. A. (2012). Selective effects of PD-1 on Akt and ras pathways regulate molecular components of the cell cycle and inhibit T cell proliferation. *Science Signaling*, *5*(230), ra46. https://doi.org/10.1126/scisignal.2002796

Patsoukis, N., Li, L., Sari, D., Petkova, V., & Boussiotis, V. A. (2013). PD-1 Increases PTEN Phosphatase Activity While Decreasing PTEN Protein Stability by Inhibiting Casein Kinase 2. *Molecular and Cellular Biology*, *33*(16), 3091–3098. https://doi.org/10.1128/mcb.00319-13

Pilon-Thomas, S., Kuhn, L., Ellwanger, S., Janssen, W., Royster, E., Marzban,

S., … Sarnaik, A. A. (2012). Efficacy of adoptive cell transfer of tumor-infiltrating lymphocytes after lymphopenia induction for metastatic melanoma. *Journal of Immunotherapy*, *35*(8), 615–620. https://doi.org/10.1097/CJI.0b013e31826e8f5f

Pittet, M. J., Speiser, D. E., Valmori, D., Cerottini, J.-C., & Romero, P. (2000). Cutting Edge: Cytolytic Effector Function in Human Circulating CD8 + T Cells Closely Correlates with CD56 Surface Expression. *The Journal of Immunology*, *164*(3), 1148–1152. https://doi.org/10.4049/jimmunol.164.3.1148

Porter, D. L., Levine, B. L., Kalos, M., Bagg, A., & June, C. H. (2011). Chimeric antigen receptor-modified T cells in chronic lymphoid leukemia. *New England Journal of Medicine*, *365*(8), 725–733. https://doi.org/10.1056/NEJMoa1103849

Potter, H., & Heller, R. (2018). Transfection by electroporation. *Current Protocols in Molecular Biology*, *121*(1), 9.3.1-9.3.13. https://doi.org/10.1002/cpmb.48

Powell, D. J., Dudley, M. E., Robbins, P. F., & Rosenberg, S. A. (2005). Transition of late-stage effector T cells to CD27+ CD28+ tumor-reactive effector memory T cells in humans after adoptive cell transfer therapy. *Blood*, *105*(1), 241–250. https://doi.org/10.1182/blood-2004-06-2482

Prickett, T. D., Crystal, J. S., Cohen, C. J., Pasetto, A., Parkhurst, M. R., Gartner, J. J., … Robbins, P. F. (2016). Durable Complete Response from Metastatic Melanoma after Transfer of Autologous T Cells Recognizing 10 Mutated Tumor Antigens. *Cancer Immunology Research*, *4*(8), 669–678. https://doi.org/10.1158/2326-6066.cir-15-0215

Qi, L. S., Larson, M. H., Gilbert, L. A., Doudna, J. A., Weissman, J. S., Arkin, A. P., & Lim, W. A. (2013). Repurposing CRISPR as an RNA-guided platform for sequence-specific control of gene expression. *Cell*, *152*(5), 1173–1183. https://doi.org/10.1016/j.cell.2013.02.022

Quail, D. F., & Joyce, J. A. (2013). Microenvironmental regulation of tumor progression and metastasis. *Nature Medicine*, *19*(11), 1423. https://doi.org/10.1038/nm.3394

Quintana, E., Piskounova, E., Shackleton, M., Weinberg, D., Eskiocak, U., Fullen, D. R., … Morrison, S. J. (2012). Human melanoma metastasis in NSG mice correlates with clinical outcome in patients. *Science Translational Medicine*,

4(159), 159ra149-159ra149. https://doi.org/10.1126/scitranslmed.3004599

Qureshi, O. S., Zheng, Y., Nakamura, K., Attridge, K., Manzotti, C., Schmidt, E. M., … Sansom, D. M. (2011). Trans-endocytosis of CD80 and CD86: A molecular basis for the cell-extrinsic function of CTLA-4. *Science*, *332*(6029), 600–603. https://doi.org/10.1126/science.1202947

Radzisheuskaya, A., Shlyueva, D., Müller, I., & Helin, K. (2016). Optimizing sgRNA position markedly improves the efficiency of CRISPR/dCas9-mediated transcriptional repression. *Nucleic Acids Research*, *44*(18), e141. https://doi.org/10.1093/nar/gkw583

Rajeshkumar, N. V., Yabuuchi, S., Pai, S. G., De Oliveira, E., Kamphorst, J. J., Rabinowitz, J. D., … Dang, C. V. (2017). Treatment of pancreatic cancer patient–derived xenograft panel with metabolic inhibitors reveals efficacy of phenformin. *Clinical Cancer Research*, *23*(18), 5639–5647. https://doi.org/10.1158/1078-0432.CCR-17-1115

Ramming, A., Thümmler, K., Schulze-Koops, H., & Skapenko, A. (2009). Homotypic T-cell/T-cell interaction induces T-cell activation, proliferation, and differentiation. *Human Immunology*, *70*(11), 873–881. https://doi.org/10.1016/j.humimm.2009.08.003

Ran, F. A., Cong, L., Yan, W. X., Scott, D. A., Gootenberg, J. S., Kriz, A. J., … Zhang, F. (2015). In vivo genome editing using Staphylococcus aureus Cas9. *Nature*, *520*(7546), 186–191. https://doi.org/10.1038/nature14299

Ran, F. A., Hsu, P. D., Wright, J., Agarwala, V., Scott, D. A., & Zhang, F. (2013). Genome engineering using the CRISPR-Cas9 system. *Nature Protocols*, *8*(11), 2281–2308. https://doi.org/10.1007/978-1-4939-1862-1_10

Rangachari, M., Zhu, C., Sakuishi, K., Xiao, S., Karman, J., Chen, A., … Kuchroo, V. K. (2012). Bat3 promotes T cell responses and autoimmunity by repressing Tim-3-mediated cell death and exhaustion. *Nature Medicine*, *18*(9), 1394–1400. https://doi.org/10.1038/nm.2871

Ren, J., Liu, X., Fang, C., Jiang, S., June, C. H., & Zhao, Y. (2017). Multiplex genome editing to generate universal CAR T cells resistant to PD1 inhibition. *Clinical Cancer Research*, *23*(9), 2255–2266. https://doi.org/10.1158/1078-0432.CCR-16-1300

Ren, J., Zhang, X., Liu, X., Fang, C., Jiang, S., June, C. H., & Zhao, Y. (2017). A versatile system for rapid multiplex genome-edited CAR T cell generation.

Oncotarget, *8*(10), 17002–17011. https://doi.org/10.18632/oncotarget.15218

Ren, X., Yang, Z., Xu, J., Sun, J., Mao, D., Hu, Y., … Ni, J. Q. (2014). Enhanced specificity and efficiency of the CRISPR/Cas9 system with optimized sgRNA parameters in Drosophila. *Cell Reports*, *9*(3), 1151–1162. https://doi.org/10.1016/j.celrep.2014.09.044

Rizvi, N. A., Hellmann, M. D., Snyder, A., Kvistborg, P., Makarov, V., Havel, J. J., … Chan, T. A. (2015). Mutational landscape determines sensitivity to PD-1 blockade in non-small cell lung cancer. *Science*, *348*(6230), 124–128. https://doi.org/10.1126/science.aaa1348

Robbins, P. F., Lu, Y. C., El-Gamil, M., Li, Y. F., Gross, C., Gartner, J., … Rosenberg, S. A. (2013). Mining exomic sequencing data to identify mutated antigens recognized by adoptively transferred tumor-reactive T cells. *Nature Medicine*, *19*(6), 747–752. https://doi.org/10.1038/nm.3161

Robert, C., Schachter, J., Long, G. V., Arance, A., Grob, J. J., Mortier, L., … Ribas, A. (2015). Pembrolizumab versus ipilimumab in advanced melanoma. *New England Journal of Medicine*, *372*(26), 2521–2532. https://doi.org/10.1056/NEJMoa1503093

Rosenberg, S. A., Lotze, M. T., Yang, J. C., Topalian, S. L., Chang, A. E., Schwartzentruber, D. J., … Steinberg, S. M. (1993). Prospective randomized trial of high-dose interleukin-2 alone or in conjunction with lymphokine-activated killer cells for the treatment of patients with advanced cancer. *Journal of the National Cancer Institute*, *85*(8), 622–632. https://doi.org/10.1093/jnci/85.8.622

Rosenberg, S. A., Packard, B. S., Aebersold, P. M., Solomon, D., Topalian, S. L., Toy, S. T., … White, D. E. (1988). Use of Tumor-Infiltrating Lymphocytes and Interleukin-2 in the Immunotherapy of Patients with Metastatic Melanoma. *New England Journal of Medicine*, *319*(25), 1676–1680. https://doi.org/10.1056/nejm198812223192527

Rosenberg, S. A., Spiess, P., & Lafreniere, R. (1986). A new approach to the adoptive immunotherapy of cancer with tumor-infiltrating lymphocytes. *Science*, *233*(4770), 1318–1321. https://doi.org/10.1126/science.3489291

Rosenberg, S. A., Yang, J. C., Sherry, R. M., Kammula, U. S., Hughes, M. S., Phan, G. Q., … Dudley, M. E. (2011). Durable complete responses in heavily

pretreated patients with metastatic melanoma using T-cell transfer immunotherapy. *Clinical Cancer Research*, *17*(13), 4550–4557. https://doi.org/10.1158/1078-0432.CCR-11-0116

Rupp, L. J., Schumann, K., Roybal, K. T., Gate, R. E., Ye, C. J., Lim, W. A., & Marson, A. (2017). CRISPR/Cas9-mediated PD-1 disruption enhances anti-tumor efficacy of human chimeric antigen receptor T cells. *Scientific Reports*, *7*(1), 737. https://doi.org/10.1038/s41598-017-00462-8

Rygaard, J., & Poulsen, C. O. (1969). Heterotransplantation of a human malignant tumour to “Nude” mice. *Acta Pathologica Microbiologica Scandinavica*, *77*(4), 758–760. https://doi.org/10.1111/j.1600-0463.2007.apm_689a.x

Santiago, C., Ballesteros, A., Tami, C., Martínez-Muñoz, L., Kaplan, G. G., & Casasnovas, J. M. (2007). Structures of T Cell Immunoglobulin Mucin Receptors 1 and 2 Reveal Mechanisms for Regulation of Immune Responses by the TIM Receptor Family. *Immunity*, *26*(3), 299–310. https://doi.org/10.1016/j.immuni.2007.01.014

Scheper, W., Kelderman, S., Fanchi, L. F., Linnemann, C., Bendle, G., de Rooij, M. A. J., … Schumacher, T. N. (2019). Low and variable tumor reactivity of the intratumoral TCR repertoire in human cancers. *Nature Medicine*, *25*(1), 89–94. https://doi.org/10.1038/s41591-018-0266-5

Schildberg, F. A., Klein, S. R., Freeman, G. J., & Sharpe, A. H. (2016). Coinhibitory Pathways in the B7-CD28 Ligand-Receptor Family. *Immunity*, *44*(5), 955–972. https://doi.org/10.1016/j.immuni.2016.05.002

Schneider, H., Martin, M., Agarraberes, F. A., Yin, L., Rapoport, I., Kirchhausen, T., & Rudd, C. E. (1999). Cytolytic T lymphocyte-associated antigen-4 and the TCR zeta/CD3 complex, but not CD28, interact with clathrin adaptor complexes AP-1 and AP-2. *Journal of Immunology*, *163*(4), 1868–1879.

Schumann, K., Lin, S., Boyer, E., Simeonov, D. R., Subramaniam, M., Gate, R. E., … Marson, A. (2015). Generation of knock-in primary human T cells using Cas9 ribonucleoproteins. *Proceedings of the National Academy of Sciences*, *112*(33), 10437–10442. https://doi.org/10.1073/pnas.1512503112

Schuster, S. J., Svoboda, J., Chong, E. A., Nasta, S. D., Mato, A. R., Anak, Ö., … June, C. H. (2017). Chimeric antigen receptor T Cells in refractory B-Cell lymphomas. *New England Journal of Medicine*, *377*(26), 2545–2554.

https://doi.org/10.1056/NEJMoa1708566

Schwartzentruber, D. J., Hom, S. S., Dadmarz, R., White, D. E., Yannelli, J. R., Steinberg, S. M., … Topalian, S. L. (1994). In vitro predictors of therapeutic response in melanoma patients receiving tumor-infiltrating lymphocytes and interleukin-2. *Journal of Clinical Oncology*, *12*(7), 1475–1483. https://doi.org/10.1200/JCO.1994.12.7.1475

Sehrawat, S., Reddy, P. B. J., Rajasagi, N., Suryawanshi, A., Hirashima, M., & Rouse, B. T. (2010). Galectin-9/TIM-3 interaction regulates virus-specific primary and memory CD8+ T cell response. *PLoS Pathogens*, *6*(5), e1000882. https://doi.org/10.1371/journal.ppat.1000882

Seki, A., & Rutz, S. (2018). Optimized RNP transfection for highly efficient CRISPR/Cas9-mediated gene knockout in primary T cells. *Journal of Experimental Medicine*, *215*(3), 985–997. https://doi.org/10.1084/jem.20171626

Shalem, O., Sanjana, N. E., Hartenian, E., Shi, X., Scott, D. A., Mikkelsen, T. S., … Zhang, F. (2014). Genome-scale CRISPR-Cas9 knockout screening in human cells. *Science*, *343*(6166), 84–87. https://doi.org/10.1126/science.1247005

Shen, C.-C., Hsu, M.-N., Chang, C.-W., Lin, M.-W., Hwu, J.-R., Tu, Y., & Hu, Y.-C. (2018). Synthetic switch to minimize CRISPR off-target effects by self-restricting Cas9 transcription and translation. *Nucleic Acids Research*, *47*(3), e13. https://doi.org/10.1093/nar/gky1165

Sheppard, K. A., Fitz, L. J., Lee, J. M., Benander, C., George, J. A., Wooters, J., … Chaudhary, D. (2004). PD-1 inhibits T-cell receptor induced phosphorylation of the ZAP70/CD3ζ signalosome and downstream signaling to PKCθ. *FEBS Letters*, *574*(1–3), 37–41. https://doi.org/10.1016/j.febslet.2004.07.083

Sheridan, C. (2018). Go-ahead for first in-body CRISPR medicine testing. *Nature Biotechnology*. https://doi.org/10.1038/d41587-018-00003-2

Shi, J., Wang, E., Milazzo, J. P., Wang, Z., Kinney, J. B., & Vakoc, C. R. (2015). Discovery of cancer drug targets by CRISPR-Cas9 screening of protein domains. *Nature Biotechnology*, *33*(6), 661–667. https://doi.org/10.1038/nbt.3235

Shi, L. Z., Gao, J., Allison, J. P., & Sharma, P. (2018). Combination therapy of

adoptive T cell therapy and immune checkpoint blockades engages distinct mechanisms in CD4+ and CD8+ T cells. *The Journal of Immunology*, *200*(1), 122.21.

Shinohara, T., Taniwaki, M., Ishida, Y., Kawaichi, M., & Honjo, T. (1994). Structure and chromosomal localization of the human PD-1 gene (PDCD1). *Genomics*, *23*(3), 704–706. https://doi.org/10.1006/geno.1994.1562

Simoni, Y., Becht, E., Fehlings, M., Loh, C. Y., Koo, S. L., Teng, K. W. W., … Newell, E. W. (2018). Bystander CD8+ T cells are abundant and phenotypically distinct in human tumour infiltrates. *Nature*, *557*(7706), 575–579. https://doi.org/10.1038/s41586-018-0130-2

Slaymaker, I. M., Gao, L., Zetsche, B., Scott, D. A., Yan, W. X., & Zhang, F. (2016). Rationally engineered Cas9 nucleases with improved specificity. *Science*, *351*(6268), 84–88. https://doi.org/10.1126/science.aad5227

Smith, F. O., Downey, S. G., Klapper, J. A., C.Yang, J., Sherry, R. M., Royal, R. E., … Rosenberg, S. A. (2008). Treatment of metastatic melanoma using Interleukin-2 alone or in conjunction with vaccines. *Clinical Cancer Research*, *14*(17), 5610–5618. https://doi.org/10.1158/1078-0432.CCR-08-0116

Smyth, M. J., Ngiow, S. F., Ribas, A., & Teng, M. W. L. (2016). Combination cancer immunotherapies tailored to the tumour microenvironment. *Nature Reviews Clinical Oncology*, *13*(3), 143–158. https://doi.org/10.1038/nrclinonc.2015.209

Snyder, A., Makarov, V., Merghoub, T., Yuan, J., Zaretsky, J. M., Desrichard, A., … Chan, T. A. (2014). Genetic basis for clinical response to CTLA-4 blockade in melanoma. *New England Journal of Medicine*, *371*(23), 2189–2199. https://doi.org/10.1056/NEJMoa1406498

Stanietsky, N., Simic, H., Arapovic, J., Toporik, A., Levy, O., Novik, A., … Mandelboim, O. (2009). The interaction of TIGIT with PVR and PVRL2 inhibits human NK cell cytotoxicity. *Proceedings of the National Academy of Sciences of the United States of America*, *106*(42), 17858–17863. https://doi.org/10.1073/pnas.0903474106

Stoddard, B. L. (2005). Homing endonuclease structure and function. *Quarterly Reviews of Biophysics*, *38*(1), 49–95. https://doi.org/10.1017/S0033583505004063

Stoddard, B. L. (2011). Homing endonucleases: From microbial genetic invaders to reagents for targeted DNA modification. *Structure*, *19*(1), 7–15. https://doi.org/10.1016/j.str.2010.12.003

Stone, J. D., & Kranz, D. M. (2013). Role of T cell receptor affinity in the efficacy and specificity of adoptive T cell therapies. *Frontiers in Immunology*, *4*, 244. https://doi.org/10.3389/fimmu.2013.00244

Sun, Y. (2016). Tumor microenvironment and cancer therapy resistance. *Cancer Letters*, *380*(1), 205–215. https://doi.org/10.1016/j.canlet.2015.07.044

Swann, J. B., & Smyth, M. J. (2007). Immune surveillance of tumors. *Journal of Clinical Investigation*, *117*(5), 1137–1146. https://doi.org/10.1172/JCI31405

Taams, L. S., Eden, W. van, & Wauben, M. H. M. (1999). Antigen presentation by T cells versus professional antigen-presenting cells (APC): differential consequences for T cell activation and subsequent T cell-APC interactions. *European Journal of Immunology*, *29*(5), 1543–1550. https://doi.org/10.1002/(SICI)1521-4141(199905)29:05<1543::AID-IMMU1543>3.0.CO;2-R

Terawaki, S., Chikuma, S., Shibayama, S., Hayashi, T., Yoshida, T., Okazaki, T., & Honjo, T. (2011). IFN-α Directly Promotes Programmed Cell Death-1 Transcription and Limits the Duration of T Cell-Mediated Immunity. *The Journal of Immunology*, *186*(5), 2772–2779. https://doi.org/10.4049/jimmunol.1003208

Thommen, D. S., Koelzer, V. H., Herzig, P., Bruijn, M. de, Voabil, P., Braber, M. van den, … Schumacher, T. N. M. (2019). Abstract B050: Identification of PD-1T TILs and CXCL13 as determinants for response to anti-PD-1 treatment using human tumor explants. *Abstracts: Fourth CRI-CIMT-EATI-AACR International Cancer Immunotherapy Conference: Translating Science into Survival; September 30 - October 3, 2018; New York, NY*. https://doi.org/10.1158/2326-6074.CRICIMTEATIAACR18-B050

Thommen, D. S., Koelzer, V. H., Herzig, P., Roller, A., Trefny, M., Dimeloe, S., … Zippelius, A. (2018). A transcriptionally and functionally distinct PD-1+ CD8+ T cell pool with predictive potential in non-small-cell lung cancer treated with PD-1 blockade. *Nature Medicine*, *24*(7), 994–1004. https://doi.org/10.1038/s41591-018-0057-z

Tirosh, I., Izar, B., Prakadan, S. M., Wadsworth, M. H., Treacy, D., Trombetta, J.

J., … Garraway, L. A. (2016). Dissecting the multicellular ecosystem of metastatic melanoma by single-cell RNA-seq. *Science*, *352*(6282), 189–196. https://doi.org/10.1126/science.aad0501

Tivol, E. A., Borriello, F., Schweitzer, A. N., Lynch, W. P., Bluestone, J. A., & Sharpe, A. H. (1995). Loss of CTLA-4 leads to massive lymphoproliferation and fatal multiorgan tissue destruction, revealing a critical negative regulatory role of CTLA-4. *Immunity*, *3*(5), 541–547. https://doi.org/10.1016/1074-7613(95)90125-6

Topalian, S. L., Solomon, D., Avis, F. P., Chang, A. E., Freerksen, D. L., Linehan, W. M., … Rosenberg, S. A. (1988). Immunotherapy of patients with advanced cancer using tumor-infiltrating lymphocytes and recombinant interleukin-2: A pilot study. *Journal of Clinical Oncology*, *6*(5), 839–853. https://doi.org/10.1200/JCO.1988.6.5.839

Topalian, Suzanne L., Hodi, F. S., Brahmer, J. R., Gettinger, S. N., Smith, D. C., McDermott, D. F., … Sznol, M. (2012). Safety, activity, and immune correlates of anti-PD-1 antibody in cancer. *New England Journal of Medicine*, *366*(26), 2443–2454. https://doi.org/10.1056/NEJMoa1200690

Tran, E., Ahmadzadeh, M., Lu, Y. C., Gros, A., Turcotte, S., Robbins, P. F., … Rosenberg, S. A. (2015). Immunogenicity of somatic mutations in human gastrointestinal cancers. *Science*, *350*(6266), 1387–1390. https://doi.org/10.1126/science.aad1253

Tran, E., Robbins, P. F., Lu, Y.-C., Prickett, T. D., Gartner, J. J., Jia, L., … Rosenberg, S. A. (2016). T-Cell Transfer Therapy Targeting Mutant KRAS in Cancer. *New England Journal of Medicine*, *375*(23), 2255–2262. https://doi.org/10.1056/nejmoa1609279

Tran, E., Turcotte, S., Gros, A., Robbins, P. F., Lu, Y. C., Dudley, M. E., … Rosenberg, S. A. (2014). Cancer immunotherapy based on mutation-specific CD4+ T cells in a patient with epithelial cancer. *Science*, *344*(6184), 641–645. https://doi.org/10.1126/science.1251102

Tran, K. Q., Zhou, J., Durflinger, K. H., Langhan, M. M., Shelton, T. E., Wunderlich, J. R., … Dudley, M. E. (2008). Minimally cultured tumor-infiltrating lymphocytes display optimal characteristics for adoptive cell therapy. *Journal of Immunotherapy*, *31*(8), 742–751. https://doi.org/10.1097/CJI.0b013e31818403d5

Valitutti, S., Müller, S., Salio, M., & Lanzavecchia, A. (1997). Degradation of T Cell Receptor (TCR)–CD3-ζ Complexes after Antigenic Stimulation. *Journal of Experimental Medicine*, *185*(10), 1859–1864. https://doi.org/10.1084/jem.185.10.1859

Van Acker, H. H., Capsomidis, A., Smits, E. L., & Van Tendeloo, V. F. (2017). CD56 in the immune system: More than a marker for cytotoxicity? *Frontiers in Immunology*, *8*, 892. https://doi.org/10.3389/fimmu.2017.00892

Van Allen, E. M., Miao, D., Schilling, B., Shukla, S. A., Blank, C., Zimmer, L., … Garraway, L. A. (2015). Genomic correlates of response to CTLA-4 blockade in metastatic melanoma. *Science*, *350*(6257), 207–211. https://doi.org/10.1126/science.aad0095

Vánky, F., Klein, E., Willems, J., Böök, K., Ivert, T., Péterffy, A., … Aparisi, T. (1986). Lysis of autologous tumor cells by blood lymphocytes tested at the time of surgery - Correlation with the postsurgical clinical course. *Cancer Immunology Immunotherapy*, *21*(1), 69–76. https://doi.org/10.1007/BF00199380

Verkuijl, S. A., & Rots, M. G. (2019). The influence of eukaryotic chromatin state on CRISPR–Cas9 editing efficiencies. *Current Opinion in Biotechnology*, *55*, 68–73. https://doi.org/10.1016/j.copbio.2018.07.005

Villadolid, J., & Amin, A. (2015). Immune checkpoint inhibitors in clinical practice: update on management of immune-related toxicities. *Translational Lung Cancer Research*, *4*(5), 560–575. https://doi.org/10.3978/j.issn.2218-6751.2015.06.06

Vollers, S. S., & Stern, L. J. (2008). Class II major histocompatibility complex tetramer staining: Progress, problems, and prospects. *Immunology*, *123*(3), 305–313. https://doi.org/10.1111/j.1365-2567.2007.02801.x

Walunas, T. L., Lenschow, D. J., Bakker, C. Y., Linsley, P. S., Freeman, G. J., Green, J. M., … Bluestone, J. A. (1994). CTLA-4 can function as a negative regulator of T cell activation. *Immunity*, *1*(5), 405–413. https://doi.org/10.1016/1074-7613(94)90071-X

Wang, Jian, Yoshida, T., Nakaki, F., Hiai, H., Okazaki, T., & Honjo, T. (2005). Establishment of NOD-Pdcd1-/- mice as an efficient animal model of type I diabetes. *Proceedings of the National Academy of Sciences of the United States of America*, *102*(33), 11823–11828.

https://doi.org/10.1073/pnas.0505497102

Wang, Jinhua, Chong, K. K., Nakamura, Y., Nguyen, L., Huang, S. K., Kuo, C., … Hoon, D. S. B. (2013). B7-H3 associated with tumor progression and epigenetic regulatory activity in cutaneous melanoma. *Journal of Investigative Dermatology*, *133*(8), 2050–2058. https://doi.org/10.1038/jid.2013.114

Wang, T., Wei, J. J., Sabatini, D. M., & Lander, E. S. (2014). Genetic Screens in Human Cells Using the CRISPR-Cas9 System. *Science*, *343*(6166), 80–84. https://doi.org/10.1126/science.1246981

Want, M. Y., Konstorum, A., Huang, R.-Y., Jain, V., Matsueda, S., Tsuji, T., … Battaglia, S. (2019). Neoantigens retention in patient derived xenograft models mediates autologous T cells activation in ovarian cancer. *OncoImmunology*, *8*(6), e1586042. https://doi.org/10.1080/2162402X.2019.1586042

Waterhouse, P., Penninger, J. M., Timms, E., Wakeham, A., Shahinian, A., Lee, K. P., … Mak, T. W. (1995). Lymphoproliferative disorders with early lethality in mice deficient in Ctla-4. *Science*, *270*(5238), 985–988. https://doi.org/10.1126/science.270.5238.985

Wei, G., Ding, L., Wang, J., Hu, Y., & Huang, H. (2017). Advances of CD19-directed chimeric antigen receptor-modified T cells in refractory/relapsed acute lymphoblastic leukemia. *Experimental Hematology and Oncology*, *6*(1), 10. https://doi.org/10.1186/s40164-017-0070-9

Wherry, E. J., Ha, S. J., Kaech, S. M., Haining, W. N., Sarkar, S., Kalia, V., … Ahmed, R. (2007). Molecular Signature of CD8+ T Cell Exhaustion during Chronic Viral Infection. *Immunity*, *27*(4), 670–684. https://doi.org/10.1016/j.immuni.2007.09.006

Wienert, B., Shin, J., Zelin, E., Pestal, K., & Corn, J. E. (2018). In vitro–transcribed guide RNAs trigger an innate immune response via the RIG-I pathway. *PLoS Biology*, *16*(7), e2005840. https://doi.org/10.1371/journal.pbio.2005840

Wolchok, J. D., Kluger, H., Callahan, M. K., Postow, M. A., Rizvi, N. A., Lesokhin, A. M., … Sznol, M. (2013). Nivolumab plus Ipilimumab in Advanced Melanoma. *New England Journal of Medicine*, *369*(2), 122–133. https://doi.org/10.1056/NEJMoa1302369

Woo, S. R., Turnis, M. E., Goldberg, M. V., Bankoti, J., Selby, M., Nirschl, C. J.,

… Vignali, D. A. A. (2012). Immune inhibitory molecules LAG-3 and PD-1 synergistically regulate T-cell function to promote tumoral immune escape. *Cancer Research*, *72*(4), 917–927. https://doi.org/10.1158/0008-5472.CAN-11-1620

Workman, C. J., Dugger, K. J., & Vignali, D. A. A. (2002). Cutting Edge: Molecular Analysis of the Negative Regulatory Function of Lymphocyte Activation Gene-3. *The Journal of Immunology*, *169*(10), 5392–5395. https://doi.org/10.4049/jimmunol.169.10.5392

Wu, Z., Yang, H., & Colosi, P. (2010). Effect of genome size on AAV vector packaging. *Molecular Therapy*, *18*(1), 80–86. https://doi.org/10.1038/mt.2009.255

Xu, F., Liu, J., Liu, D., Liu, B., Wang, M., Hu, Z., … He, F. (2014). LSECtin expressed on melanoma cells promotes tumor progression by inhibiting antitumor T-cell responses. *Cancer Research*, *74*(13), 3418–3428. https://doi.org/10.1158/0008-5472.CAN-13-2690

Yang, Y., Wang, L., Bell, P., McMenamin, D., He, Z., White, J., … Wilson, J. M. (2016). A dual AAV system enables the Cas9-mediated correction of a metabolic liver disease in newborn mice. *Nature Biotechnology*, *34*(3), 334–338. https://doi.org/10.1038/nbt.3469

Yao, X., Ahmadzadeh, M., Lu, Y. C., Liewehr, D. J., Dudley, M. E., Liu, F., … Robbins, P. F. (2012). Levels of peripheral CD4+ FoxP3+ regulatory T cells are negatively associated with clinical response to adoptive immunotherapy of human cancer. *Blood*, *119*(24), 5688–5696. https://doi.org/10.1182/blood-2011-10-386482

Yossef, R., Tran, E., Deniger, D. C., Gros, A., Pasetto, A., Parkhurst, M. R., … Rosenberg, S. A. (2018). Enhanced detection of neoantigen-reactive T cells targeting unique and shared oncogenes for personalized cancer immunotherapy. *JCI Insight*, *3*(19), e122467. https://doi.org/10.1172/jci.insight.122467

Yu, X., Harden, K., Gonzalez, L. C., Francesco, M., Chiang, E., Irving, B., … Grogan, J. L. (2009). The surface protein TIGIT suppresses T cell activation by promoting the generation of mature immunoregulatory dendritic cells. *Nature Immunology*, *10*(1), 48–57. https://doi.org/10.1038/ni.1674

Zacharakis, N., Chinnasamy, H., Black, M., Xu, H., Lu, Y. C., Zheng, Z., …

Feldman, S. A. (2018). Immune recognition of somatic mutations leading to complete durable regression in metastatic breast cancer. *Nature Medicine*, *24*(6), 724–730. https://doi.org/10.1038/s41591-018-0040-8

Zak, K. M., Kitel, R., Przetocka, S., Golik, P., Guzik, K., Musielak, B., … Holak, T. A. (2015). Structure of the Complex of Human Programmed Death 1, PD-1, and Its Ligand PD-L1. *Structure*, *23*(12), 2341–2348. https://doi.org/10.1016/j.str.2015.09.010

Zetsche, B., Gootenberg, J. S., Abudayyeh, O. O., Slaymaker, I. M., Makarova, K. S., Essletzbichler, P., … Zhang, F. (2015). Cpf1 Is a Single RNA-Guided Endonuclease of a Class 2 CRISPR-Cas System. *Cell*, *163*(3), 759–771. https://doi.org/10.1016/j.cell.2015.09.038

Zhang, F., Cong, L., Lodato, S., Kosuri, S., Church, G. M., & Arlotta, P. (2011). Efficient construction of sequence-specific TAL effectors for modulating mammalian transcription. *Nature Biotechnology*, *29*(2), 149–153. https://doi.org/10.1038/nbt.1775

Zhang, X., & Piedrahita, J. A. (2014). Advances in the Generation of Transgenic Domestic Species via Somatic Cell Nuclear Transfer. In *Principles of Cloning: Second Edition* (pp. 95–106). https://doi.org/10.1016/B978-0-12-386541-0.00008-4

Zheng, C., Zheng, L., Yoo, J. K., Guo, H., Zhang, Y., Guo, X., … Zhang, Z. (2017). Landscape of Infiltrating T Cells in Liver Cancer Revealed by Single-Cell Sequencing. *Cell*, *169*(7), 1342–1356. https://doi.org/10.1016/j.cell.2017.05.035

Zhou, J., Shen, X., Huang, J., Hodes, R. J., Rosenberg, S. A., & Robbins, P. F. (2005). Telomere Length of Transferred Lymphocytes Correlates with In Vivo Persistence and Tumor Regression in Melanoma Patients Receiving Cell Transfer Therapy. *The Journal of Immunology*, *175*(10), 7046–7052. https://doi.org/10.4049/jimmunol.175.10.7046

Zhu, C., Anderson, A. C., Schubart, A., Xiong, H., Imitola, J., Khoury, S. J., … Kuchroo, V. K. (2005). The Tim-3 ligand galectin-9 negatively regulates T helper type 1 immunity. *Nature Immunology*, *6*(12), 1245–1252. https://doi.org/10.1038/ni1271

Zincarelli, C., Soltys, S., Rengo, G., & Rabinowitz, J. E. (2008). Analysis of AAV serotypes 1-9 mediated gene expression and tropism in mice after systemic

injection. *Molecular Therapy*, *16*(6), 1073–1080. https://doi.org/10.1038/mt.2008.76

8. Appendix

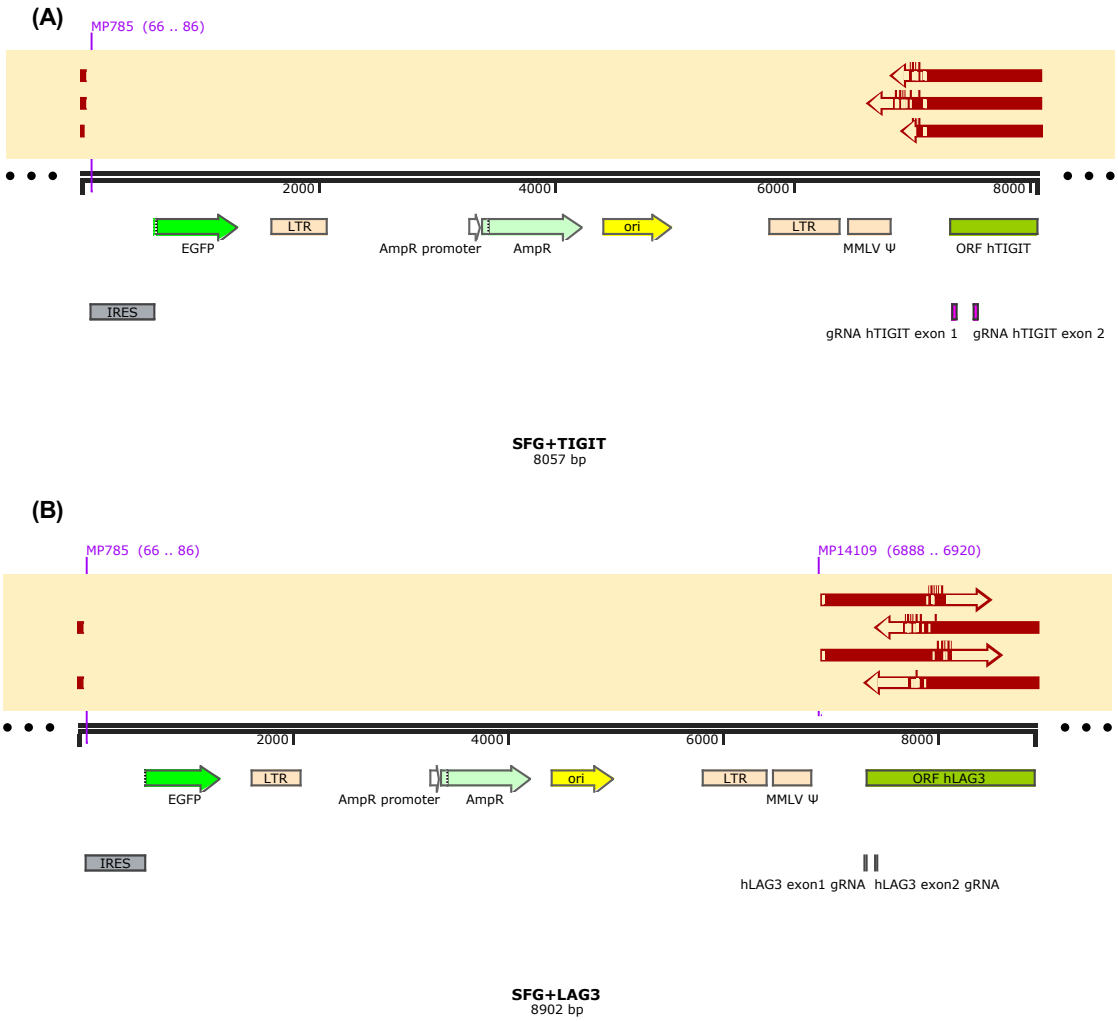

Supplementary Figure 8.1. Validation of correct ligation via Sanger sequencing. (A) Schematic representation of SFG.TIGIT plasmid. Three clones were sent for sequencing with the reverse primer 'MP785' (marked in purple) that starts at the IRES site and continues towards the TIGIT ORF (marked in green rectangle). The sequences (three red arrows) were aligned to the reference plasmid and showed perfect alignment up to the point where the sequence reads start to decrease in quality (end reads). **(B)** Schematic representation of SFG.LAG3 plasmid. Two clones were sent for sequencing with both forward ('MP14109') and reverse ('MP785') primers (marked in purple) that flanked the LAG3 ORF (marked in green rectangle) (forward and reverse primers were used because of the size of the insert). The sequences (four red arrows) were aligned to the reference plasmid and showed perfect alignment up to the point where the sequence reads start to decrease in quality (end reads).

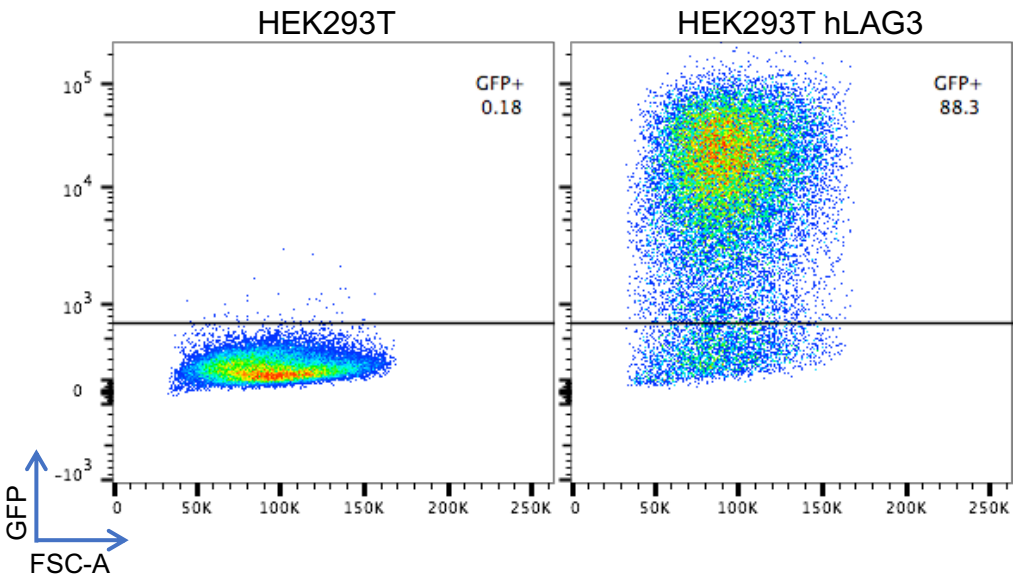

Supplementary Figure 8.2. GFP expression of HEK293T cells transfected with SFG.LAG3 plasmid. Percentage of GFP$^+$ HEK293T cells after transfection of SFG.LAG3 plasmid (gated on live cells).

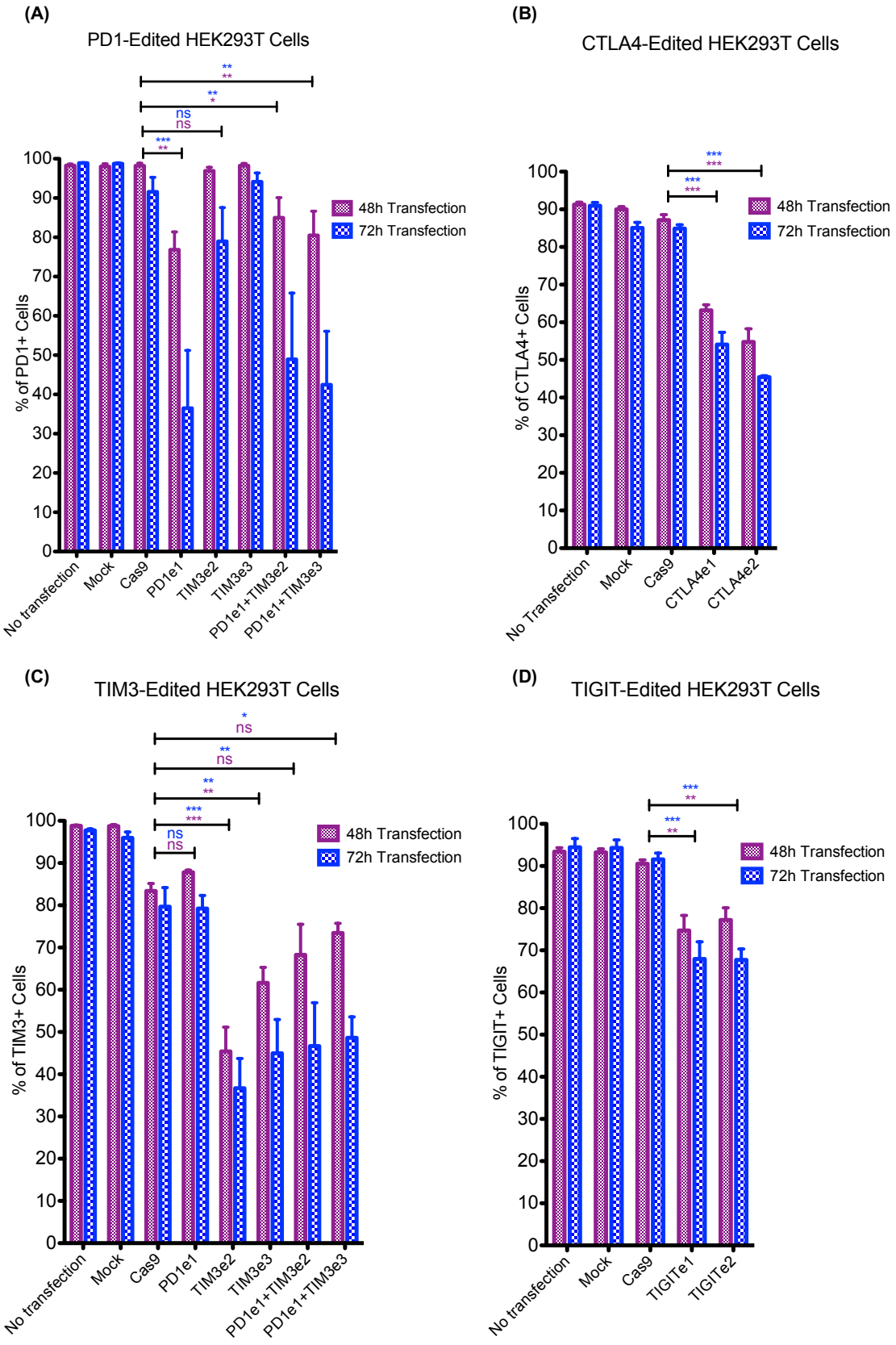

Supplementary Figure 8.3. Percentage of HEK293T cells expressing targets of interest after gene editing. HEK293T cells engineered to constitutively express the targets of interest were edited with plasmids encoding Cas9 and gRNAs targeting **(A)** PD1, **(B)** CTLA4, **(C)** TIM3,

and **(D)** TIGIT. The percentage of cells expressing these targets after gene editing is shown (gated on live cells); n=3 (mean ± SEM). For all of the graphs, one-way repeated measures ANOVA followed by Dunnett's Multiple Comparison was performed for each timepoint.

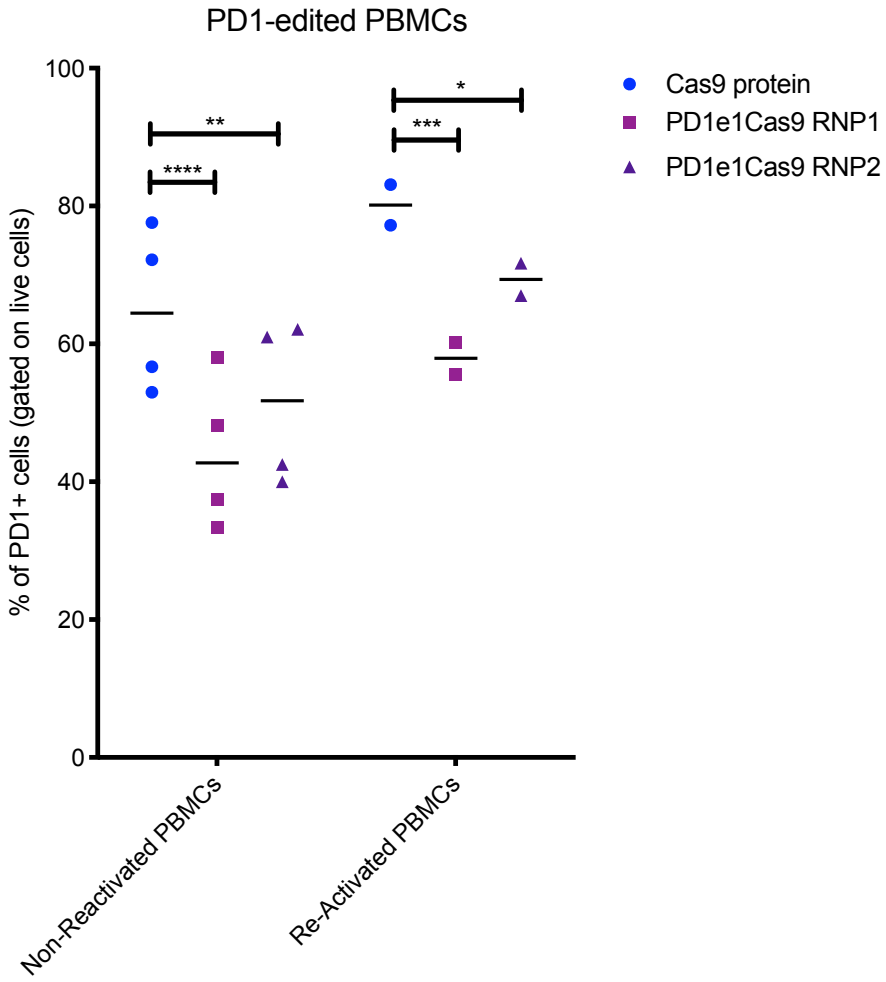

Supplementary Figure 8.4. Percentage of PD1 expression on edited PBMCs. PBMCs were electroporated with either Cas9 protein alone (blue dots), with PD1e1 Cas9 RNP1 (magenta squares), or with PD1e1 Cas9 RNP2 (gRNA from Ren *et al.*, 2017) (purple triangles). Percentage of PD1 positive cells is shown (gated on live cells). Two-way repeated measures ANOVA followed by Dunnett's Multiple Comparison was performed.

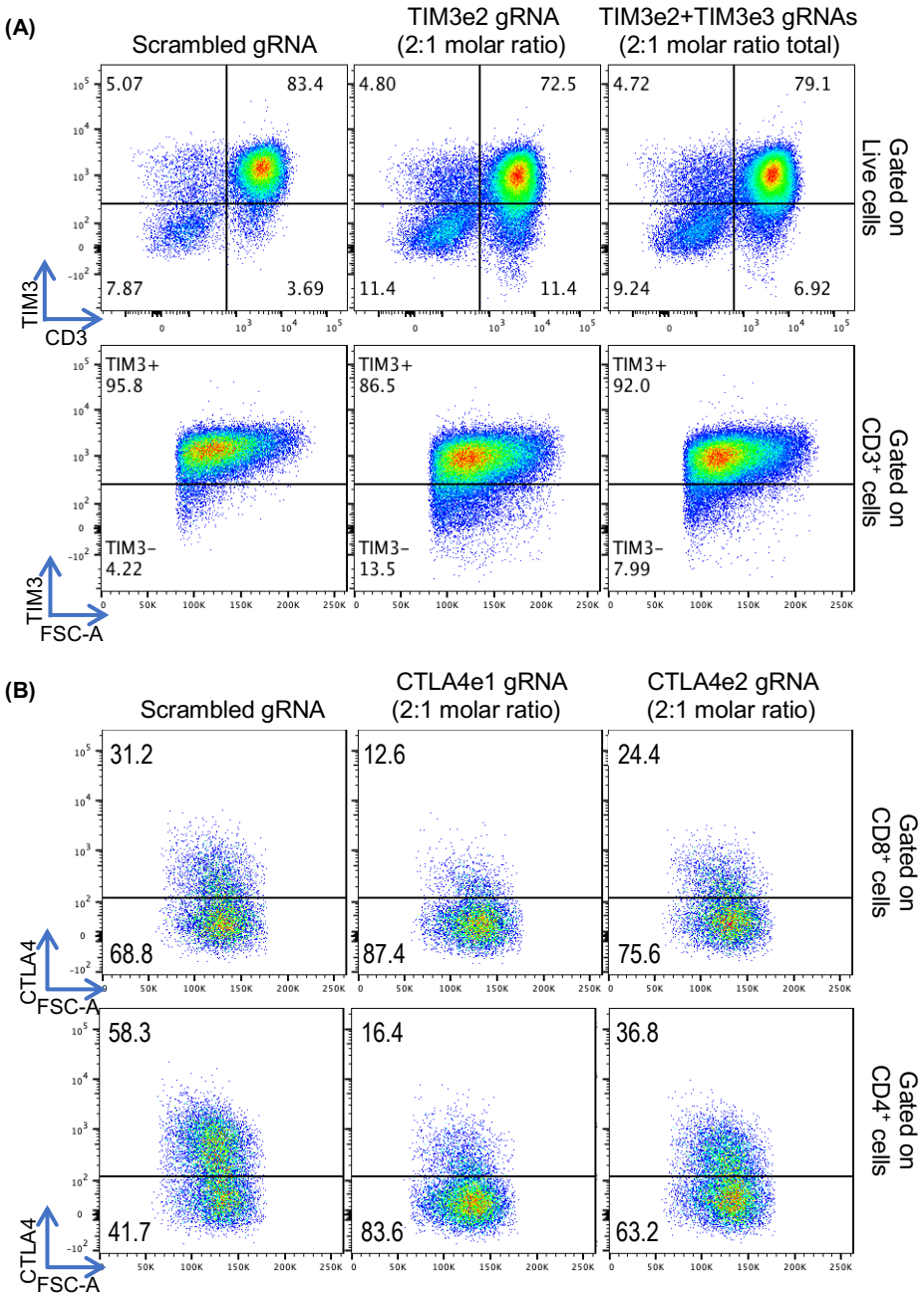
(A)
Scrambled gRNA
TIM3e2 gRNA (2:1 molar ratio)
TIM3e2+TIM3e3 gRNAs (2:1 molar ratio total)
5.07
83.4
7.87
3.69
4.80
72.5
11.4
11.4
4.72
79.1
9.24
6.92
Gated on Live cells
TIM3
CD3
TIM3+ 95.8
TIM3- 4.22
TIM3+ 86.5
TIM3- 13.5
TIM3+ 92.0
TIM3- 7.99
Gated on CD3+ cells
TIM3
FSC-A
(B)
Scrambled gRNA
CTLA4e1 gRNA (2:1 molar ratio)
CTLA4e2 gRNA (2:1 molar ratio)
31.2
68.8
12.6
87.4
24.4
75.6
Gated on CD8+ cells
CTLA4
FSC-A
58.3
41.7
16.4
83.6
36.8
63.2
Gated on CD4+ cells
CTLA4
FSC-A
(C)
CTLA4-Edited Reactivated PBMCs
% of CTLA4+ cells
ns
***
***
****
Scrambled ctrl
CTLA4e1
CTLA4e2
CD8+
CD4+

Supplementary Figure 8.5. TIM3 and CTLA4 gRNA validation in healthy donor PBMCs. (A) Flow cytometry plots showing the expression of TIM3 (top row: gated on live cells, bottom row: gated on $CD3^+$ cells) on healthy donor PBMCs edited with either TIM3e2 gRNA, TIM3e3 gRNA, or a combination of both. **(B)** Flow cytometry plots showing the expression of CTLA4 on $CD8^+$ cells (top row) and $CD4^+$ cells (bottom row) edited with either CTLA4e1 gRNA or CTLA4e2 gRNA. Representative of 4 different healthy donor PBMCs **(C)** Quantification of the percentage of $CTLA4^+$ cells on both $CD8^+$ and $CD4^+$ cells on reactivated PBMCs that were edited with either scrambled gRNA (blue dots), with CTLA4e1 gRNA (magenta squares), or with CTLA4e2 gRNA (purple triangles). One-way repeated measures ANOVA followed by Dunnett's Multiple Comparison was performed for each cell type.

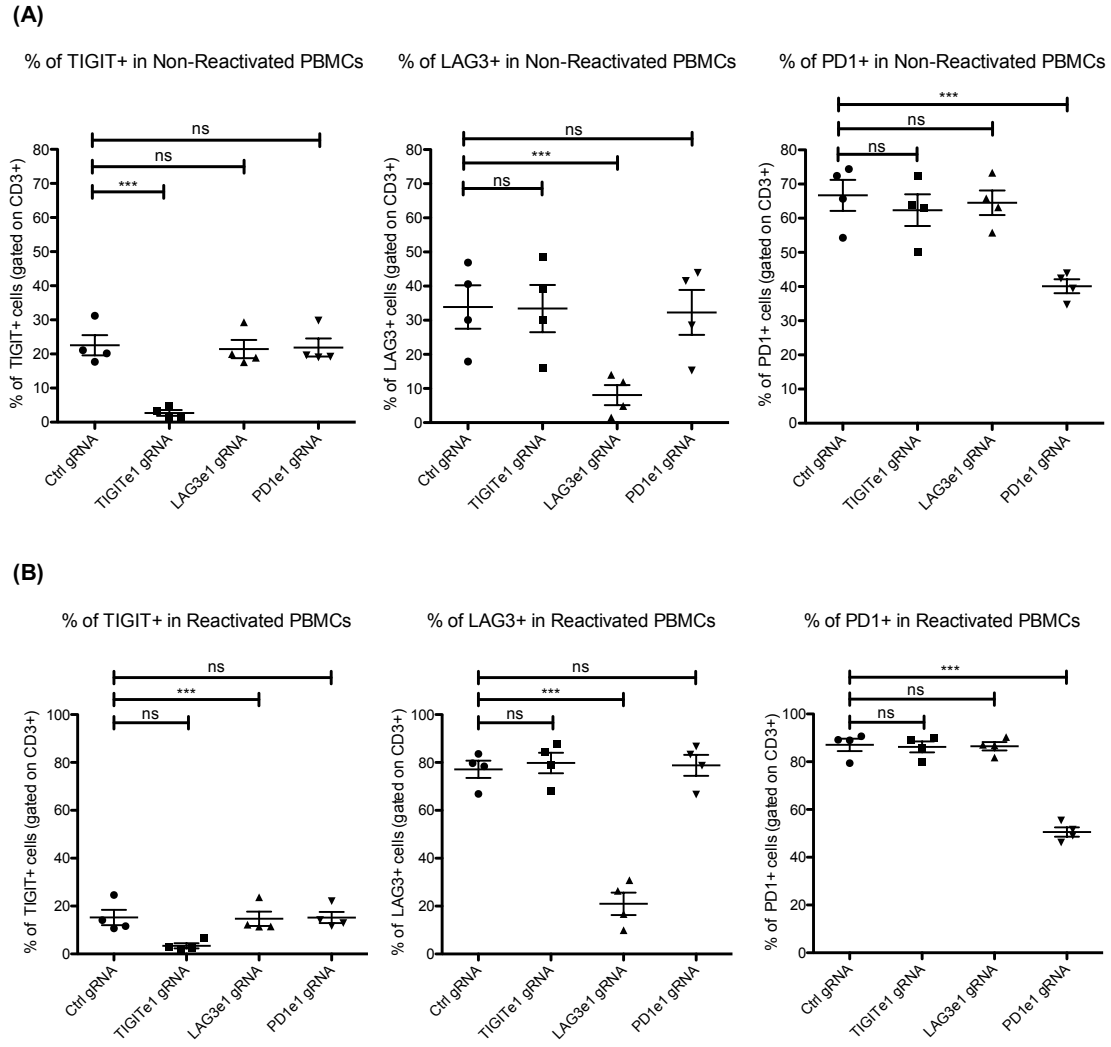

Supplementary Figure 8.6. Gene editing of four different healthy donors PBMCs with either PD1, TIGIT, or LAG3 gRNA. (A and B) Quantification of the percentage of $TIGIT^+$ (left column), $LAG3^+$ (middle column), or $PD1^+$ (right column) cells (gated on $CD3^+$ cells) in either **(A) '**Non-Reactivated' PBMCs or **(B)** 'Reactivated' PBMCs. One-way repeated measures ANOVA followed by Dunnett's Multiple Comparison was performed for each group of cells.

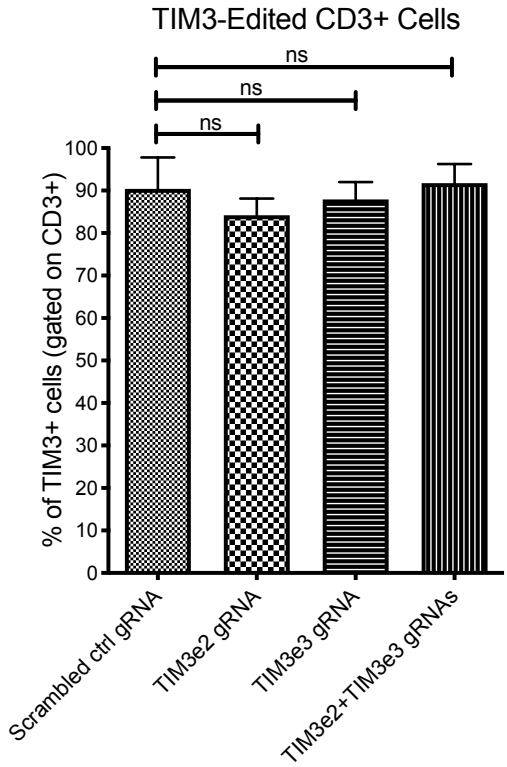

Supplementary Figure 8.7. Gene editing of MX063 TILs with gRNAs targeting TIM3. Quantification of percentage of $TIM3^+$ cells (gated on $CD3^+$ cells); n=5 (mean ± SEM). One-way repeated measures ANOVA followed by Dunnett's Multiple Comparison was performed.

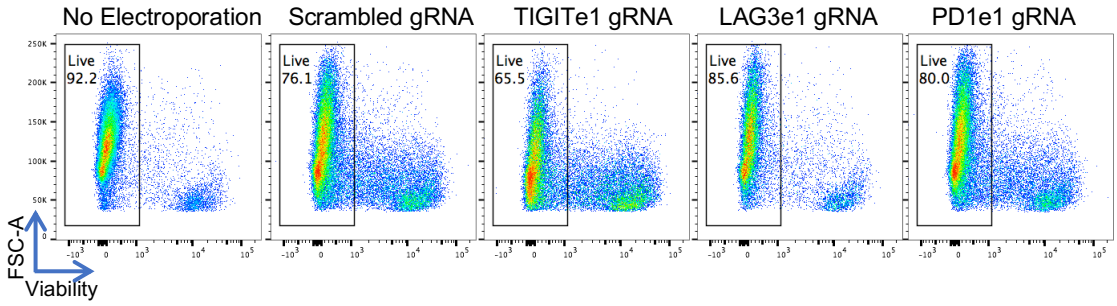

Supplementary Figure 8.8. Viability of TILs edited during REP. Representative flow plots of viability of TILs three days post-editing when the electroporation took place whilst the cells were undergoing rapid expansion.

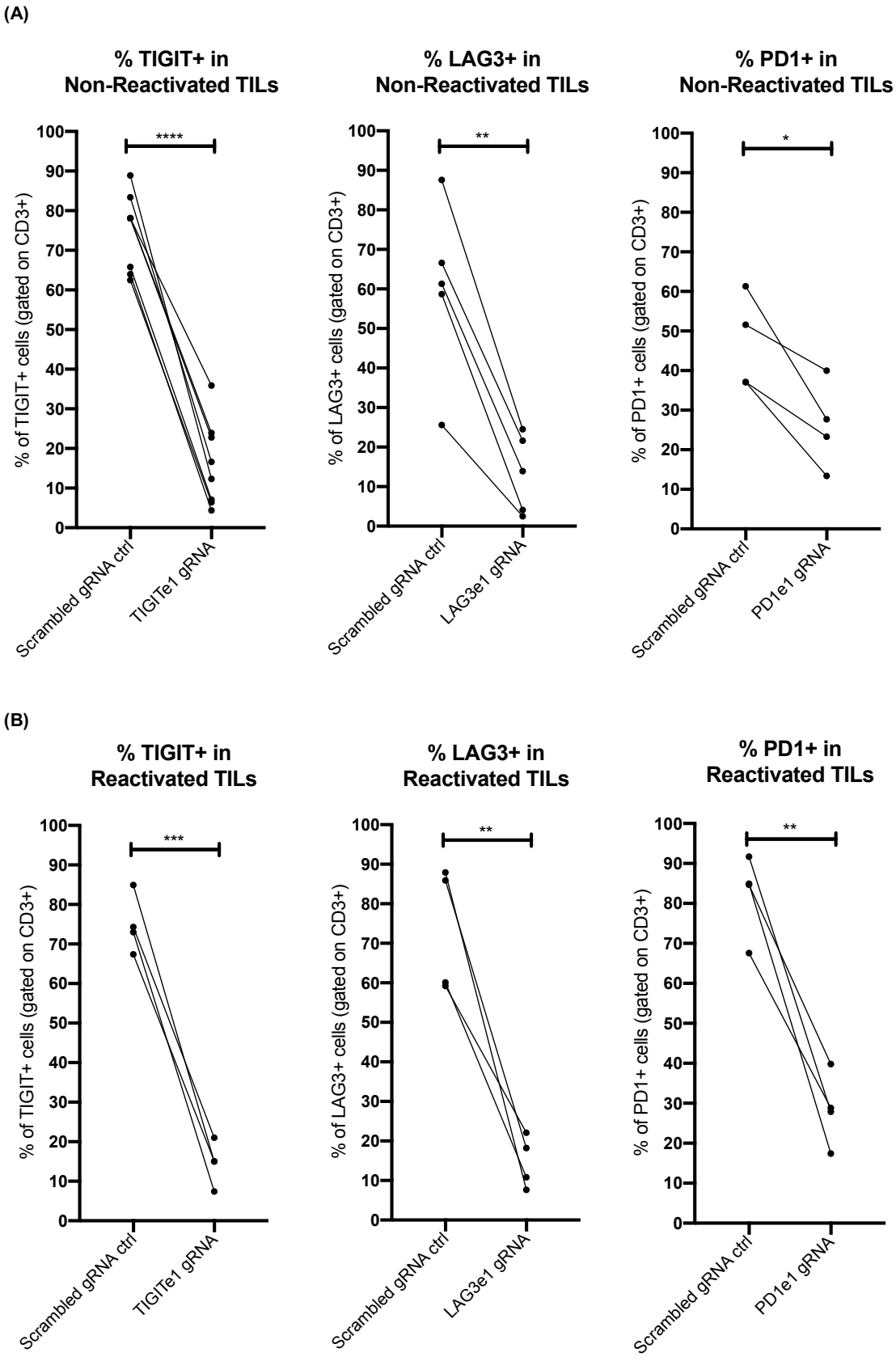

Supplementary Figure 8.9. Gene editing of TILs during REP. (A and B) Quantification of the percentage of TIGIT$^+$ (left column), LAG3$^+$ (middle column), or PD1$^+$ (right column) cells (gated

on CD3$^+$ cells) in either **(A)** 'Non-Reactivated' TILs or **(B)** 'Reactivated' TILs. Paired t-tests were performed for each graph.

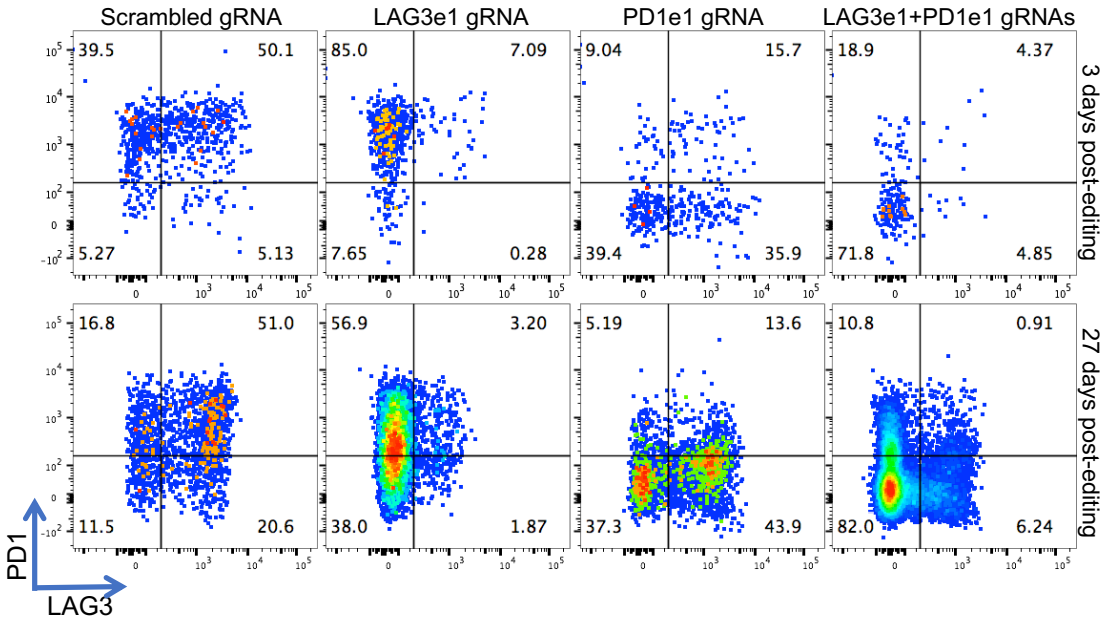

Supplementary Figure 8.10. Efficient and persistent co-editing of PD1 and LAG3 on LTX1000 TILs. Flow cytometry plots showing expression of PD1 and TIM3 in 'Reactivated' TILs on day 3 post-editing (top row) and day 27 post-editing (bottom row) (gated on CD3$^+$ cells).

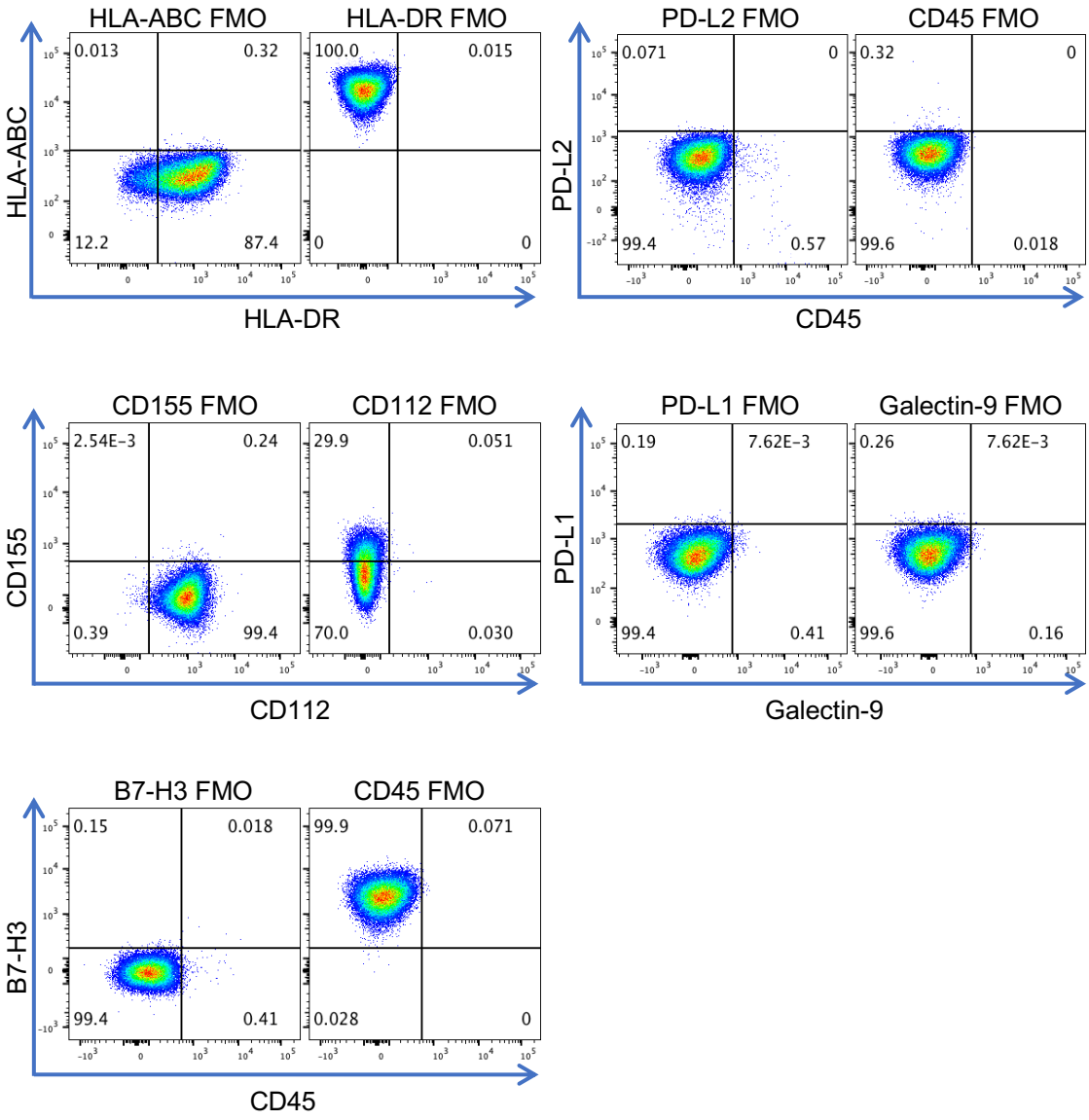

Supplementary Figure 8.11. Fluorescence minus one (FMO) controls for the staining of MX063 primary tumour cell line. Flow cytometry plots of the FMO controls used to set the gates.

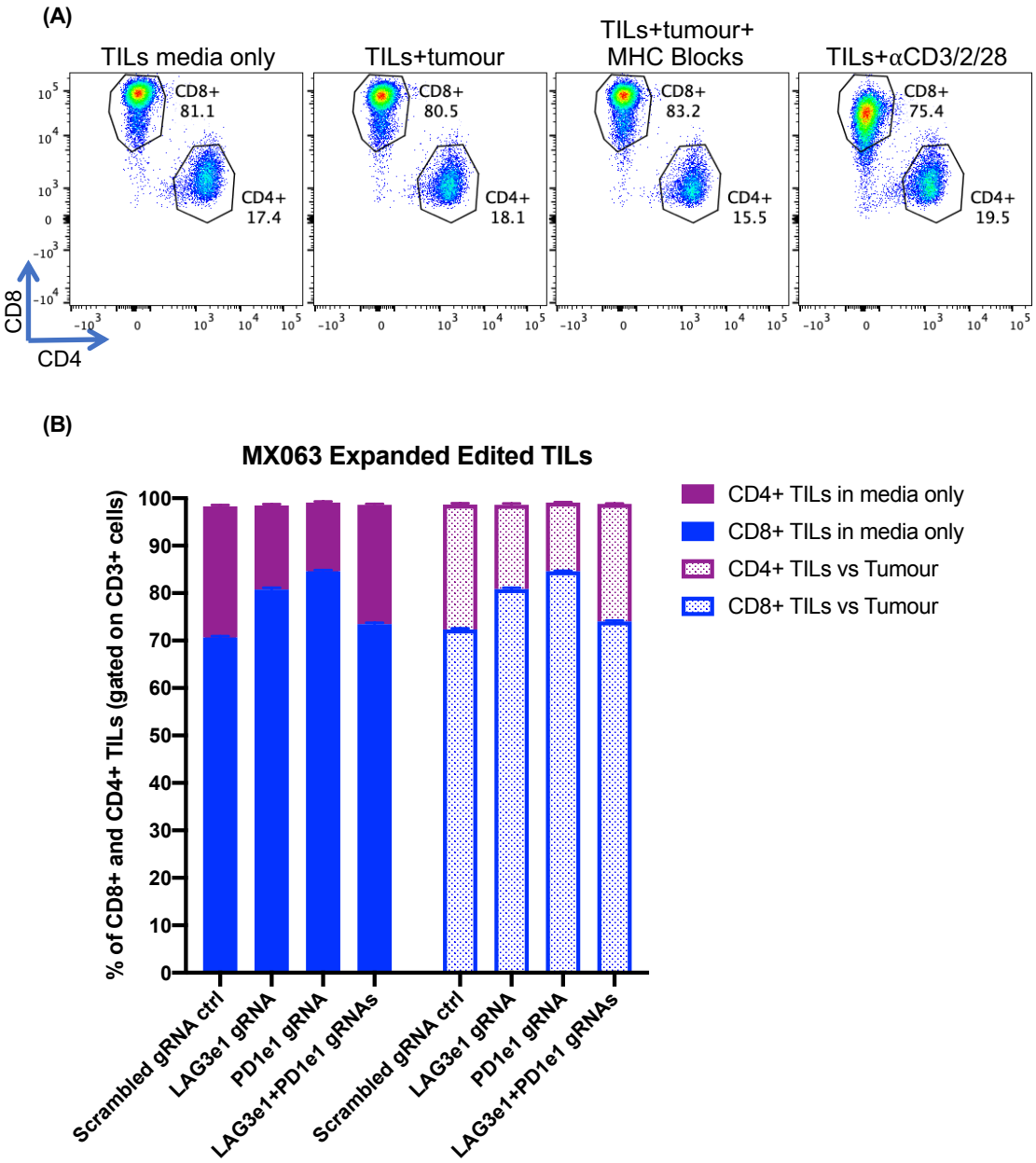

Supplementary Figure 8.12. Percentage of CD4⁺ and CD8⁺ cells in expanded MX063 TILs that were edited to knockdown either LAG3, PD1, or a combination of both. (A) Representative flow plots showing the expression of CD8 and CD4 in edited TILs (gated on CD3⁺ cells). **(B)** Quantification of the percentage of CD8⁺ and CD4⁺ TILs (gated on CD3⁺ cells) in edited and non-edited TILs; n=3 (mean ± SEM) (blue: % of CD8⁺ TILs (in media alone), purple: % of CD4⁺ TILs (in media alone), light blue: % of CD8⁺ TILs (incubated with tumour cells), light purple: % of CD4⁺ TILs (incubated with tumour cells)).

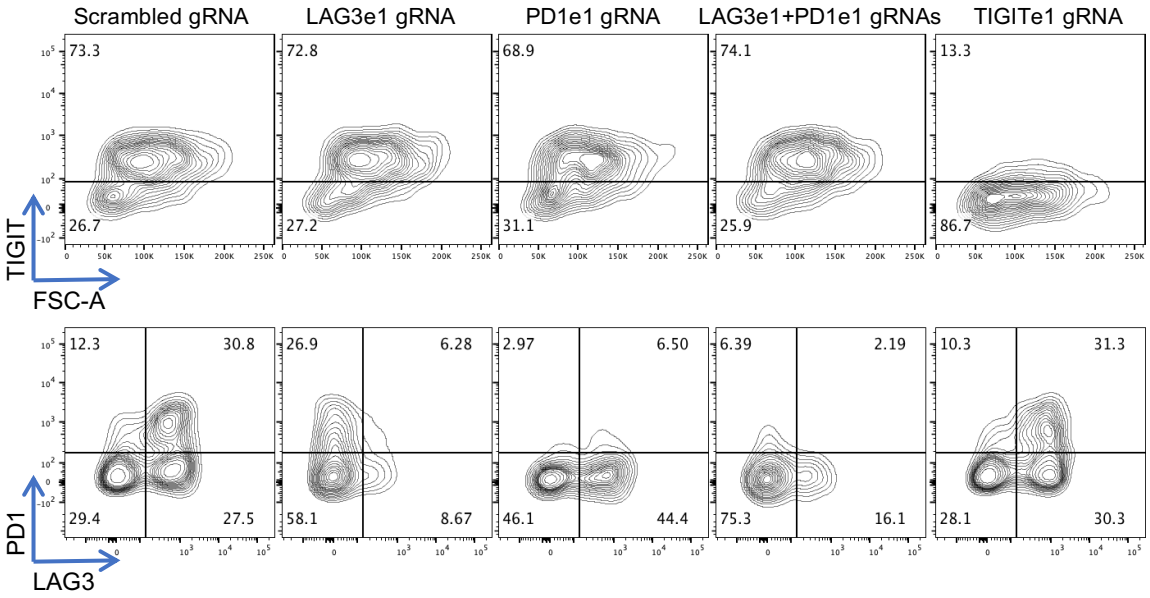

Supplementary Figure 8.13. Successful gene editing of TIGIT, LAG3, PD1, and combination of LAG3 and PD1. MX063 expanded TILs were re-expanded using the REP ('REP 2') and while expanding they were edited using the CRISPR/Cas9 technology to knockdown either LAG3, PD1, a combination of both, or TIGIT. Flow cytometry analysis showing the expression of TIGIT (upper row) or of PD1 and LAG3 (lower row) is presented here.